Investigating Interleukin-1β Processing, Secretion and Targeting in a Zebrafish model

Nikolay Vasilevich Ogryzko

Submitted for the degree of Doctor of Philosophy

Department of Cardiovascular Science

Sepember 2012

Abstract

Uncontrolled inflammation contributes to a number of autoinflammatory pathological conditions, and is a significant factor in a number of other areas such as atherosclerosis the leading cause of death in the developed world. The inflammatory response is very tightly regulated, and controlled at its apex by Interleukin-1β, a key proinflammatory cytokine. This key initiator provides an ideal target for therapeutic intervention, yet many aspects of its biology are poorly understood, including its novel release mechanism. Mammalian in vitro studies have demonstrated IL-1β is processed by a protein complex called the inflammasome and that this processing is linked to release via membrane-derived microvesicles from the cell surface. However, it has not yet been possible to show the functional release of IL-1β microvesicles *in vitro*, determine the mechanism of release and how it is linked to processing and the biological function of these vesicles upon downstream cells. We hypothesise that components of the ESCRT complex are responsible for IL-1β secretion; however, the tools to test this hypothesis in vitro have not yet been developed.

IL-1β structure is highly conserved between zebrafish and humans based on structure prediction software, which shows zebrafish IL-1β shares the same secondary and tertiary structural elements. Zebrafish IL-1β mRNA is induced in response to injury and the inflammatory response is downregulated in response to treatment with IL-1β pathway inhibitors. To investigate IL-1β processing *in vivo*, I have tested a FRET based reporter for caspase-3 activation and characterised the use of such a reporter in the zebrafish as a proof of concept. I have also designed a version of this reporter specific to caspase-1 activation.

Alongside the work on an inflammasome reporter, I also show the first in vivo evidence of IL-1β secretion from inflammatory cells in response to injury using a macrophage specific IL-1β fusion reporter.

In this thesis I demonstrate the utility of the zebrafish as a model of IL-1β biology with regards to induction of IL-1β signaling and the susceptibility of the zebrafish innate immue response to treatment with IL-1β pathway inhibitors, and I present the first evidence of putative IL-1β containing microvesicle release from macrophages *in vivo*.

Acknowledgements

I would like to thank my supervisors whose help was greatly appreciated in this project. Thank you Heather Wilson for my training in tissue culture, molecular biology, writing and critical thinking, but mostly for her patience with me. Many thanks to Steve Renshaw for training in microscopy and zebrafish work, help with writing and understanding the literature, but also for helping to provide a such a positive atmosphere in the Renshaw lab. I would also like to thank my personal tutor Endre Kiss-Toth for his help and advice.

I'd also like to thank Catherine Loynes for training in zebrafish microinjection and embryo handling, Phil Elks for training in light microscopy, and Adrienne Angyal for training in tissue culture.

Thank you to the aquarium staff and technical staff at both the Centre for Developmental and Biomedical Genetics and in the Department of Cardiovascular Science.

And finally many thanks to Aleksandra Bojarczuk, Katy Henry, Caroline MacCalman and Anne Robertson for moral support.

The construct for generating the NF-κB reporter line was a kind gift of Michelle Kanther and John Rawls (University of North Carolina), The *mpeg1* entry clone was provided by Felix Ellett (Walter and Eliza Hall institute, Melbourne), *nsfB* constructs were provided by Mike Parsons (Johns Hopkins), the lyz promoter entry clone was provided by Xingang Wang (Institute of Molecular and Cell Biology, Singapore) and the IL-1β coding sequence was a kind gift of Sara Kohal (University of Sheffield)

Abbreviations

AP, Alkaline Phosphatase; **ASC**, apoptosis-associated speck-like protein containing a CARD; **BAX**, Bcl-2 associated x protein; **BCPIP**, 5-Bromo-4-chloro-3-indolyl phosphate; **(B) (F) RET**, (Bioluminescent) (Förster) Resonance Energy Transfer; **BLAST**, Basic Local Alignment Search Tool; **BSA,** Bovine Serum Albumin; **BzATP**, 2'(3')-O-(4-Benzoylbenzoyl)adenosine-5'-triphosphate; **CARD**, Caspase Recrutment Domain; **(c) DNA**, (complementary) Deoxyribonucleic Acid; **CHMP**, Charged multivesicular body protein; **CHT,** Caudal Hematopoietic Tissue; **(d) (A) (G) (C) (T) ATP**, (deoxy)(Adenosine) (Guanosine) (Cytosine) (Thymidine) Triphosphate; **DAMP**, Damage Associated Molecular Pattern; **DIG**, Digoxygenin; **DMEM**, Dulbecco's Modified Eagle medium; **DMSO,** Dimethyl Sulphoxide; **(E) (B) (C) (G) (Y) FP**, (enhanced) (Blue) (Cyan) (Green) (Yellow) Fluorescent Protein; **EDTA**, Ethylenediaminetetraacetic acid; **ER**, Endoplasmic Reticulum; **ESCRT,** endosomal sorting complex required for transport; **EST,** Expressed Sequence Tag; **FCS,** Fetal Calf Serum; **HIV**, Human Immunodeficiency Virus; **Hpf**, Hours Post Fertilisation; **IκB**, nuclear factor of kappa light polypeptide gene enhancer in B-cells inhibitor; **IKK**, IκB Kinase; **IL-1,** Interleukin-1; **IL-1R**, Interleukin-1 Receptor; **IL-1F7**, Il-1 Family member 7; **IMAGE**, Integrated Molecular Analysis of Genomes and their Expression Consortium; **IRAK**, Interleukin receptor associated kinase; **LAMP**, Lysosomal-associated membrane protein; **LMP**, low Melting Point; **LRR**, Leucine Rich Repeat; **LPS**, Lipopolysaccharide; **MCPIP**, monocyte chemoattractant protein-induced protein; **MCS**, Multiple Cloning Site; **ME**, Middle Entry; **MMP**, Metric Metalloproteinase; **(m) (si) (t) RNA**, (message) (short interfering) (transfer) Ribonucleic Acid; **MTX**, Maitotoxin; **MyD88**, Myeloid differentiation primary response gene; **NA**, Numerical Aperture; **NBT**, nitroblue tetrazolium; **NCBI**, National Center for Biotechnology Information; **NEB**, New England Biolabs; **nF**, netFRET; **NF-κB**, nuclear factor kappa-light-chain-enhancer of activated B cells; **NIK**, NF-κB inducing kinase; **NLR(P)(C),** NOD like receptor (Pyrin) (CARD) domain containing; **PAMP**, Pathogen Associated Molecular Pattern; **PBS**, Phosphate Buffered Saline; **PFA**, Paraformaldehyde; **PMA**, phorbol 12-myristate 13-acetate; **PPADS**, pyridoxalphosphate-6-azophenyl-2',4'-disulfonic acid; **PRR**, Pattern Recognition Receptor; **PS**, Phosphatidyl Serine; **PSF**, Point Spread Function; **PYD**, Pyrin Domain; **RAcP**, Receptor Acessory Protein; **RHD**, Rel

Homology Domain; **ROS**, Reactive Oxygen Species; **SLS**, Scientific Laboratory Supplies;**SSC**, Saline Sodium Citrate; **TILLING**, Targeting Induced Local Lesions in Genomes; **TIR**, Toll/Interleukin-1 receptor; **TLR**, Tol Like Receptor; **TUNEL**, Terminal deoxynucleotidyl transferase dUTP nick end labeling; **UAS**, Upstream Activating Sequence; **UTR**, Untranslated Region; **VLR**, Variable Lymphocyte receptor; **WISH**, Whole-mount in situ Hybridisation;

Table of Contents

Figures and Tables

Chapter 1: Introduction

1.1 Evolution of the Immune response

The evolution of multicellular life presented many challenges, perhaps foremost of these was competition and interaction with more primitive, pathogenic microorganisms, leading to the evolution of immunity as a mechanism to distinguish self from non-self and to combat invading microorganisms. The earliest example of invertebrate immunity was documented by Metchnikoff in 1882 who described the attempted phagocytosis of a rose thorn puncturing a starfish by cells which were later termed coelomocytes (reviewed in Beck and Habicht, 1996).

Since then, primitive immune responses have been observed in a variety of invertebrate organisms in the study of immunity and evolution. *Hydra* has been shown to mount a potent antimicrobial response regulated by neuronal cells (Kasahara & Bosch 2003), and genome data-mining has permitted the discovery of pattern recognition receptors (PRRs) in other members of the cnidarian lineage. These PRRs use leucine rich repeats (LRRs) as the basis of their pattern recognition and were discovered as homologues for Toll like receptors (TLR) and Interleukin 1 receptors (IL-1R) (DJ Miller et al. 2007). These receptors link to innate immunity through the NF-κB pathway, which activates transcription of immune related genes and was also found in cnidarian genomes (DJ Miller et al. 2007; J. Sullivan et al. 2007). The Toll pathway has been linked to development in a number of organisms, such as *drosophila,* but in mammalian lineages acts as an activator of immunity (Medzhitov et al. 1997). The evolution of the Toll pathway, has been implicated as occurring after the evolution of sponges (Hemmrich et al. 2007). LRRs as a mechanism of pathogen recognition are also present in plants to a great extent, demonstrating the evolution of these components very early on (DA Jones & D. Takemoto 2004; Nürnberger et al. 2004)

Sensing of pathogens and non-self material leads to the production of antimicrobial compounds and activation of phagocytosing cells, as those described by Metchnikoff in starfish but also present in insects (Lanot et al. 2001), implying their evolution before the divergence of these lineages. In horseshoe crabs, this response is also potentiated by the precursors of the complement system (Y. Zhu

et al. 2005) which later developed to regulate the interaction between innate and adaptive immunity (Carroll 1998).

As immune systems evolved, so did pathogens, and LRRs as a mechanism of pathogen recognition have been suggested as evolutionarily burdensome due to the necessity of maintaining a large pattern recognition "library" (Pancer & Cooper 2006). This difficulty was surmounted by the evolution of a family of VLR proteins in sea lampreys which were capable of rapid rearrangement to generate a vast array of combinations for improved pathogen sensitivity (Pancer et al. 2004), alongside the evolution of the first adaptive immune cells; lymphocytes (Shintani & Terzic 2000). These were the precursor to more advanced immunoglobulin domain based antibodies which first evolved in jawed fish, and the evolution of varied lymphocyte populations (Kaufman 2002), however, immunoglobulin containing proteins were also implicated in earlier lamprey immunity (Fujii et al. 1979).

We can see that as organisms gained complexity, so did their immune systems, as layers of additional defense were added to protect against pathogens (Flajnik & Du Pasquier 2004). The most "modern" development in immunity, Immunoglobulin genes, are under fierce selection pressure in response to pathogen evolution, as evidenced by the differences observed between mouse and human immune genes (Hughes 1997). However, the more evolutionarily ancient immune pathways remain more conserved as demonstrated by the role of PRRs and phagocytosis. However, despite their useful role in host defense, the release of antimicrobial compounds and the activation of immune cells is potentially dangerous for the host organism and therefore mechanisms of regulation, and signalling have evolved to ensure tight control of these systems. Cytokines are an evolutionarily ancient mechanism to recruit immune cells and correctly activate the host response (Beck & Habicht 1991a); key amongst these is the interleukin 1 (IL-1) family. These genes are similarly ancient, yet retain a conserved function: IL-1 like proteins have been identified in starfish and *tunicates* and have furthermore been able to elicit an IL-1β like response in murine fibroblasts and human cell lines (Beck & Habicht 1991b).

Human IL-1 itself was first discovered as a "leukocytic pyrogen" identified by its pleiotropic effects and was later found to consist of two separate proteins,

IL-1α and IL-1β. IL-1α has been described as an intracellular and local mediator, whereas IL-1β has instead been designated as a more general, systemic mediator (Dinarello 1996) and has since been described as a "gatekeeper of inflammation" (Dinarello 2011a) due to its apical role in the initial stages of the inflammatory response.

1.2 Summary of IL-1β synthesis and release

As a key regulator of immunity, IL-1β release must be strictly controlled, and over the course of evolution, numerous adaptations have provided tight control of the IL-1β pathway. On a basic level, the release of IL-1β from innate immune cells, such as macrophages, has numerous distinct controls, each requiring a potentially differing external signal to activate. These control the action of IL-1β at the transcriptional level as well as the functional level. The IL-1β message is transcribed and stabilised upon the reception of a pathogen or damage associated molecular pattern (PAMP or DAMP) by pattern recognition receptors on the cell surface. This signal is transduced through the NF-κB signalling pathway resulting in the induction of IL-1β transcription as the inactive propeptide pro-IL-1β. Pro-IL-1β is converted into an active cytokine through the action of caspase-1 which itself is proteolytically activated via the reception of secondary PAMP and DAMP signalling through intracellular PRRs making up complexes termed inflammasomes. IL-1β is then packaged and released from the cell via an unknown secretion mechanism, not dependent on the traditional ER/Golgi release pathway. IL-1β is regulated at transcription, translation, post translational and release pathways sensitive to a variety of stimuli and under a complex set of controls (Figure 1.1).

1.3 Pro-IL-1β induction

1.3.1 Pattern recognition in IL-1β induction

IL-1β is released by monocyte and myeloid lineage cells (Kominato et al. 1995) in response to external stimuli, notably pathogen associated molecular patterns (PAMPS), as well as injury and other inflammation inducing stimuli such as other cytokines and stress factors (see (Dinarello 2009a) for more detail)

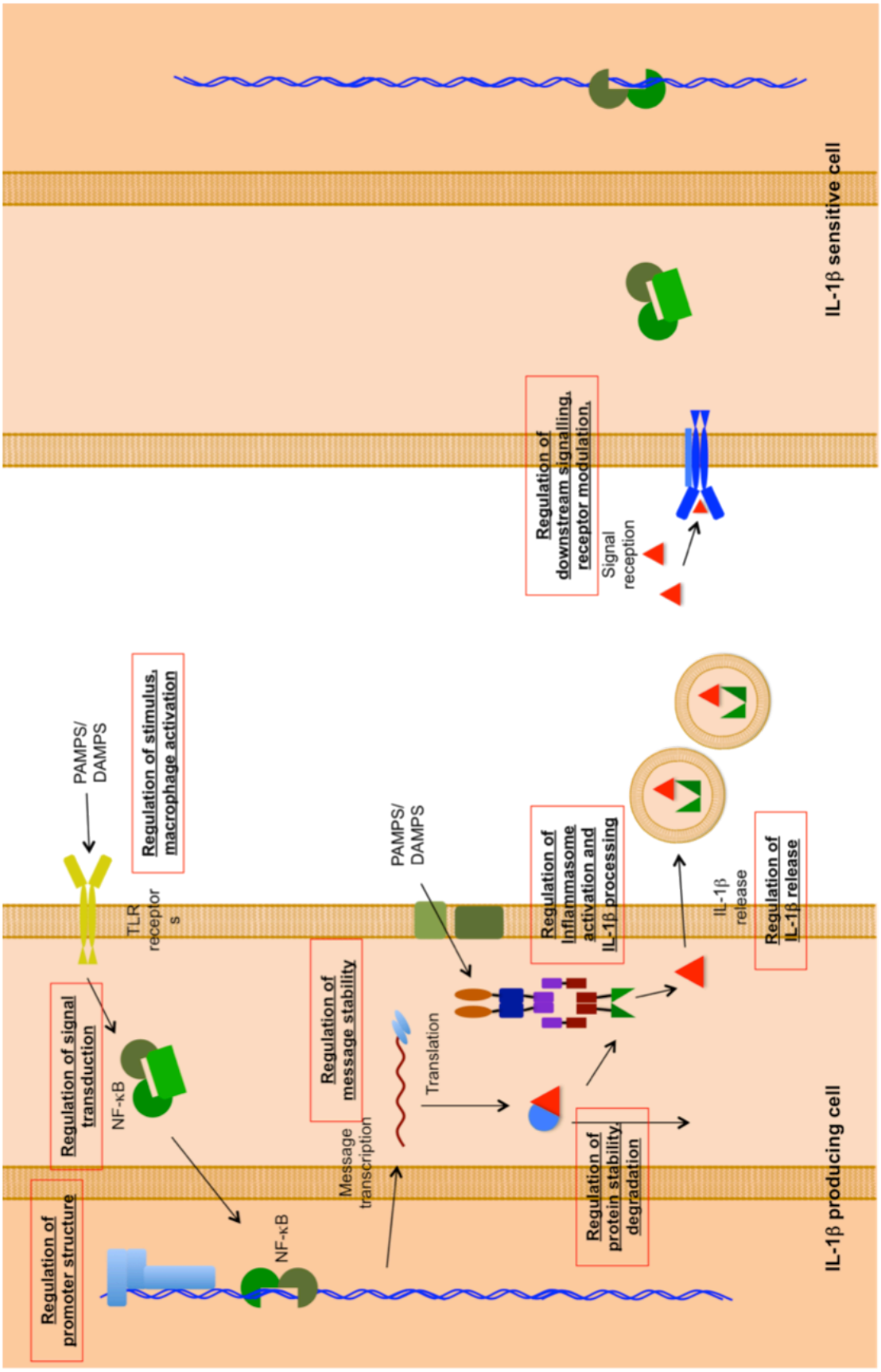
IL-1β sensitive cell
Regulation of downstream signalling, receptor modulation,
Signal reception
IL-1β producing cell
Regulation of stimulus, macrophage activation
PAMPS/ DAMPS
TLR receptor s
Regulation of signal transduction
NF-κB
Regulation of promoter structure
NF-κB
Regulation of message stability
Message transcription
Translation
PAMPS/ DAMPS
Regulation of Inflammasome activation and IL-1β processing
Regulation of protein stability, degradation
IL-1β release
Regulation of IL-1β release

Figure 1.1. IL-1β signalling is subject to tight regulation on a number of levels. IL-1β is induced in response to a number of inflammatory stimuli, via the canonical NF-κB pathway, and expressed from a promoter architecture "poised" for a rapid response. Both the mRNA and pro-peptide of IL-1β are subject to regulated turnover and degradation and inflammatory stimuli are necessary for stability. IL-1β processing is mediated by caspase-1, itself subject to activation by inflammasome complexes responsive to varied stimuli. Inflammasome action is coupled to IL-1β release by a number of pathways sensitive to inflammatory signalling, and signal sensitivity is controlled by downstream decoy receptors and an endogenous antagonist.

activating TLR receptors on the cell surface. Chromatin at the IL-1β gene locus in IL-1β producing cells exists in an "open and ready" arrangement due to the permanent binding of a transcription factor complex to promoter sites on the gene (M. Liang et al. 2006; Unlu et al. 2007), limiting the amount of time needed to initiate transcription on the reception of an inflammatory stimulus. IL-1β transcription is triggered by the activation of NF-κB and its subsequent translocation to the nucleus following reception of Toll like receptor (TLR) ligands by TLRs on the cell surface (Sabroe et al. 2008), or in fact by IL-1β itself (Dinarello et al. 1987) (Figure 1.2).

1.3.2 NF-κB complexes and transcriptional control

IL-1β transcription is a product of active NF-κB binding to NF-κB response elements upstream of the IL-1β coding sequence, however, because of the potency of genes potentially activated by NF-κB, this activation itself strictly controlled. Cytosolic NF-κB is a multimeric protein complex composed of IκB and two NF-κB protein subunits: the p50 or p52 subunit, and the p65 subunit, RelA (Baeuerle 1988). These subunits all contain a protein domain called the Rel homology domain (RHD), containing both immunoglobμlin like folds and the IκB interaction sites. However, on RelA, the DNA binding sites are present on the IPT domain (immunoglobulin-like, Plexin and transcription factor domain) (Aravind & Koonin 1999). In its inactive state, the nuclear localisation signals present on NF-κB

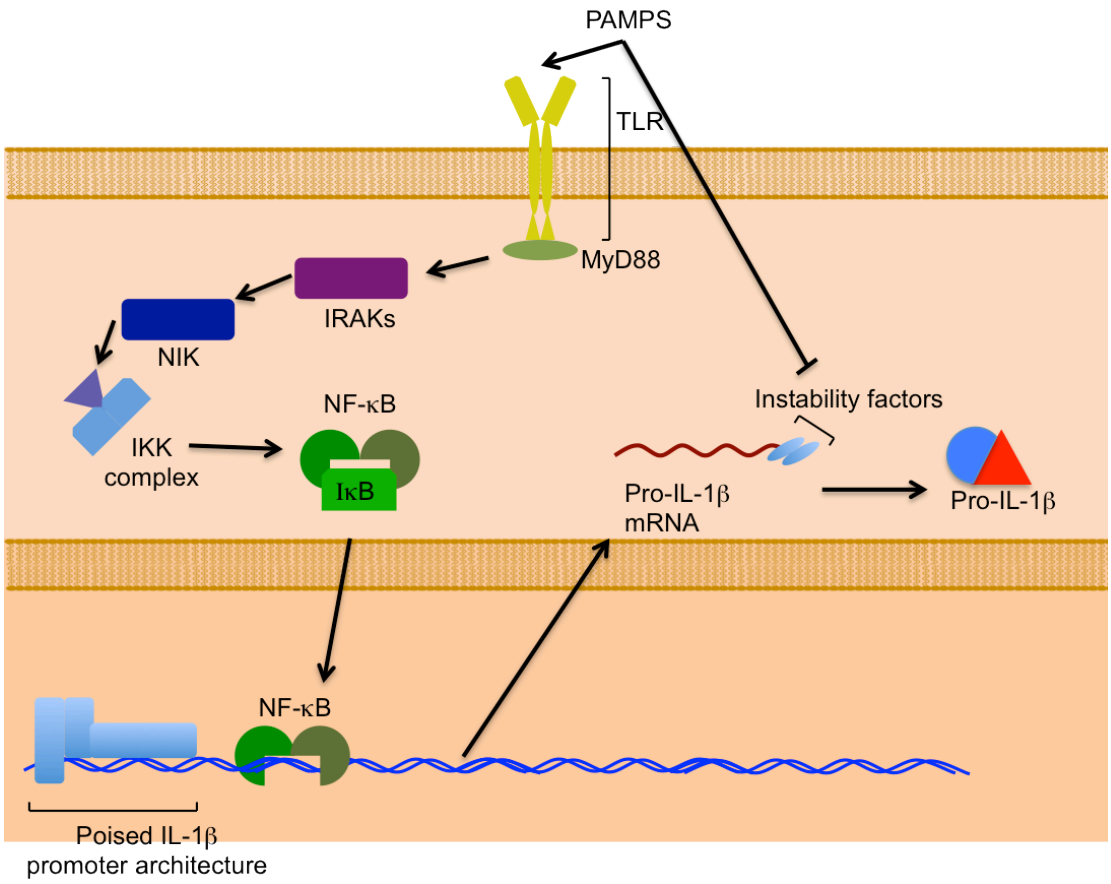

Figure 1.2. IL-1β transcription induction in response to Pathogen associated Molecular Patterns (PAMPS). IL-1β is induced in response to activation of TLR receptors on the cell surface by PAMP ligands. The signal is transduced through the canonical NF-κB pathway where it induces IL-1β transcription from a rapid-response promoter architecture. IL-1β is also controlled on an mRNA stability level via instability elements in the 3' UTR and potential internal RNAse sites; message stability is dependent on the continued presence of inflammatory stimuli.

subunits are masked by the binding of IκB to the complex in a 1:1 manner using the ankyrin repeats present on IκB and the RHD (Jacobs & S. Harrison 1998). Multiple modes of activation exist for NF-κB, the foremost being the kinase cascade culminating in the phosphorylation of IκB by IKK (IκB kinase). This phosphorylation prevents IκB binding to NF-κB and exposes the PEST (sequences rich in Proline, Glutamic acid, Serine and Threonine residues), sites present on IκB (Shumway et al. 1999) and allows IκB to be ubiquinated, which targets IκB for degradation by the proteosome.

With IκB unbound and degraded, the nuclear localisation signals on NF-κB become exposed and the protein is shuttled to the nucleus (Carlotti et al. 2000) where it can bind NF-κB response elements and start the transcription of IL-1β .

IκB itself is degraded by a the IKK complex, consisting of two effector kinases IKKα and IKKβ (DiDonato et al. 1997; Mercurio et al. 1997); and the regulatory subunit IKKγ (DiDonato et al. 1997; Mercurio et al. 1997; Rothwarf et al. 1998), which itself is regulated by NIK (NF-κB inducing kinase) (Regnier et al. 1997).

NIK function is mediated by further factors, dependent on the nature of the stimuli in question. The most common in the study of IL-1β biology is MyD88, a signal transducer and TLR adaptor, in this context specifically TLR4, which is responsible for detecting bacterial LPS (lipopolysaccharide). MyD88 transduces these signals to IRAKs (interleukin-1 receptor associated kinases); which are the first step of this phosphorylation cascade (Croston et al. 1995), or are able to bind to IKK directly (Cooke et al. 2001).

1.3.3 Translational control of IL-1β

Pro-IL-1β production is under further control at the mRNA stability level. The production of pro-IL-1β mRNA is induced without further protein synthesis and adhesion stimuli are sufficient for this response (Schindler et al. 1990), however, in response to LPS, a rapid increase, followed by a rapid degradation of IL-1β mRNA was described (Fenton et al. 1987). Conversely low level induction of IL-1β transcription by phorbol 12-myristate 13-acetate (PMA) resulted in a more stable message, indicating more than one pathway for regulation of mRNA stability

(Fenton et al. 1988). The suggested mechanisms behind the control of IL-1β mRNA translation differ and multiple mechanisms have been proposed.

Bufler *et al.* (2004) propose the involvement of instability elements detected by homology to described elements in the coding sequence of IL-1F7, although alignment data presented in this study was not compelling. However, similar elements were found in other proteins (Tierney & Medcalf 2001).

The 3' UTR region of IL-1β mRNA has been implicated in the speed of ribosomal translation of the mRNA where downstream binding of a protein may inhibit ribosome velocity (Kaspar & Gehrke 1994). This instability and translational control is regulated by TLR ligands, the most common experimentally used is bacterial LPS, a ligand of TLR4. Binding of this ligand increases the stability of IL-1β mRNA and allows more pro-IL-1β to be produced (Bufler et al. 2004).

More recently, the involvement of an RNase, MCPIP, a product of the *ZC3H12A* gene, has been implicated in the transcriptional control of IL-1β by premature degradation of the IL-1β message (Mizgalska et al. 2009). Induction of the *ZC3H12A* gene was later shown to be a result of IL-1β stimulation itself, suggesting a negative feedback control mechanism for IL-1β translation (Kasza et al. 2010).

Altering IL-1β stability at the message level could provide cells with an additional layer of control over IL-1β signalling and allow the removal of excess transcripts in the event of a transient inflammatory insult, mRNA could be rapidly degraded without initiating protein translation.

1.4 Post-Translational processing.

1.4.1 NLRs and Inflammasomes

In mammalian cells, IL-1β is released from cells as a mature cytokine following its conversion from pro-IL-1β by proteolytic cleavage; separating the bioactive IL-1β subunit from the pro-domain. This action is performed by the Interleukin 1 converting enzyme now known as caspase-1 (DK Miller et al. 1993). Although in this process caspase-1 is essential for the release of mature IL-1β, it has also been linked to the processing of at least 77 other extracellular proteins involved in initiating and recovering from inflammatory processes (M. Keller et al. 2008)

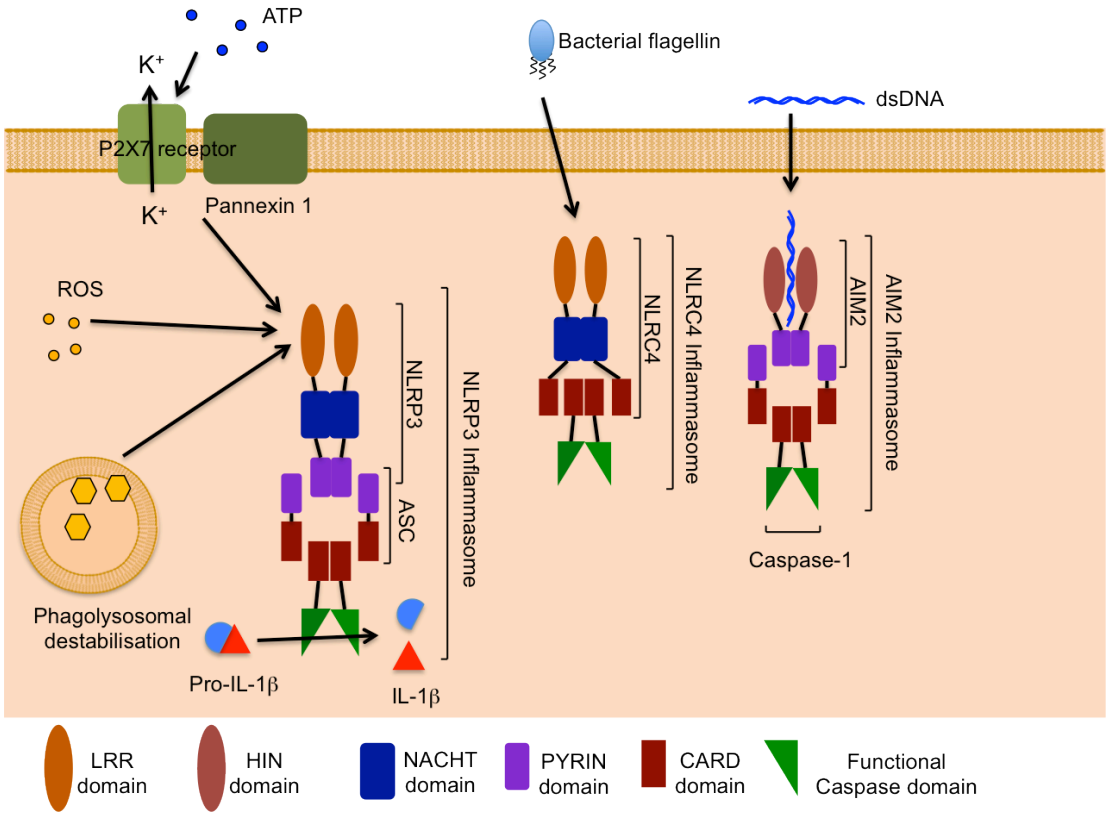

Figure 1.3. Inflammasomes are mediators of IL-1β processing and share common domain architectures. IL-1β is processed by caspase-1, which in turn is activated by inflammasome complexes. Inflammasomes are responsive to a wide range of stimuli, via activation of different Pattern Recognition Receptors (PRRs). Different PRRs oligomerise into different inflammasomes with a unique set of ligands. Inflammasomes bind caspase-1 via a caspase recruitment domain (CARD) present either on the PRR protein, or via apoptosis-associated speck-like protein containing a CARD (ASC), an adaptor protein. Displayed are NLRP, NLRC and AIM inflammasomes. (adapted from Rathinam *et al*,.(2012))

Caspase-1 itself is produced as a pro-peptide and is proteolytically activated (Ayala et al. 1994) by an autocatalytic method (K. Wilson et al. 1994) following the reception of a secondary inflammatory signal, a PAMP or DAMP, often distinct from the stimulus necessary for the induction of IL-1β, such as the ATP mediated IL-1β response in LPS primed monocytes (MacKenzie et al. 2001). Hereby, the release of mature IL-1β requires a secondary stimulus and an additional layer of regulatory control. This secondary signal initiates the assembly and activation of the large multiprotein complex known as the Inflammasome, whose function is to produce mature IL-1 β through the activation of Caspase-1 (P. Li et al. 1995; B. Miller et al. 1995) (Figure 1.3)

A number of proteins are necessary for the function of an inflammasome, but key to these are a number of protein domains. At the most basic level, to perform the function of an inflammasome, a caspase recruitment domain (CARD) able to interact with the CARD domain of caspase-1, and a PRR capable of sensing an inflammatory stimulus are necessary (Martinon et al. 2002; Franchi et al. 2006). Inflammasome PRRs take the form of Nod like receptors or NLR proteins, containing LRR domains for pattern recognition. NLRs have a number of other features exemplified in the most characterised, and perhaps the most complex inflammasome based on the NACHT, LRR and PYD domains-containing protein 3 (NLRP3). In an NLRP3 inflammasome, NLRP3 acts as the primary PRR and has a multidomain structure (Martinon et al. 2002); the LRR domain acts as the sensor for inflammatory stimuli, the NACHT domain is responsible for oligomerisation of NLRP3 proteins, and the Pyrin domain is indirectly responsible for the recruitment of caspase-1 via the presence of an adaptor protein (ASC), itself composed of a Pyrin domain and a CARD domain. NLRP3 inflammasomes are responsive to a wide array of stimuli (Rathinam et al. 2012).

Other inflammasome complexes, making use of differing arrangements of these domains have been described. NLRP proteins, like NLRP3, rely on ASC for caspase recruitment, whereas NLRC proteins have a CARD domain of their own in lieu of a Pyrin, thereby not requiring ASC (Mariathasan et al. 2004). Inflammasome PRRs do not always take the form of a Leucine rich repeat as in NOD like proteins (NLRs) of the NLRP and NLRC families. AIM2 inflammasomes, composed of a Pyrin domain and a HIN domain, instead detect double stranded DNA by binding directly

via their HIN domain. Although AIM2 inflammasomes have a limited ability to recognise self-DNA, the presence of double stranded DNA in the cytosol is most often a sign of bacterial or viral infection.

Although Inflammasome PRR proteins containing pyrin domains, such as NLRP and AIM based inflammasomes, require apoptosis-associated speck-like protein containing a CARD (ASC) for their function (Hornung et al. 2008; Hornung et al. 2009). ASC is also capable of potentiating the response of NLRC inflammasomes, which can mediate caspase-1 activation through their own CARD domain, but show a decrease in IL-1β production in ASC-/- cells demonstrating that caspase-1 is activated more effectively in the presence of ASC in these inflammasomes (Miao et al. 2006).

The precise mechanism of activation of inflammasomes is poorly characterised. The activation of NLRC4 inflammasomes through direct detection and binding of bacterial flagellin by the NAIP protein family and interaction of this protein with NLRC4 has been demonstrated (Kofoed & Vance 2011; Y. Zhao et al. 2011), as has the ability of AIM2 inflammasomes to bind directly to dsDNA (Hornung et al. 2009; Bürckstümmer et al. 2009). However, the activation of the archetypal NLRP3 inflammasome (Jin & Flavell 2010) remains to be understood.

NLRP3 is present as a multimeric protein in the cytoplasm of immune cells, it oligomerises through an LRR domain, with assembly into the inflammasome based on a pyrin domain interaction with ASC. The sensory, and presumably activation functions of NLRP3 are performed by a NACHT domain. However, it has also been shown that the pyrin domain of NLRP3 can itself inhibit inflammasome function, so perhaps inflammasome activation results in the change or removal of this domain from caspase-1 (Chae et al. 2006). NLRP3 is essential for the primary IL-1 β release pathway of IL-1 β from macrophages (Sutterwala, Ogura, Zamboni, et al. 2006; Sutterwala, Ogura, Szczepanik, et al. 2006) and it seems that mature IL-1 β also depends on the presence of ASC to be released (Pelegrín et al. 2008). The NLRP3 inflammasome is assembled in response to pathogen stimulation, as shown by the nuclear distribution of ASC until stimulation with PAMPs (Bryan & Dorfleutner 2009); at which point ASC is shuttled to the cytoplasm and associates

into aggregate complexes with Caspase-1, some near the cell surface at possible IL-1 β release sites (Pelegrín & Surprenant 2009b).

NLRP3 inflammasomes assemble and activate in response to a broad range of stimuli, ranging from bacterial and viral pathogens (Meixenberger et al. 2010; S. Kim & Bauernfeind 2010; I. Allen et al. 2009), to danger signals such as silica, asbestos and uric acid crystals (Gasse et al. 2009; Dostert et al. 2008; Hornung et al. 2008), and such a wide assortment of mechanisms implies that NLRP3 does not directly sense these stimuli. Instead, three potential mechanisms for this activation have been proposed (Jin & Flavell 2010). NLRP3 inflammasomes can be activated directly by potassium efflux from the cell (Pétrilli et al. 2007), by reactive oxygen species (ROS) produced from mitochondria (Cruz et al. 2007) and by the disruption of phagolysosomes by crystalline compounds (Hornung et al. 2008). Interestingly, both K^+ efflux and ROS production can be linked to the detection of extracellular ATP by the P2X7 receptor (Pelegrín & Surprenant 2009b)(Cruz et al. 2007; Pétrilli et al. 2007). Blocking the P2X7 receptor with a selective antagonist in an inflammatory macrophage subtype (M1) (Scotton et al. 2005; Martinez et al. 2006) prevents NLRP3 activation through the other methods, not just the ATP dependant pathway, but the mechanisms were unclear (Pablo Pelegrin & Annmarie Surprenant 2009a).

1.4.2 Non-caspase-1 mediated mechanisms of IL-1β processing.

Although caspase-1 is the primary mediator of IL-1β processing, other mechanisms of IL-1β cleavage have been described. Mice deficient in caspase-1 were still capable of developing arthritic symptoms, and mature IL-1β was recovered from synovial joints and inflammatory lesions (Guma et al. 2009) (Joosten & Netea 2009). Elastase and chymase activity has been proposed as a mechanism for cleavage, inhibition of which lessened arthritic symptoms (Guma et al. 2009). Caspase-1 deficient mice were also capable of producing a bioactive IL-1β in response to turpentine treatment (Fantuzzi et al. 1997). IL-1β cleavage resulting in a molecule with 30% bioactivity of mature IL-1β was reported due to granzyme A mediated cleavage (Irmler et al. 1995), and Matrix Metalloproteinase

mediated cleavage was observed for MMP2, 3 and 9 (Schönbeck et al. 1998). Other caspases have also been implicated in the processing of IL-1β, which is also cleaved at the caspase-1 cleavage site by caspase-8 (Maelfait et al. 2008).

Bacterial proteins have also been implied in IL-1β cleavage, with the suggestion that this is an attempt to maintain an inflammatory niche in *C. albicans* and *S. aureus* infection, however it was also shown that these varying forms of IL-1β cleavage were less bioactive than caspase-1 processed IL-1β and that this was a function of the increased size of the molecule (R. Black et al. 1988; Schönbeck et al. 1998). Extracellular processing mechanisms have been proposed as a route for the production of mature IL-1β cytokine post pyroptosis by cells in inflammatory lesions, a mechanism possibly subverted by bacterial processing.

1.4.3 P2X7 receptor function.

Rapid release of IL-1β from innate immune cells is triggered by reception of an exogenous ATP danger signal by the P2X7 receptor on the cell surface (Sanz & Di Virgilio 2000). The P2X7 receptor is a purinergic receptor that forms a cation pore on binding extracellular ATP signal (Perregaux & Gabels 1994; Rassendren et al. 1997). In this context, receptor activation leads to the efflux of K+ ions from the cell (Surprenant et al. 1996), but is also coupled to the much larger pannexin-1 channel, which it can activate to make the cell membrane permeable to much larger sized molecules of up to 900Da (Ferrari et al. 2006; Pelegrín & Surprenant 2006; Pétrilli et al. 2007; Pelegrín et al. 2008). Pelegrin and Surprenant (2006) posit that since a pannexin-1 siRNA knockdown inhibits IL-1β processing, the cation efflux is not itself responsible for the activation of the NLRP3 inflammasome and that the pannexin channel may offer a novel way that extracellular ATP can enter the cell and activate IL-1β processing by a more direct method. Nevertheless, it is also clear that pannexin-1 is essential for the activation of the inflammasome through recruitment by P2X7 (Kanneganti et al. 2007; Locovei et al. 2007). It has now been suggested that pannexin-1 itself is activated by high extracellular concentrations of K+, and that the presence of these cations outside the cell in a locally high concentration is responsible for the activation the channel (Silverman & Vaccari 2009).

An interesting development is the proposition of novel mechanisms of inflammasome control; Pelegrin and Surprenant (2009a) have shown that the inflammasome is inhibited in the M2, or resolution type, macrophage by ATP acting independently of the P2X7 receptor. This process occurs through the direct reduction of ROS production, and the rearrangement of the cell's cytoskeleton to confine inflammasome components and restrict the formation of the complex. This gives an indication that perhaps IL-1β release can be controlled in M1 macrophages through the manipulation of these same mechanisms.

1.5 IL-1β release

Numerous mechanisms for the release of IL-1β from immune cells have been described, and although these mechanisms may not be entirely IL-1β specific, these highlight the evolutionary importance of the control of IL-1β signalling. It has been proposed that these mechanisms occupy a "spectrum" of release dependent on the severity of stimuli that the immune cells experience with low level continual release a feature of local inflammation, protected release a response to stronger stimuli with the most severe inflammatory insults resulting in a "terminal" release of IL-1β. Furthermore, it is also likely that more than one of these mechanisms can be engaged in response to a stimulus (López-Castejón & Brough 2011), and it must be made clear that *in vitro* studies of IL-1β release may not accurately represent this full spectrum by concentrating on a specific stimulus rather than considering the whole cell microenvironment in its totality.

1.5.1 Low level release mechanisms

Early in the history of IL-1β research it was shown that IL-1β lacks a signal peptide or leader sequence required for its release via conventional protein secretion pathways (Auron & Webb 1984), and that IL-1β was processed prior to its release from the cell (Auron et al. 1987). IL-1β release from monocytes was shown to be independent of cell death and insensitive to inhibition by golgi/ER pathway inhibitors (Rubartelli et al. 1990), and these data pointed to a novel secretory pathway for IL-1β. Rubartelli *et al.* (1990) demonstrated that IL-1β was contained within monocyte fractions resistant to trypsin degradation unless first treated

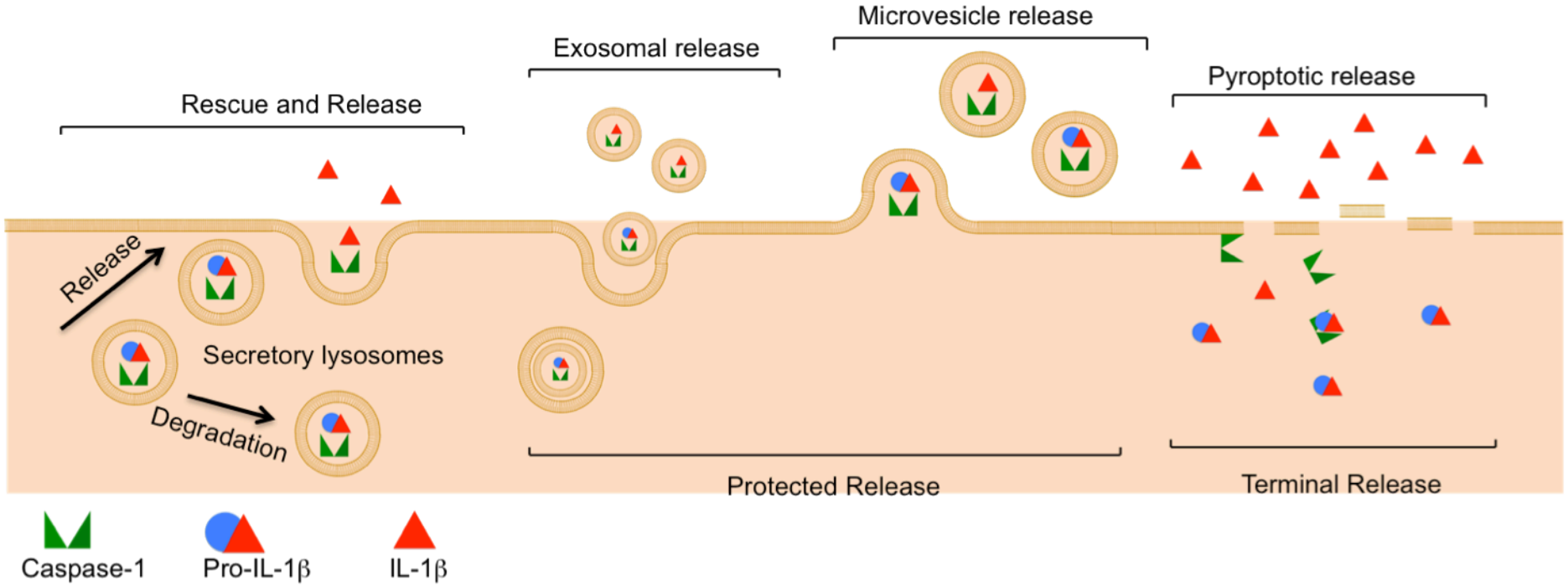

Figure 1.4. Spectrum of IL-1β release. A potential unifying mechanism for IL-1β release is a dependence release mechanism on the strength of inflammatory insult (López-Castejón and Brough, 2011). Low-level secretion from secretory lysosomes is dependent on the redirection of IL-1β from its constant degradation by lysosomes to local release. More powerful stimuli release membrane bound IL-1β for trafficking to more distant inflammatory loci whereas pyroptotic release results from extended exposure to insult or infection with intracellular pathogens. (Adapted from Lopez-Castejon & Brough (2011))

with detergent, providing evidence that IL-1β was present in intracellular vesicles, later shown to be endolysosomes (Andrei et al. 1999). These IL-1β containing endolysosomal bodies are targeted for degradation via the autophagy pathway, disruption of which results in an increase in IL-1β secretion from the cell, a mechanism suggested as a limit to secretion of the cytokine (Saitoh et al. 2008; Harris et al. 2011). It has been hypothesized that IL-1β is constantly turned over within the cell, and that this release pathway redirects this turnover to secretion under the appropriate stimuli, a mechanism termed "rescue and release" (López-Castejón & Brough 2011). Alongside this pathway, a direct transport mechanism for IL-1β independent of secretory lysosomes has also been proposed (Brough & Rothwell 2007) (Figure 1.4).

1.5.2 Pyroptosis as a mechanism for IL-1β release

IL-1β has been demonstrated as a product of the inflammatory macrophage cell death pathway pyroptosis (Le Feuvre et al. 2002; Bergsbaken et al. 2010). Pyroptosis is an inflammatory programmed cell death, related to apoptosis but with key differences: like apoptosis, pyroptosis is mediated by caspases, though in this case, the inflammatory caspase-1, is required for pyroptosis to occur (Hersh et al. 1999). Unlike apoptosis, which does not trigger an inflammatory reaction by packaging cellular material into apoptotic bodies later phagocytosed by immune cells, pyroptosis is a pro-inflammatory lysis of innate immune cells (Brennan & Cookson 2000). Immune cells undergoing pyroptosis experience caspase-1 mediated membrane pore formation (Fink et al. 2008) resulting in loss of membrane asymmetry demonstrated by dye uptake and phosphatidylserine (PS) flip on the cell surface, a process differing from apoptosis where PS flip is observed but membrane integrity is maintained (Brennan & Cookson 2000). Pore formation allows osmotic lysis of macrophages as excess water crosses the membrane into the cell and results in the release of the cell contents into the cellular milieu, concurrently releasing large amounts of processed IL-1β alongside other cytokines (Fink & Cookson 2006). Pyroptosis is entirely caspase-1 dependent as inhibiting caspase-1 also inhibits this cell death pathway (Hersh et al. 1999; Brennan & Cookson 2000). Pyroptosis is independent of caspase-3 activation (Brennan & Cookson 2000), and apoptotic pathways remain mechanistically independent of

pyroptosis (P. Li et al. 1995) delineating this as two separate pathways to cell death.

Certain intracellular pathogens, such as *legionella* (L. Y. Gao & Abu Kwaik 1999) and *Yersinia* (Bergsbaken & Cookson 2007) can initiate a sterile, apoptotic cell death dependent upon caspase-3 in macrophages. However, this can be switched to a pyroptotic death if this infection is in pre-activated rather than naïve cells (Bergsbaken & Cookson 2007). Although pyroptosis has been described for sterile stimuli, such as prolonged P2X7 receptor activation, pyroptosis has most commonly been detected in response to potent intracellular pathogens, such as *Yersinia*, *Legionella*, *Salmonella* and anthrax toxin (Hersh et al. 1999; L. Y. Gao & Abu Kwaik 1999; Fink et al. 2008) and this proposes an evolutionary basis for pyroptosis; as a number of these pathogens induce apoptosis in host cells as a possible mechanism for further infection, pyroptosis could act as a switch to warn nearby cells of this attempt to subvert cellular machinery. As such, pyroptosis sends a very "urgent" and potent signal to surrounding cells with the effectively uncontrolled release of normally strictly controlled, intracellular, pro-inflammatory factors such as mature IL-1β and tumour necrosis factor α (TNFα) (Bergsbaken et al. 2010).

1.5.3 Vesicular and endosomal release pathways

Alongside rescue and release mechanisms, and the localised release of IL-1β from inflammatory cell death, an interesting IL-1β release mechanism via the membrane-derived microvesicles from macrophages has been described. These vesicles contain both mature, biologically active IL-1β as well the ability to process pro-IL-1β using packaged inflammasome components such as caspase-1, suggesting that the site for the release of these vesicles is close to the site of inflammasome mediated caspase-1 activation, and that the release and processing pathways are likely related (Pelegrín & Surprenant 2009b), Mackenzie *et al.,* (MacKenzie et al. 2001) demonstrate that the release of microvesicles is distinct from cell lysis and is a very rapid process, however the mechanism by which these vesicles are packaged and released is unknown. This microvesicle based IL-1β release pathway has also been demonstrated in microglia (Bianco et al. 2005) and

dendritic cells (Pizzirani et al. 2007), and its presence in these cell types implies its functions as a release mechanism within tissues as well as in the bloodstream. Microvesicles are capable of releasing IL-1β in response to ATP stimulation of P2X7 receptors on their cell membranes (Pizzirani et al. 2007), and that this mechanism is due to lysis of these vesicles (Bianco et al. 2005).

IL-1β is also found within smaller membrane bound vesicles termed exosomes, first identified in murine macrophages by the presence of endolysosomal markers, such as LAMP1. These exosomes act as a mechanism of IL-1β release with significantly different kinetics from membrane derived microvesicle release in terms of LPS priming (Qu et al. 2007). Exosomal release of IL-1β is highly dependent on the NLRP3 inflammasome, however is paradoxically not dependent on caspase-1, as it still occurs in macrophages derived from caspase-1 deficient mice (Qu et al. 2009). Exosomes are significantly smaller than membrane microvesicles, being 50-80nm in diameter, rather than 100-600nm for microvesicles (Qu et al. 2009).

Vesicles and exosomes could be an evolutionary mechanism to deliver IL-1β to sites of inflammation and overcome the limited half-life of IL-1β in the circulation (Kudo et al. 1990), but also as a potential response to the potency of IL-1β and the danger of unnecessary proinflammatory signalling and off target effects on surrounding cells. The potential benefit of release using vesicular bodies is that IL-1β, and in fact other proteins co-released with the vesicles are delivered to target cells at a high concentration. Such packaging avoids dilution within the extracellular environment (Hugel & Martínez 2005) confers protection from degradation due to their membrane encapsulation. These mechanisms have therefore been termed “protected release” (López-Castejón & Brough 2011).

1.6 Mechanisms of microvesicle formation and release.

1.6.1 Phosphatidylserine signalling

Preceding the release of IL-1 containing vesicles, a phosphatidylserine (Eisenberg et al. 1990) flip from the internal to external membrane face is detectable on the surface of releasing cells (MacKenzie et al. 2001), which may be

related to the method of release and/or may provide a method for these vesicles to interact and "dock" with their target cells. This PS flip has been confirmed as dependent on P2X7 receptor stimulation and extracellular calcium (Pizzirani et al. 2007) defining these vesicles as distinct from the exosomes released during apoptosis and other processes (Aupeix et al. 1997; Heijnen et al. 1999) but related to other microvesicles produced in processes such as coagulant and healing activity (Dachary-Prigent et al. 1993; Satta et al. 1994). Therefore this suggests that this pathway of IL-1β release may well utilise a pre-existing mechanism of vesicle release as opposed to one specifically evolved for the secretion IL-1β.

1.6.2 Membrane structure and vesicle formation

Phosphatidyl serine is a membrane lipid that usually lies on the inner face of a lipid bilayer, providing an ideal signal to detect changes in cell state or signalling as a result of its relocation to the outer face of the membrane (Fadok et al. 1992; Fadok et al. 1993; S. Martin et al. 1995). In order to control this process and maintain membrane asymmetry, cells have an ATP driven translocase, an active enzyme responsible for maintaining PS on the inner face of the membrane (Seigneuret 1984). Loss of membrane asymmetry and thus PS externalisation is achieved through the activity of a Scramblase enzyme dependent on Ca^{2+} influx into the cell for its activation (Stout et al. 1996; Q. Zhou et al. 1997). In red blood cells, the proposed mechanism for the release of these microvesicles following the loss of membrane asymmetry is the activation of calpain by increased Ca^{2+} concentration, resulting in the calpain mediated cleavage of the underlying cytoskeletal structure (Zwaal & Schroit 1997). Its been proposed that the increased cellular Ca^{2+} concentration also results in the activation of enzymes responsible for the cleavage of $PI(4,5)P_2$; a membrane lipid responsible for anchoring the underlying cytoskeleton to the plasma membrane, osmotic pressure then results in the separation of the membrane from the skeleton and the formation of a membrane bleb (H. Keller et al. 2009). It has been suggested that this blebbing is a function of the release of IL-1β in microparticles, however due to the timescale it occurs at; significantly later than the release of microvesicles, it may be a result of the cell's ability to release microvesicles being overwhelmed, or

that continuous exposure to ATP initiates blebbing to engulf macrophages and trigger a negative feedback response, thereby controlling inflammation (Marguet et al. 1999; Verhoef & Estacion 2003): vesicle shedding is visible within seconds of a secondary stimulus such as ATP, reception and the accompanied tethered blebbing from the plasma membrane takes place over the timescale of a few minutes. The two processes, though temporally linked, have been shown to be independent of each other. Blebbing is inducible upon maitotoxin (MTX) uptake or by non-specific large pore opening following treatment with high concentrations of extracellµlar K^+ (Verhoef et al. 2004), supporting the role of the P2X7 receptor and extracellular K^+ in IL-1β processing and release.

1.6.3 Candidate microvesicle release proteins

The release of membrane-derived microvesicles remains poorly understood, and although specific proteins have been implicated in the pathway, the exact mechanism of release remains to be determined. Bianco *et al.,* (2009) propose a central role for sphingomyelinase in this release pathway, citing its importance in P2X7 mediated IL-1β release alongside previous data indicating the role of sphingomyelinase in the release of vesicles from artificial microspheres (Nurminen et al. 2002), and its role in membrane blebbing during apoptosis (Tepper et al. 2000; Lépine et al. 2006). Bianco *et al.,* (2009) suggest that sphingomyelinase mediates vesicle release through altering membrane structure, however this provides no insight into the packaging of microvesicle contents.

A novel binding partner of caspase-1, Rab39a has also been implicated in the release of IL-1β (C. Becker et al. 2009). Rab39a is a member of the RAB GTPase family, members of which are responsible for membrane fusion and organisation (Stenmark et al. 2001; Zerial & McBride 2001). Becker *et al.,* (2009) have shown that Rab39a is required for IL-1β secretion, and was induced by LPS stimulation, however it was unclear which of the IL-1β secretion pathways Rab39a could be involved in.

A potential mechanism for the release of microvesicles is the Endosomal Sorting complex required for Transport (ESCRT) complexes. ESCRT proteins have been shown to allow the budding of HIV virions from the surface of the cell

(Garrus et al. 2001; Demirov et al. 2002; von Schwedler et al. 2003; Morita et al. 2011), a process shown to be similar to the release of membrane microvesicles (Gan & Gould 2011). The importance of the ESCRT complexes has been shown in membrane scission in cytokinesis (Morita et al. 2007; Dukes et al. 2008) which also involve the same proteins as viral budding (Carlton & Martin-Serrano 2007). ESCRT III, the complex responsible for membrane scission, is capable of mediating the formation of intraluminal vesicles in an isolated system (Wollert et al. 2009). The proposed mechanism behind this relies on the ability of the ESCRT III components, CHMP proteins, to self assemble into a helical structure *in vitro* through the formation of a spiral oligomer (Lata et al. 2008). Interactions between these spiral oligomers and the membrane to which they bind proposes a mechanism by which the membrane could buckle, resulting in a vesicular "bud" (Lenz et al. 2009; Henne et al. 2011). This mechanism provides an ideal candidate pathway for the biogenesis and release of microvesicles from the surface of a plasma membrane and has been significantly better characterised than proposed sphingomyelinase pathways, for which mechanistic details are less clear.

1.7 IL-1β receptors and signal modulation

1.7.1 IL-1RI

Evolution has adapted further regulation onto IL-1β signalling with the strict regulation of IL-1 signals received by IL-1β sensitive cells. IL-1β has two distinct types of receptors, IL-1R1 and IL-1R2, both with differing functions in IL-1β sensitive cells. The IL-1R1 receptor is a member of the TIR domain receptor superfamily (Mitcham et al. 1996; Y. Xu et al. 2000), linked to TLR proteins and other Toll based receptors (Medzhitov et al. 1997). Control over the efficiency of signal transduction by these receptors is provided through the existence of receptor subtypes that transduce signals less efficiently or not at all, acting as sinks for the IL-1β present.

IL-1R1 is the signal transducing IL-1 receptor and is a complex of two proteins, the receptor unit (J. Sims et al. 1988; Vigers et al. 1997) and the IL-1 receptor accessory protein (RAcP), which is necessary for signal transduction (Greenfeder et al. 1995; Korherr et al. 1997; Cullinan et al. 1998), IL-1RAcP is

recruited to IL-1R to form a receptor complex but does not directly contact IL-1β (Casadio et al. 2001). The IL-1RI IL-1β complex is also internalised by the cell (Qwarnstrom et al. 1988) after ligand binding, reducing the capability of the cell to receive further signals (Figure 1.5).

1.7.2 IL-1RII

IL-1RI signalling is tempered by another controlling factor in the form of the IL-1RII receptor, which lacks the TIR domain present on IL-1RI (Mcmahan et al. 1991). IL-1RII can be cleaved from the cell surface and released into the bloodstream though the actions of an aminopeptidase (Cui et al. 2003). In both cases the functional role of this receptor is to act as an IL-1β sink, sequestering the cytokine and reducing the amount of free IL-1β that can reach and induce a response in IL-1RI (Colotta et al. 1993; Kollewe et al. 2000; Neumann et al. 2000). IL-1RII can also sequester the IL-1RAcP, necessary for IL-1β signal transduction, preventing it forming functional complexes with IL-1RI (Lang et al. 1998; Malinowsky & Lundkvist 1998). Soluble IL-1RAcP also binds to the soluble variant of IL-1RII, enhancing its binding properties and allowing it to sequester IL-1β more effectively (D. Smith et al. 2003).

1.7.3 IL-1Ra and Anakinra

IL-1 receptor antagonist (RA) was discovered in a sequence search for IL-1β matching genes (Eisenberg et al. 1990), as such IL-1RA is on the same genomic region as IL-1α and IL-1β, showing a common ancestry for this gene and indicating an evolution based on gene duplication (Nicklin & Weith 1994). IL-1RA is a natural competitive inhibitor (Schreuder et al. 1997) of IL-1β signalling as it binds to the same receptors but cannot initiate signalling due to its inhibition of IL-1RAcP binding and blockage of the IL-1RI complex formation during IL-1β signalling (Greenfeder et al. 1995). Recombinant IL-1RA has been marketed under the name Anakinra, which has been approved for the treatment of rheumatoid arthritis (Bresnihan et al. 1998; Jiang et al. 2000; S. Cohen et al. 2002; Mertens & Singh 2009) and is being investigated for the treatment of other inflammatory conditions (So & De Smedt 2007). Numerous studies have also been conducted on Anakinra

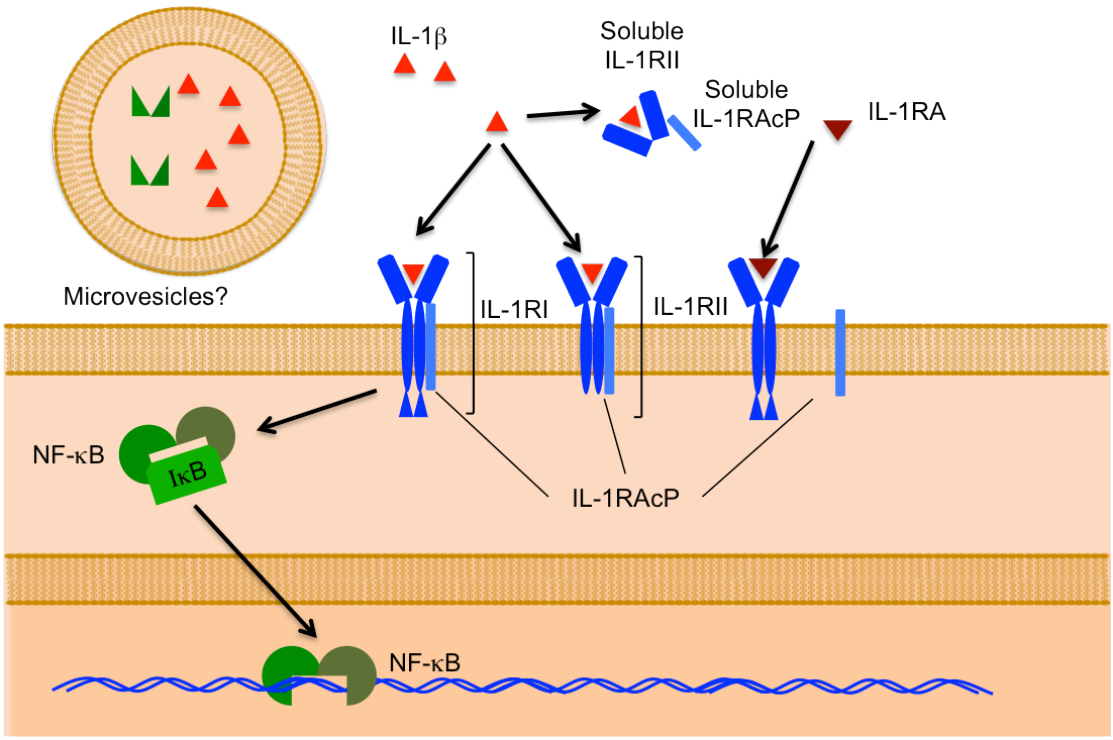

Figure 1.5. IL-1β signalling is subject to control at the signalling level. The receptor for IL-1β, IL-1RI requires an accessory protein, IL-1RAcP, to transduce a signal. Downstream genes are activated via NF-κB signalling, which is both upstream and downstream of the IL-1β pathway. Receptor signalling is regulated by decoy receptor IL-1RII, in both membrane bound and soluble forms, incapable of transducing a signal and acting as sinks for both IL-1β and IL-1RAcP, IL-1RAcP is also present on soluble receptors, enhancing IL-1β binding. IL-1β is further regulated by endogenous ligand IL-1Ra, capable of binding IL-1RI, but preventing binding of IL-1RAcP.

safety (Nuki et al. 2002; Fleischmann et al. 2006), with possible side effects arising from the immunosuppressive effect of inhibiting inflammatory initiation. Anakinra has also been investigated in the treatment of heart disease, where inflammation plays an important role in the development of atherosclerotic plaques (Abbate et al. 2008; Salloum et al. 2009). However, its expense, short lifetime and intravenous delivery method leave a niche for alternative therapies.

1.8 Investigating IL-1β signalling and regulation.

The evolutionary history and conservation of immune regulation, as well as the strict control of the IL-1β pathway confirm its importance in inflammation. IL-1β is under strict regulation at all pathway steps. IL-1β is induced in response to a variety of stimuli, as a function of the modular TLR receptors ensuring its sensitivity to multiple types of inflammatory insult. In IL-1β producing cells, the IL-1β promoter is poised for transcription, allowing a quick response, but the IL-1β message is subject to further controls based on its stability, and the resulting pro-protein subject to similar controls and premature degradation. IL-1β processing and secretion are linked, responsive to yet further stimuli and regulation in the form of the varied inflammasome complexes responsible for caspase-1 activation, and a concurrent spectrum of release. Control at the IL-1 receptor level has evolved an additional layer to modulate the IL-1β signal through decoy receptors sequestering the IL-1β signal (Figure 1.6).

The complexity of IL-1β signalling demonstrates the importance of control of IL-1β, itself described as a master switch of inflammation. Yet for its importance, key components of the pathway are not yet understood. The mechanisms behind inflammasome activation, its link to release, the release mechanisms themselves and the relation this release has to downstream reception of the IL-1β signal has yet to be elucidated.

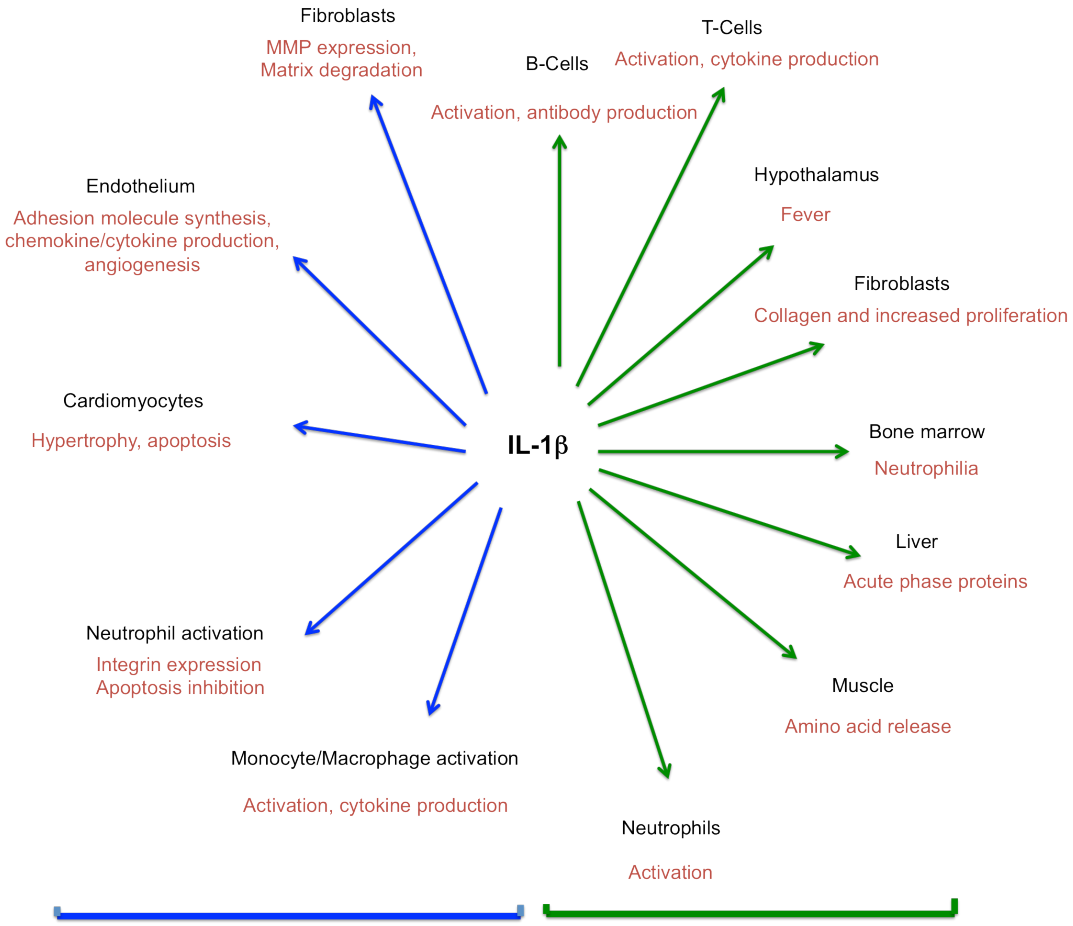

Figure 1.6. Downstream effects of IL-1β signalling. IL-1β has a pleiotropic spectrum of activity and is a key cytokine in the initiation of inflammation. Alongside its autoinflammatory role in the pathogenesis of atherosclerosis, a major contributor to mortality in the developed world (blue, adapted from Bujak & Frangogiannis (2009), it has a wide range of downstream effects in multiple other tissues (green, adapted from C Dinarello (2011)

1.9 Investigating the consequences of unregulated IL-1β release

1.9.1 Clinical relevance of IL-1β

IL-1β has been linked to the development of a number of diseases such as the development of plaques and cholesterol metabolism in atherosclerotic disease (Elhage et al. 1998; Isoda et al. 2004; Isoda et al. 2005), as well as significantly contributing to the development of autoinflammatory and autoimmune diseases (Dinarello 1996; Dinarello 2009b) and neuronal injury (Relton & Rothwell 1992; Boutin et al. 2001; Allan et al. 2005) (Figure 1.6). IL-1β signalling initiates a cascade response in target cells at the site of inflammation, multiplying the initial signal received by these first cells by orders of magnitude. This is a very powerful response to the initial infection as it quickly mobilises innate immunity in a large region of the surrounding tissue; naturally such a strong response must also be strictly controlled (Dinarello 2009b). The prognosis of autoinflammatory conditions such as rheumatoid arthritis, cryopyrinopathy-associated periodic syndrome and Adult onset stills disease have been improved by treatment with Anakinra, which has also shown promising results in the treatment of diabetes and ST elevated myocardial infarction (reviewed in Dinarello, 2011).

Although therapeutically it may be beneficial to inhibit IL-1β signalling in its entirety, it may also be pragmatic to consider specifically targeting the IL-1β release mechanism as a way to avoid systemic immunosuppression. One could hypothesise that allowing low level and terminal release events to proceed uninhibited could prove protective against infection and local inflammatory insult, however better control of the protected release pathway could result in the reduction of systemic inflammatory conditions, such as cardiovascular diseases, where microvesicles have been demonstrated as an important factor (Nomura et al. 1995; Huber et al. 2002).

Nevertheless, the mechanisms involved in the release events described here are poorly characterised, and small molecule modulators of the microvesicle release pathway could prove an invaluable tool for therapeutic intervention in both inflammatory diseases and atherosclerosis.

1.9.2 IL-1β pathway models.

The current paradigm of IL-1β function and release has largely been developed using *in vitro* tissue culture methods in cell lines or macrophage type cells in isolation. The use of cell monoculture techniques, *in vitro* study and lack of cellular microenvironment presents an artificial system for studying the release of IL-1β from cells, hence examining the situation *in vivo* could provide very valuable insight into these pathways. It is difficult to determine how IL-1β release operates in a living organism and how IL-1β containing vesicles are trafficked to sites of inflammation based on cell culture methods and it is likely that significantly more detail about the nature of microvesicle signalling could be discovered in a live organism unconstrained by the limitations of cell culture, and that greater insight could be gained from the ability to track both the release and targeting of microvesicles with greater fidelity than possible *in vitro*. Currently there are no *in vivo* models of IL-1β release and signalling that would allow real-time visualisation of the IL-1β release process.

1.9.3 Zebrafish as a model system.

Current studies of IL-1β in mouse and human macrophages are limited by their lack of interaction with the cellular milieu, and if we want to examine these interactions an *in vivo* model is the ideal tool. To visualise the secretion of a molecule in response to inflammatory insult would require and model amenable to genetic manipulation and to high power microscopy, requirements that are met by the zebrafish (*Danio rerio*). Zebrafish are transparent as larva (Kimmel 1989), and their genetic tractability make them ideal for the expression of reporters based on the IL-1β pathway.

1.9.3.1 Zebrafish transgenesis tools

The main tool in the arsenal of zebrafish transgenesis is the tol2 transposon system, derived from the *Medaka* and allowing the efficient generation of transgenic lines (K. Kawakami et al. 2004; Urasaki & Asakawa 2008). Alongside this, the Gal4/UAS tools used in genetic studies of drosophila (Scheer 1999; E. Scott et al. 2007) have also been adapted to zebrafish to allow the tissue specific promotion of reporter lines (Asakawa & K. Kawakami 2008) adding to the genetic

amenability of zebrafish. Furthermore, zebrafish genes can be specifically knocked down using antisense technology such as morpholinos (Ekker 2000; Nasevicius & Ekker 2000; Draper et al. 2001).

1.9.3.2 Imaging in the zebrafish

Zebrafish are amenable to genetic modification, which combined with their larval transparency make them ideal as an *in vivo* model. These advantages are perhaps best exemplified by the recent development of fluorescent calcium sensors, which have enabled the real time imaging of neuronal activation and brain activity on a single cell basis (Ahrens et al. 2013; Muto et al. 2013). Such breakthroughs are possible in this model specifically due to its amenability to live imaging and genetic manipulation and demonstrate the utility of the zebrafish as a platform for in vivo study. Furthermore, the small size and short generation time of zebrafish has also enabled the use of microCT for phenome screening of the whole organism to catalogue the characteristics of specific mutations (Cheng et al. 2011).

1.9.3.3 Zebrafish as disease models

More relevant to the study of IL-1β biology is the study of innate immunity in zebrafish (Meeker & Trede 2008; Renshaw & Trede 2012; Henry et al. 2013) enabled by the characterisation of the various immune cell lineages during development and their behaviour. Zebrafish macrophages were initially characterised by their morphology and expression of early myeloid and leukocyte markers (Herbomel et al. 1999; Herbomel et al. 2001) and more recently, zebrafish macrophages have been fluorescently labelled using the *mpeg1* (Ellett et al. 2010) and *fms* (Gray et al. 2011) promoters. However even before these lines were developed it was possible to visualise microglia, a specialised macrophage subtype, using the *APO-E* and *pu.1* transgenic markers (Peri & Nüsslein-Volhard 2008) enabling the characterisation of the highly dynamic microglial response to calcium signalling using the aforementioned GCaMP calcium sensor(Sieger et al. 2012).

Other innate immune cell types have also been characterised in the zebrafish. By using the zebrafish orthologue of Myeloid specific peroxidase (mpx), Lieschke et al. (2001) characterised embryonic neutrophils. The promoter involved was later used to generate the *mpx:gfp* neutrophil marker line (Renshaw

et al. 2006) later complemented by lines bearing the *lyz* promoter (CJ Hall et al. 2007).

Combined, these technologies have enabled the characterisation of the varying roles of neutrophils and macrophages in the innate immune response; such as their movement dynamics (Ellett et al. 2010; Gray et al. 2011); susceptibility to pharmacological manipulation (Loynes et al. 2010) and induction of hypoxic signalling (Elks et al. 2011); differing roles in phagocytosis (Colucci-Guyon et al. 2011); and their roles in wound healing (L. Li et al. 2012); as well as the ability of these systems to be subverted into a trophic phenotype by the signalling molecules released during tumour initiation (Feng et al. 2012).

It has also been possible to characterise other immune components in the zebrafish; such as the definition of mast cells, a neutrophil subtype expressing the cpa5 marker; and the identification of dendritic cells (Lugo-Villarino et al. 2010), eosinophils (Balla et al. 2010)and T-cells (Langenau et al. 2004) from adult zebrafish. The pathways involved in the immune response, MyD88 expression (CJ Hall et al. 2009) chemokine signalling (Oehlers et al. 2010), and PI3K activity have also been studied in the zebrafish. Novel imaging tools useful in the study of innate immunity include hydrogen peroxide sensors; which reveal the role of H_20_2 in the initiation of inflammation in response to injury (Niethammer et al. 2009) and the role of H_20_2 signalling in tumour initiation (Feng et al. 2010); and dynamic apoptosis sensors (Van Ham et al. 2010) which could reveal the pathways involved in inflammation resolution and in the processes involved in membrane asymmetry.

In trying to combat the growing threat of antibiotic resistance, and to further elucidate the pathways involved, a number of zebrafish models of infection have been established (C. Sullivan & C. Kim 2008; A. Meijer & Spaink 2011). Problematic, drug resistant bacteria such as *S. aureus* and *M. turberculosis* have been modelled in zebrafish using various strains of *S. aureus* (Prajsnar et al. 2008; Prajsnar et al. 2012) and the marine pathogen *M. marinum* (Tobin et al. 2010; C. Yang et al. 2012). E. coli (Colucci-Guyon et al. 2011) and S. enterica (Van der Sar et al. 2006) have been used to study more general phagocytic and signal transduction pathway dynamics. Finally, zebrafish have also been used to study aquaculture

pathogens, such as *V. anguilarum* (Z. Xu et al. 2011). These models provide an insight into the mechanisms involved in the host response to infection and allow these processes to be visualised *in vivo.*

Alongside their role in in infection models, zebrafish have also been used in the study of a number of other diseases (Lieschke & Currie 2007), ranging from ototoxicity (Buck et al. 2012) and epilepsy (Baxendale et al. 2012) to muscular disease (Ingham 2009) and atherosclerosis (Stoletov et al. 2009).

The zebrafish has been key to a number of advances that are in part impractical or uneconomical in other models, but a number of these advances, such as the aforementioned neuronal imaging (Ahrens et al. 2013), are almost impossible in a model without the attributes of the zebrafish. The combination of genetic amenability and transparency during larval development enable the zebrafish to be used as a powerful tool for *in vivo* imaging, which is perhaps the greatest advantage of the zebrafish over mammalian models, and make it key in studying complex pathways for which *in vivo* imaging is necessary.

1.9.3.4 Innate immune pathway conservation in the zebrafish

The use of zebrafish as a tool to study IL-1β biology is possible because of the high degree of homology between zebrafish and mammals. As discussed earlier, the evolution of the innate immune system predates vertebrate development and zebrafish have an extensive complement of innate immune genes. Zebrafish macrophages develop shortly after fertilisation and perform a phagocytosing role in zebrafish larva (Herbomel et al. 1999; Herbomel et al. 2001). Signalling and induction in the innate immune pathway are mediated by zebrafish homologues of TLR pattern recognition receptors (Jault et al. 2004; A. Meijer et al. 2004) through a conserved NF-κB pathway including MyD88 (Van der Sar et al. 2006), NF-κB (Correa et al. 2004), and its activation pathway (reviewed by Stein *et al.,* 2007). Zebrafish inflammatory caspases have been described (Masumoto et al. 2003; Eimon et al. 2006), as well as ASC (Masumoto et al. 2003; Y. Sun et al. 2008) and inflammasome like proteins (Laing et al. 2008). Zebrafish also show conservation of P2X7 receptors in both structure and function (López-Castejón, M. Young, et al. 2007) and pannexin-1 (Prochnow et al. 2009). IL-1 protein family and

receptor family conservation has also been extensively described (Huising et al. 2004), however, the present state of these receptors is complicated by errors in sequencing and genome assembly (see Chapter 3).

1.20 Project aims

The zebrafish innate immune system shows a high degree of conservation with human immunity and should provide the ideal subject for the development of an *in vivo* model of IL-1β biology.

In IL-1β research, there are a number of key questions relating to the IL-1β pathway that remain unanswered. How is the processing of IL-1β activated and how can this be modulated? What is the mechanism by which IL-1β is packaged into vesicles, how is this linked to processing, how are these vesicles release and what regulatory steps are necessary? In addition how are IL-1β containing vesicles transported to their site of action, which downstream signalling pathways are responsible for targeting them to IL-1β sensitive cells and what triggers the release of their contents? And what are the key control points that may serve as therapeutic targets?

The biogenesis and release of microvesicles is difficult to observe in cell culture, and the mechanisms behind these processes have not yet been described. The involvement of microvesicles has been described for a number of proteins as a non-conventional mechanism of cellular release, implying the evolutionary conservation of the pathway machinery, and its significance as a biological process. Studying this pathway *in vivo* is the logical extension for its characterization, and would yield valuable insight into not only the mechanism as a whole, but how it pertains to IL-1β. Inhibiting release could therefore become a valuable therapeutic tool in conditions where this pathway is responsible for the release of bioactive signals.

My hypothesis is that microvesicular IL-1β release and microvesicular biogenesis is dependent on the ESCRT pathway and that mechanisms linking this pathway to secretion rely on Rab adaptor proteins to link caspase-1 mediated processing to secretion. Furthermore I hypothesise that the release of IL-1β from microvesicles is dependent on receptors on the surface of sensitive cells, and that this signalling is highly context dependent. Unfortunately the tools to test these hypotheses *in vivo* are currently unavailable.

Thus, the aims of this thesis are primarily to develop a zebrafish *in vivo* model of IL-1β biology. Specifically I aim to

1. Validate the zebrafish as a viable model of the IL-1β pathway through both bioinformatics analysis and through inhibition of components of the IL-1β pathway.
2. Develop a FRET based reporter of IL-1β processing by measuring caspase-1 activation to enable spatial and temporal localisation of IL-1β processing and its link to release
3. Develop an in vivo reporter of IL-1β secretion to allow visualisation of the release event and downstream signalling to sensitive cells.

Chapter 2: Materials and Methods

Unless otherwise stated, all reagents were purchased from Sigma-Aldrich

2.1 Buffers

20x saline sodium citrate buffer (SSC)

3M sodium chloride

300 mM sodium citrate

Adjusted to pH 7 with citric acid.

Hybridisation Buffers

Wash hybridisation buffer:

50% formamide

5 × SSC

0.1% Tween 20

adjusted to pH 6 with Citric acid.

Pre-hybridisation buffer:

As wash-hybridisation buffer, with the addition of

50 μg/ml heparin (Scientific Laboratory Supplies (SLS))

500 μg/ml tRNA

Probe-hybridisation buffer:

Pre-hybridisation buffer with the addition of

1:200 dilution of AP-labelled probe in 80% formamide

E3 medium

5 mM sodium chloride

170 μM potassium chloride

330 μM calcium chloride

330 μM $MgSO_4$

0.00005% methylene blue

2.2 Bioinformatic study

2.2.1 Sequence Searching and Gene alignments

BLAST searching was performed using the National Center for Biotechnology Information (NCBI) Basic Local Alignment Search Tool (BLAST) tool (http://blast.ncbi.nlm.nih.gov/) domains were delimited by the BLAST location of domains on query sequences. Protein alignments were performed using clustalW. Gene searching was performed using the Ensembl genome browser (http://www.ensembl.org/index.html) against Human or zebrafish genomes. Data were updated during the study to use the latest zebrafish genome assembly (Zv9).

2.2.2 Zebrafish IL-1β structure prediction

The Zebrafish IL-1β protein sequence (accession: NP_998009.1) was submitted to the Phyre (Kelley & Sternberg 2009) (http://www.sbg.bio.ic.ac.uk/~phyre/), RaptorX (Peng & J. Xu 2011; Källberg et al. 2012) (http://raptorx.uchicago.edu/), I-TASSER (Y. Zhang 2008; A. Roy et al. 2010) (http://zhanglab.ccmb.med.umich.edu/I-TASSER/) and the UCL PsiPred Server (Buchan et al. 2010) (http://bioinf.cs.ucl.ac.uk/). The resulting models were analysed by comparison with the human IL-1β protein structure (accession AAA59135.1) and the nearest protein orthologues provided by each server.

2.3 Functional study

2.3.1 Whole mount *in situ* Hybridisation (WISH) probe synthesis

An IL-1β coding sequence containing vector (A kind gift of Sara Kohal, University of Sheffield) was linearised with a HindIII restriction digest. 20μg of vector was mixed with 20μl of New England Biolabs (NEB) restriction Buffer 2, 0.5μl HindIII (NEB) in a total volume of 200μl of distilled water and incubated at 37 °C for 3 hours. The linearised DNA was phenol:chloroform precipitated: 200μl of Phenol:Chloroform:Isoamyl Alcohol 25:24:1 Saturated with 10 mM Tris, pH 8.0, 1 mM EDTA was added to the reaction mixture and vortexed thoroughly for 3 minutes. The mixture was centrifuged at 14000 rpm for 7 minutes and the top layer added to a new tube. An equal volume of chloroform was added to this layer which was then vortexed thoroughly. This was centrifuged at 14000 rpm for 5

minutes and the top layer again removed. This was mixed 10:1 with 3M sodium acetate then 1:1 with isopropanol. The mixture was kept at -20 °C for 1 hour then pelleted by centrifuging at 4 °C and 14000 rpm for 20 minutes. The supernatant was removed and the pellet was washed gently with 200 μl of 70% ethanol, which was then removed after a further 5 minute, 14000 rpm centrifugation at 4 °C. After removal of the ethanol, the pellet was air-dried for 10 minutes and resuspended in 20μl of sterile water. The DNA was quantified on a Nanodrop™ 1000 spectrophotometer (Thermo Scientific).

A DNA probe was transcribed using a T7 RNA digoxygenin (DIG) labelling kit (Roche). 2μg of linearised DNA was mixed with 4μl DIG labelling mix, 2μl RNAse inhibitor, 2μl T7 polymerase in a total volume of 40μl sterile water then incubated for 2 hours at 37 °C. The DNA template was removed with a 30 minute digestion with an additional 4μl of DNAse then precipitated with lithium chloride: the reaction was mixed with 1μl pH8 0.5M EDTA, 2.5μl 4M LiCl and 75μl ethanol and kept at -80°C for 1 hour, then pelleted by centrifugation at 4 °C, 14000rpm for 30 minutes. The supernatant was removed and the pellet was gently washed with 100μl ethanol, which was also removed following a 10 minute centrifugation at 4 °C, 14000 rpm. After removal of the supernatant, the pellet was air-dried for 5 minutes and resuspended in sterile water. Presence of RNA was confirmed by gel electrophoresis of 1μl of resuspension on a 1% agarose gel. 80μl of formamide was added to resuspension which was then stored at -80 °C.

An antisense probe was synthesised by linearising with an Apa1 digest, and Sp6 polymerase.

2.3.2 WISH protocol

Embryos were fixed overnight in phosphate buffered saline (PBS) (Fisher Scientific) with 4% paraformaldehyde (PFA) at 4°C, then transferred into 100% methanol and stored at -20 °C at no more than 20 embryos per eppendorf.

The embryos were rehydrated by washing in 500ml of a methanol series of 3:1, 1:1, and 1:3 methanol:PBS for 5 minutes in each wash. The embryos were washed 4 times with PBT (0.1% tween 20 in PBS) for 5 minutes each. This was followed by a treatment in 10mg/ml of proteinase K for 15 minutes for 24hpf

embryos, 30 minutes for 48 hpf embryos and 60 minutes for 72 hpf embryos, followed by fixing for a second time in 4%PFA-PBS for 20 minutes.

The embryos were incubated in a pre-hybridisation buffer for 5 hours at 70 °C then incubated with probe-hybidisation buffer for 18 hours at 70 °C. the probe was removed by successively washing with 3:1, 1:1 and 1:3 washes of the hybridisation buffer and 2x SSC for 15 minutes each wash. A final wash 2x SSC was then followed by 2 30 minute washes with 0.2x SSC at 70 °C, which was then diluted with 3:1, 1:1 and 1:3 washes of 0.2x SSC and PBT buffer at 20 °C for 10 minutes each with a final wash of PBT for 10 minutes.

The embryos were incubated in blocking buffer (PBT, 2% sheep serum (Stratech) and 2mg/ml BSA) for 3 hours on a rocking platform. The embryos were then incubated with an anti-DIG-AP (Roche) antibody in blocking buffer at a 1:5000 dilution for 18 hours at 4 °C with gentle rocking. This was washed off with 6 × 15 minute washes in PBT. The embryos were washed 3 times in staining wash (100mM pH 9.5 tris HCL, 50mM magnesium chloride, 100 mM sodium chloride and 0.1% tween 20). Embryos were then stained with staining solution (staining wash with 100mg/ml NBT (Roche) and 50 mg/ml BCPIP (Roche)) until staining developed. The reaction was stopped by replacing this wash with 1mM EDTA in PBS with pH adjusted to 5.5. The embryos were refixed in PBS with 4% PFA, then stored at -20 °C in methanol.

2.4 Tol2 mRNA synthesis

Tol2 mRNA was generated using the pCS2FA-transposase construct from the Tol2Kit (plasmid 396). The pCS2FA-transposase plasmid was linearised with a Not1 digestion (NEB) as described previously and transcribed using an Sp6 mMESSAGE mMACHINE® kit (Ambion). 1 μg of template DNA was mixed with 2 μl enzyme mix, 2 μl reaction buffer, 10 μl NTP/CAP mixture in a total volume of 10 μl nuclease-free water. The reaction was mixed gently then briefly centrifuged then incubated for 2 hours at 37 °C. the template DNA was degraded with a 15 minute digestion at 37 °C with Turbo DNAse. The RNA was recovered using phenol: chloroform extraction as described previously and resuspended in 20 μl nuclease free water. The yield of mRNA was estimated on an agarose gel.

2.5 PCR amplification

PCR reactions were set up with 1μl of 10μM dNTPs (a mix of dATP, dTTP, dCTP, dGTP at 2.5μM each) (Promega) with 0.25 μl Phusion polymerase (NEB), 1.25 μl each of 10 μM forward and reverse primers, 100 ng of template DNA and 4 μl of Phusion GC buffer (NEB) in total volume of 20 μl nuclease free water. The basic PCR conditions were:

98 °C for 30 seconds

then 30 cycles of
98 °C for 30 seconds for denaturation,
60°C 50 seconds for annealing,
72°C 30 seconds for extension,

with a final extension of
72 °C for 10 minutes

The annealing temperature was optimised for each primer pair by performing a gradient PCR between 55 and 65 °C and extension time was increased to 3 minutes for the FRET mutagenesis.

PCR primers are described in Table 1.

2.6 Embryo Treatment

All zebrafish experiments and transgenic line maintenance were performed under a Home Office animal-handling license to conform to Animals (Scientific Procedures) Act 1986.

2.6.1 Tail transection

2.6.1.1 Tail transection of pigmented WT embryos post 72 hpf

Pigmented day 72 hpf embyos were anaesthetised in MS-222 and placed onto reversed scotch tape to help remove excess liquid. The tail was amputated at the most distal point of the pigment gap perpendicular to the circulation of the

aorta using a microscalpel (World precision instruments) under a dissecting microscope. Embryos were placed into fresh E3 immediately post injury and allowed to recover at 28.5 °C

2.6.1.2 tail transection of non-pigmented (nacre) and less than 72hpf embryos

Embryos were transferred to fresh E3 at a density of 20-25 per plate and anaesthetised with MS-222. Tail transection was performed midway between the terminal point of the aortic venous loop and the distal most part of the tail using a number 15 scalpel blade under a dissecting scope. Embryos were placed in E3 to allow recovery as above.

2.6.2 Zebrafish egg microinjection

Tanks of paired fish, 10 of each sex, were marbled overnight. Embryos were collected and injected no more than 20 minutes post fertilization during the one cell stage. Embryos were collected and ~50 were aligned onto a microinjection plate. Injections were performed using a palled Kwik-Fil™ borosilicate glass capillary (World Precision Instruments) loaded with the DNA sample using a gel loading pipette tip, the end of the needle was then broken off using fine forceps to create the injection aperture (~50 μm -150μm in diameter). DNA injection concentration was optimized to 50ng/μl at~1nl DNA solution per embryo, Tol2 RNA was optimized to 30ng/μl. *V anguillarum* DNA was injected at one tenth the stock concentration of 65ng/μl (a kind gift of Victor Mulero, Murcia). Phenol red was added as at a concentration of 1μl in 10μl to enable clearer visualisation of the injection. Consistency of injection volume was ensured using a pneumatic picopump (PV830, World Precision Instruments) and air compressor, using a micromanipulator to manoeuvre the needle into place and a microscope to visualize the injections. Post injection, the fish were placed in E3 medium at 50 embryos per plate and incubated at 28.5 ^{o}C for 6 hours, after which dead and unviable embryos were removed from the medium. The fish were kept at 28.5 ^{o}C. Transgenic embryos were selected using relevant markers/reporters by fluorescence microscopy and maintained at no more than 80 embryos per plate. These embryos were then manually dechorionated 48-72 hpf.

2.6.3 Chemical treatment

For chemical treatment, embryos were split into a 24 well plate at a density of 5 per well, in 0.5ml of fresh E3. Compounds were made up to double strength concentration at 0.5ml per each well being treated and mixed thoroughly before experimental blinding and addition to each well. The plates were swirled gently to evenly mix each compound. Final treatment concentrations were 50μm for AC-YVAD-CMK (Calbiochem) and Q-VD.Oph (R&D systems), 1μM for Brilliant Blue G, 10 μM for KN62 (Calbiochem) and 1μg/ml LPS (E. coli serotype R515, Alexis Biochemicals). Embryos were kept at 28^{o}C for the course of the treatment.

Tg(BACmpo:FRET DEVD)sh237 embryos were subjected to isopimpinellin treatment by addition of 25μM isopimpinellin (R&D systems) to the low melting point agar used for mounting and the maintenance of an E3 layer over the agar with a concentration of 25 μM isopimpinellin.

For treatment of *Tg(lyz:nsfB.mCherry)sh260* embryos, metronidazole was added at a concentration of 5 μM to a 30 ml plate of embryos for 4 hours before imaging.

2.7 Construct generation

2.7.1 Transformation

25μl of competent Top10 cells (Invitrogen) were thawed on ice. 1μl of prepped plasmid or 2.5μl of reaction were added to the cells, which were then gently mixed. The cells were incubated on ice for 30 minutes then heat shocked for 45 seconds at 42^{o}C. The cells were left on ice for a further 10 minutes then 150μl of room temperature SOC medium (Invitrogen) was added and the cells were mixed vigorously for 1 hour at 37 ^{o}C on a shaker at 200rpm. The cells were then plated out onto warmed selection plates with the relevant antibiotic and left to grow overnight at 37^{o}C. Selection plates were made with autoclaved LB agar and either kanamycin or carbenicillin antibiotic at 50μg/ml

2.7.2 DNA purification

Post transformation, bacterial colonies were selected and inoculated into either 3ml or 50ml of autoclaved LB broth with added kanamycin or carbenicillin (as

above) and shaken vigorously at 200rpm overnight at 37°C. Plasmid cultures were purified using the alkaline lysis method and a commercial kit (QIAgen). For sequencing, diagnostic digests and subcloning applications, the miniprep protocol and a 3ml culture volume was used; for larger volumes of DNA necessary for vector construction, transfection and microinjection, the high speed midiprep protocol and a 50ml culture volume was used. Column purification was also used in gel extraction following restriction digests (QIAgen). DNA concentration was measured using a Nanodrop™ 1000 spectrophotometer (Thermo Scientific).

2.7.3 Vector construction

The Gateway recombination reaction is described in detail in Chapter 6. (Figure 6.2)

2.7.3.1 Conversion of DNA concentration

DNA concentration as ng/µl was converted to femtomoles using the following equation:

$$ng\ of\ DNA\ required = (femtomoles\ required \times size(bp)) \times \frac{660}{10^6}$$

2.7.3.2 Vector maps and sequence construction.

Vector maps and sequences were assembled using ApE software (http://biologylabs.utah.edu/jorgensen/wayned/ape/). ApE was used to generate restriction maps for diagnostic digests and the recombination tool was used to generate entry clone and expression vector sequences for BP and LR recombination.

2.7.3.3 BP cloning

The gene of interest was amplified using attB site containing primers (Table 1) and gel purified as described. 15 femtomoles of the PCR product was combined with 100ng of donor plasmid in TE buffer in a total volume of 4µl. 1µl of BP clonase II enzyme mix (Invitrogen) and vortexed briefly. The resulting reaction was left at 18 °C for 20 hours then transformed into Top10 cells and plated onto kanamycin selection medium. Entry clone recombination was confirmed by sequencing with M13 forward and reverse primers.

2.7.3.4 LR cloning

5 femtomoles of each entry clone were combined with 10 femtomoles of destination vector in a final volume of 4μl. 1μl of LR clonase II plus (Invitrogen) was added to the mixture and vortexed briefly. The reaction mix was kept at 18 °C for 20 hours then transformed into Top10 cells and plated onto carbenicillin selection medium. Correct integration was performed using a diagnostic digest: 3-6 colonies were miniprepped and subjected to restriction digest at 37 °C for 3 hours, the resulting products were resolved using gel electrophoresis. Restriction enzymes were selected to yield 4-5 restriction fragments of differing sizes, preferably with restriction sites present in each entry clone.

2.7.3.5 pDEST(MPEG1:Gal4.VP16:polyA)

The MPEG1 5' entry clone (Ellett et al. 2010) was eluted from the delivered filter with 5μl of TE buffer and retransformed into Top10 cells then midiprepped. The entry clone was recombined using LR cloning with the pME-Gal4.VP16 and p3E-PolyA (387 and 302 from the Tol2kit respectively) in the pDESTTol2pA2 (394) backbone. pDEST(MPEG1:Gal4.VP16:polyA) diagnostic digest was performed with Kpn1 (NEB), and a correct plasmid was selected and midiprepped.

2.7.3.6 pDEST(lyz:nsfB.mCherry)

The p5E-*lyz* entry clone (a kind gift of Xingang Wang, Institute of Molecular and Cell Biology, Singapore) and pME-*nsfB* (a kind gift of Mike Parsons, Johns Hopkins) were eluted and retransformed as described above. These clones were combined with p3E-mCherrypA (388) and pDESTTol2pA2 in an LR recombination reaction. Correct recombination was confirmed using an AlwN1 (NEB) restriction digest.

2.7.3.7 pME-MCS-zfIL-1β

The IL-1β middle entry vector was constructed using the middle entry multiple cloning site entry vector pME-MCS. Primers designed from the deposited zebrafish IL-1β sequence (accession: AAQ16563.1) including a 5' HindIII restriction site and a 3' BamHI site were used to amplify the IL-1β coding sequence from 48hpf zebrafish DNA. The purified PCR product was ligated into an Invitrogen TOPO blunt vector (Invitrogen). The ligated vector was transformed into Top10 cells and grown up on kanamycin selection medium. Colonies were analysed for

correct ligation using an EcoRI restriction digest. The purified plasmid and the pME-MCS entry vector were subjected to a HindIII and BamHI restriction digest and resolved using gel electrophoresis. The bands representing the empty pME-MCS vector and the IL-1β insert were gel extracted into a final volume of 10μl elution buffer each. The IL-1β fragment was ligated into the linearised pME-MCS entry clone vector in a ratio of 3ml IL-1β fragment to 1ml entry clone in a final volume of 10ml using T4 ligase (NEB). The ligation mix was kept overnight at 18 °C and transformed into Top10 cells, which were grown on kanamycin selection plates, selected and miniprepped. The purified plasmids were subjected to a HindIII, BamHI restriction digest to check for correct insertion of the IL-1β sequence.

2.7.3.8 pDEST(UAS:MCS-zfIL-1β.EGFP), pDEST(UAS:MCS-zfIL-1β.mCherry)

pME MCS IL-1β was combined with p5E UAS, pDESTTol2pCG2 (395) and either p3E-EGFPpA (366) or p3E-mCherrypA in an LR recombination reaction to generate an EGFP or mCherry fusion protein respectively. Correct recombination was confirmed using a Kpn1 restriction digest.

2.7.3.9 pDEST(4xUAS:zfIL-1β.EGFP), pDEST(4x UAS:zfIL-1β. mCherry)

pME-zfIL-1β was generated using BP cloning as described previously using accession sequence AAQ16563.1 for primer design. p5E 4xUAS was amplified from a 4xUAS:nsfB.mCherry expression plasmid (a kind gift from Mike Parsons, Johns Hopkins) using the provided sequence data and as described previously for BP cloning.

pME-zfIL-1β and p5E 4xUAS were combined with pDESTTol2pCG2 (395) and either p3E-EGFPpA or p3E-mCherrypA in an LR recombination reaction to generate an EGFP or mCherry fusion protein respectively. Correct recombination was confirmed using an Xba1 (NEB) restriction digest.

2.7.3.10 pDEST(MPEG1:IL-1β.EGFP), pDEST(MPEG1:IL-1β. mCherry)

pME-zfIL-1β was combined with the Mpeg1 5' entry clone, pDESTTol2pCG2 (395) and either p3E-EGFPpA or p3E-mCherrypA in an LR recombination reaction to generate an EGFP or mCherry fusion protein respectively. Correct recombination was confirmed using an AlwN1 restriction digest.

2.7.4 FRET YVHD mutagenesis

The FRET DEVD plasmid (Rehm et al. 2002) consisting of a FRET construct of CFP and YFP separated by nucleotides encoding the optimal Caspase 3 cleavage site, DEVD, on a PcDNA3 vector was mutagenized to the Caspase 1 cleavage site present on IL-1β, YVHD (Rano et al. 1997; Thornberry et al. 1997). The primers were designed according to the parameters provided in the Stratagene Quikchange mutagenesis protocol; as the primers were intended to replace 5 nucleotides the primer length was kept at the maximum recommended 45 base pairs and the highest possible GC content to ensure robust binding of the elongated primer arms. The Primers were extended by PCR to create a new plasmid followed by the degradation of the existing plasmid with a 1 hour digestion with Dpn1 (NEB) at 37 ^{o}C. The plasmids were transformed into Top10 cells and grown up overnight at 37 ^{o}C on ampicillin selection plates. Colonies were miniprepped and confirmed by sequencing.

2.8 Zebrafish Line generation

2.8.1 Zebrafish embryo generation

For injection, and single transgenic line experiments, embryos were generated by marbling. Wire mesh tanks suspended over a solid container were covered with a layer of marbles and gently placed into the bottom of the aquarium tank at 4-8 pm the day before embryos were needed. For injection, embryos were collected every 15 minutes after aquarium lighting was turned on. Embryos were strained from the marble tans and placed into fresh E3 and marble tanks were placed back into the aquarium tanks. For non-injection uses, embryos were collected 4 hours after aquarium lights were turned on.

For line crosses, embryos were generated by pair mating. Single male or female fish from each line were placed into a single pair mating tank with a plastic divider which was removed an hour after aquarium lighting was activated. The adults were separated after 4 hours and embryos strained from these tanks. Embryos were selected as described.

2.8.2 Line generation and maintenance

For line generation, injected embryos were selected by transgenic markers were possible; *Tg(pNF-κB:EGFP)* positive embryos were selected by EGFP expression, *Tg(lyz:nsfB.mCherry)* embryos selected by mCherry expression in myeloid cells, *Tg(mpeg1:Gal4.VP16)* embryos were grown unselected. Injected embryos were grown at a density of 20 per tank (Techniplast) and screened after 2 months. *Tg(pNF-κB:EGFP)* and *Tg(lyz:nsfB.mCherry)* embryos were screened by crossing to Nacre wild types. The offspring were screened for transgene expression. Multiple founders were identified for the *Tg(pNF-κB:EGFP)* line, and one was selected as a line founder and designated with the Allele number *sh235*. A single founder was identified for *Tg(lyz:nsfB.mCherry)* and the resulting progeny raised under the allele number *sh260*.

Tg(mpeg1:Gal4.VP16) adults were crossed to *Tg(UAS:Kaede)* and screened for GFP expression in myeloid cells. A number of founders were identified and the progeny from one of these was raised under the allele designation *sh256*.

The *Tg(BACmpo:FRET DEVD)* founder showed very low rates of allele transmission to its progeny. And only 3 of the embryos raised survived to adulthood. These were outcrossed to WIK wildtypes and the resulting progeny grown to generate the line, under the allele number *sh237.*

For routine line maintenance, embryos were grown at 30 per tank to encourage even sex ratios. A *Tg(BACmpo:FRET DEVD)sh237; Tg(lyz:nsfB.mCherry)260* compound transgenic line was made by pair mating these two lines into a compound transgenic.

2.9 Cell culture

2.9.1 HEK293T

2.9.1.1 Maintenance

HEK293T cells were maintained in Dulbecco Modified Eagle Medium (DMEM) (Invitrogen) supplemented with 10% heat inactivated low endotoxin FCS (SourceBioScience), 0.1 mg/ml penicillin (Invitrogen), 0.1 mg/ml streptomycin (Invitrogen) and 0.1 mg/ml L-glutamate in a water saturated incubator with 5% CO_2. Cells were passaged every 2-3 days when reaching 80% confluence with 2

quick washes with warmed PBS and 5 minute treatment with 1 ml 0.05 % Trypsin (Invitrogen). Cell density was determined using a haemocytometer and cells were split 1:10 into 10ml of warm media.

2.9.1.2 Transfection

A single 20mm circular coverslip was placed into each well of a 24 well plate and HEK293T cells were seeded into these wells at a density of 2.5×10^4 cells per well in a volume of 0.5ml of warm media. Cells were maintained in an incubator as described above. The following day, the cells were washed twice with PBS and provided with 0.5ml warm media. The cells were transfected by adding 1μg of DNA, 1μl of Turbofect (Fermentas) in a total volume of 100μl of serum free DMEM and swirled gently. 4 hours post transfection, caspase inhibitors were added for 20 hour overnight treatment.

Cells were fixed by first briefly washing twice with PBS, then 20 minute treatment with 4% PFA/PBS. This was followed by a further 3 washes in distilled water, after which the coverslips were removed and overturned onto microscope slides with a drop of VECTASHIELD® (Vector Labs) and sealed with nail varnish.

2.9.2 THP-1

2.9.2.1 Maintenance

THP-1 cells (ATCC) were maintained in RPMI-1640 (Invitrogen) supplemented with 10% heat inactivated low endotoxin FCS (SourceBioScience), 0.1 mg/ml penicillin (Invitrogen), 0.1 mg/ml streptomycin (Invitrogen) and 0.1 mg/ml L-glutamate with 50 μM 2-mercaptoethanol. In a water saturated incubator with 5% CO_2. Cells were passaged every 3 days by splitting 1:5 into a T75 flask.

2.9.2.2 Transfection

Cell density was measured using a haemocytometer allowing 10^6 THP-1 cells per transfection to be centrifuged and pelleted at 200g and 22 ^oC. Cells were resuspended in a mixture of 82 μl Nucleofection buffer and 18 μl buffer supplement (Nucleofector® Kit V) with 1μg of plasmid DNA per reaction. The cells were electroporated using a Nucelofector™ (Lonza) and the inbuilt THP-1 high viability protocol. Cells were quickly returned to 2ml of warmed RPMI media

containing 20nM PMA to differentiate them. Transfected THP-1 cells were washed daily with PBS and supplied with fresh media containing the inhibitor or PAMP treatment described.

2.10 Imaging

2.10.1 WISH mounting and imaging

WISH embryos in methanol were rehydrated with brief washes in 3:1, 1:1 and 1:3 methanol:PBS, which was then replaced with 80% glycerol. The embryos were rocked gently until they sank into the glycerol. They were stored at -20 °C until imaging. Whole fish were imaged on a Nikon SMZ1500 stereomicroscope with a DS-Fi1 camera using NIS elements software to generate focused images from multiple z plane acquisitions (Nikon). For higher resolution images, the embryo tails were removed and mounted in glycerol with no. 0 coverglass (SLS) and imaged on a Bx51 compound, with a Camedia C-3030ZOOM camera and a 40x NA 1.15 water immersion objective using Cell B software.

2.10.2 Mounting live embryos for imaging.

Embryos were anaesthetised by transferring them to clean E3 medium and adding MS-222 dropwise until cessation of movement. Embryos were mounted in a 40mm dish with a section of the base replaced by a No.0 microscopy glass coverslip (SLS). They were arranged and immobilised in molten 0.75 % low melting point (LMP) agarose at ~32 ^{o}C containing 0.017% MS-222. The embryos and agarose were prevented from drying out by the addition of a 2ml MS-222 containing layer of E3 placed on top of the agarose during imaging.

2.10.3 *Tg(pNF-κB:EGFP)sh235* mounting and imaging (long term and 8h).

Tg(pNF-κB:EGFP)sh235 embryos were injured 72 hpf and kept at 28 ^{o}C for 30 minutes. Embryos were then mounted in LMP agarose and imaging was initiated an hour after injury using a TE-2000U microscope (Nikon) with a Orca-AG Camera (Hamamatsu) running Volocity™ imaging software (Perkin Elmer). Images were acquired using a 10x NA 0.3 PlanFluor objective, at 2.5 minute intervals over a focal depth of 100μM with 10 z planes. Volocity™ was used to generate a calculated point spread function (PSF) based on the objective used and EGFP emission

frequency and the images were deconvolved using Volocity™ for 30 iterations to generate the final images.

For compound treatment, embryos were injured and treated as described. After an 8 hour incubation at 28 ^{o}C, the embryos were mounted in LMP agarose and imaged. A 100μM focal depth was used, divided into 10 focal planes centred on the circulation in the dorsal aorta-venous loop. The images were compressed into a single plane and a region of interest was drawn around the site of injury, delimited by the extent of the pigment line gap, but ignoring neuromast support cells. The average intensity across this ROI was recorded.

2.10.4 Leukocyte recruitment count

Post injury and treatment with selected compounds, the embryos were kept at 28 ^{o}C for 6 hours. After this time, any dead embryos were removed and the rest of the embryos manually counted for leukocyte recruitment. Embryos were anaesthetised with 0.017% MS-222 as described previously and the number of neutrophils at the site of injury were counted from the proximal most point of the pigment line parallel to the injury to the line of the injury itself using an M165FC stereomicroscope (Leica)

2.10.4 HEK293T FRET image acquisition

Fixed cells as described previously were imaged on a TE-2000U microscope (Nikon) with a Orca-AG Camera (Hamamatsu) using Volocity™ imaging software (Perkin Elmer) under the following exposure and emission settings. For each FRET acquisition, 3 images were taken. The cells were imaged with a D436/20x CFP excitation filter and a D480/40m CFP emission filter to aquire an image of the donor fluorescence, then with a HQ500/20x YFP excitation filter and a HQ535/30m emission to aquire an image of the YFP fluorophore with a CFP to YFP image taken with the CFP excitation and the YFP emission filter. A 455DCLP dichroic mirror was used for these images (filters and dichroic from Chroma). Exposure settings were determined by autoexposure to the YFP emission channel and maintaining the same exposure setting in all 3 channels. 3-4 random fields of view were imaged for each repeat yielding a total of 10 images per treatment group from 3 repeats. Images to calculate CFP and YFP spectral bleedthrough constants were acquired with these settings on cells expressing either CFP or YFP

separately. Images were acquired at 10x magnification using a 0.3NA PlanFluor objective (Nikon).

2.10.5 HEK293T FRET processing/analysis

Spectral bleedthrough constants were calculated using Volocity™ software: regions of interest (ROI) were drawn around 10-12 cells of varying intensity and Volocity™ was used to calculate the bleedthrough constant. FRET was calculated by Volocity™ using these constants. Background corrections were determined by Volocity™ from a cell-free region of interest. Threshold corrections were performed by carrying over these background constants into the "threshold" dialogue box. Cell measurements were performed by Volocity™, objects were defined in the 6th percentile of CFP intensity with a size-guide of 250μm^2. These data were exported to excel where the average intensity for each FRET calculation method used was calculated across each field of view. Figures were generated and statistical analysis performed using Prism® (Graphpad).

2.10.6 Tg(BACmpo:FRET DEVD)sh237 isopimpinellin acquisition and processing

Six embryos at a 72 hpf developmental stage were injured as described above and kept at 28 ^oC for 30 minutes. They were mounted as described with the addition of Isopimpinellin to the LMP agarose, and E3 layer. Embryos treated with 1% DMSO were injured and mounted at the same time as a control. The embryos were imaged for 8 hours with acquisition initiated 1 hour post injury under the same acquisition settings described above with images taken every 180 second, with the observer blinded to the experimental condition. Volocity™ was used to generate an nF channel with threshold set at 150% of the mean intensity of the signal from a cell free ROI. Spectral bleedthrough was determined from previously fixed HEK293T samples. The image sequences were compressed to a single z-plane. The images were investigated for instances of neutrophil apoptosis by the loss of FRET but retention of YFP signal and these data were recorded and quantified.

2.10.7 Tg(BACmpo:FRET DEVD)sh237;Tg(lyz:nsfB.mCherry)sh260 acquisition

The *Tg(BACmpo:FRET DEVD)sh237* was crossed to *Tg(lyz:nsfB.mCherry)sh260*. At 72 hpf, embryos were treated with metronidazole then mounted for imaging after 4 hours. The embryos were imaged on a UltraVIEW VoX spinning disk confocal

microscope (Perkin Elmer) mounted on a Axiovert 200M (Zeiss) running Volocity™ software for image acquisition (Perkin Elmer). Images were captured at the Caudal Haematopoetic Tissue (CHT) of the embryos. 4 fluorescent settings were captured for each image. CFP was imaged with a 440 nm laser line for excitation and a 485/705nm dual band-pass filter for emission, YFP was imaged with a 514 laser line for excitation and a 587 filter for emission, and the FRET channel was imaged with the CFP excitation and YFP emission settings. The mCherry channel was acquired with a 561 nm laserline for excitation and a 525/640 dual band-pass filter for emission. The images were acquired using a 40x PlanFLN NA 1.3 oil immersion objective. This yielded images of the *mpx* FRET reporter and allowed colocalisation with cells expressing nsfB.mCherry. The images were processed as described above and visualised for apoptotic events.

2.10.8 THP-1 FRET YVHD acquisition

THP-1 cells transfected with FRET YVHD, or with FRET DEVD being used as a control, were differentiated with 20nm PMA as described previously onto LabTek™ 8 chambered coverglass (Thermo Scientific). Controls were as follows: 2 well YVHD, 2 wells YVHD with Caspase 1 inhibitor treatment, 2 wells DEVD, 2 wells DEVD with Caspase 1 inhibitor treatment. 24 hours post transfection, the media was replaced and control chambers of cells were treated with 50nm AC-YVAD-CMK Caspase 1 inhibitor for 18 hours. After AC-YVAD-CMK treatment the cells were primed with 1μg/ml LPS for 3 hours. Cells were imaged as described with HEK293T cells above at the timepoints indicated. 3 ROIs were designated randomly within each chamber. Immediately before initiation of acquisition, the cells were stimulated with 500nm 3'-O-(4-benzoyl)benzyl-ATP (BzATP).

2.10.9 THP-1 FRET YVHD analysis

Spectral bleedthrough was determined from previously fixed HEK293T samples. nF/Donor was determined as described previously and exported to Excel (Microsoft). The nF/Donor intensity for each object was averaged across each field of view and figures were generated in Prism® (Graphpad).

2.10.10 THP-1 IL-1β.EGFP

THP-1 cells transfected with the IL-1β.EGFP expression plasmid and seeded onto 6 well plates. Cells were then differentiated with 20nm PMA. 48 hours post transfection cells were stimulated with 500nm BzATP and imaged at 5 minute intervals using a 10x 0.3NA PlanFLuor objective on a TE-2000U microscope (Nikon) with a Orca-AG Camera (Hamamatsu).

2.10.11 *Tg(fms:Gal4.VP16)i186;Tg(UAS:nsfB.mCherry)i149 pDEST(UAS:MCS-zfIL-1β.EGFP)* image acquisition

FMS UNM embryos were injected with *pDEST(UAS:MCS-zfIL-1β.EGFP)* and selected for *Cmlc2*EGFP and mCherry expression at 48 hpf. Embryos were injured 72 hpf and mounted in LMP agarose after 10 minutes. The site of injury was imaged every 2 minutes using a 10x 0.3NA PlanFLuor objective on a TE-2000U microscope (Nikon) with an Orca-AG Camera (Hamamatsu).

2.10.12 pDEST(MPEG1:IL-1β.EGFP) image acquisition.

AB wildtype embryos were injected with *pDEST(mpeg1:IL-1β.EGFP)* as described and selected for cmlc2EGFP expression after 48h. At 72 hpf embryos were injured and incubated for 30 minutes at 28 ^{o}C. after 30 minutes, embryos were mounted in LMP agarose and imaged using a UltraVIEW VoX spinning disk confocal microscope (Perkin Elmer) mounted on a Axiovert 200M (Zeiss) running Volocity™ software for image acquisition (Perkin Elmer). A 40x PlanFLN NA 1.3 oil immersion objective was used. Images of single cells were acquired, upper and lower limits of the focal depth defined by the limits of the cell, and 6 focal planes were used. Gain was set at 125 to keep exposure to a minimum. Images were acquired every 15 seconds.

2.11 Data collection and statistical analysis

Data was collected either from Volocity™ or visual counting and input manually into Prism® (Graphpad), which was used to generate figures and statistical analyses. The observer was blinded to experimental treatments throughout to avoid experimental bias. Throughout the study, "*" refers to a p value of ≤0.05, "**" to ≤0.01 and "***" to ≤0.001

Table 2.1 PCR primers

Gateway sequencing primers	
5' forward sequencing	CTATGACCATGATTACGCCAAGCTA
5' reverse sequencing	CTGCTTTTTTGTACAAACTTG
ME forward sequencing	CAAGTTTGTACAAAAAAGCAG
ME reverse sequencing	CCACTTTGTACAAGAAAGCTG
3' forward sequencing	CAGCTTTCTTGTACAAAGTGG
3' reverse sequencing	CAGTGAATTATCAACTATGTA
FRET mutagenesis primers	
Forward	CGTCCGAGCTCAGCGGATATGTGCACGATGGTACCAGCGGAAGCG
Reverse	CGCTTCCGCTGGTACCATCGTGCACATATCCGCTGAGCTCGGACG
FRET mutagenesis sequencing primer	
Forward	AGTGGATCCGACGAGATG
pME-zfIL-1β	
Forward	GGGGACAAGTTTGTACAAAAAAGCAGGCTTGATGGCATGCGGGCAATATGAAGTC
Reverse	GGGGACCACTTTGTACAAGAAAGCTGGGTCGATGCGCACTTTATCCTGCAGCTC
pME-MCS-zfIL-1β	
Forward	GATTAAAGCTTATGGCATGCGGGCAATATGAAGTC
Reverse	CGGTGGATCCGATGCGCACTTATCCTGCAGCTC
p5E 4xUAS	
Forward	GGGGACAACTTTGTATAGAAAAGTTGAACGGTGGCTTCTAATCCGTGA
Reverse	GGGGACTGCTTTTTTGTACAAACTTGACTTCGAGGTCGAGGGAATTC

Chapter 3: Bioinformatic Investigation of Zebrafish as a model of Interleukin-1β Biology

Zebrafish and humans share significant conservation in elements of their immune system. Zebrafish orthologues exist of TLRs and other pattern recognition receptors, NF-κB, and more. To use zebrafish as a viable model of IL-1β biology, this pathway in zebrafish must share enough conservation with the human IL-1β pathway that any discoveries made in zebrafish on IL-1β modulation could be transferred to human medicine with a chance of success. To this end I undertook a bioinformatics study of the immune components in the zebrafish IL-1β pathway that have not already been studied starting with zebrafish IL-1β itself.

3.1 Zebrafish IL-1β function and processing

The fish immune system encodes orthologues of IL-1β, however, these sequences lack a consensus caspase-1 cleavage site like that found in mammalian IL-1β orthologues (Zou et al. 1999; Bird, Zou, et al. 2002; Bird, T. Wang, et al. 2002; Hong et al. 2004; Angosto et al. 2012). It is unclear whether IL-1β therefore functions in a similar way in the zebrafish as it does in mammalian cells. The induction of the IL-1β message has been described in response to peptidoglycan injection in carp (T. Kono et al. 2002); *Francisella* in zebrafish (Vojtech et al. 2009); *V. anguillarum* DNA, flagellin and LPS in pufferfish (MP Sepulcre et al. 2009); LPS in catshark (Bird, T. Wang, et al. 2002) and LPS in trout (Zou et al. 1999); which indicate that the role of IL-1β as a proinflammatory cytokine is conserved between mammalian and fish lineages. Processing of IL-1β into a mature cytokine has been demonstrated in trout (Hong et al. 2004) and seabream (López-Castejón, M Sepulcre, et al. 2007), however the caspase-1 dependence of these processing mechanisms has been questioned.

The caspase-1 cleavage site is poorly conserved outside the mammalian clade (Figure 3.1), however these orthologues contain an IL-1β family signature (Bird, Zou, et al. 2002). The human IL-1β gene is present in a cluster of Interleukin

1 like genes, but this cluster is highly polymorphic and the presence of so many IL-1 gene family members around the same chromosomal region suggests their evolutionary origin from a single gene (Dunn et al. 2001; Brocker et al. 2010). This appears to have occurred at some point in mammalian evolution, as there are fewer interleukins present on the same linkage group in mice than in human genome (Figure 3.2).

In zebrafish, the IL-1β gene clusters separately from other interleukins on chromosome 10, with no other nearby interleukins. For human IL-1β, both pro and mature sequences (accession AAA59135.1 and AAC03536.1 respectively) align most closely to the annotated zebrafish IL-1β protein (accession NP_998009.1) which also has human pro IL-1β as its best reciprocal BLAST hit. However, there were no hits for human IL-1α and IL-1RA alignment, which matches previous studies which failed to find zebrafish homologues (Huising et al. 2004). Huising *et al* also found IL-18 homologues in *Medaka* and *Fugu*, but I failed to find a similar IL-18 homologue in the zebrafish genome.

An alignment of these two proteins shows that the proteins have overall high homology (Figure 3.3 A). An alignment of the IL-1β cytokine post processing with the putative active IL-1β region, defined by BLAST as starting at residue 106, shows an even higher homology, which would be expected if this was the active region of the molecule. The zebrafish IL-1β sequence was analysed using RaptorX (Källberg et al. 2012) and Phyre (Kelley & Sternberg 2009). Phyre predicted a β-sheet rich structure very similar to that of human IL-1β (Priestle et al. 1988) for the c terminal domain of the protein (Figure 3.4). However, the structural model produced by RaptorX disagreed on where this IL-1β like domain began and generated an α-helix prediction for what would be the equivalent of the receptor activation residues on the cytokine. This split also differs from that assigned by BLAST and other alignment tools. To test whether other tools detected this segment as an α-helix or β-strand, the protein sequence was submitted into I-TASSER (Y. Zhang 2008; A. Roy et al. 2010) and PsiPred (Buchan et al. 2010). PsiPred yielded very similar results to Phyre using a different methodology not based on the template method that Phyre or RaptorX uses and I-TASSER confirmed the results of Phyre, whilst also predicting structures where the Pro-domain blocked access to the first β–strand. These results also both show that the most

conserved residues map to the predicted beta sheet regions on the protein (Figure 3.5). I-TASSER also predicted that this structure most likely interacted with IL-1R and that by GO terms, the protein was most likely to bind to IL-1R have an extracellular function involved in inflammation and immunity.

Overall, zebrafish IL-1β has high degree of sequence homology and a conserved structure based on structural prediction tools.

3.2 Zebrafish IL-1 receptors.

IL-1 receptors in zebrafish have proved much more difficult to explore bioinformatically. Human IL-1RI maps most closely to the RAcP like 1 sequence and the hypothetical proteins IL-1R like 2 and IL-1R like 2, predicted by automated sequence analysis (accession NP_001136054.1, XP_001339654.4 and XP_002663470.2 respectively.)

Zebrafish IL-1RI has been annotated by Huising *et al* (2004) (accession ENSDARP00000012342) and maps to chromosome 3, where it encodes a peptidase like protein. López-Castejón et al. (2007), however, define IL-1RI using the accession ENSDARP00000055956 and IL-1RII using the accession ENSDARP00000064952, which have not been available since the Zv8 release of the zebrafish genome. Meijer *et al.* (2004) have cloned a partial message of the zebrafish IL-1R mRNA (deposited as AAQ91322.1), which still maps to the same message fragment on the Zv9 assembly, however, remains poorly annotated and only codes for the TIR domain. Alignments were not made to IL-1R due to this lack of clarity.

Figure 3.1. Zebrafish IL-1β does not align to give a direct match for the consensus mammalian caspase-1 recognition and cleavage site. Clustal alignment of pro-IL-1β sequences from various vertebrate species followed by accession number. The human caspase-1 cleavage site is shown by the black box, indicating no conservation of the cleavage site outside the mammalian clade.

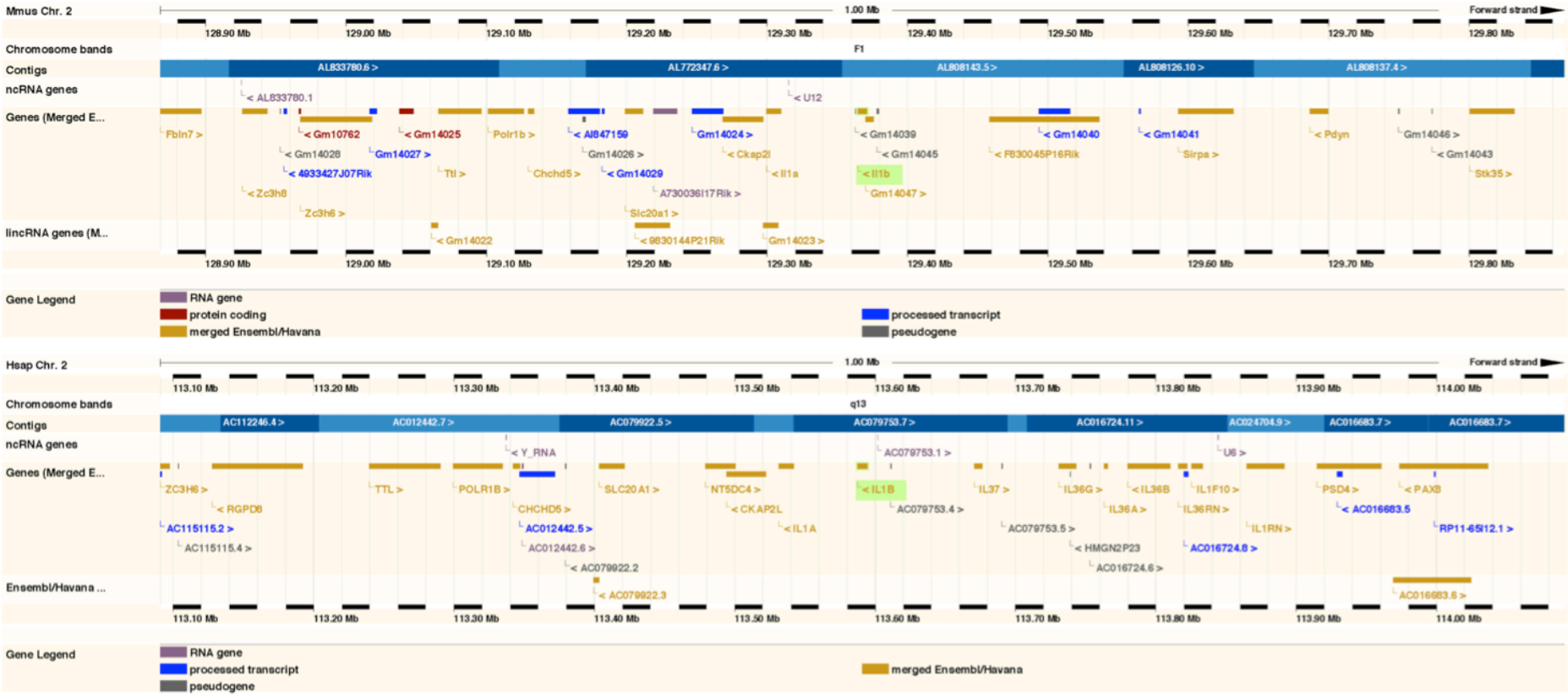

Figure 3.2. The IL-1 locus is shows an evolutionary expansion in the mammalian lineage. Ensemble contig alignment of the IL-1 locus on human C2 shows its position near a number of other IL-1 family members. Though the position of IL-1β is conserved in mice, this cluster contains only IL-1α.

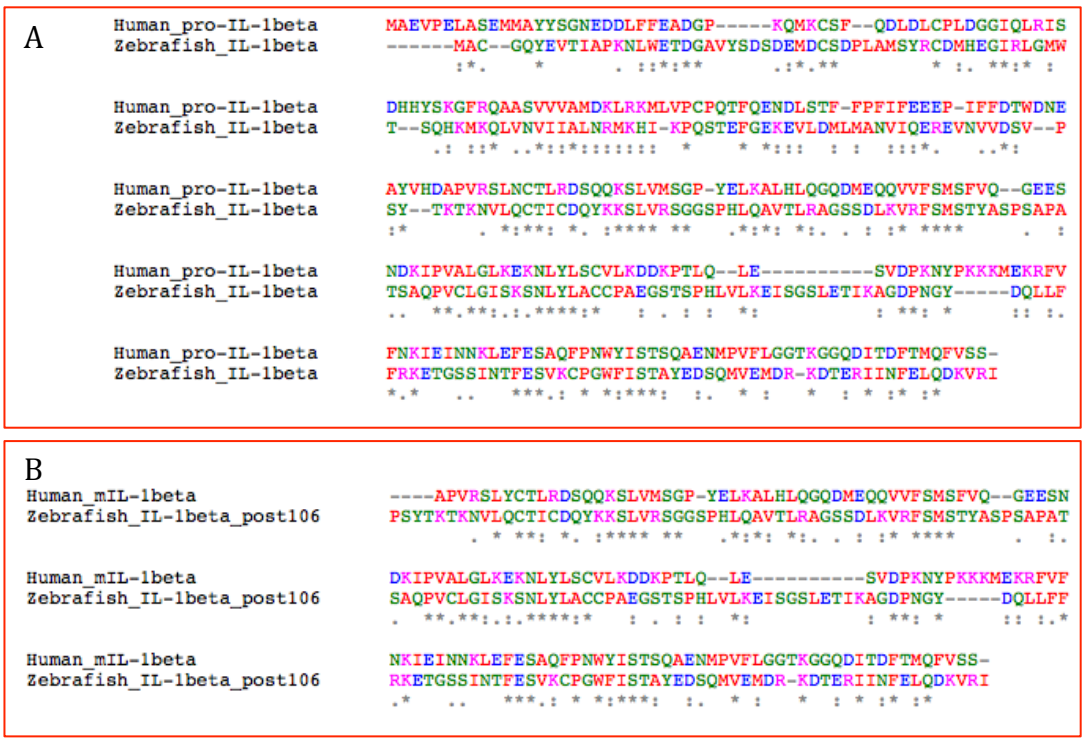

Figure 3.3. The mature IL-1β cytokine has higher homology between humans and zebrafish than an overall alignment of the entire pro-protein would otherwise suggest. Clustal alignment of the human IL-1β pro-protein, accession AA59135.1, and the zebrafish IL-1β, accession NP_998009.1 shows the overall similarity between the two proteins (A), but has more conserved residues when the mature cytokine (accession AAC03536.1) is compared to the c-terminus of the zebrafish IL-1β protein (B).

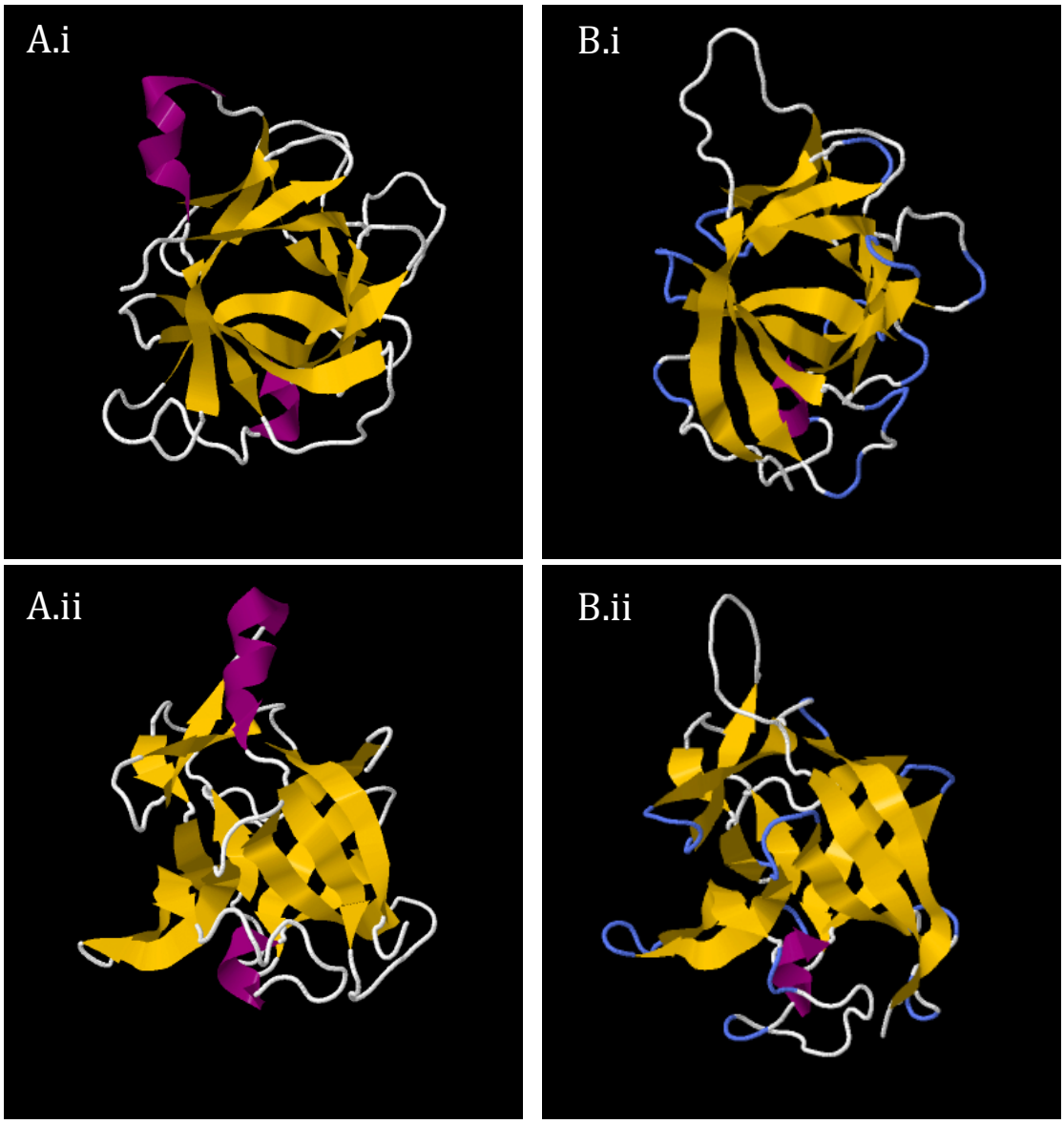

Figure 3.4. Human and zebrafish mIL-1β is a trefoil structure composed primarily of β-sheets. JMOL image of mIL-1β (accession AAA59135.1) (Ai and Aii) and of zfIL-1β (Bi and Bii) predicted using Phyre from two different angles shows a highly similar trefoil structural arrangement composed of β-sheets.

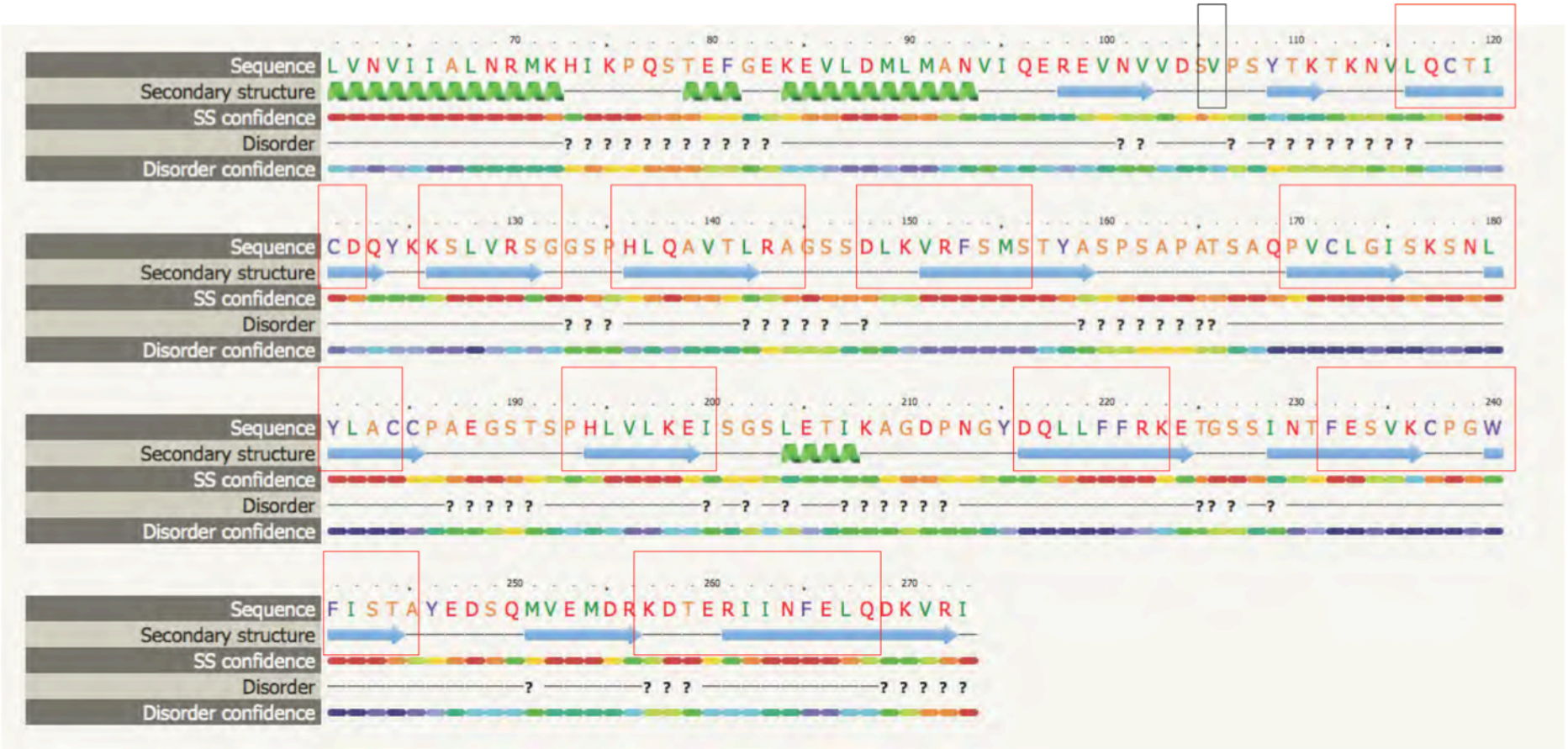

Figure 3.5. Zebrafish mature IL-1β cytokine b-strand secondary structure regions match areas of high conservation between zebrafish and human IL-1β. Phyre prediction of the zebrafish IL-1β structure shows a largely of b-strand composition. The positioning of these strands matches regions of conservation between zebrafish and human IL-1β (red boxes)

3.3 IL-1β processing by caspase-1 orthologues

Although IL-1β structure remains relatively homologous, it is unclear whether IL-1β is cleaved and processed in zebrafish. There are numerous pieces of evidence that suggest that this may not be the case. The human cleavage site is not conserved outside of mammalian caspase-1 orthologues (Figure 3.1), and a number of studies have failed to identify cleavage sites in the IL-1β orthologues of other fish species, such as trout (Zou et al. 1999) and gilthead seabream (Angosto et al. 2012). In trout, the cleavage of IL-1β by caspase equivalents was not investigated and the study lacked a secondary stimulus for inflammasome activation. However, in seabream, Angosto *et al* showed that despite IL-1 release as a smaller isoform, corresponding to the mature cytokine, the processing was not dependent on caspase-1.

Whether this applies to zebrafish would be dependent on the evolutionary relationships between these caspase and IL-1β orthologues. Huising et al (2004) show that zebrafish caspase-A and -B are phylogenetically most similar to mammalian caspase-1 orthologues, however functional activity was not assessed. Caspase A and B, the closest orthologues to mammalian caspase-1 and 5 (Masumoto et al. 2003) have highly conserved catalytic domains, but less conserved N-terminal domains (Figure 3.6). Whereas the N-terminus of caspase-1 is a caspase recruitment or CARD domain, caspase-A and -B instead have pyrin domains, a related death-fold domain (Martinon et al. 2001) with less conservation to the N terminus of Capase 1.

Overall, the phylogenetic alignment of the human caspase-1 protein with mouse, chicken and seabream caspase-1 and zebrafish caspase-A show that zebrafish caspase-A is evolutionarily further from human caspase-1 than its seabream orthologues (Figure 3.7 A), however when considering just the functional caspase domain, this effect is reversed (Figure 3.7 B).

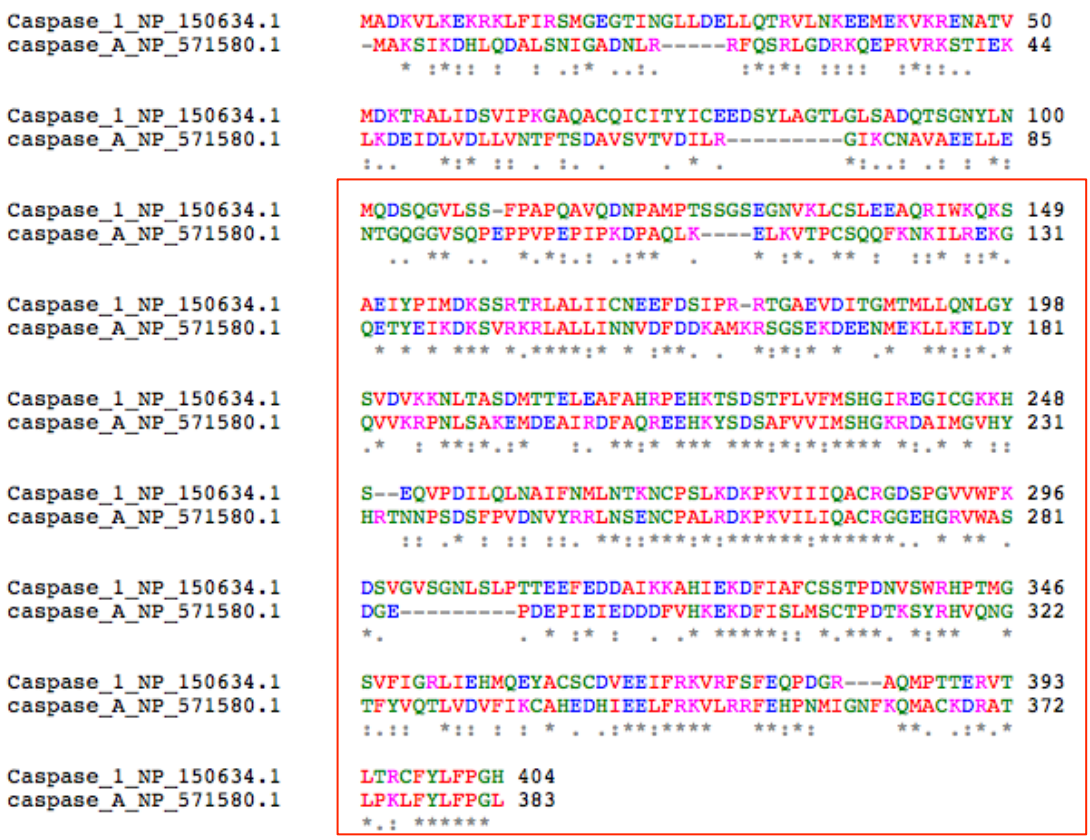

Figure 3.6. Alignment of Human caspase-1 and zebrafish caspase-A shows high conservation of the active caspase domain. Clustal alignment of human caspase-1 and zebrafish caspase A. Caspase domains are highlighted with the red box.

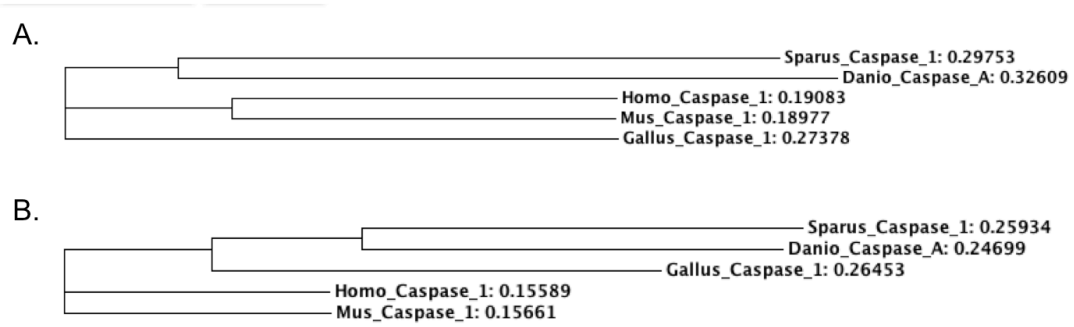

Figure 3.7. Caspase-1 phylogenetic tree. Caspase-1 alignments show phylogenetic difference between zebrafish and human caspase-1 orthologues as further than Seabream caspase-1 (A), unless only caspase functional domains are considered (B). Functional domain based on López-Castejón et al., (2008)(Accession numbers *Sparus*: CAM32183.1, *Danio*: NP_571580.1, *Homo*: NP_150634.1, *Mus*: NP_033937.2, *Gallus*: AAC69917.1). Generated using Clustal Omega.

3.4 Discussion.

In order to develop *in vivo* reporters of IL-1β, it is essential to ensure that the model organism used is appropriate. The advantages of the zebrafish as a model for inflammation were laid out in chapter 1, where the current understanding of the conservation of immune genes and functions in vertebrates is summarised. Numerous components in innate immune pathways are conserved however, it is still uncertain how the divergence between fish and mammals affects the IL-1β pathway.

In mammals, the IL-1β locus is highly polymorphic, with the suggestion that a number of the Il-1 family members evolved from a single locus. This appears to have happened in the mammalian lineage as so many related IL-1 proteins were not found in fish. The syntenic difference between mice and humans demonstrates the magnitude of the divergence of this locus in the mammalian clade, however, the expansion of the IL-1 family into so many paralogues highlights the evolutionary importance of IL-1 itself.

From a protein sequence perspective, the C-terminal region of zfIL-1β, corresponding to the protein sequence of the mature human IL-1β cytokine is highly conserved between humans and zebrafish. As no role has yet been confirmed for the pro domain of IL-1β, residing in the N-terminus of the coding sequence, it is highly likely that its role is mostly inhibitory. This could occur through allosteric blocking of important residues on mature IL-1β or through increasing the size of the cytokine for export, although as IL-1β secretion is coupled to its processing, the latter is unlikely. Nevertheless, if its function is purely inhibitory, there would be weak evolutionary selection pressure against any mutants unless they affected its function. In contrast, the C-terminal region of the protein corresponding to the mature cytokine would be under much stronger selection pressure to retain its sequence and its function, as changes here would likely affect the ability to bind to its receptor and transduce a signal. It is therefore expected that this region of the protein would retain much more similarity between species than the N-terminal propeptide. Analysis of these protein regions demonstrated that this was indeed the case; the prodomain equivalent region on zebrafish IL-1β has far fewer identical residues, but has large regions of similarity,

whereas the C-terminal domain, corresponding to the human mature IL-1β sequence has significantly more identical residues (Figure 3.3). Furthermore, structural prediction of the protein sequence using Phyre and RaptorX support these hypotheses and suggest a β-trefoil shape for IL-1β composed primarily of β-sheets. However, these approaches may introduce a certain bias. Both Phyre and RaptorX base their prediction on homology to existing models, which they use as templates and may introduce error if a template for a closer homologue is not available. In this study, the closest structural match in Phyre was the chicken IL-1β protein, whereas RaptorX used a series of human IL-1β mutants as a structural template. The difference between these approaches was addressed by combining further methods such as the UCL Psipred server to investigate these differences. Psipred attempts to predict secondary structure rather than to generate a tertiary structure for the entire protein, and was used here to look at the difference in secondary structure predicted by the two newer methods. Overall, whilst the use of structure prediction does not provide as robust a method for generating a structure as a solved crystal structure for zebrafish IL-1β, it does provide supporting evidence for the similarity in structure between IL-1β orthologues.

Although the evolutionary importance and conservation of IL-1β as a cytokine has been suggested via its sequence and structural homology, the zebrafish IL-1β receptor is poorly characterized. There is disagreement about the coding sequence for the receptor, and presently there are no orthologues annotated as either IL-1RI or IL-1RII on the latest genome assembly (Zv9) except for the automated hypothetical entries IL-1RI-like-1 and -2. From these data it is very difficult to determine the comparability between the zebrafish IL-1 receptors and their human orthologues. Further detail would be gained from molecular cloning of these receptors and investigating their exon structure, domain organization and expression, however currently this information is not available.

One major potential problem with using zebrafish as a model for IL-1β is the lack of an obvious conserved caspase cleavage site on zfIL-1β that maps to mammalian orthologues. Another is the lack of *in vitro* data to support a lack of IL-1β cleavage in fish (Angosto et al. 2012). However, existing data may be

incomplete and these caveats may not apply to the current study. Angosto *et al*. (2012) show that mIL-1β is released from seabream leukocytes, and is unaffected by inhibition with AC-YVAD-CMK and AC-ZVAD-FMK. However, previous publications show that seabream P2X7 receptors respond differently to ATP stimulation than their human and rat counterparts, and were not capable of inducing caspase-1 mediated cleavage of human IL-1β, with this incapability localized to the intracellular domain of seabream P2X7; demonstrated by the ability of a seabream extracellular domain-rat intracellular domain chimaeric protein to activate caspase-1 in response to ATP. Conversely, zebrafish P2X7 was able to trigger IL-1β processing and functioned in a similar way to rat P2X7 in response to inhibition, although the inhibitors used; Brilliant Blue G, PPADS, suramin and magnesium; were less effective than for Human P2X7 (López-Castejón, M. Young, et al. 2007). Human and zebrafish caspase-1 orthologues were also shown to only share 36.4 and 35.9 % amino acid similarity with seabream caspase-1 (López-Castejón et al. 2008) and it is known that the seabream and zebrafish show great phylogenetic divergence (Sarropoulou et al. 2007).

From these sources, it is uncertain whether studies of seabream caspase processing of IL-1β are directly applicable to studies of zebrafish IL-1β biology, and recent publications in the field show that this may not be the case. Recently, Vojtech *et al* (2012) have demonstrated that Zebrafish caspases -A and -B mediated IL-1β cleavage of zebrafish IL-1β and that this processing is at aspartic acid residues 104 and 122 for caspase-A and -B respectively. These residues are in the putative caspase recognition sites NVVD and TICD on zf IL-1β (Figure 3.7), which are located close to the equivalent human cleavage site YVHD. Furthermore, zebrafish leukocytes are also capable of secreting mature IL-1β and that zebrafish caspases were sensitive to inhibition by AC-YVAD-CMK (Vojtech et al. 2012).

Overall, these bioinformatic data suggest that IL-1β is structurally highly conserved, between zebrafish and humans, and that the components required for processing IL-1β and signaling also share a significant degree of homology. *In silico*, the zebrafish appears to be a viable model of IL-1β biology but further experimental confirmation is required, as undertaken in chapter 4.

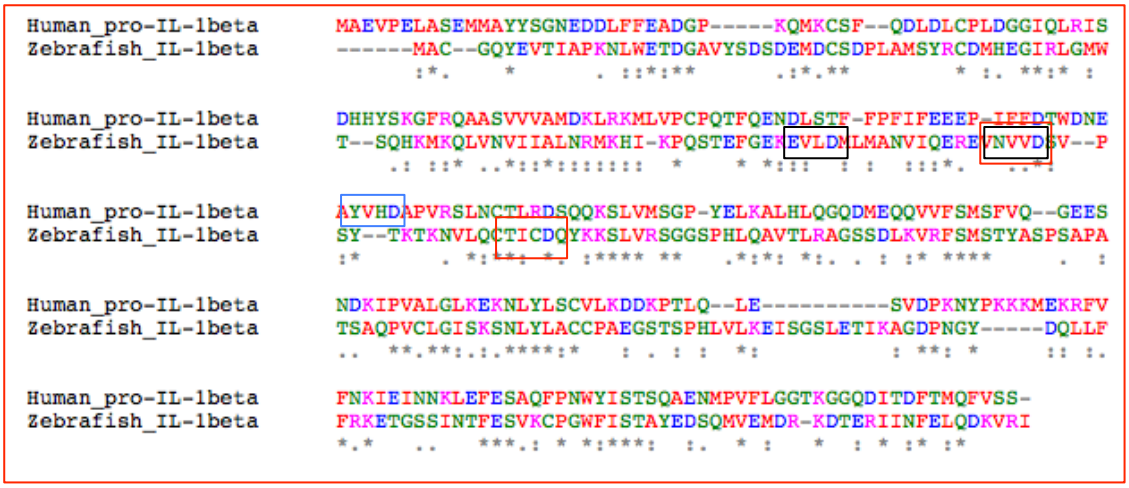

Figure 3.8. Proposed caspase-A and -B cleavage sites on zebfafish IL-1β. Human IL-1β, accession AAA59135.1, with caspase-1 cleavage site (blue box) aligned to zebrafish, NP_998009.1, with caspase-A cleavage sites EVLD and NVVD (black boxes) and caspase-B cleavage sites NVVD and TICD (red boxes) as described by Vojtech *et al.* (Vojtech et al. 2012)

Chapter 4: Functional Validation of Zebrafish as a model of Interleukin-1β Biology

I have previously shown that zebrafish and human IL-1β protein orthologues share both sequence and structural similarity, and alongside other published results these data suggest that proinflammatory cytokine IL-1β function is conserved between zebrafish and mammals. In order to further characterise zebrafish IL-1β function to support this hypothesis, I investigated IL-1β expression in response to inflammatory and infectious stimuli, and observed the effect of mammalian IL-1β pathway inhibitors on measures of inflammation in zebrafish.

4.1 IL-1β message expression

4.1.1 IL-1β is expressed at low levels in zebrafish embryos in the absence of inflammatory stimuli.

Whole mount *in situ* hybridization (WISH) was used to determine the spatial expression of IL-1β in zebrafishand its response to inflammatory stimuli. Using an *in situ* RNA probe generated from a zebrafish IL-1β cDNA construct kindly provided by Sara Kohal, the expression of IL-1β mRNA was studied in embryos 24, 48 and 72 hours post fertilisation (hpf) embryos.

In 24 hpf embryos IL-1β expression was found to be localised to the site of early leukocyte haematopoiesis above the yolk sac, the first site of primitive macrophage development (Herbomel et al. 1999), and is localized in a punctate manner similar to the distribution of leukocytes during this development phase (Figure 4.1 A). Expression in 48hpf embryos is localized to these areas, but appears less intense. (Figure 4.1 B). This effect was not seen in the sense control probe (Figure 4.1 C)

4.1.2 Injury is a powerful inducer of IL-1β mRNA in zebrafish embryos compared to LPS and *Vibrio anguillarum* DNA

Published data has previously demonstrated the responsiveness of the zebrafish immune system to inflammatory and infectious stimuli such as LPS (MP Sepulcre et al. 2009). Furthermore DNA isolated from the fish pathogen *Vibrio anguillarum* (MP Sepulcre et al. 2009) was shown to induce an inflammatory response. These stimuli were investigated for IL-1β induction using WISH, However, neither LPS treatment nor injection of *V. anguillarum* DNA showed a significant increase in staining for IL-1β mRNA in LPS treated fish [Figure 4.2 B,C]. Furthermore any apparent increase in staining in *V. anguillarum* injected fish may also be attributable to the non sterile injection technique used in administering the treatment. The lack of IL-1β staining following these treatments is recapitulated in 48hpf fish where the same lack of response to LPS and *V. anguillarum* treatment can be seen (Figure 4.3 B, C). Following these results I decided to move on to an injury based inflammatory stimulus.

Injury has long been a mainstay of inflammatory assays in zebrafish embryos (Renshaw et al. 2006) and as a powerful inflammatory stimulus might be expected to induce IL-1β signalling. When tested, injury by tail transection induced the transcription of the IL-1β mRNA message. In 24hpf embryos injury stimulated the expression of IL-1β when probed 2 hours post injury (Figure 4.4). This staining persisted at 8 hours post injury, although to an apparently lower level than at the initial 2-hour timepoint. The staining is localised at the site of injury and to punctate bodies around the injury site and the caudal hematopoietic tissue (CHT) Injured fish also show more staining away from the site of injury around the aforementioned early hematopoietic regions 2 hours post injury. Close examination of these staining patterns shows them to be localized within what appear to be leukocytes based on their irregular morphology and localization to the CHT (Figure 4.5). At 26 hpf, these cells are most likely early macrophages, but could also be early neutrophil progenitor cells. A number of cells display a mononuclear morphology and are likely to be monocytic in origin (Figure 4.5).

Injuring 48hpf embryos demonstrates a very similar staining pattern (Figure 4.6), with peak staining seen at 2 and 4 hours post injury, and less at 6 and

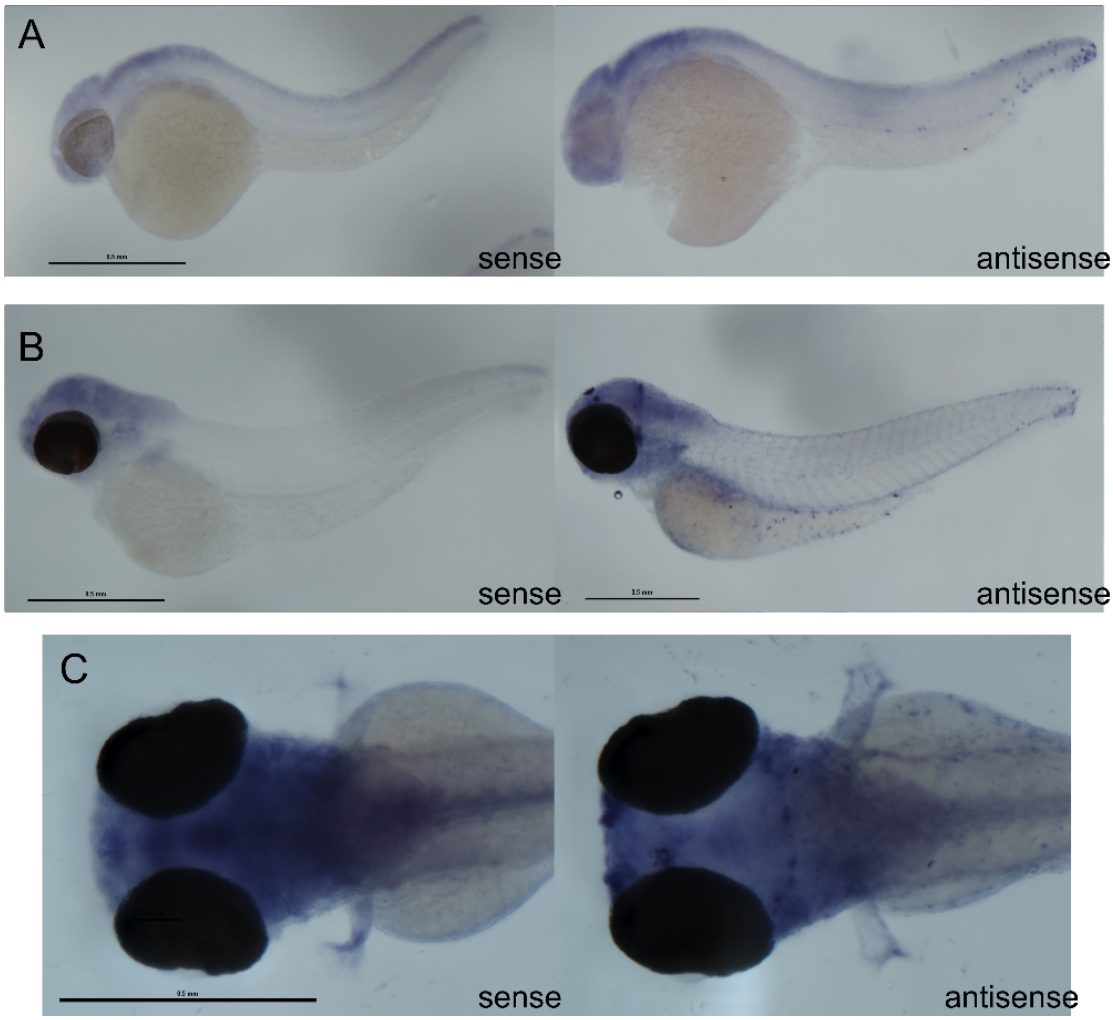

Figure 4.1. IL-1β expression in response to injury using WISH with sense controls. 24 and 48 hpf embryos (A and B respectively) stain for IL-1β mRNA in punctate cells around the yolk and sites of injury, 72 hpf embryos have symmetrical staining localized in the head and brain region. WISH with a sense probe (C) show no staining except for a delocalised faint staining in the hindbrain indicative of non-specific probe trapping. Scale bar = 500 μm

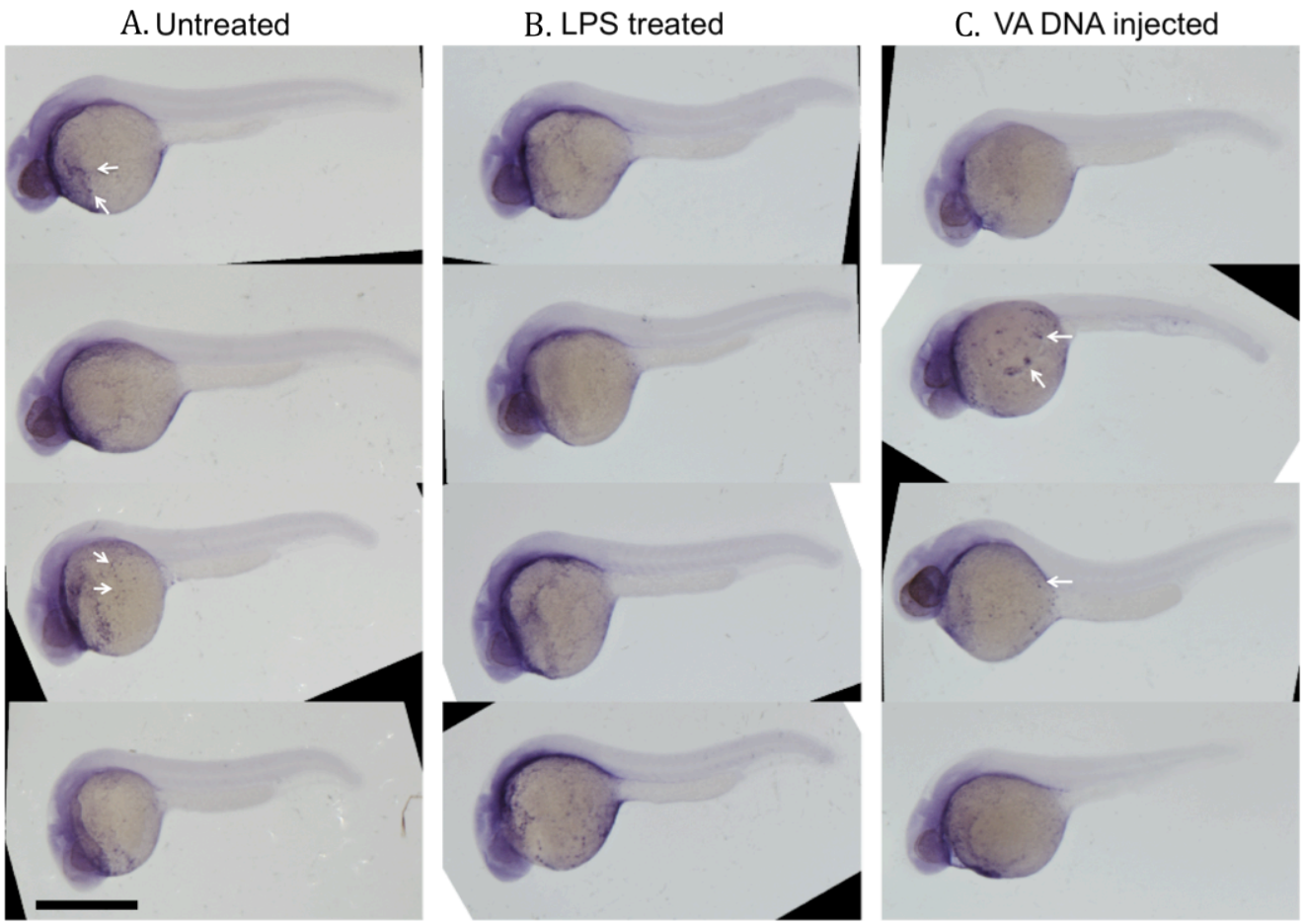

Figure 4.2. IL-1β mRNA is weakly expressed without inflammatory stimuli and shows a small response in embryos injected with *V anguillarum* DNA. 24 hpf embryos treated overnight with 1mg/ml with LPS (B) or injected with *V. anguillarum* DNA shortly after fertilization (C) appear to have no more induction of IL-1β message transcription than control embryos (A) when assayed via WISH for IL-1β. Untreated embryos show some IL-1β mRNA staining in a punctate pattern over the yolk sac, possibly within macrophage progenitors, also present in LPS and VA DNA treated embryos (arrows). Scale bar =500μm

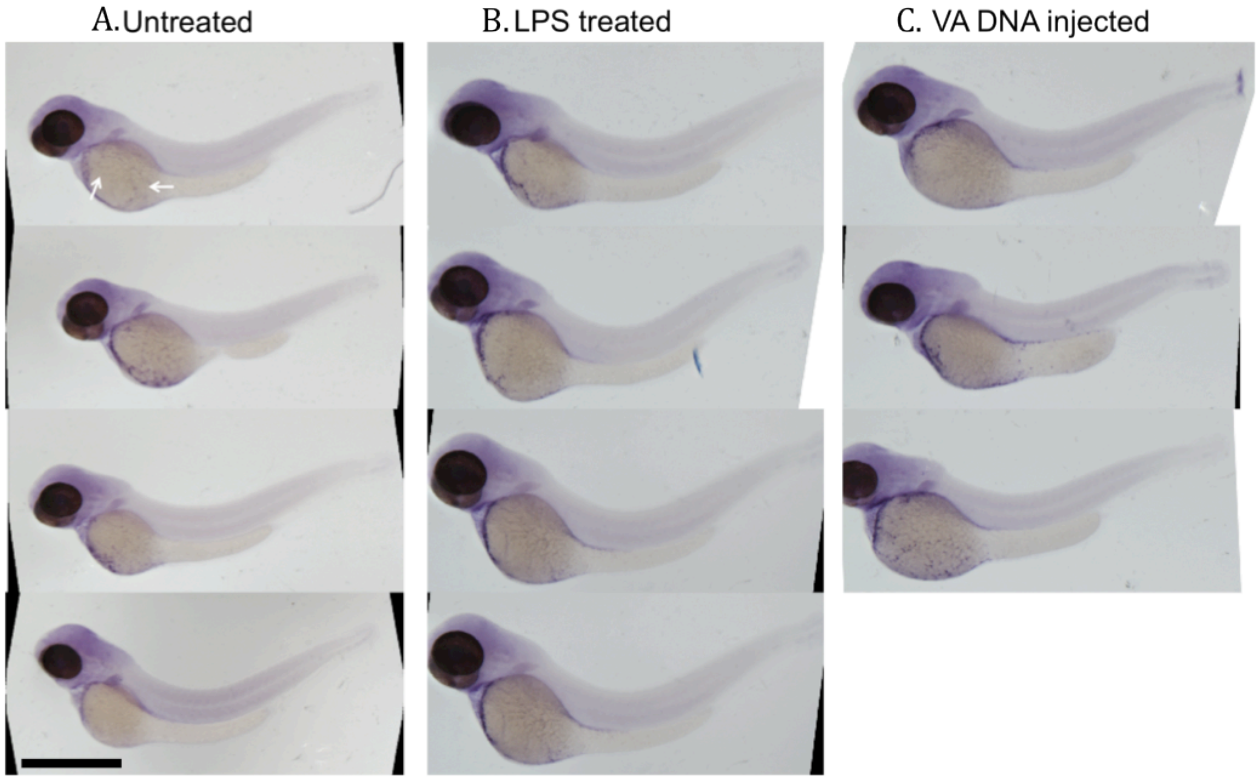

Figure 4.3. at later developmental stages, IL-1β expression is limited to a weak signal over the yolk sac which can be partly induced by injection with *V. anguillarum* DNA. 48 hpf embryos treated overnight with 1mg/ml with LPS (B) or injected with Vibrio Anguillarum DNA shortly after fertilization (C) appear to have no more induction of IL-1β message transcription than control embryos (A) when assayed via WISH for IL-1β column). Untreated embryos show some IL-1β mRNA staining in a punctate pattern over the yolk sac, possibly within macrophage progenitors, also present in LPS and VA DNA treated embryos (arrows). Scale bar = 500 μm

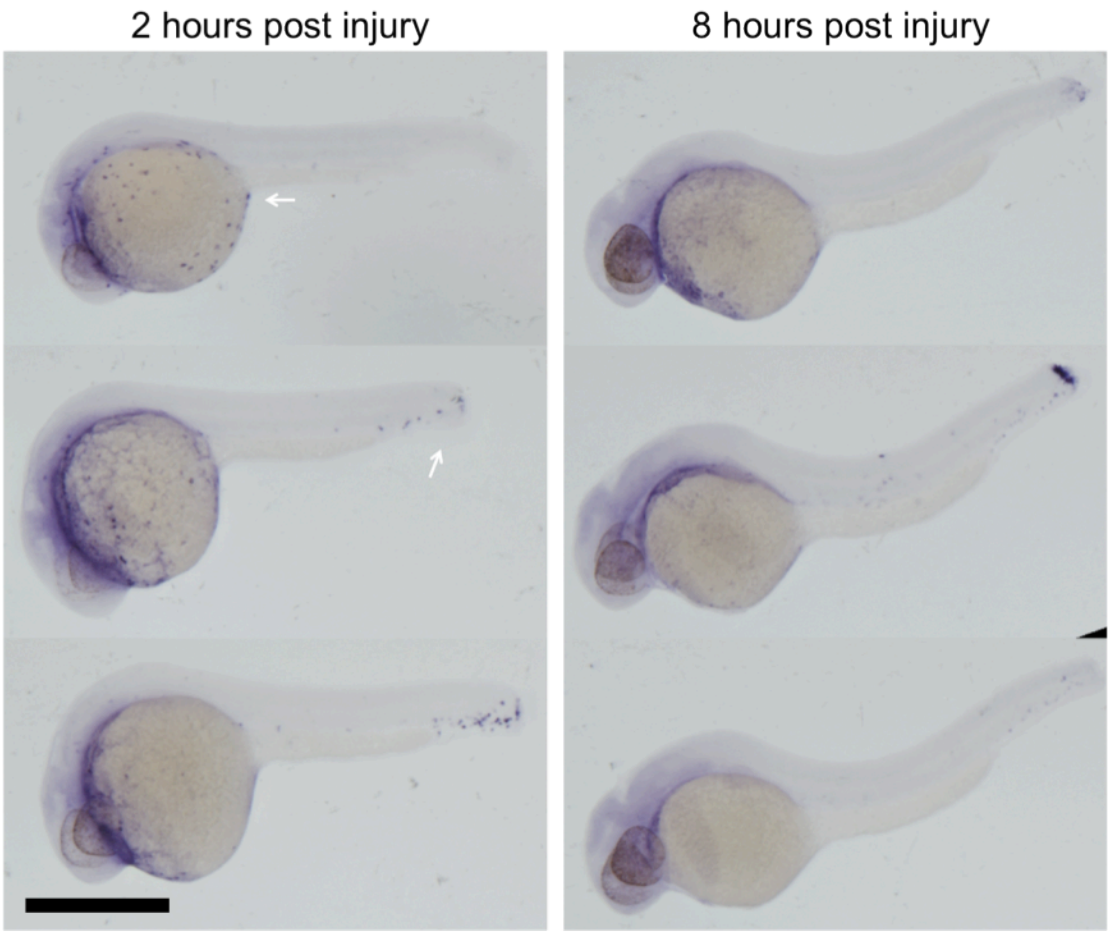

Figure 4.4. Injury is a potent inducer of IL-1β mRNA expression in early embryos. 2 hours post injury, 24 hpf embryos show significant IL-1β mRNA upregulation at the site of injury and over the yolk sac (arrows) to a greater extent than those shown in untreated embryos (Figure 4.1A). 8 hours post injury there are less stained cells in the rest of the embryos, but IL-1β expression remains at the site of injury. Scale bar = 500μm

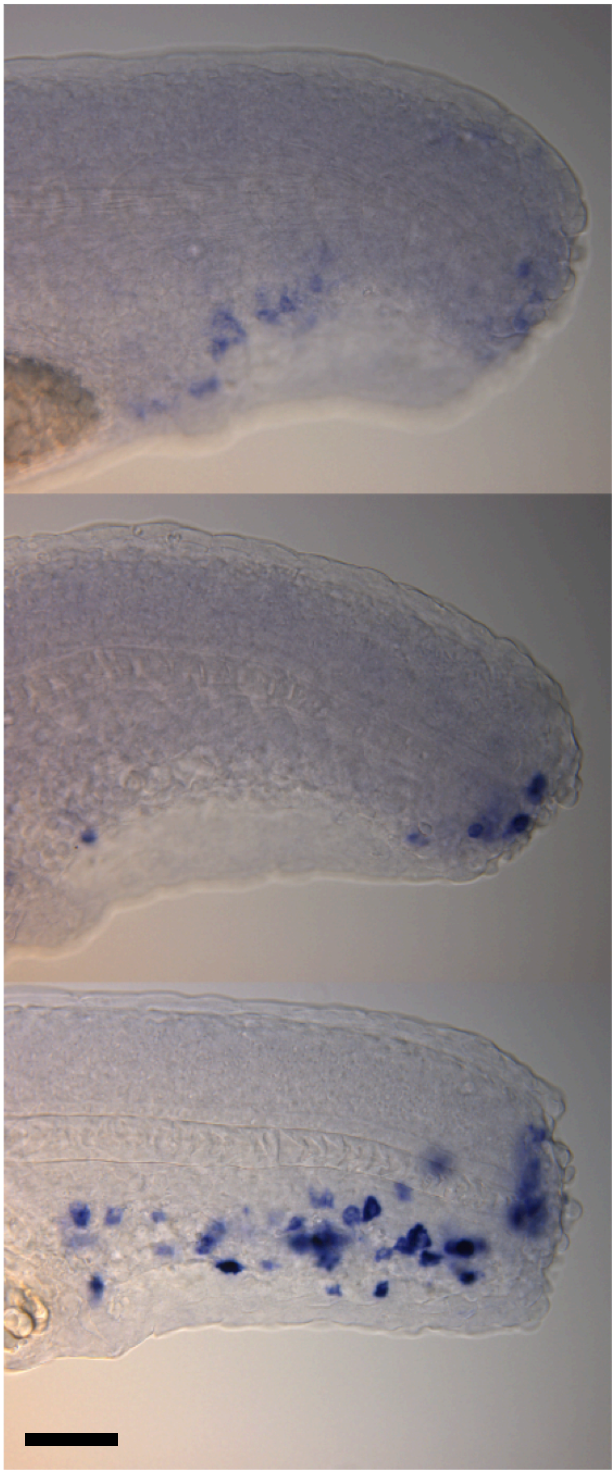

Figure. 4.5. IL-1β is expressed in macrophage like cells in response to injury in 24hpf embryos. High-resolution compound light microscopy, using a 40x objective, of multiple representative embryos reveals that cells stained for IL-1β mRNA via WISH have a very leukocyte-like morphology and appear to have moved from the CHT towards the site of injury. These cells have an irregular morphology and stain strongly for IL-1β mRNA. Scale bar= 50 μm

8-hour timepoints, though it should be stressed that many other factors can affect the strength of staining of a WISH and that this should not be considered a quantitative assay. Very intense staining can be seen in a few embryos at the site of injury, yet its absence in other embryos and injured embryos stained with a sense probe (Figure 4.1) implies that this effect is unlikely to be due to non specific staining of damaged or necrotic tissue at the site of injury.

The exact cellular localisation of the staining at these sites remains unclear and is difficult to determine due to the intensity of the signal. A closer look at the stained cells under higher power microscopy again reveals them as having very leukocyte like morphology, with single nuclei (Figures 4.5, 4.8). These cells also appear to cluster around the endothelium of the aorta and intersegmental vessels, which has previously been shown to act as a conduit for macrophage migration towards sites of injury (Figure 4.7) (Gray et al. 2011). Together these observations imply that the stained cells are likely to be a monocyte/macrophage lineage. Whole embryo imaging shows that staining away from the site of injury is strongest at 2hpi (Figure 4.5), where more cells can be seen in the rest of the fish and over the yolk sac; the presence of cells elsewhere in the fish is reduced progressively throughout the response and in most embryos is gone by later timepoints, leaving staining localized mostly to the site of injury. In the characterisation of embryonic zebrafish macrophages, Herbomel *et al*. (1999) also note that macrophages throughout the embryo adopt an activated phenotype in response to inflammatory insults.

These data show that IL-1β is more strongly induced by injury than by the other methods of inflammatory insult tested. In response to injury, IL-1β is expressed in cells exhibiting morphology, developmental timescale and apparent behaviour of macrophages. The strongest time for IL-1β induction is at 2-4 hours post injury, with a reduction in signalling after 6 hours.

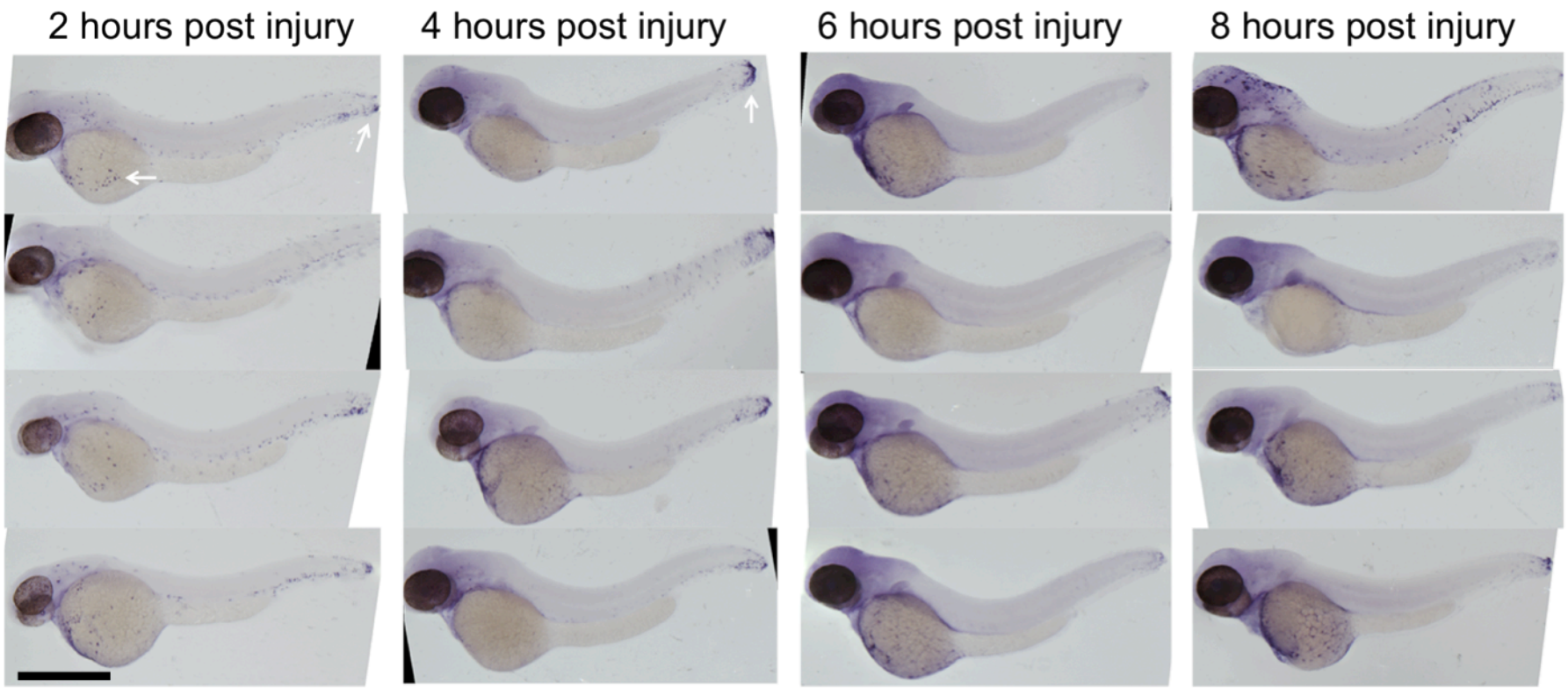

Figure 4.6. Injury is a potent inducer of IL-1β mRNA in day 2 fish. Zebrafish embryos injured at 48h post injury show a very strong induction of IL-1β mRNA after 2 hours when assayed by WISH. Labelled cells can be seen throughout the embryos, especially around the yolk sac, a site of early macrophage haematopoiesis. The response at the site of injury appears strongest after 4 hours, but with less staining throughout the rest of the embryos implying that IL-1β is induced in cells far from the site of injury as an early response to injury. This staining appears to be less intense at later timepoints. Scale bar = 500μm

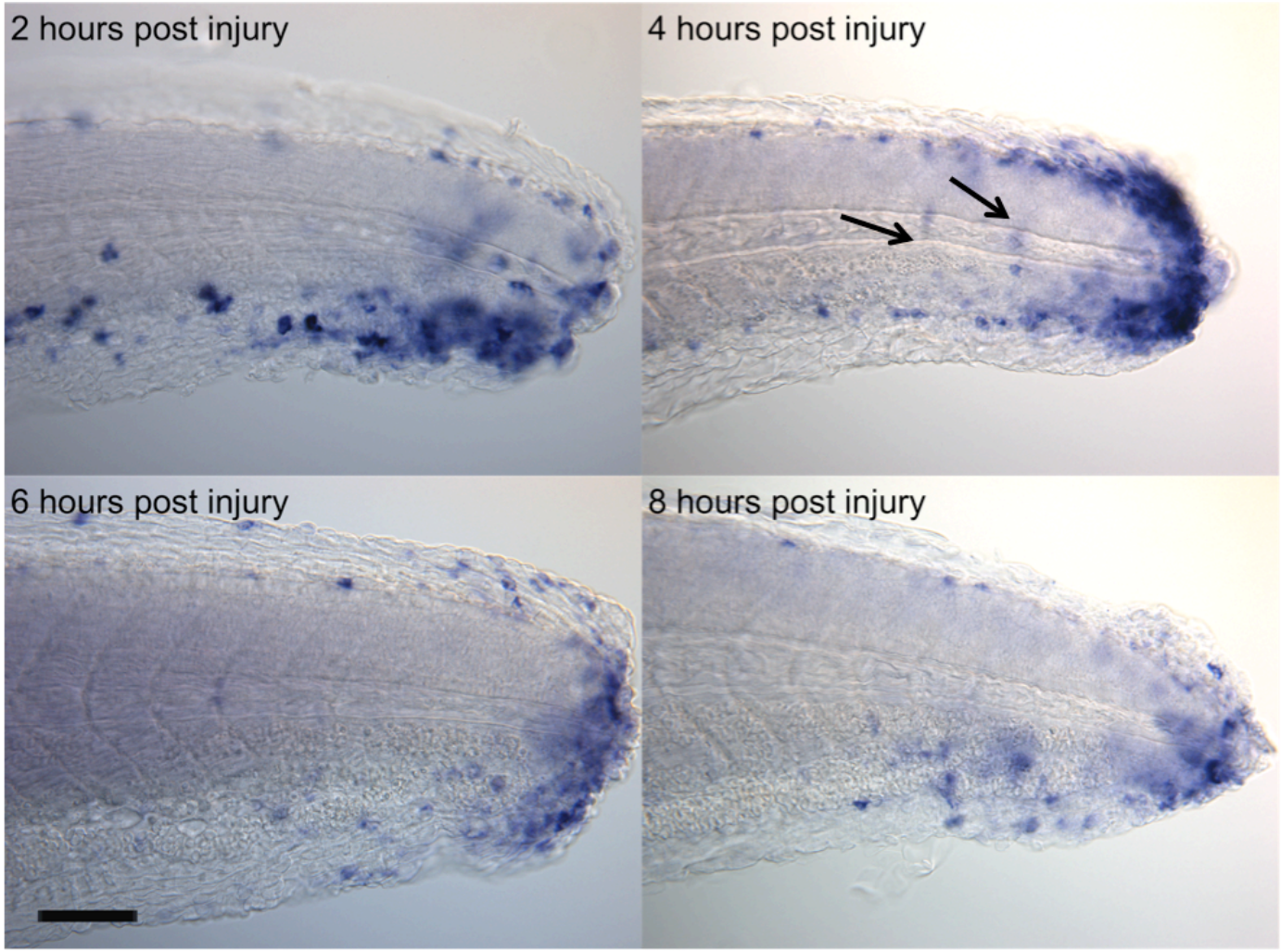

Figure 4.7. IL-1β staining reveals that stained cells cluster in patterns similar to the distribution of endothelial tissue and the site of injury in a tail fin injury assay. High-resolution compound microscopy using a 40x objective of IL-1β WISH embryos shows the induction of IL-1β transcription in response to injury. Arrows indicate clustering of stained cells around the expected location of intersegmental vessels and dorsal aorta. Scale = 50 μm

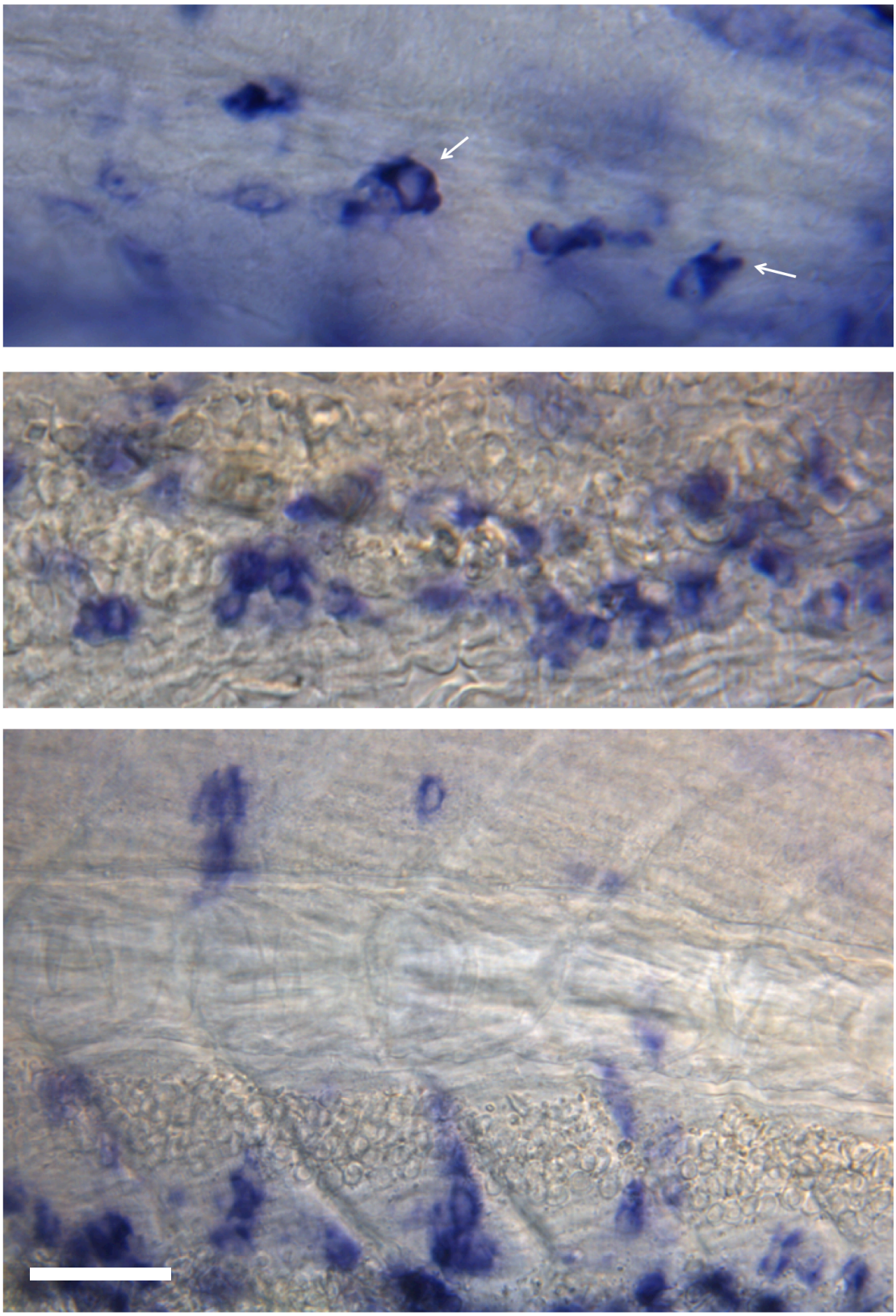

Figure 4.8. IL-1β expression is upregulated in macrophage like cells in response to injury. High-resolution microscopy of injured 48hpf embryos show WISH staining is localized to large mononuclear, morphologically irregular and non-localised cells. scale bar= 20 μm

4.2 Caspase and P2X7 inhibition on markers of inflammation

4.2 1 NF-κB signaling reporters

NF-κB is a critical component of the IL-1β signaling pathway and, as described previously, is responsible for inducing its transcription. NF-κB plays an important role in a number of further inflammatory processes as well as in development and regeneration in the zebrafish (Kanther et al. 2011). Kanther *et al* (2011) have previously described the construction of an NF-κB reporter transgenic zebrafish in which EGFP is induced in cells in response to the activation of NF-κB. This group kindly provided the construct used to generate this reporter line enabling me to generate a new allele of this reporter line by injecting this reporter into WIK wild-type embryos. Once grown, screening by pair mating to wild types showed that approximately 15% of the adults were capable of transmitting the transgene to their progeny. Of these adults, approximately 10% had progeny of mixed intensities.

During development, *Tg(pNF-κB:EGFP)sh235* expresses EGFP in neuromast support cells, muscle, epithelium, immune cells, and endothelial cells (Figure 4.9); indicating active NF-κB in these tissues during growth and development. The line founder transmitted the allele to more than the 50% of progeny expected for a single allele of the transgene, and embryos derived from this founder had a mix of fluorescent intensities (Figure 4.10); indicating the presence of more than a single allele and therefore multiple insertions of the transgene.

Based on their fluorescent intensity it was decided that embryos with multiple insertions would make a more effective reporter with regards to reducing exposure and decreasing acquisition time during imaging, however, the presence of larvae with various levels of EGFP expression is a potential source of experimental error and therefore necessitated the development of an experimental strategy to reduce this error.

Larvae derived from the F1 generation showed a mix of fluorescent intensities corresponding to a mixture of copy numbers carried by each offspring. Quantitative assays using this line require an unbiased and fluorescently homogenous baseline intensity to reduce error; therefore, sufficient embryos of approximately the same fluorescent intensity were selected from each embryo

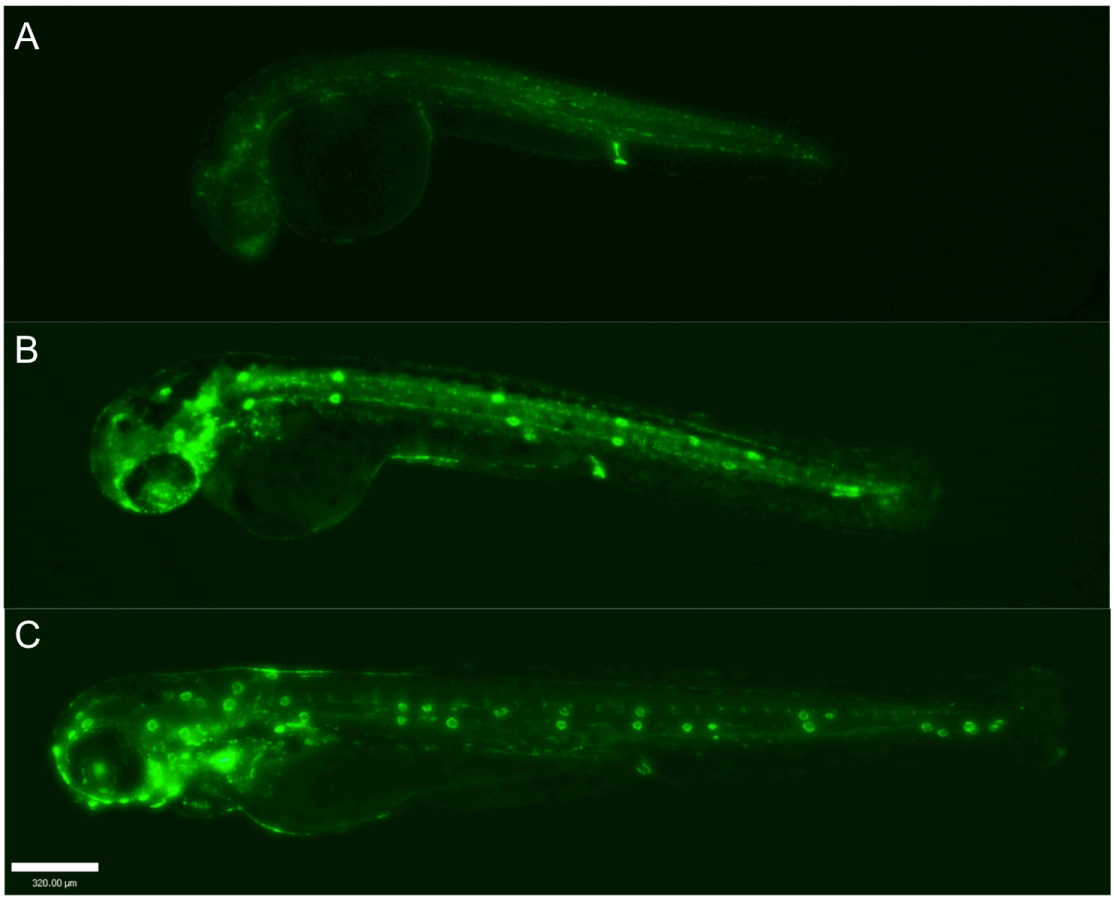

Figure 4.9. T*g(NF-κB:EGFP)sh235,* a reporter of NF-κB activation, shows significant activity of NF-κB during development. *Tg(pNF-κB:EGFP)sh235* demonstrates the temporal and spatial pattern of NF-κB activation during development. (A) At 24hpf, NF-κB is active in the musculature, with further expression in neuromast support cells and endothelium at later timepoints of 48 (B) and 72 hpf (C). Scale bar =320 μm

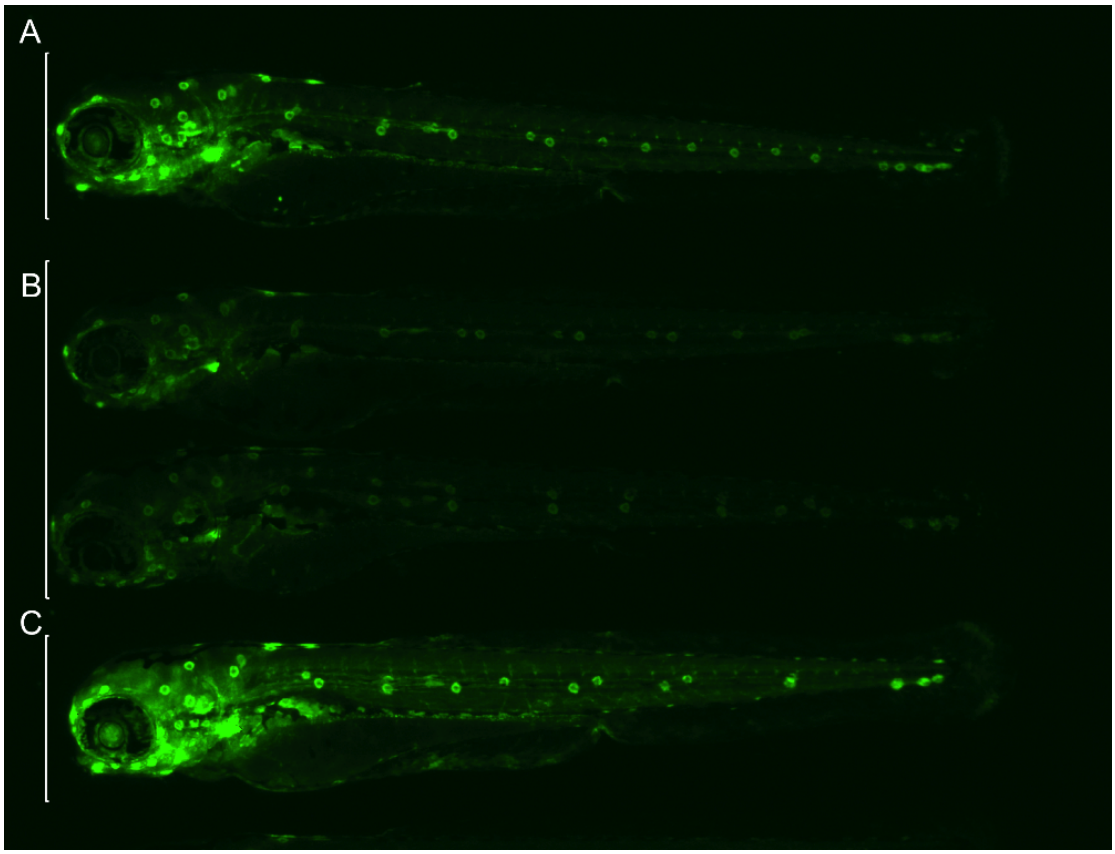

Figure 4.10. *Tg(pNF-κB:EGFP)sh235* siblings show a varying intensity of EGFP indicating multiple insertions of the expression vector. 72hpf sh235 embryos from the same clutch show at least 3 different brightnesses (A, B and C). Homozygous and heterozygous embryos would only account for two phenotypic variants, therefore more than 1 allele of the gene must be present.

clutch collected for each experiment. Consequently, results from these embryos must also be normalized to the particular intensity of the control embryos from each experiment in order for results between experiments to be compared. This will also correct for any differences in hardware functioning with regards to fluorescent transmission efficiency between experiments.

For quantitative assays with this line, the control sample numbers were increased to 30 to provide increased statistical power to account for the variation in embryo intensity and microscope function between experiments.

The large numbers of controls were averaged for each repeat experiment and these averages compared between experimental repeats to determine the proportional change in intensity due to the embryo selection and any alterations made to microscopy hardware between experiments. The difference was used to generate a multiplication factor for the change, which was used to normalise every data point in each experiment by the average intensity difference between each experiment denoted by this factor. This enabled the normalised data to be pooled between experimental repeats for statistical analysis.

4.2.2 *Tg(pNF-κB:EGFP)sh235* as a reporter of inflammation

I hypothesised that inhibition of IL-1β pathway components will reduce IL-1β release and consequently inflammation at the site of injury in zebrafish. In WISH assays (Figures 4.3-4.8), injury was the most powerful stimulant of IL-1β mRNA production. Here, I used an injury assay to investigate the effects of P2X7 and caspase-1 inhibitors on assays of inflammation.

In mammals, the P2X7 receptor is responsible for the activation of the NLRP3 inflammasome via reception of the DAMP stimulus extracellular ATP. Due to the high levels of conservation between mammalian and zebrafish P2X7 receptors (López-Castejón, M. Young, et al. 2007), I hypothesised that P2X7 inhibition would have a similar effect on IL-1β production (Figure 4.11). This response was not directly observable due to the lack of a characterised IL-1β specific reporter and was measured indirectly using the *Tg(pNF-κB:EGFP)sh235* line as a readout of inflammatory signalling at the site of injury. I initially

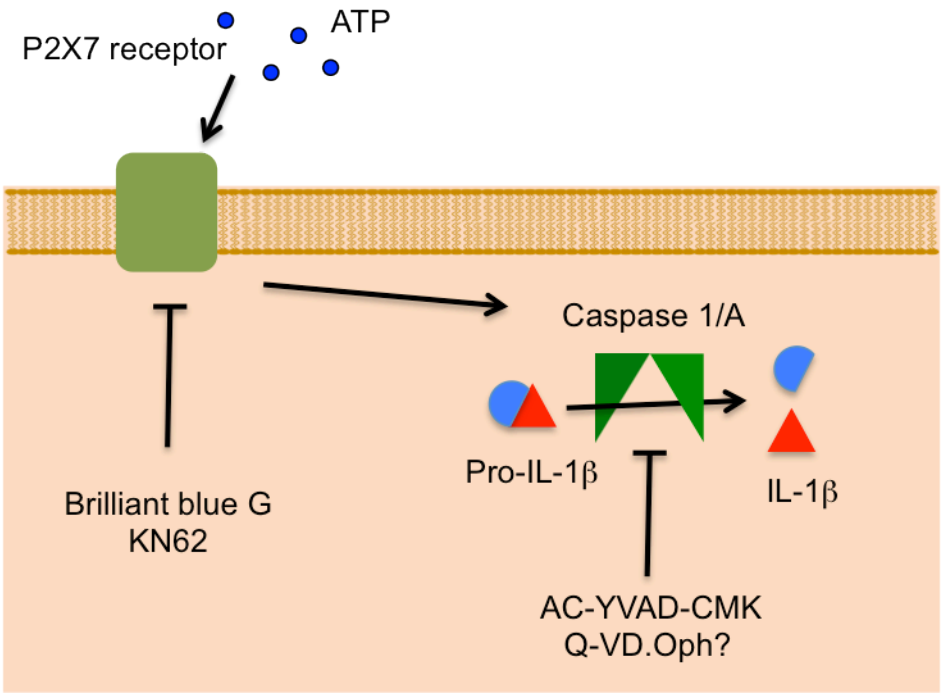

Figure 4.11 Inhibition of P2X7 (Sanz & Di Virgilio 2000) **and caspase-1** (B. Miller et al. 1995) **function leads to a reduction in mature Il-1β production**. Reduction of IL-1β signalling via P2X7 and caspase-1 inhibition reduces inflammatory signalling, and I hypothesise that inhibiting this pathway in zebrafish would result in a reduction of inflammatory signalling in inflammatory assays.

characterised the injury response in these fish; embryos mounted and imaged from an hour post injury revealed that NF-κB activation measured by EGFP intensity increases at the site of injury over the 8-hour experimental time course (Figure 4.12 A). Concurrent with the increase in fluorescence induced by injury, leukocytes, distinguished by their irregular morphology and rapid movement (Figure 4.12 B) (visible in a time lapse movie), can be seen migrating towards the site of injury; however, most of the EGFP signal at the site of the injury originates from the damaged tissues themselves.

The increase in EGFP fluorescence was used as a readout of fluorescence and an assay around the modulation of this signal was developed. 72hpf *Tg(pNF-κB:EGFP)sh235* embryos were injured and treated with P2X7 inhibitors Brilliant Blue G and KN62 and imaged 8 hours post injury (hpi). The fluorescence at the site of injury was compared with untreated embryos (Figure 4.13) and showed a trend towards decrease that did not reach statistical significance. A power calculation performed on the mean of this data revealed that sample sizes would have to be increased to 30 for Brilliant blue and 70 for KN62 to have 90% confidence in the statistical difference.

To more directly measure the effect of caspase A activation, the experiment was repeated with caspase-1 inhibitor AC-YVAD-CMK. The caspase-1 and caspase-A proteins share similar sequence specificities (Masumoto et al. 2003) and I hypothesised that AC-YVAD-CMK would therefore inhibit caspase-A. *Tg(pNF-κB:EGFP)sh235* embryos treated with AC-YVAD-CMK showed a significant decrease in NF-κB activation at the site of injury compared to DMSO control treated embryos (Figure 4.14). This effect was not repeated with the pan-caspase inhibitor Q-VD.OPh. These data indicate that the NF-κB pathway is susceptible to inhibition with the caspase-1 specific inhibitor AC-YVAD-CMK, and potentially sensitive to P2X7 inhibition, supporting the hypothesis that inhibiting proteins in the IL-1β processing and release pathway negatively regulates the inflammatory response.

4.2.3 Caspase A inhibitor AC-YVAD-CMK and P2X7 inhibitors KN62 and Brilliant blue G reduce neutrophil recruitment to sites of injury

Tg(pNF-κB:EGFP)sh235 acts as a reporter based on NF-κB activation, a pathway relevant in significantly more than the inflammatory signalling

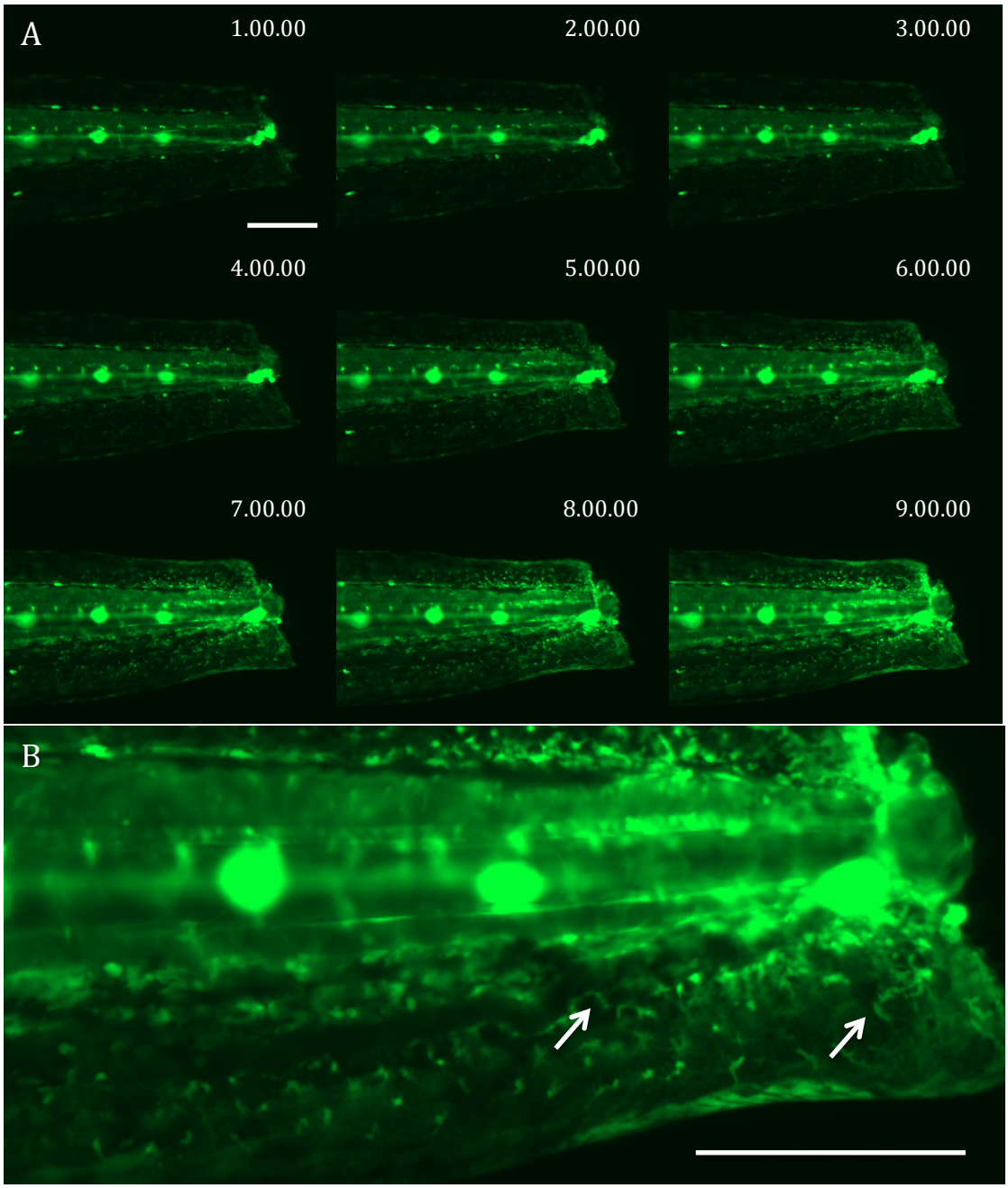

Figure 4.12. NF-κB is activated in response to injury. 72hpf *Tg(pNF-κB:EGFP)sh235* embryos injured by tail transection show the induction of EGFP at the site of injury in response to NF-κB activation over a 9 hour timespan measured by widefield microscopy (A). Images taken every 120 seconds and viewed as a timelapse show that EGFP fluorescence is present in motile cells with an irregular morphology, signifying NF-kB activation in this cell population (B, white arrows). time in hh:mm:ss –displaying hours post injury, Scale = 300μm

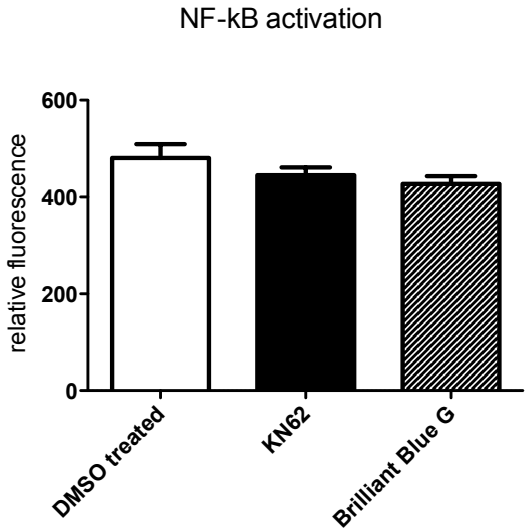

Figure 4.13. P2X7 inhibitors Brilliant Blue G and KN62 have no significant effect on NF-κB activation in response to injury. NF-κB activation at the site of injury assayed using *Tg(pNF-κB:EGFP)sh235* as an NF-κB activation reporter, is not significantly affected by mammalian P2X7 inhibitors Brilliant Blue G and KN62 (one way ANOVA with Dunnet's post test, n=3, 20 fish per treatment group)

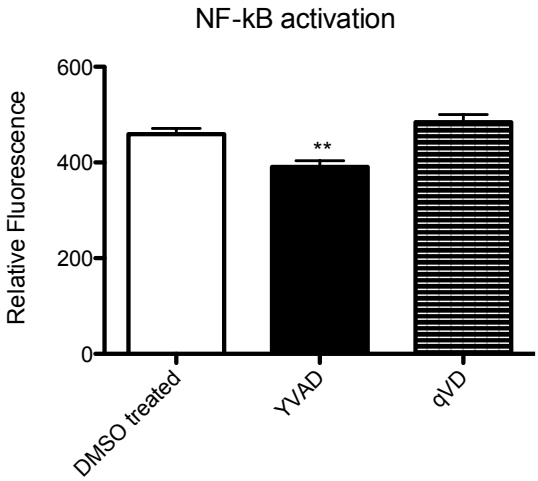

Figure 4.14 Caspase-1 inhibitor AC-YVAD-CMK downregulated the activation of NF-κB at the site of injury. NF-κB activation at the site of injury assayed using *Tg(pNF-κB:EGFP)sh235* as an NF-κB activation reporter, is reduced when treated with mammalian caspase-1 inhibitor AC-YVAD-CMK 8 hours post injury. Pan-caspase inhibitor Q-VD.OPh has no effect. (one way ANOVA with Dunnet's post test, n=3, 20 fish per treatment group)

investigated here, and a proportion of the signal detected here in response to injury is also likely to be linked to wound healing and regeneration of the injured tissue. In order to look at the inflammatory pathways in more detail, a more specific assay of inflammation was required. *Tg(mpx:EGFP)i114* (Renshaw et al. 2006) specifically labels neutrophils and allows the monitoring of their behaviour in response to inflammatory stimuli. This line has been used in the study of recruitment and resolution of inflammation at sites of injury (Ellett et al. 2010), also investigated using other leukocyte markers (L. Li et al. 2012). I used this as a more specific assay of inflammation to investigate P2X7 and caspase-A inhibition. Injured 3dpf *Tg(mpx:EGFP)i114* were treated with P2X7 inhibitors Brilliant blue G and KN62 and neutrophils recruited to the site of injury were counted after 6 hours. Both inhibitors significantly reduced the recruitment of neutrophils to the injury (Figure 4.15), indicating a negative effect on the overall inflammatory response. Treatment with caspase inhibitors AC-YVAD-CMK and Q-VD.OPh, resulted in a decrease in neutrophil recruitment after AC-YVAD-CMK treatment, but not treatment with pan-caspase inhibitor Q-VD.OPh (Figure 4.16). Inflammatory signalling at the sites of injury was reduced by the inhibition of P2X7 and caspase-A in zebrafish on the basis of neutrophil recruitment to sites of injury.

4.3 Macrophage recruitment as a reporter of inflammation

4.3.1 Macrophage recruitment to sites of injury.

The inflammatory response involves a number other cells as well as neutrophils and as discussed in chapter 1, studies of mammalian models of IL-1β biology have revealed the importance of macrophages in the production and signaling pathways of IL-1β. IL-1β is also detected by mammalian macrophages, inducing the expression of other inflammatory signals and responses. *In situ* data presented in this study (Figures 4.3-4.8) suggest that IL-1β is expressed in macrophages in response to injury, but were unclear whether zebrafish macrophages also respond to this cytokine.

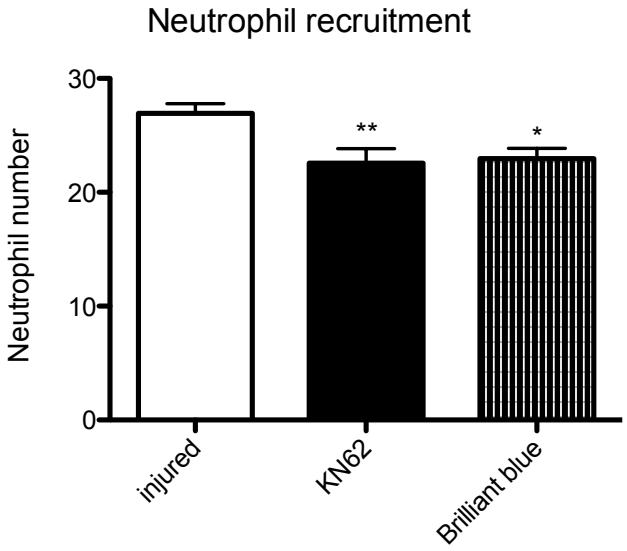

Figure 4.15. Neutrophil recruitment in *Tg(mpx:EGFP)i114* is reduced by treatment with P2X7 inhibitors Brillaint Blue G and KN62 *Tg(mpx:EGFP)i114* show a reduction in neutrophil recruitment 6 hpi when treated with Brilliant Blue G and KN62 (one way ANOVA, Dunnett's post test. n=3, 8 fish per treatment group)

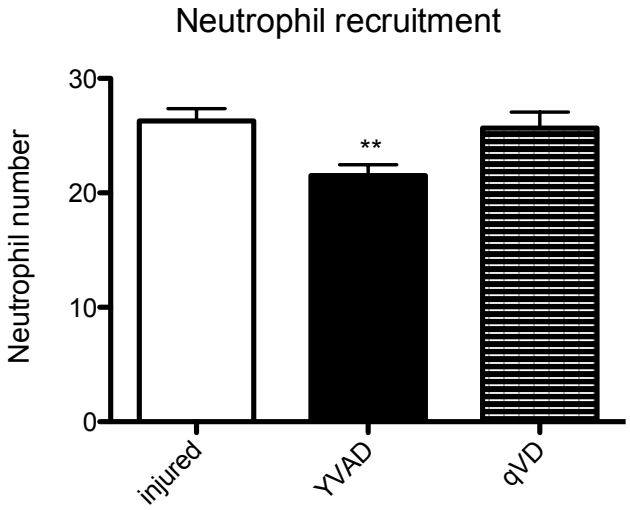

Figure 4.16. Mammalian caspase inhibitor AC-YVAD-CMK reduces neutrophil recruitment to the site of injury. AC-YVAD-CMK significantly decreases neutrophil recruitment to the site of injury in *Tg(mpx:EGFP)i114* 6 hours post injury in a tail fin injury assay, pan caspase inhibitor Q-VD.OPh has no significant effect. (one way ANOVA, Dunnett's post test. n=3, 8 fish per treatment group)

4.3.2 Macrophage specific transgenic lines

Tools to study macrophage behaviour were limited to the *Tg(fms:Gal4.VP16)i186;Tg(UAS:nsfB.mCherry)i149* compound line. The *fms* promoter drives Gal4-VP16 in macrophages, xanthophores, neuromasts and hindbrain; and is therefore not macrophage specific. Macrophages can be identified from other labelled cells only by their motility, morphology and size. The driver line is crossed to a UAS driven mCherry tag, however, a significant part of the mCherry signal has been lost over successive generations (Figure 4.17). The occurrence of UAS promoter silencing has been previously reported (Akitake et al. 2011), however in the majority of these fish the silencing is severe enough to prevent the identification of more than a minority of macrophages. The use of these fish for the previously described recruitment assays is further complicated by the presence of a large number of xanthophores in the tissue of the tail fin, making macrophage counting at the site of injury more difficult. Macrophages in the *Tg(fms:Gal4.VP16)i186;Tg(UAS:nsfB.mCherry)i149* can still be identified using confocal microscopy to select a focal plane excluding the epithelial layers where xanthophores are localized, however, the limited thickness of the fish around the tail where injury assays are performed limits this approach. For these reasons, I looked for alternatives for investigating macrophage recruitment and macrophage behaviour.

Recently, Ellet *et al* (2010) have published the discovery of a significantly improved macrophage specific reporter. The *mpeg1* promoter line is macrophage specific during the larval stage, making it far more effective as a macrophage label than the *fms* promoter line in zebrafish embryos due to the lack of expression in other cell types.

I used the *mpeg1* promoter entry clone described in the Ellet *et al.* (2010) paper to generate a Gal4 expression vector using gateway cloning. The 5' *mpeg1* entry clone was combined with the middle entry Gal4 entry clone, the 3' entry polyA entry clone and the PA2 destination vector from the Tol2Kit (Kwan et al. 2007)

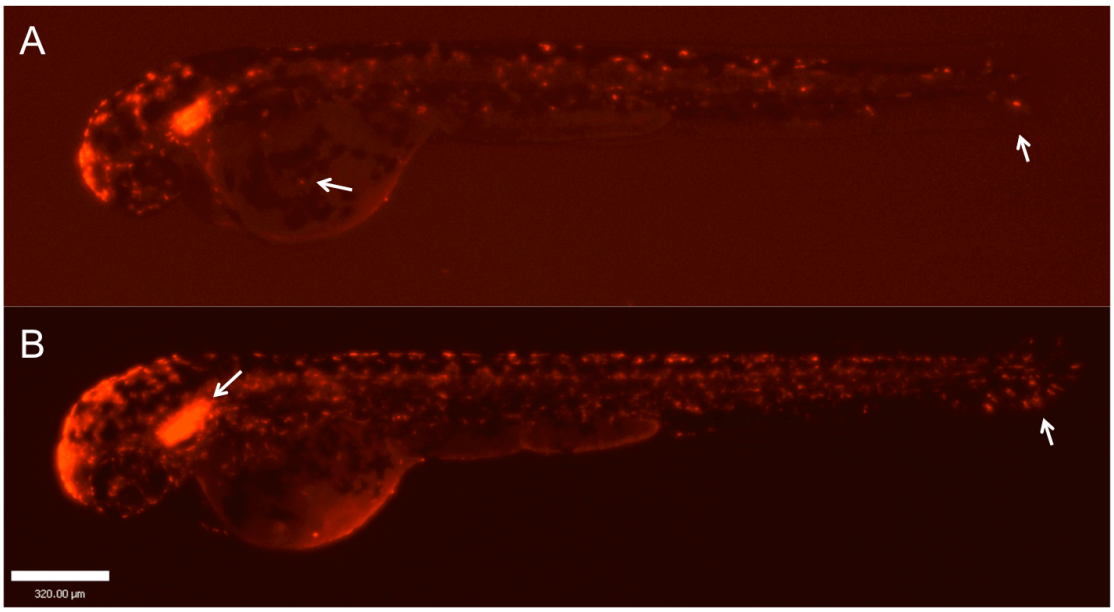

Figure 4.17. *Tg(fms:Gal4.VP16)i186;Tg(UAS:nsfB.mCherry)i149* is a transgenic marker of macrophages. *Tg(fms:Gal4.VP16)i186;Tg(UAS:nsfB.mCherry)i149* expresses the nitroreductase mCherry fusion protein in a number of tissues, including macrophages, xanthophores, hindbrain and neuronal cells. Xanthophores in the tissue of the tail (arrows show xanthophores at the tail, expression in the hindbrain and neuronal cells and macrophages over the yolk) make distinguishing macrophage recruitment and resolution in response to injury particularly problematic. Siblings from the same clutch, (A) and (B), imaged at differing exposure settings to demonstrate markedly different levels of expression and fluorophore intensity, probably releated to significant methylation of the UAS promoter (Akitake et al. 2011). Scale bar = 320 μm

to yield a tol2 equipped *mpeg1*:gal4 construct. I injected this construct into AB wild types alongside tol2 mRNA. Once grown, the fish were crossed to a *Tg(UAS:Kaede)* fish line and screened for fluorophore expression. A founder was identified by the expression of Kaede in macrophages. The *Tg(UAS:Kaede)* line used has been generated relatively recently and so shows a low level of UAS silencing remaining useable for quantitative assays, however, care must be taken when selecting a group of embryos for the assay to ensure all embryos have approximately the same number of labelled macrophages. As shown in Figure 4.18, our *Tg(mpeg1:Gal4.VP16)sh256*, *Tg(UAS:Kaede)* has significantly more macrophage specificity than *Tg(fms:Gal4.VP16)i186;Tg(UAS:nsfB.mCherry)i149*, with far less off target expression. Labelled macrophages can be seen in both fish lines (Figure 4.18 B and C) however the *fms* promoter makes it very difficult to distinguish macrophages from other cell types, which interfere with visualizing macrophages directly when using non-confocal microscopy.

4.3.3 Macrophage rectruitment to sites of injury is inhibited by caspase-1 Inhibitor AC-YVAD-CMK and P2X7 inhibitors Brilliant Blue G and Kn62

With a reliable macrophage *mpeg1* marker it was possible to investigate the effects of AC-YVAD-CMK on macrophage recruitment. Published data describes the role of macrophages in wound healing and inflammation resolution, as well as the development of endothelial tissue in angiogenesis; however, the recruitment of macrophages at an early stage of inflammation, the upregulation of IL-1β mRNA in response to injury and the role of macrophages in mammalian inflammation imply that macrophages are important in the initial stages of inflammation. *Tg(mpeg1:Gal4.VP16)sh256*:*Tg(UAS:Kaede)* embryos were injured as described previously and treated for 6 hours with AC-YVAD-CMK and Q-VD.OPh. The number of macrophages at the site of injury was counted after 6 hours. AC-YVAD-CMK significantly decreased the recruitment of macrophages to the wound whereas Q-VD.OPh had no effect (Figure 4.19). P2X7 inhibitors Brilliant Blue G and KN62 also significantly reduced macrophage recruitment to the site of injury (Figure 4.20).

4.4 Effects of caspase-1 and P2X7 inhibitors on inflammatory markers

In summary, these data show that the IL-1β mRNA message is induced in response to injury and to a lesser extent in response to the injection of *Vibrio anguillarum* DNA, though it is unclear whether this response is due to the presence of the pathogen DNA, or due to the non sterile nature of the injection. This message is stained in mononuclear cells with an irregular morphology which cluster around the yolk sac, CHT and expected sites of intersegmental vessels and appear to have been fixed in the process of migrating towards the site of injury, all behaviours characteristic of macrophages. Futhermore, using NF-κB activation, neutrophil recruitment and macrophage recruitment as markers of inflammation, these data show that mammalian caspase-1 inhibitor AC-YVAD-CMK decreases the inflammatory response, as do mammalian P2X7 inhibitors Brilliant Blue G and KN62.

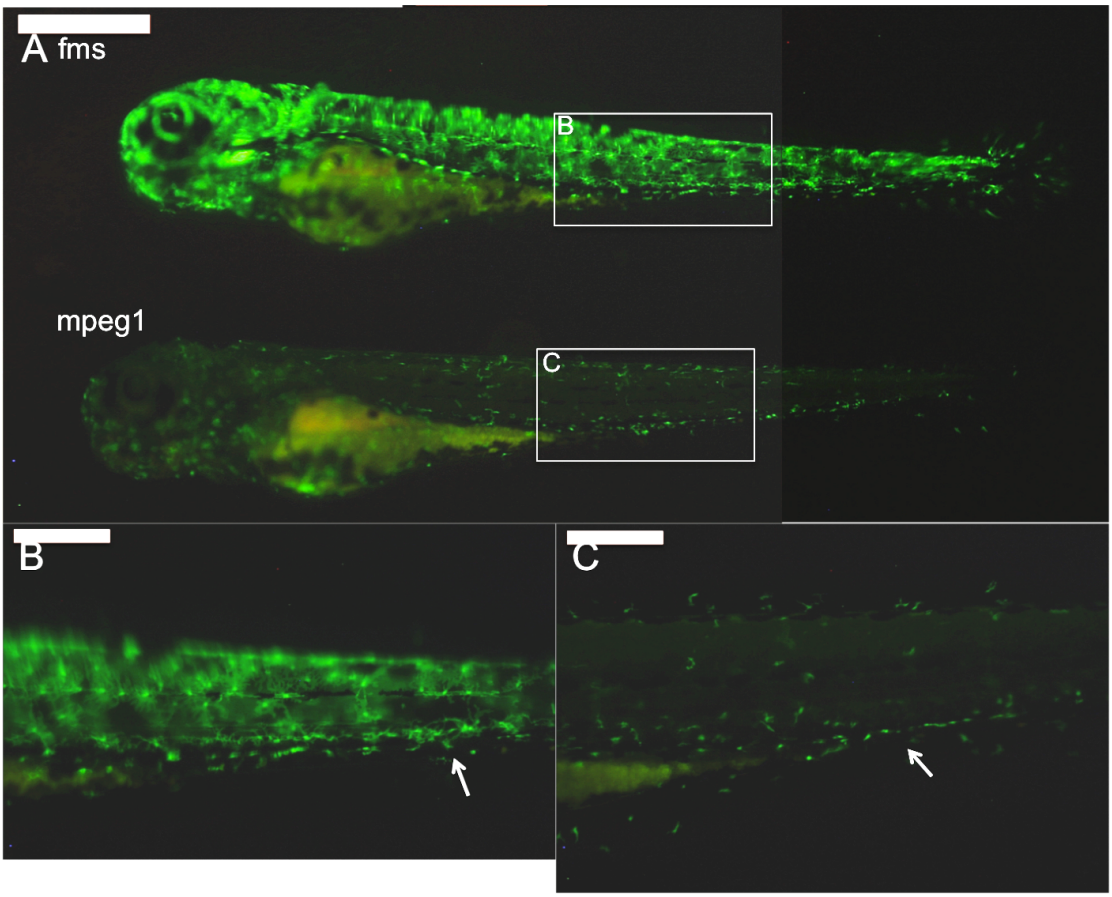

Figure 4.18. *Tg(mpeg1:Gal4.VP16)sh256* is a more reliable macrophage marker than *Tg(fms:Gal4.VP16)i186 in embryonic zebrafish.* A. the *fms* promoter and *mpeg1* promoter driving *Tg(UAS:Kaede).* The *mpeg1* promoter has significantly improved macrophage specificity than *fms*, with fewer non-macrophage tissues labelled. Macrophages can be seen throughout the fish and within the tissue of the CHT (arrows). Scale = 500 μm (A), 200μm (B, C)

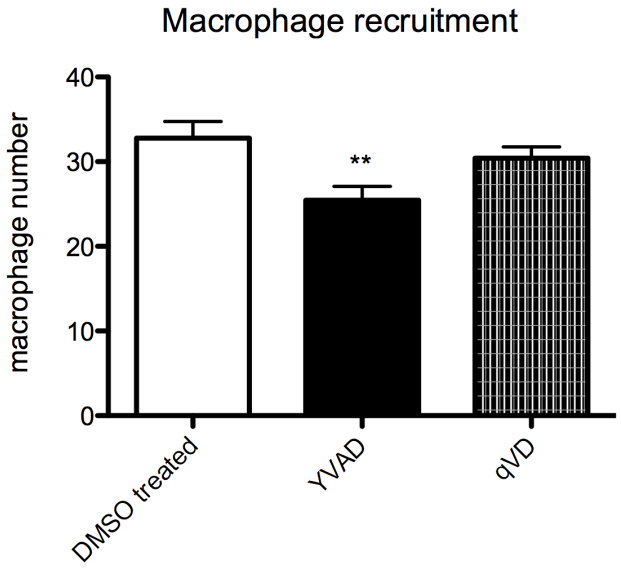

Figure 4.19. Macrophage recruitment to the site of injury is inhibited by mammalian caspase-1 inhibitor AC-YVAD-CMK. Caspase-1 inhibitor AC-YVAD-CMK reduces recruitment of macrophages to the site of injury in *Tg(mpeg1:Gal4.VP16)sh256*, *Tg(UAS:Kaede)* embryos when assayed at 6hpi. (one way ANOVA, Dunnett's post test. n=3, 8 fish per treatment group)

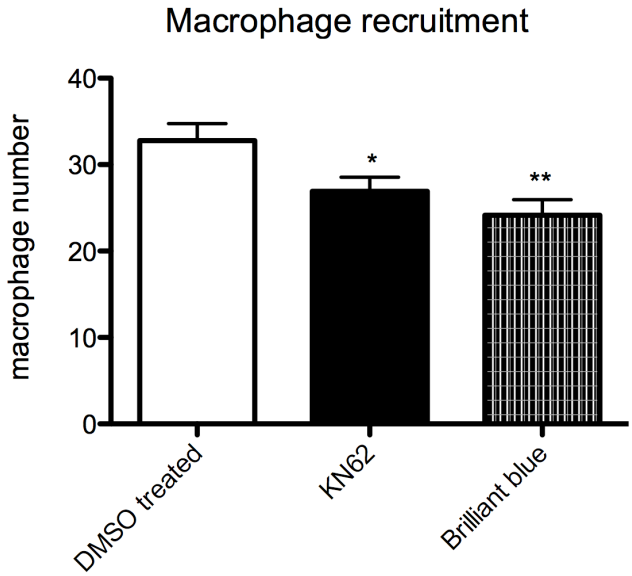

Figure 4.20. Macrophage recruitment to the site of injury is inhibited by mammalian P2X7 inhibitors KN62 and Brilliant Blue G. P2X7 inhibitors Brilliant Blue G and KN62 reduce the recruitment of macrophages to the site of injury in *Tg(mpeg 1:Gal4.VP16)sh256*, *Tg(UAS:Kaede)* embryos when assayed at 6hpi. (One way ANOVA, Dunnett's post test. n=3, 8 fish per treatment group)

4.5 Discussion

4.5.1 *V. anguillarum* DNA as an inducer of inflammation

IL-1β signaling did not appear to be induced by infectious stimuli. Neither LPS nor V. anguillarum DNA increased the staining for IL-1β mRNA via WISH, which is particularly puzzling due to the way the V. anguillarum DNA was prepared. The V. anguillarum DNA sample was a kind gift of Victor Mulero (Murcia Spain). It is a miniprep of a liquid culture of VA, and as such it is expected that the miniprep protocol will not have removed many pathogen associated molecular patterns present in such a culture. The failure of this to elicit a response implies that, as a pathogen, VA DNA doesn't stimulate the IL-1β pathway in zebrafish. Alternatively, if the miniprep was too efficient at removing genomic bacterial DNA leaving just inserted plasmids, it wouldn't have contained any of the molecular patterns necessary to induce IL-1β; in which eventuality an induction of pro inflammatory pathways downstream of IL-1β wouldn't be expected at all, unless this DNA was capable of inducing TLR signalling. When injected into *Tg(pNF-κB:EGFP)sh235* embryos, VA DNA greatly increases the fluorescent intensity of EGFP throughout the fish, indicating that the pathway is activated by the injection, however, with the presence of multiple NF-κB:EGFP alleles in the line, it is impossible to quantitively assay this response and perform further experiments on whether this is due to the presence of the VA DNA sample, or the injection itself. This could be investigated with the preparation of a new sample of V. anguillarum DNA using a more stringent purification method, such as a phenol chloroform extraction or with injection in sterile conditions. The latter would indicate whether the injection itself was promoting an inflammatory response, whereas the former would inform on whether the response was due to sample preparation. I think its unlikely that the response is due to the presence of the pathogenic DNA, and that it is more likely due to other factors in the sample or injection. Pattern recognition receptors would be more likely to be activated by PAMPs than by the bacterial DNA and it is more likely that this is what causes the response seen in the *Tg(pNF-κB:EGFP)sh235* line however, the injection protocol is not sterile, so could induce NF-κB signalling on its own.

Induction of IL-1β message by pro-inflammatory stimuli

The *in situ* data using an IL-1β hybridization probe supports the hypothesis that the increase in NF-κB activity is due to injection. As Figures 4.2 and 4.3 show, the injected embryos show a slight increase in IL-1β mRNA expression but also show some abnormal development (second and fourth fish in Figure 4.2 and second fish in Figure 4.3), but as a WISH, this is difficult to quantify. Abnormal development is a typical response when >1nl is injected into zebrafish embryos from an early stage and can be seen in RNA, DNA and morpholino injections to varying degrees. An effect on the gross morphology on the fish would also be expected to result in aberrant transcription factor signalling, such as increased NF-κB activation. For these reasons, It is more likely that any effects seen from injecting the DNA are more likely due to injection trauma. This leaves the injury as the most viable technique to investigate inflammatory responses. It is important to note that WISH reports the presence of mRNA, and does not report signal induction. It is possible that injury is stimulating mRNA stability (Bufler et al. 2004), and the resulting signal could be a result of both induction and increased mRNA stability.

The induction of IL-1β mRNA was very strong in response to injury and demonstrates the importance of this cytokine in the inflammatory response. The pattern of induction suggests that IL-1β is more important at earlier stages of injury where IL-1β is induced in immune cells throughout the embryo 2 hours after injury and the strongest response appears to be after around 4 hours. This suggests that IL-1β is important in inducing parts of the inflammatory response rather than in its resolution, which matches data in mammalian cells where IL-1β is described as a pro inflammatory cytokine. Interestingly, there is also less probe trapping at the site of injury at 2 hpi, than in 4-8 hpi embryos (Figure 4.6) and from these data it is difficult to determine whether this indeed is a result of probe trapping, or a physiological response to injury. This could be investigated by determining the cellular localisation of the IL-1β staining through double WISH staining. In *Tg(pNF-κB:EGFP)sh235* embryos, NF-κB signalling is active in other, non leukocyte tissues (Figure 4.11) implying the activation of inflammatory pathways in these tissues. It may be possible to use a similar system to investigate

IL-1β specific gene activation by using the IL-1β promoter to drive EGFP rather than NF-κB response elements.

The data suggest that due to expression at such an early developmental stage, before the appearance of neutrophils, staining in cells with leukocytic morphology and large, single nuclei and localization to sites of haematopoiesis over the yolk and in the CHT, that these stained cells are macrophages. In later developmental stages there appears to be an induction of the IL-1β message in a greater number of cells, which could correspond to either the increase in macrophages at later developmental stages, as these cells develop or the induction of IL-1β in other immune cells such as neutrophils. In future work, I would investigate IL-1β localisation using a double *in situ* for IL-1β and a macrophage marker to determine whether the IL-1β signal is in fact in macrophages, and whether other cell types are also responsible for this response. Nevertheless, these data suggest that the evolutionary importance of IL-1β in response to injury in the inflammatory response is conserved between humans and zebrafish.

4.5.2 *Tg(pNF-κB:EGFP)sh235* as a tool to study inflammation

Though the *Tg(pNF-κB:EGFP)sh235* line proved useful for this study, it has significant limitations when performing quantitative assays. Crosses to yield transgenic embryos must be carefully performed to control the number of alleles each embryo has as this has a direct effect on the intensity of the zebrafish. However, the line has limited fluorescent intensity with just a single insertion, so a mechanism to increase the brightness of the transgene, such as increase in copy number, is necessary. The fish is most reliable as a homozygote with a single allele insertion, but best imaged and measured with multiple insertions or alleles. In this study I approached the issue by first sorting the embryos at 4 hpf to remove any embryos born earlier or later than this timepoint so all embryos were at the same developmental stage to reduce any difference in protein expression due to development for each experiment, at 72hpf, the embryos were again sorted by eye under a fluorescence dissecting scope to select embryos of approximately the same brightness, these were randomly allocated to treatment groups without the use of a fluorescence microscope to avoid experimental bias. This approach avoids errors

introduced through changes in transgene intensity brought about by copy number or developmental level, but uses embryos of a sufficient fluorescent intensity to be easily imaged and quantified. The importance of compensating for copy number or fluctuations in intensity due to developmental status cannot be overstated, and an approach that limits the errors due to these factors yet maintains a strong fluorescent intensity for quantitation, like the approach described in this study, is recommended.

The change in the NF-κB signal upon treatment with the inhibitors tested appeared to be very small, leading to a large number of embryos needed in order to increase statistical power. NF-κB is important in zebrafish development as evidenced by its expression in a large number of cell types at 72hpf when these assays were performed (Figure 4.9), and the role of NF-κB in wound healing and regeneration has already been reported. A tail fin injury assay of NF-κB activation in response to injury would be expected to initiate both inflammatory and wound healing responses, and it is only the inflammatory responses that are expected to be susceptible to modulation by caspase-1 and P2X7 inhibitors; therefore, the change in signal from NF-κB activation is expected to be very small. To achieve the statistical power necessary for quantifying this response, it is necessary to remove as much experimental error and noise from this system as possible. In this study, this approach necessitated the use of larger numbers of embryos than for the leukocyte recruitment assays.

In this study I used NF-kB activation as a marker of inflammatory signalling, however, NF-kB is important in significantly more than inflammatory function (Baeuerle & Baltimore 1996), further evidenced by the activation of NF-kB not only in injury but also in developmental processes (Figure 4.9). the roles of NF-κB in these functions questions its reliability as an inflammatory reporter. A more specific reporter would require EGFP induction under a gene induced by inflammatory stimuli, such as IL-1β itself, also capable of being induced by itself (Dinarello et al. 1987), and it would be interesting to repeat these assays in such a reporter.

4.5.3 Effects of caspase-A and P2X7 inhibition on inflammatory signalling

Experimentally, mammalian caspase-1 inhibitor AC-YVAD-CMK decreased both NF-κB activation at the site of injury, as well as decreasing the recruitment of macrophages and neutrophils to the wound. Although it is unclear whether AC-YVAD-CMK inhibits the zebrafish caspase-1 equivalent caspase-A, published data (Masumoto et al. 2003; Vojtech et al. 2012) suggest that this is likely to be the case based on the target sequence specificity of caspase-A. This study shows that AC-YVAD-CMK affects inflammatory initiation and therefore suggests a homologous role for caspase-A in zebrafish inflammatory signalling. NF-κB is downstream of IL-1β signalling in IL-1 sensitive cells and an inhibition of IL-1β release would effect this downstream signalling and reduce the fluorescent signal from NF-κB activation. A resulting reduction in the activation of downstream cells would also inhibit the release of further inflammatory factors and result in a reduction in the inflammatory response and the recruitment of further immune cells to the site of injury. The reduction of neutrophil and macrophage recruitment to the site of injury could also be due to a more direct effect of caspase A inhibition and the reduction in direct IL-1β exposure of these cells.

A pan-caspase inhibitor, Q-VD.OPh had no effect on the recruitment of leukocytes and NF-κB activation at the site of injury, however it would be expected to at least match the effect of AC-YVAD-CMK on caspase A. As a pan caspase inhibitor, Q-VD.OPh would also be expected to affect pro apoptotic caspases. Three possible explanations for the lack of response to Q-VD.OPh treatment on NF-κB activation and leukocyte recruitment are that perhaps Q-VD.OPh either does not penetrate the fish to sites of activity as well as AC-YVAD-CMK does; that Q-VD.OPh is not compatible with zebrafish caspases, or that any decrease in caspase-A based inhibition is offset by an increase in cells being targeted towards a necrotic rather than apoptotic cell death pathway, a subsequent increase in necrotic cell debris and the consequent increase in additional inflammatory signalling. This increase could mask a reduction in caspase-1 mediated signalling and I would expect would also result in a larger increase in the inflammatory markers investigated than was shown. It is therefore more likely that zebrafish are insensitive to Q-VD.OPh via either its incompatibility with zebrafish caspases, or its inability to reach sites of

caspase activation. Other studies in the Renshaw lab have failed to show an effect of this inhibitor in inflammation resolution assays.

The similarities in zebrafish and mammalian P2X7 receptors have already been studied, however, the data in this study imply that P2X7 is also functionally conserved in zebrafish. Treatment with P2X7 inhibitors negatively affected leukocyte recruitment at the site of the injury demonstrating its role in inflammatory signalling. However, the same inhibitors failed to affect NF-κB activation at the site of injury. This could be a statistical effect due to a lack of power in the experiment or that these inhibitors may not be very effective in zebrafish, although the latter conclusion is unsupported by the decrease in leukocyte recruitment. It is more likely that these inhibitors had an effect that fell below the threshold for statistical significance, a conclusion supported by Figure 4.11, which shows a trend towards a decrease.

Although we cannot be certain that AC-YVAD-CMK, brilliant blue and KN62 are inhibiting caspase-A or zebrafish P2X7 respectively, these data in combination, along with the similarities in IL-1β sequence, alongside the similarities in the components of the IL-1β processing and release components imply the role of IL-1β is conserved between mammals and zebrafish. A more definite conclusion could be reached by investigating the cleavage of caspase-A substrates, such as IL-1β, and would be possible with an anti zebrafish IL-1β specific antibody used in western blot assays to determine whether caspase-A is active with treatment. However, western blots are difficult to quantify and this may result in a false conclusion if there are other pathways active other than P2X7 that can activate IL-1β, or if AC-YVAD-CMK has less efficacy in some of the cell types being investigated. Further assays on caspase-A activity *in vivo* could provide a wealth of data on IL-1β signalling in zebrafish, but for the purpose of this study, I have shown that mammalian caspase-A and P2X7 inhibitors reduce inflammation at the site of injury and likely do this through inhibition of IL-1β signalling.

Alongside these data, is the generation and further characterization of *Tg(pNF-κB:EGFP)s235* and *Tg(mpeg1:gal4.VP.16)sh256* as described, which will

undoubtedly be useful tools for the study of innate immune function. The *mpeg* promoter is a valuable tool for the study of macrophage function *in vivo* in zebrafish as described by Ellet *et al*. (2010) and allows the behaviour of macrophages to be visualized, which has not been possible before. This is made easier by its format as an entry clone compatible with the gateway system, which makes it possible to use it as a direct driver for a macrophage label, bypassing the need for a Gal4-UAS system and allowing more reliable data collection. In this study we have taken advantage of the entry clone to generate a number of useful tools, which will be described later.

Chapter 5, Development of a FRET based caspase-1 activation reporter.

5.1 Introduction.

5.1.1 Inflammasome function in IL-1β processing

The inflammasome complex is assembled in response to pro inflammatory stimuli such as PAMPs detected by the cell. In mammalian models, the inflammasome mediates the cleavage and activation of pro-caspase-1, which in turn is responsible for the cleavage of pro-IL-1β into a bioactive cytokine. Current methods of studying inflammasome function have utilized antibody techniques such as immunoprecipitation and fluorescent staining, on fixed cells. These mechanisms provide insight into inflammasome function, but operate on a single timepoint, so may miss important insights into inflammasome mechanisms. Mechanisms of inflammasome function, activation and localization have yet to be fully identified, and the pathway, as well as its relation to IL-1β release and processing remains poorly understood.

The IL-1β processing stage mediated by inflammasome activation precedes IL-1β signalling and provides an ideal step for therapeutic intervention, so understanding this pathway is essential to controlling IL-1β signalling and downstream inflammatory processes. I hypothesise that an *in vivo* live imaging reporter of inflammasome activation would provide valuable insights on the temporal and spatial aspects of inflammasome function, and allow these aspects to be further characterised. Such a reporter would act to bridge any gaps in understanding between inflammasome action and the release of IL-1β in living systems.

5.1.2 Förster Resonance Energy Transfer (FRET) as an active caspase reporter.

Förster Resonance Energy Transfer (FRET) is a technique based on resonant energy transfer between two fluorophores of similar excitation and

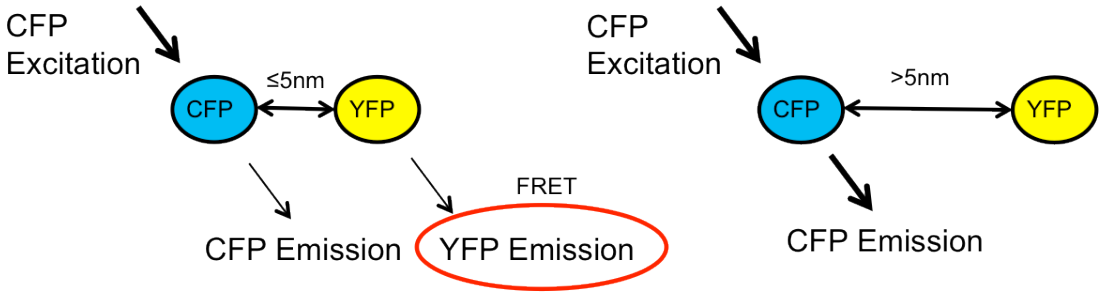

Figure 5.1. Förster Resonance Energy Transfer (FRET) in a CFP/YFP fluorophore pair. FRET is a non-radiative transfer mechanism that occurs over distances of approximately 5nm. At these distances, energy is transferred from the donor fluorophore (CFP) to the acceptor fluorophore (YFP). The FRET signal is therefore the emission of CFP excitation energy at the YFP emission peak. Separation of the fluorophores results in the loss of this signal.

emission spectra. In FRET, two spectrally similar fluorophores, commonly BFP-GFP or CFP-YFP are imaged under excitation and emission frequencies that excite both fluorophores individually. In any FRET pair, one fluorophore has a smaller wavelength and a higher excitation energy and is called the Donor fluorophore (BFP or CFP in previous examples), whereas the other has a longer wavelength and correspondingly lower excitation energy and is referred to as the Acceptor (GFP or YFP). If there is enough spectral overlap between the emission wavelength of the donor and the excitation wavelength of the acceptor then it is possible that when excited, the emission energy of the donor fluorophore can excite the acceptor fluorophore, resulting in a signal corresponding to acceptor emission in the absence of input energy of the right frequency to excite the acceptor fluorophore directly.

FRET is a non-radiative transfer mechanism, and as such behaves differently from a radiative energy transfer mediated by photons. Detectable FRET can only occur over small distances of 5-10nm, distances significantly smaller than the emission wavelengths of the fluorophores involved at 470-550nm and is mediated by virtual photons (Andrews 1989). The efficiency of this transfer mechanism relies on the distance between the two fluorophores and is governed by the following equation:

$$(1) \qquad E = \frac{1}{1 + \left(\frac{r}{R_0}\right)^6}$$

Where r is the distance between the fluorophores, and R_0 is the distance at which E is at 50% efficiency. Rather than the radiative transfer commonly associated with fluorescent proteins, which attenuates to the 2nd power with distance, FRET is far more sensitive to distance and loses efficiency to the 6th power. FRET is incredibly dependent on maintaining a distance between the fluorophores that is less than the R_0 and is consequently most efficient when the two molecules are directly linked with the minimum spacer distance between the fluorophores as possible; Xia and Liu (2001) demonstrated that an increase of 22 amino acid residues in the linker sequence between fluorophores can reduce the measured FRET intensity by >40%.

Because of its sensitivity to distance, the most common applications of FRET are to investigate the colocalisation of different proteins to cellular and membrane compartments and their interactions, acting as a very precise molecular ruler; however a FRET approach has also been used to successfully develop a reporter of caspase-3 activation in apoptosis (X. Xu et al. 1998; Rehm et al. 2002; Tian et al. 2007). Xu *et al.* (1998) have developed an expression cassette encoding a CFP YFP FRET pair linked by a short sequence encoding the human caspase-3 cleavage site DEVD; in response to caspase-3 activation, this site is cleaved resulting in the separation the fluorophore pairs and a loss of FRET. In this study I aim to modify this system to develop a reporter of caspase-1 activation in human macrophage like cells, and to further expand this into an *in vivo* reporter of inflammasome function in a transgenic zebrafish.

In designing a FRET-based reporter for caspase-1 activity it is important to consider the ideal conditions to achieve optimal energy transfer, as well as the parameters required in order that it is detected most effectively. The details of the design and detection are therefore described in detail below.

In previous studies (Morgan et al. 2001; Tyas et al. 2000; Rehm et al. 2002; Tian et al. 2007; Koopmans et al. 2007) FRET has been measured by calculating

changes in the CFP/YFP ratio for a CFP-YFP FRET pair. Resonant energy used to excite an acceptor fluorophore from a donor excitation input is energy not released as visible light at the emission wavelength of the donor, as such, when FRET occurs, the acceptor operates as a fluorescent quencher of the donor. Separation of the fluorophores disables the quencher activity of the acceptor resulting in an increase in donor emission. This will result in a change in the ratio of CFP to YFP in a CFP-YFP FRET pair as donor emission intensity increases.

5.2. Results

5.2.1 *In vitro* characterisation of FRET DEVD

The published caspase-3 apoptosis reporter (Rehm et al. 2002) was initially tested in order to establish that FRET measurement and processing was possible due to a biological response, using the equipment available. HEK293 cells were transfected with the caspase-3 DEVD FRET reporter plasmid (Rehm et al. 2002) and a plasmid encoding the pro-apoptotic protein Bcl-2 associated x protein (BAX) a kind gift of Dr. David Huang (Eliza and Walter Hall Institute, Melbourne)(Renshaw et al. 2004), a Bcl-2 family member. 24 hour treatment with the pan-caspase inhibitor Q-VD.OPh was used as a negative control. 24 hours after transfection, these cells were fixed in VECTASHIELD® (Vector Labs) and imaged. Volocity™ was used to generate a channel for the ratio of the CFP channel (CFP excitation, CFP Emission) to the YFP channel (YFP excitation, YFP Emission) (ratio hereby reffered to as C/Y), which was then analysed by using a measurement function to define objects of cellular size with a fluorescent intensity in the 6th percentile of the CFP channel. These parameters are strict enough to remove most false positives, but did, however, remove a number of transfected cells as well. The intensities for these objects were averaged across each field of view to quantify the C/Y for each treatment group. This protocol removes any data not defined as a cell by the software based on the CFP channel, which tended to be less intense than the YFP, as selecting objects by YFP could result in the inclusion of low intensity cells where the CFP emission signal could fall below the threshold of detection.

It was possible to further refine this cell population using background and threshold corrections. A background correction subtracts a defined background signal from each channel before calculating C/Y, whereas threshold alters every pixel falling below the value set to zero, effectively discounting the signal defined as background. A background correction therefore decreases the entire signal from any images, including signal contributing to FRET increasing the risk of false negatives and removing a significant amount of data. Conversely threshold correction may not properly correct for background signal overlapping FRET expressing cells and may allow the introduction of experimenter bias if not performed correctly. With regards to C/Y, the FRET signal is derived as change in the fluorescent ratio.

The data were corrected with both mechanisms and plotted to investigate background correction further. In uncorrected data, treatment with BAX increased the C/Y compared to untreated samples and treatment with Q-VD.OPh (Figure 5.2A). The effect of background corrections vary; correcting the ratio channel with the background function and threshold yield similar results (Figure 5.2 B and C), however, with a much greater spread of values and consequently a greater standard error.

Technically, when using C/Y, threshold correction is not necessary as the cells imaged are selected by the software based on their size and fluorophore expression, thereby only measuring pixels in cells expressing the FRET construct. However, as the aim is to develop this system in an *in vivo* model it is necessary to refine the generation of a FRET channel to enable the processing of FRET in zebrafish. C/Y directly compares donor and acceptor fluorophore intensity during FRET, taking advantage of its role as a fluorescent quencher, however it generates an aberrant signal because the C/Y is also calculated for non-cell containing regions. Any background should therefore be corrected when using C/Y. This can be seen in Figure 5.2 C where thresholding, mostly falling at a very low level, whereas background correction (Figure 5.2B) yields a result much closer to the uncorrected data. Using both background and threshold correction seems to greatly increase the range of values the result shown by a threshold correction, reducing most data points to below 0.01 and inverting the result expected from previous studies (Rehm et al. 2002). Clearly, the spread of data and correction of

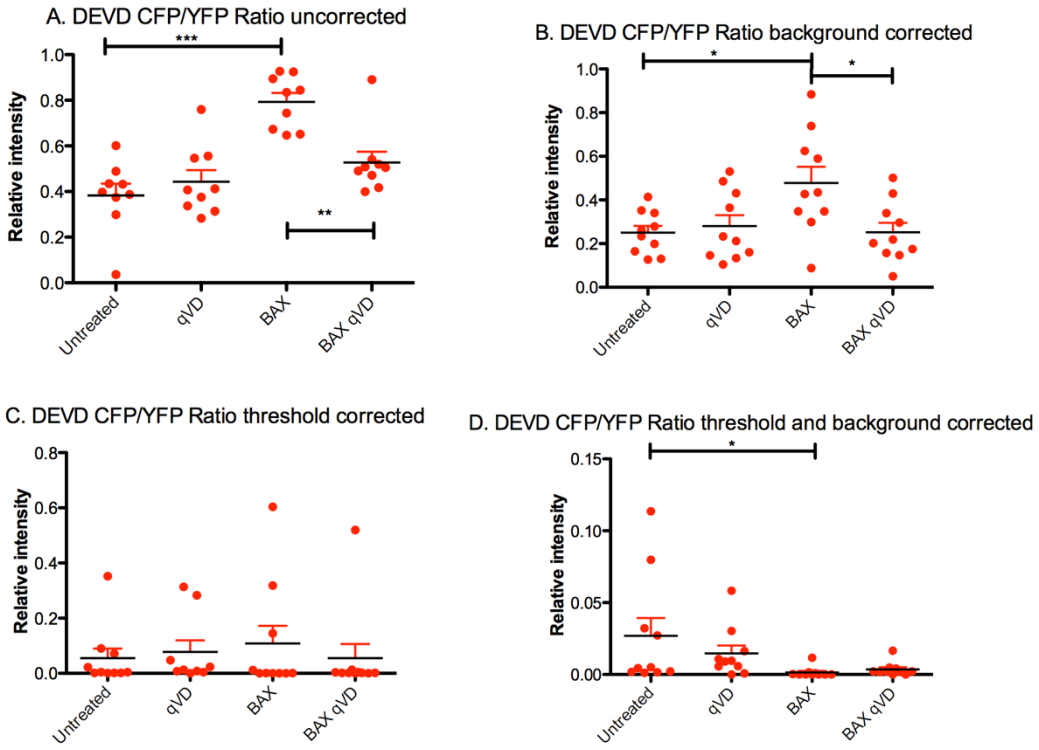

Figure 5.2. FRET signal from the caspase-3 reporter plasmid is reduced in response to BAX overexpression when expressed as a CFP/YFP ratio (C/Y). HEK293T cells cotransfected with the FRET DEVD reporter plasmid and proapoptotic protein BAX show an increase in C/Y compared to cells treated with pan-caspase inhibitor Q-VD.OPh (qVD) and cells without BAX transfection (A). B, C and D are the same data showing background, threshold and multiple methods of correction respectively. (n=3, 3-4 samples per experiment. Statistics: One way ANOVA followed by Dunnets post test)

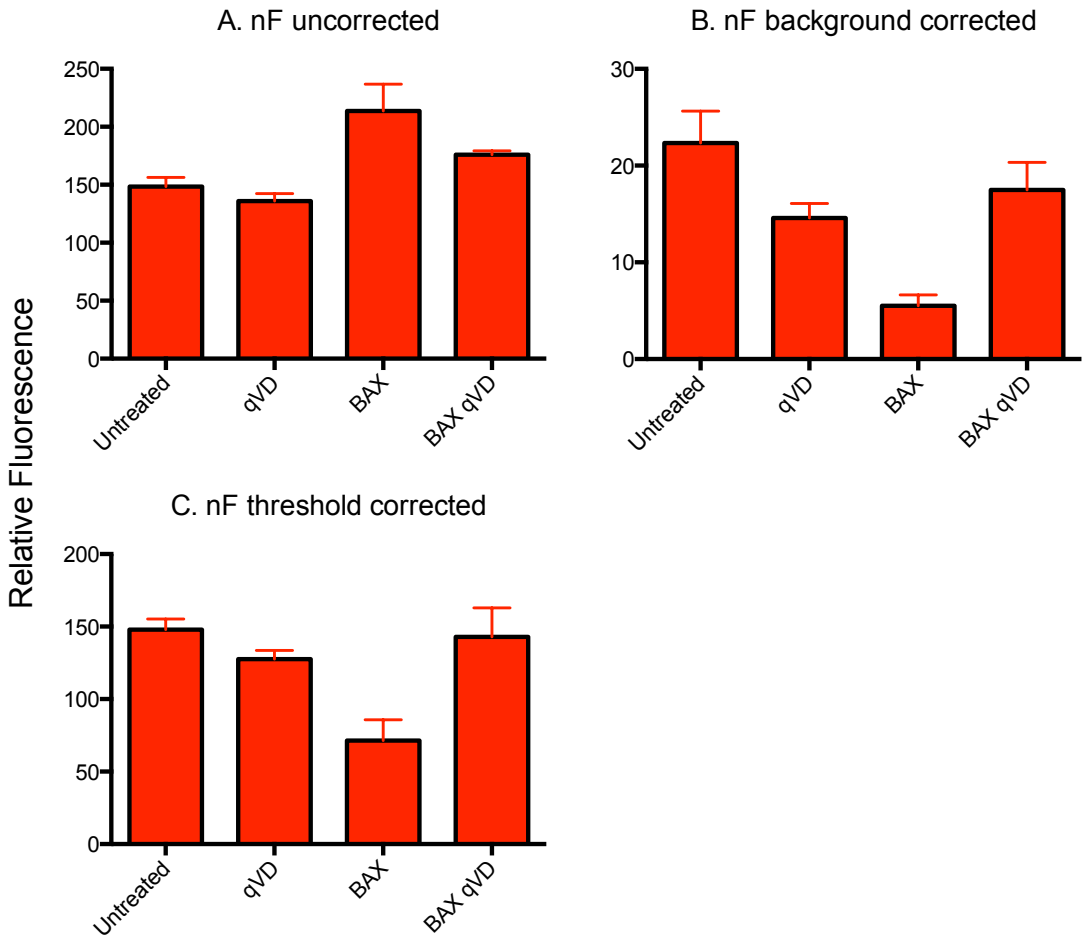

Figure 5.3. FRET signal from the caspase-3 reporter plasmid is reduced in response to BAX overexpression when expressed as netFRET (nF). HEK293T cells cotransfected with the FRET DEVD reporter plasmid and proapoptotic protein BAX show a decrease in nF compared to cells treated with pan-caspase inhibitor Q-VD.OPh (qVD) and cells without BAX transfection (A). B and C show background and threshold methods of correction respectively. Data are mean ± SEM for n=3, 3-4 samples per experiment.

most values to below 0.2 and 0.01 using threshold and combined threshold and background correction informs that this is an unviable strategy for generating a FRET channel. However, a background correction could still prove useful. Other studies (Tyas et al. 2000; Morgan et al. 2001) have used a C/Y ration to detect FRET, however, differences in processing from these these groups could present a problem. In these studies, cells were annotated manually rather than relying on software processing. In a live organism with multiple cells at a site of injury over a long timelapse microscopy aquisition, such a strategy is unviable, so other mechanisms of detecting FRET were also investigated.

5.2.2 Measures of FRET

As opposed to using C/Y, it is possible to make a more direct measure of FRET. Youvan *et al.* (1997) have developed an algorithm to calculate netFRET (nF). Defined as:

$$(2) \qquad nF = FRET - \big((Acceptor \times A) + (Donor \times B)\big)$$

The imaging parameters to generate nF are substantially different from those used to measure C/Y. C/Y requires the acquisition of images of CFP emission following CFP excitation and YFP emission following YFP excitation and relies entirely on the quenching ability of the YFP fluorophore to generate a ratio, which is then altered by the separation of the fluorophores. nF requires the addition of a third channel, that being YFP emission following CFP excitation and is effectively a more direct measurement of the FRET process as it quantifies the component of the YFP signal derived from the resonant transfer. The advantage of nF over C/Y is that it corrects for spectral overlap between the two fluorophores more effectively, necessary because of the very similar spectra of CFP and YFP (Pawley 2006). *In vivo*, nF will also provide a more useful visualisation of FRET as either a presence or absence of a signal rather than an increase in a signal, this will be discussed in more detail later. (section 5.3)

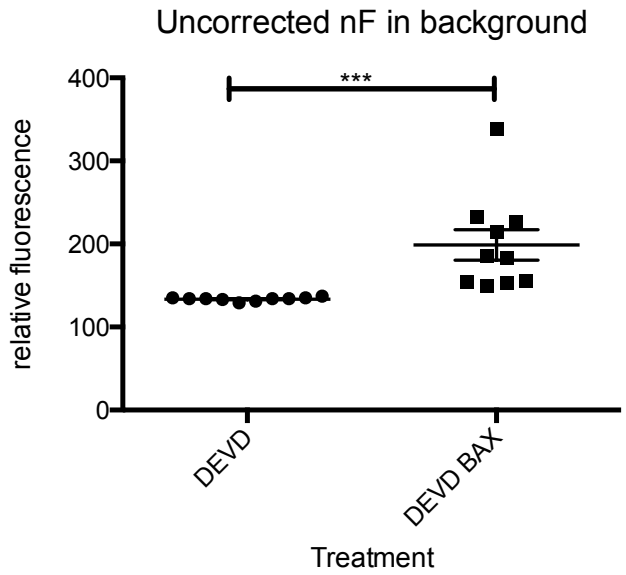

Figure 5.4. Post-apoptotic cellular debris has a significant amount of nF signal derived from auto-fluorescence. Background regions selected by drawing ROI in regions lacking a YFP signal have a high background level of nF. (n=3, 3-4 samples per experiment, statistics: two tailed t-test.)

The nF of the above experiment was plotted and background and threshold corrections again performed (Figure 5.3). Like C/Y, these corrections must be carefully considered. However, unlike C/Y as the signal is the product of a single channel with subtractions to account for spectral bleedthrough, it is possible that the best correction will differ from this method to C/Y. Varying corrections have been used in a number of studies, however, none of these directly relate to a *in vivo* model. Most studies have used a straight background correction when generating derivatives of nF (Youvan et al. 1997; G. Gordon et al. 1998; Z. Xia & Y. Liu 2001), however have concentrated on single cells rather than an average across a field of view. In this instance, both background and threshold corrections give results as expected (Figure 5.3B,C), based on experience of the C/Y ratio; both corrections were not applied simultaneously.

It is confounding that applying a background correction gives the inverse of the expected results (Rehm et al. 2002),and in order to understand this, the data must be examined more closely. In this protocol, cells are defined and selected by fluorescence in the CFP wavelength, a fluorophore significantly less intense than YFP (Pawley 2006) which radiates weakly above the high background of the

experiment. While it is possible to capture more exposed images of CFP emission, this would have an adverse effect on the YFP fluorophore by overexposing it thereby making a reliable quantification of FRET impossible, therefore CFP emission will often fall below a level of detection. At such low intensities it may be difficult to distinguish between cells containing CFP from auto-fluorescing cell debris without correcting for background in the other channels, as removal of cells which don't fluoresce above a set threshold in the YFP of FRET channel will remove these data. The magnitude of this effect can be quantified by generating an uncorrected nF channel for images exposed to the BAX apoptotic stimulus, or control cells and quantifying the nF in a non cell containing region (Figure 5.4) quantification shows a significant difference between the background signal of control and apoptotic cells which can only be attributed to transfection with the BAX pro-apoptotic protein. Plotting an uncorrected nF against a threshold corrected channel shows the complete reversal of just the BAX treated cells, demonstrating the necessity of correcting for background (Figure 5.3).

5.2.3 Normalising FRET

As shown by equation 2, nF itself is dependent on the direct intensity of the FRET channel corrected for spectral bleedthrough from the donor and acceptor channels. Thereby, an increase in intensity of the fluorophores based on an increased concentration of fluorophores in any given cell increases nF; whereas lower concentrations of fluorophores will yield an equivalently lower nF (a perceived erroneous result as a lower concentration does not automatically imply a loss of FRET from the caspase reporter). Therefore, for accuracy in a wide selection of cells, nF must be corrected for fluorophore concentration. Gordon et al (1998) propose a simple correction based on dividing directly by the intensity of both fluorophores, defining FRETN as:

$$(3) \qquad FRETN = \frac{FRET - ((Acceptor \times A) + (Donor \times B)}{Acceptor \times Donor} = \frac{nf}{Acceptor \times Donor}$$

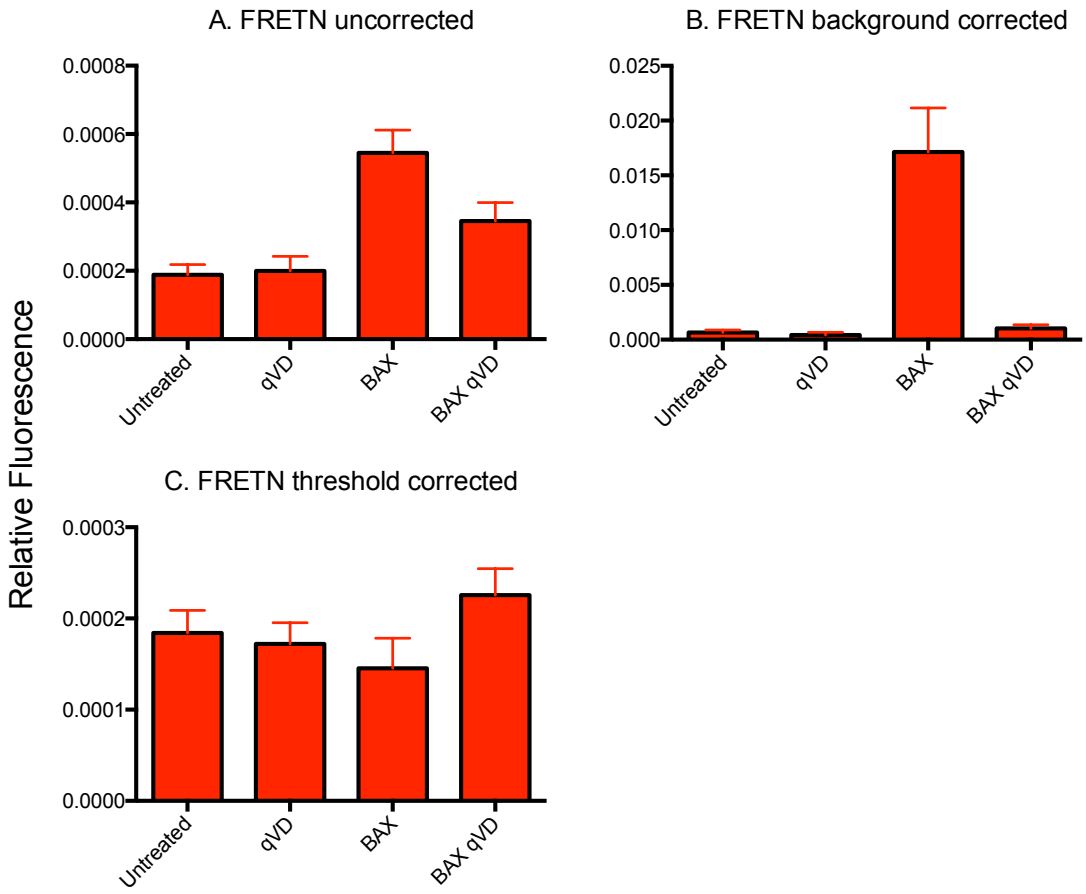

Figure 5.5. FRET signal from the caspase-3 reporter plasmid shows no change in response to BAX overexpression when expressed as FRETN. HEK293T cells co-transfected with the FRET DEVD reporter plasmid and pro-apoptotic protein BAX show no response compared to cells treated with pan-caspase inhibitor Q-VD.OPh (qVD) and cells without BAX transfection when measured using FRETN (A). B and C show background and threshold methods of correction respectively. Data are mean ± SEM for n=3, 3-4 samples per experiment.

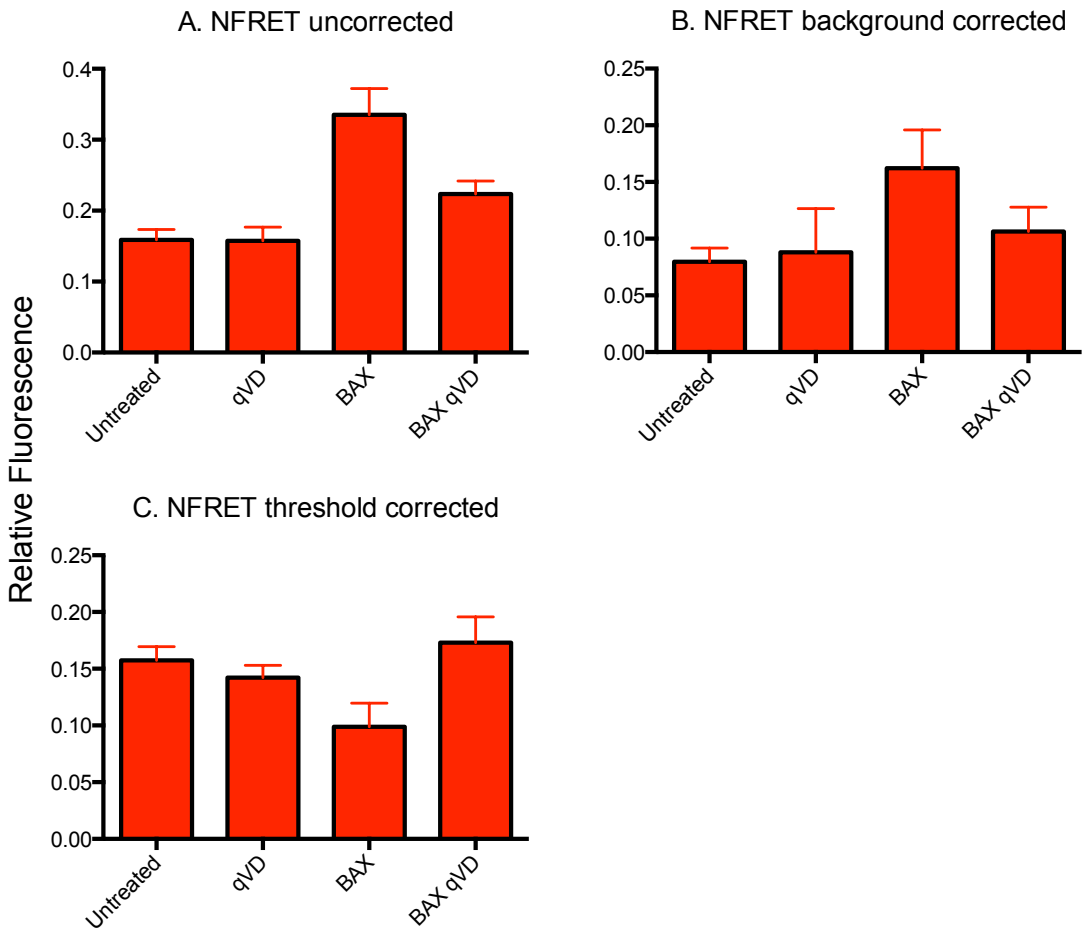

Figure 5.6. FRET signal from the caspase-3 reporter plasmid shows no change in response to BAX overexpression when expressed as N_{FRET} unless using a threshold correction. HEK293T cells co-transfected with the FRET DEVD reporter plasmid and pro-apoptotic protein BAX show no response compared to cells treated with pan-caspase inhibitor Q-VD.OPh (qVD) and cells without BAX transfection when measured using N_{FRET} (A). B and C show background and threshold methods of correction respectively. Only threshold correction is shown to match previous data. Data are mean ± SEM for n=3, 3-4 samples per experiment.

Here, the FRET value is substantially reduced due to its decrease by the inverse factors of both acceptor and donor fluorophores. Plotting FRETN, without correction thereby gives an even larger erroneous result (Figure 5.5A) with Volocity™ mistakenly annotating background signal as cell objects rather than apoptotic debris and measuring this as FRET thereby failing to be corrected by a YFP divisor, and exacerbating the signal seen in nF (Figure 5.2A). Threshold

correction removes this aberrant result, yielding a measurement far closer to results for C/Y and corrected nF, whereas a background correction greatly exacerbates this.

In a different study, Xia and Liu (2001) propose that FRETN is an unreliable normalisation mechanism and can yield results with errors of more than 80%. Instead they develop a different correction mechanism to account for fluorophore concentration named N_{FRET}:

$$(4) \quad NFRET = \frac{FRET - \big((Acceptor \times A) + (Donor \times B)\big)}{\sqrt{(Acceptor \times Donor)}} = \frac{nf}{\sqrt{Acceptor \times Donor}}$$

N_{FRET} normalises by the square of acceptor and donor intensity and analysing the previous data this way yields a similar pattern to that shown by FRETN, though with a smaller spread of results and a closer fit to nF and C/Y data (Figure 5.6). However, it is unclear whether this analysis is necessary. Both FRETN and N_{FRET} correct for the donor and acceptor concentrations, a correction important in measuring FRET interactions between two molecules, which could be expressed in different concentrations. This correction is unnecessary when considering a fusion protein as both fluorophores will be expressed equimolarly before caspase-3 mediated cleavage and the subsequent loss of FRET. Xia and Liu (2001) describe a further normalisation method, nF/Donor:

$$(5) \qquad \frac{NFRET}{Donor} = \frac{FRET - \big((Acceptor \times A) + (Donor\ x\ B)\big)}{Donor} = \frac{nf}{Donor}$$

(defined incorrectly as N_{FRET}/Donor by Volocity) which they quantify as yielding an error of <10%, compared to their measured error of <7% for N_{FRET}. When plotted, nF/Donor yields results remarkably consistent with those for uncorrected nF and C/Y with and both background corrections.

In *in vitro* studies using cell lines, transfection will result in fluorescent cells having a spread of intensities, so if FRET is to be quantified its necessary to normalise for fluorophore concentration, however, from the processing of the *in*

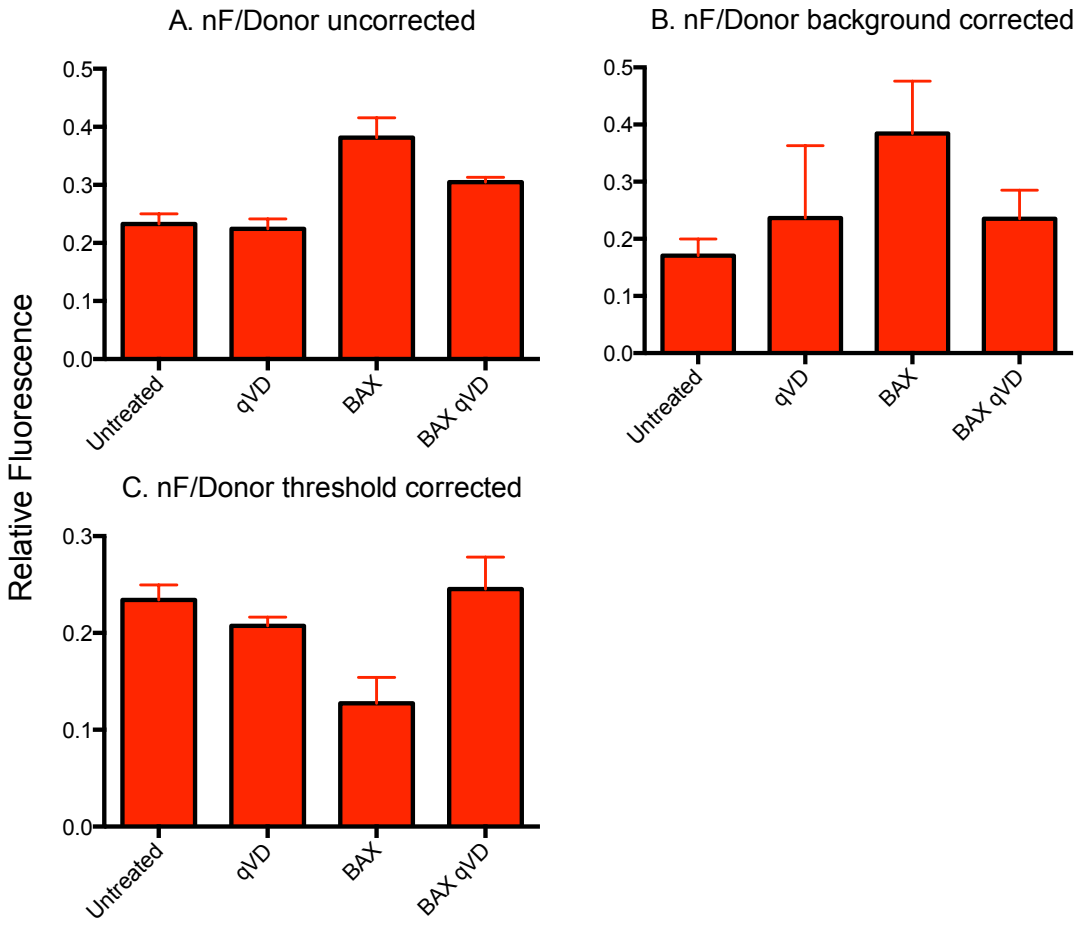

Figure 5.7. FRET signal from the caspase-3 reporter plasmid shows no change in response to BAX overexpression when expressed as nF/Donor unless using a threshold correction. HEK293T cells cotransfected with the FRET DEVD reporter plasmid and proapoptotic protein BAX show no response compared to cells treated with pan-caspase inhibitor Q-VD.OPh (qVD) and cells without BAX transfection when measured using nF/Donor (A). B and C show background and threshold methods of correction respectively. Data are mean ± SEM for n=3, 3-4 samples per experiment.

vitro data, we can see that background correction substantially alters the results of the experiment. Threshold corrections for C/Y removes a large amount of signal from annotated objects. Therefore, the need for a background correction should be questioned. The experimental setup defines objects by the donor intensity; as not all of the cells in the experiment are transfected with the FRET reporter, only a proportion express it, these must therefore be defined by Volocity™. This already selects out non-FRET areas, which is the function of the background and threshold correction. Because C/Y is a simple division and Equations 2-4 are not used, no bleed-through between channels is calculated. Furthermore, as this data is based on a ratio channel and the reporter plasmid expresses CFP and YFP in equimolar concentrations (as these proteins are expressed from the same open reading frame/cDNA).

5.3 *In vivo* FRET

5.3.1 Measuring neutrophil apoptosis *in vivo* using FRET DEVD

As demonstrated, the reliability of FRET in *in vitro* cell culture is dependent on a number of factors; background correction and normalisation being the most important. If these techniques are to be applied *in vivo*, the same corrections must also be applied. Moreover, the mounting of live embryos and cells is substantially different from cell-based assays; cells are seeded onto microscope coverglass, leaving no tissue, or media between the coverglass and the fluorescent cells resulting in a lightpath with minimal to no distortion. Alternatively, zebrafish must be mounted in agarose and constitute a living mass of tissue. It was therefore likely that further optimisation would be required before the development of a caspase reporter *in vivo*.

In order to investigate the *in vivo* activity of an apoptosis reporter, a model with demonstrated apoptosis was required; apoptosis has been proposed as a mechanism for the clearance of neutrophils from sites of injury during the inflammation and is necessary for its successful resolution (Loynes et al. 2010). This would prove an ideal model to characterise a FRET based *in vivo* reporter of

apoptosis and to further develop the imaging techniques necessary for an inflammasome reporter.

To generate a zebrafish model expressing the caspase-3 FRET reporter previously described, the FRET pair construct was targeted to the MPO BAC (Renshaw et al. 2006) using BAC recombineering (E. Lee et al. 2001). This generated a vector for the generation of a line expressing devdFRET under the control of a neutrophil specific promoter. The *Tg(BACmpo:FRET DEVD)sh237* transgenic line was generated using this construct. Expression vector construction and line generation was performed by Catherine Loynes.

5.3.2 Acceptor Photobleaching in FRET

To test whether the fluorescent signal emitted from these cells was actually FRET, an acceptor photobleaching experiment was performed. The YFP acceptor protein was bleached using a spinning disc confocal with a wavelength of 514nm and the resulting fluorescence quantified. FRET was lost after acceptor photobleaching along with the signal from the YFP channel (Figure 5.8). As FRET functions as a fluorescent quencher it is expected that the emission of the CFP would increase with the destruction of the YFP fluorophore, however this was not seen (Figure 5.8). A fluctuation corresponding to the timepoint of the photobleaching showed a slight reduction in intensity in the CFP channel, which could indicate that the 514 laser line may have bleached the CFP fluorophore and masked any increase in the CFP emission after loss of quenching, which would be expected given the spectral similarity of CFP and YFP. This hypothesis was tested by photobleaching the YFP with the next available wavelength, 561nm, which would have less overlap with the CFP excitation frequency, so would not be expected to bleach CFP; but this failed to disrupt the YFP fluorophore. The increase in fluorescent emission energy of the CFP fluorophore, whilst significant, is expected to be spread across a large emission range, and the increase at any given frequency is predicted to be very small (Figure 2B in Youvan et al. 1997) (notably for a BFP rather than CFP protein) so may fall below the threshold of detection for the instruments used. Furthermore previous studies of acceptor photobleaching have used a 532nm laser for the bleaching of a YFP fluorophore, equipment not available at this facility.

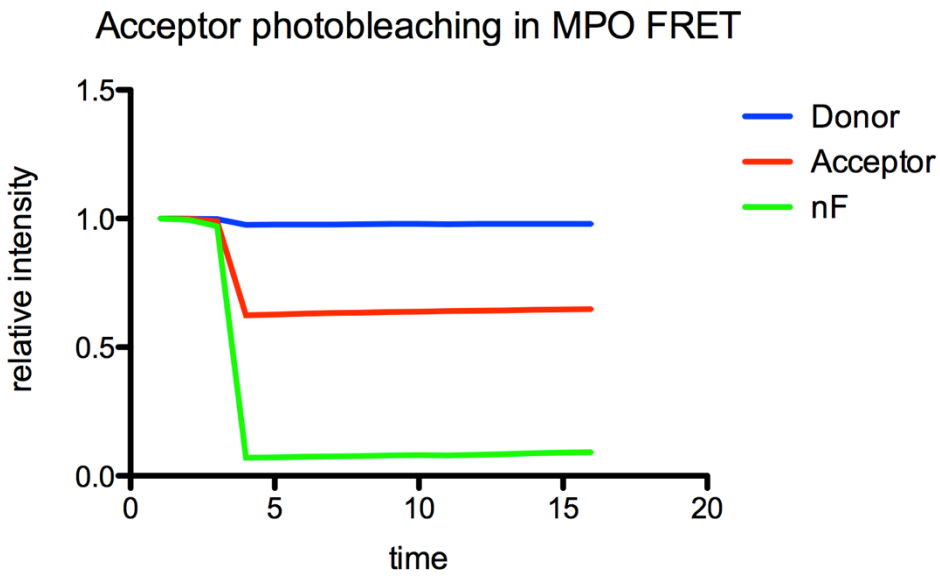

Figure 5.8. bleaching of the acceptor fluorophore results in loss of FRET (nF). *Tg(BACmpo:FRET DEVD)sh237* embryos imaged under 20x NA 0.45 obejctive using a spinning disc confocal lose nF signal in response to acceptor photobleaching with a 514nm laser.

5.3.3 Isopimpinellin induces neutrophil apoptosis in the resolution of inflammation

To investigate the functional use of this transgenic line as a reporter of apoptosis, a compound implicated in neutrophil apoptosis was used to treat fish post injury to elicit an accelerated resolution of the inflammatory response. The naturally occurring coumarin isopimpinellin has been shown to have anti cancer properties in mouse experiments (Kleiner et al. 2001; Prince et al. 2006). Furthermore, a recently performed small molecule screen has shown that isopimpinellin can accelerate the resolution of neutrophilic inflammation in a zebrafish model through a pro-apoptotic pathway (unpublished data, Anne Robertson). The action of isopimpinellin on *Tg(BACmpo:FRET DEVD)sh237* following injury was investigated. 78 hpf embryos were injured and mounted in agarose containing 25um isopimpinellin for imaging. The embryos were imaged every 2.5 minutes for 11 hours. These images were processed using nF and threshold correction and displayed in a merged channel image with the acceptor for normalization to fluorophore concentration during visualisation. Unlike the previously described normalisation methods (equations 3-5, Gordon et al. 1998;

Xia & Liu 2001), nF was expressed overlayed on the acceptor image for each timepoint in the acquisition to enable visualisation of the loss of FRET over the timecourse and enable tracking of neutrophil fate after the loss of FRET (Figure 5.9).

Neutrophils at the site of injury can be seen adopting an apoptotic, spherical morphology at which point the FRET signal is lost. After loss of FRET, YFP expression remains for approximately 5 minutes until this signal is lost, recapitulating the morphology seen by Loynes et al (2010) during neutrophil apoptosis. After the loss of FRET, neutrophils remain for 5-15 minutes before emission from the fluorophores is lost. This has been described as occurring prior to apoptosis as neutrophil "corpses" remain after loss of fluorescence of GFP derived proteins (Loynes et al. 2010) and is most likely due to changes in pH within the cell denaturing these fluorophores (Pawley 2006). Isopimpinellin significantly increased the occurrence of neutrophil apoptosis at the site of injury (Figure 5.10).

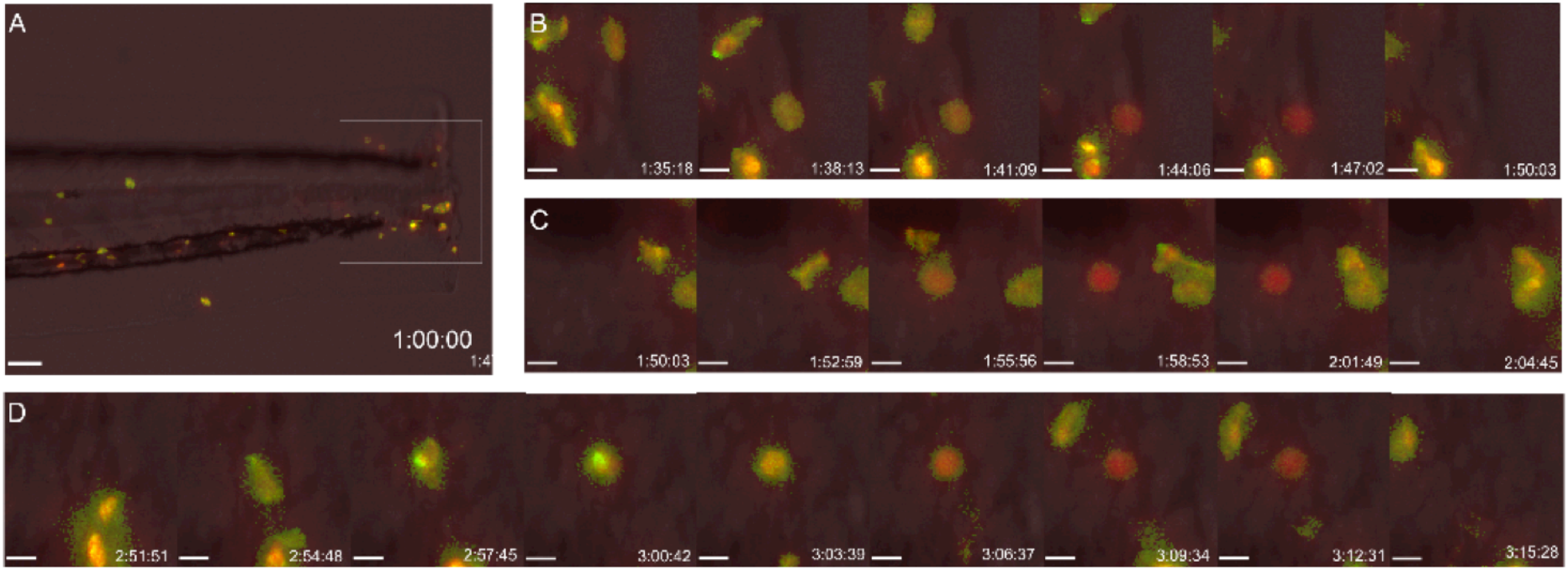

Figure 5.9. *Tg(BACmpo:FRET DEVD)sh237* is an *in vivo* reporter of Caspase-3 activation in neutrophil apoptosis during the resolution of inflammation. 72 hpf *Tg(BACmpo:FRET DEVD)sh237* embryos were imaged from 1 hour after injury by tail transection and treatment with isopimpinellin using a 10x NA 0.3 objective. Neutrophils at the site of injury (A) were observed for apoptotic morphology. nF, calculated using Volocity™ (green), is lost 10-15 minutes prior to loss of signal from the acceptor fluorophore (red) (B, C and D) (inset). scale is 110 μm for A and 10 μm for B-D, time post injury shown in lower right of each frame as hh:mm:ss.

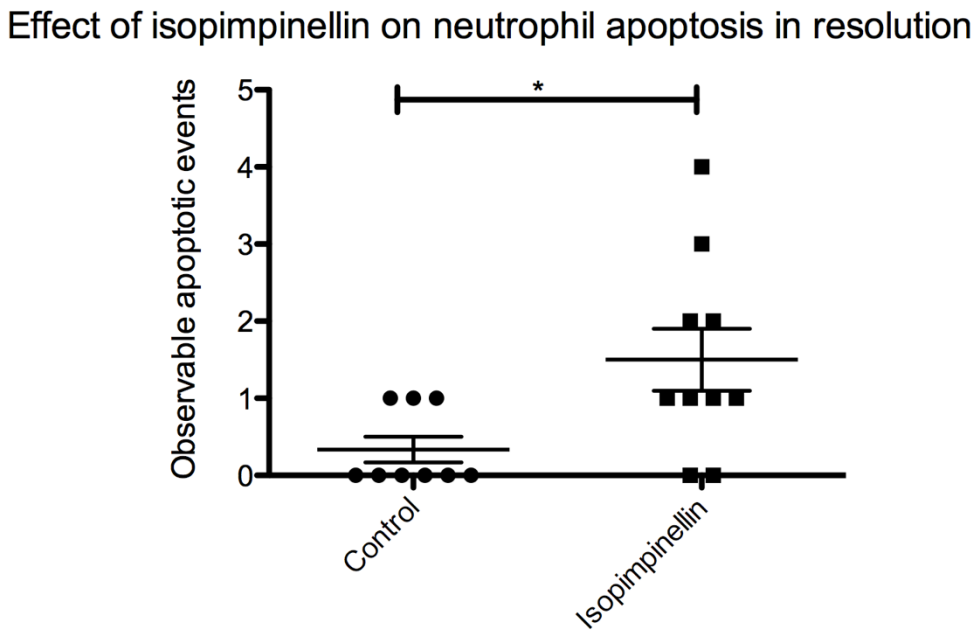

Figure 5.10. Isopimpinellin increases neutrophil apoptosis during inflammation. *Tg(BACmpo:FRET DEVD)sh237* imaged 1 hour post injury show a greater number of observable apoptotic events when treated with isopimpinellin than embryos treated with a DMSO control. (n=2, 10 fish in total. Unpaired t-test.)

5.3.3 Nitroreductase converts metronidazole into a pro-apoptotic metabolite

As an additional validation of the responsiveness of the *in vivo Tg(BACmpo:FRET DEVD)sh237* reporter to apoptosis, another functional test was developed. Nitroreductase, the protein product of the *nsfb* gene converts metronidazole into a toxic metabolite (Curado et al. 2008; X. Zhao et al. 2009) and can be used to ablate specific cell populations. I used the tol2kit Gateway™ system (Kwan et al. 2007) to generate a neutrophil specific nitroreductase mCherry fusion construct by combining a LyzC 5' promoter entry clone, with an nsfb middle entry clone lacking a stop codon and a 3' mCherry entry clone to generate *pol2DEST(Lyz:nsfb.mCherry)* and to subsequently generate the *Tg(Lyz:nsfb-mCherry)sh260* transgenic line enabling the targeted ablation of neutrophils. This line was crossed to *Tg(BACmpo:FRET DEVD)sh237. Tg(BACmpo:FRET DEVD)sh237, Tg(Lyz:nsfb-mCherry)sh260* embryos were treated with metronidazole, and imaged 4 hours after metronidazole treatment mounted in metronidazole containing agarose. An nF channel was generated for this acquisition and merged with the

acceptor channel to visualise apoptosis (Figure 5.11). Over this timelapse, apoptotic neutrophils are clearly distinguishable by their morphology; as well as loss of FRET and nitroreductase.mCherry fluorescence. The complexity of this compound zebrafish line necessitated taking images at 5 minute intervals rather than the 2.5 minute intervals used previously (Figure 5.9) due to the time necessary to change 4 filter sets and laser lines rather than 3. The apoptotic process occurred over a similar duration to that described previously with Isopimpinellin treatment.

The key to successful *in vivo* FRET imaging appears to be the management of background signal and the acquisition of images using the correct filter settings. While exposure was kept to a minimum, the FRET reporter protein was less susceptible to bleaching *in vivo* than it was in transfected cells. However, as predicted, there was substantially more background signal in the zebrafish, with significant autofluorescence in the CFP and FRET channel arising from the pigment cells. This was removed from nF images by increasing the YFP threshold as the autofluorescence was not present in this channel, and was the reason why a threshold correction was used for *in vivo* imaging in this study. Furthermore, necrotic tissue in embryos that died over the course of the acquisition was also autofluorescent and generated its own "nF" signal independent of a fluorophore (Figure 5.12), further supporting the use of a correction in the *in vitro* experiments described earlier (Figure 5.4).

Tg(BACmpo:FRET DEVD)sh237 successfully reports on apoptosis *in vivo*, recapitulating *in vivo* data of isopimpinellin efficacy via TUNEL staining. (Anne Robertson, data not shown). From this model, a viable methodology for imaging and displaying FRET in an *in vivo* system has been demonstrated. From this point it was possible to move onto generating an *in vivo* reporter of IL-1β processing using caspase-1 specific FRET cleavage.

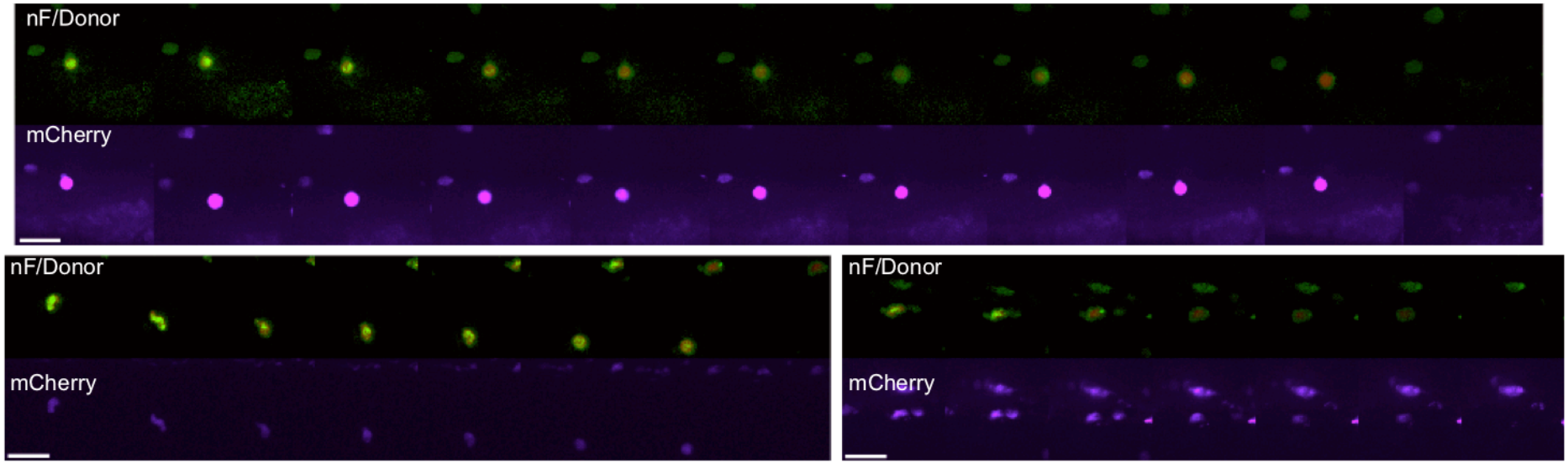

Figure 5.11. *Tg(BACmpo:FRET DEVD)sh237, Tg(lyz:nsfb.mCherry)sh260* ablates neutrophils by apoptosis when treated with pro-drug metronidazole. 72 hpf *Tg(BACmpo:FRET DEVD)sh237;Tg(lyz:nsfb.mCherry)sh260* embryos were imaged following 4 hour treatment with metronidazole using a 40x NA 1.3 oil immersion objective on a spinning disc confocal, with images taken at 5 minute intervals. 3 examples of neutrophils adopting a rounded, apoptotic morphology and losing FRET protein and nfsb.mCherry fluorescence in response to tissue specific ablation. nF, calculated using Volocity™ (green), is lost 20-30 minutes prior to loss of signal from the acceptor fluorophore (red) (upper frames) mCherry fluorescence from the nitroreductase-mCherry fusion protein is also lost at this time (purple, lower frames). Scale bar =35μm

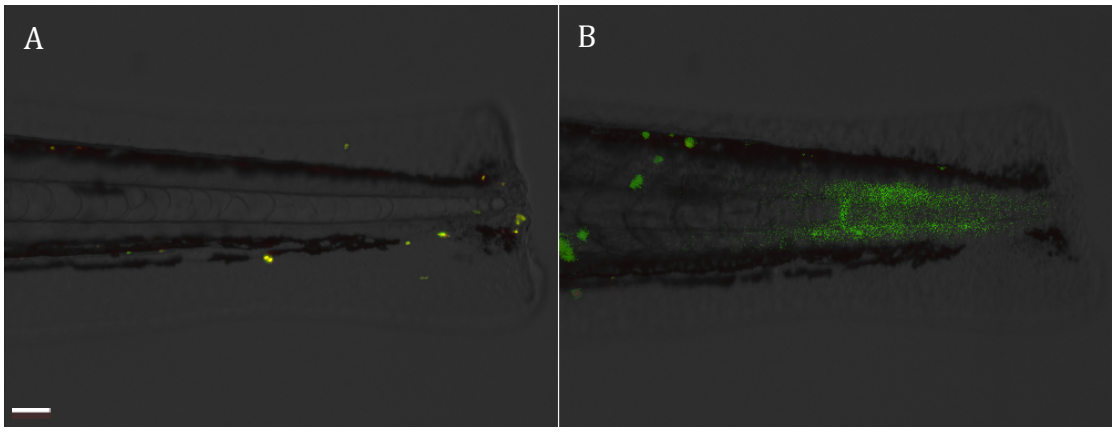

Figure 5.12. nF is detected from autofluorescence as a function of necrosis. A proportion of *Tg(BACmpo:FRET DEVD)sh237* embryos injured 72 hpf and imaged for 8 hours die as a result of the experimental process. These embryos show an increase in nF (green) throughout the fish (B) when compared to the initial 1 hour post injury timepoint (A) and demonstrate the importance of considering the contribution autofluorescence can make when measuring FRET in a live organism. Scale bar = 110 μm

5.4 FRET as a reporter of caspase-1 activation

5.4.1 *In vitro* testing of inflammasome reporter constructs.

Using site directed mutagenesis, the caspase-3 cleavage site DEVD was mutated to the caspase-1 optimal cleavage site WEHD (Rano et al. 1997): primers were designed complementary to the sequence on either side of the DEVD cleavage site with the centre residues instead encoding WEHD. These primers were used to amplify the FRET cassette and vector via PCR, then the template was degraded with methylated DNA specific restriction enzyme Dpn1. Success of the site directed mutagenesis was confirmed by sequencing. An additional mutant, encoding the caspase-1 cleavage site present on IL-1β, YVHD, was also generated.

In order to develop a caspase-1 FRET reporter an appropriate cell model was required. Only specific cell types are responsible for IL-1β processing and release *in vivo*; as mentioned these are mainly monocytes and macrophages (Dinarello 1996). A model of IL-1β processing must therefore be as close to these cell types as possible but remain amenable to cell culture techniques. The ultimate aim was to develop this into an *in vivo* model, but *in vitro* testing was required as a proof of concept in order to determine whether the FRET reporter was responsive to inflammasome activation. Initially, mouse RAW264.7 macrophage cells were used as a model of inflammasome activation, these cells are amenable to transfection, but retain a macrophage like phenotype. Shortly after commencing this work it was shown by Pelegrin *et al.* (2008) that RAW264.7 cells lack the ASC protein and are unable to process IL-1β, so were unsuitable for testing our inflammasome reporter. Instead, the human monocyte cell line THP-1 was chosen, having been previously characterised for IL-1β release by caspase-1 inhibitor AC-YVAD-CMK (YVAD) (MacKenzie et al. 2001). These cells are difficult to transfect and a number of transfection techniques were attempted. Nucleofection (Amaxa) proved the most efficient method of transfecting THP-1 cells, mirroring published data (Martinet et al. 2003), however the maximum transfection efficiency achieved was 5%, as opposed to the 80% described. It was found that transfection efficiency decreased substantially as a function of passage number.

5.4.2 FRET YVHD is unable to detect caspase-1 activation in transfected THP-1 cells *in vitro*.

It was confirmed that FRET YVHD was insensitive to cleavage by caspase-3 using the previously described assay (Figure 5.13).

To test investigate caspase-1 mediated cleavage of FRET YVHD, THP-1 cells were transfected with the FRET-YVHD reporter construct and treated with PMA to differentiate them into a more macrophage like, adherent phenotype, responsive to IL-1 secretion and amenable to imaging. The cells were primed with LPS 48 hours after transfection for 3 hours then imaged. Cells were stimulated with BzATP at the beginning of image acquisition in order to activate caspase-1 via P2X7 receptor activation. The cells were imaged for 20 minutes post ATP stimulation with images taken every 30 seconds. 6 fields of view were imaged per treatment. As Volocity™ was not able to keep track of the same cells over the timecourse, cells were annotated manually for each field of view and tracked across multiple time points. An nF/donor channel was generated for each field of view and these data were averaged per field of view.

Bleaching is a confounding issue with this experiment as generation of a FRET channel requires taking 3 imaged for each frame, the FRET signal decreases very strongly for all channels as a result of bleaching, which nF/Donor was unable to compensate for.

The FRET YVHD signal appeared to decrease significantly faster than in the controls, with the AC-YVAD-CMK treated FRET YVHD signal decreasing at a rate somewhere between this and the DEVD non caspase-1 cleavable control. To be sure that this is a result of the caspase-1 cleavage the experiment was further refined. Fluorescent exposure was reduced by increasing the time between image acquisition to 2.5 minutes (Figure 5.15) and 10 minutes (Figure 5.16). Bleaching was still a significant problem at 2.5 minutes, but as before, nF /Donor in FRET YVHD decreased faster than in other treatments, implying that this difference could again be due to the action of caspase-1. This was not detected using 10 minute intervals between exposures where no change was measured.

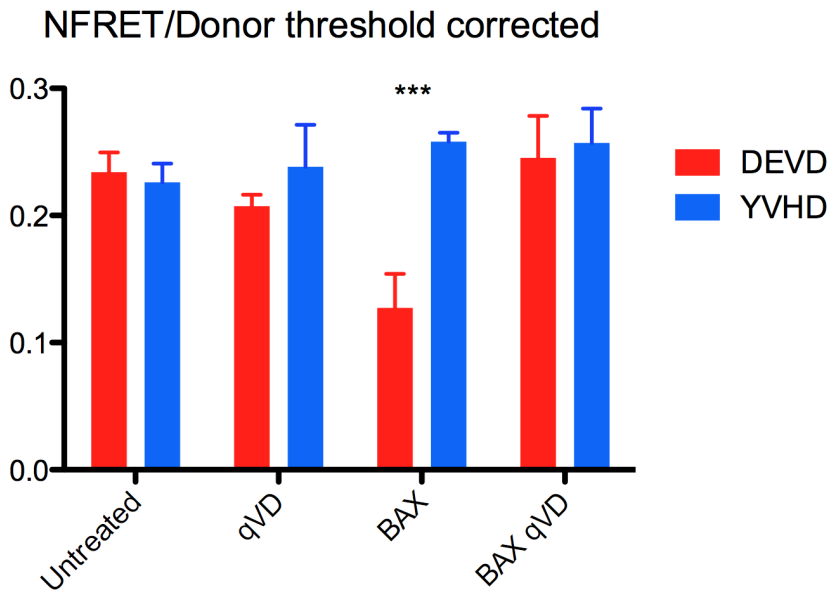

Figure 5.13. DEVD YVHD is not sensitive to caspase-3 activation by overexpression of BAX. HEK293T cells cotransfected with DEVD or YVHD FRET reporter plasmids and BAX only show a decrease in nF in the DEVD reporter with no change in the nf signal from the YVHD reporter plasmid. Data are mean ± SEM for n=3, 3-4 samples per experiment. Statistics: One way ANOVA followed by Boneferroni post test, threshold correction applied.

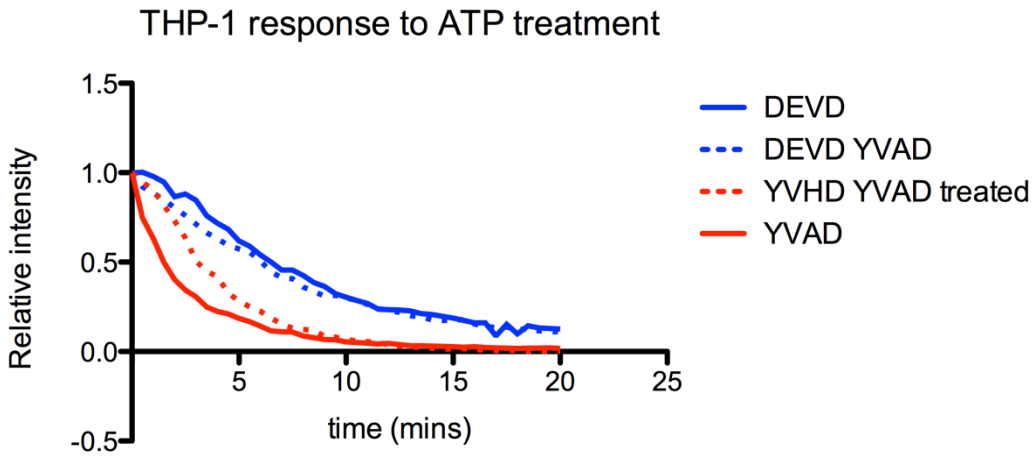

Figure 5.14. Differentiated and primed THP-1 monocytes show a faster decrease in nF signal in the FRET YVHD reporter when stimulated with ATP. THP-1 monocytes, transfected with DEVD or YVHD reporter plasmids show a decrease in nF signal due to overexposure and photobleaching, loss of FRET is uninhibited.

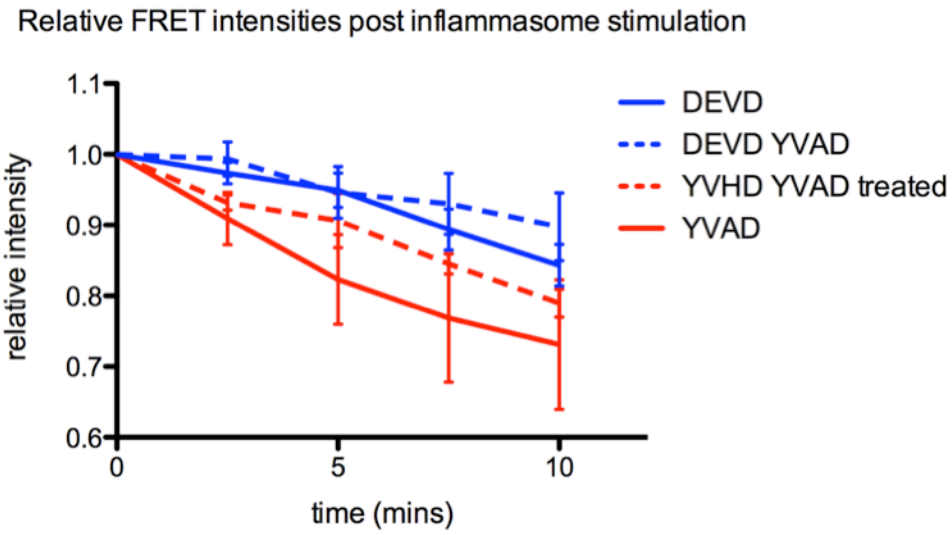

Figure 5.15 Differentiated and primed THP-1 monocytes show a faster decrease in nF signal in the FRET YVHD reporter when stimulated with ATP. THP-1 monocytes, transfected with DEVD or YVHD reporter plasmids show a decrease in nF signal due to overexposure and photobleaching, loss of FRET is uninhibited by caspase-1 inhibitor AC-YVAD-CMK (YVAD) however, nF signal from Untreated YVHD declines at a faster rate, possibly indicating inflammasome activation.

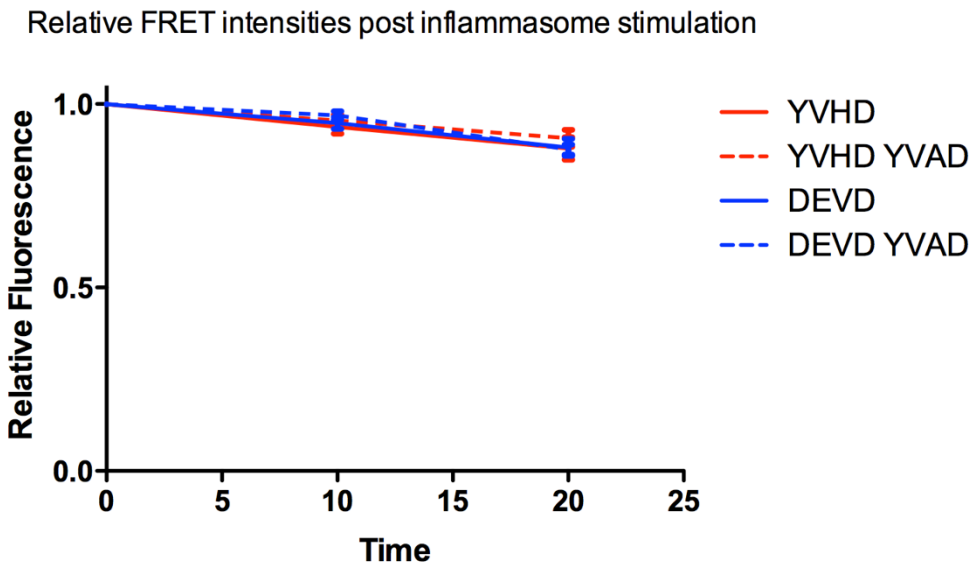

Figure 5.16. Differentiated and primed THP-1 monocytes show no change between caspase-3 and caspase-1 reporters when imaged at 10 minute intervals. THP-1 monocytes, transfected with DEVD or YVHD reporter plasmids show no change in nF signal over 20 minutes of stimulation with BzATP.

5.5 Discussion

5.5.1 FRET calculation methodology.

The hardware available for the experimental measurement of FRET has expanded over time, and Xia and Liu (2001) have described the use of three different acquisition systems for experimental use; a spectrofluorometer, a widefield fluorescence microscope and confocal microscopy. Microscopy was described as more effective for live cell imaging due to the ability to spatially and temporally define FRET signals with a greater level of accuracy at the microscopic level. This study also used similar light microscopy techniques because of the emphasis on using FRET techniques at the cellular level. However, because of the hardware limitation, the software available for processing was limited to Volocity™. Although other methodologies for calculating FRET exist, the four FRET measurements presented here are the only methods available in Volocity™, as although other software examples, such as PixFRET (Feige et al. 2005), exist, the necessity of high throughput for processing inflammatory timelapse microscopy required the use of Volocity™.

Although described methods for normalising FRET (G. Gordon et al. 1998; Z. Xia & Y. Liu 2001) require correction for the concentration of both fluorophores, in this example it was not necessary. The FRET cleavage reporter is a fusion protein expressing CFP and YFP in a 1:1 ratio, therefore the concentration of CFP-YFP will be the same. However, some form of normalisation was still required as in transfected cells, there was a range of intensities resulting from the transfection in both HEK293T cell lines and monocyte cell lines. Although from the experimental data, it was clear that FRETN (G. Gordon et al. 1998)was the least accurate methodology for normalisation.

5.5.2 *In vivo* FRET as a reporter of apoptosis

Normalisation was less of an issue in *in vivo* zebrafish images, as there was less difference in intensity between cells, however, when imaging across a number of planes, error could still be introduced in objects appearing less bright if falling

outside a focal plane. For this reason, normalisation may still be required. In this study, *in vivo* images of nF were expressed relative to their acceptor fluorescence, with nF shown over the acceptor signal. Showing the data this way demonstrates that the FRET signal is lost before the cell undergoes apoptosis as the YFP signal; and in the nitroreductase example, mCherry; persists after the loss of FRET. This gives a qualitative on/off FRET signal for each cell, which can be quantified across an organism by considering the number of cells undergoing apoptosis, but would be inappropriate if the magnitude of FRET in each cell was to be considered. In this situation, normalisation by nF/Donor would be necessary.

A further issue with the *in vivo* study is the use of widefield microscopy; cells falling outside focal planes suffer optical distortion and appear out of focus, which makes identification of cells difficult. Removal of this signal would be possible using deconvolution, a function present in the Volocity software package, but would require generating CFP and YFP beads in order to reliably measure an accurate Point Spread Function (PSF), and while it is possible to calculate a PSF based on wavelength and numerical aperture, this results in a less accurate deconvolution.

As shown, the noise of a system has a large impact on the FRET signal and can easily affect the experimental output. It was unclear which method of background correction was most accurate with both background and threshold corrections yielding similar results with respect to loss of FRET following BAX transfection, however both demonstrated the necessity of a correction, confirmed by the high nF background signal present in BAX treated cells. Thresholding was preferentially used in this study due to its effects across a larger number of normalisation methods and its ability to correct both FRETN and N_{FRET}, encouraging its use for any further FRET experiments which may require normalisation for differing fluorophore concentrations rather than using a fusion protein, though this may not be appropriate for *in vivo* experiments.

In vivo FRET in zebrafish, may introduce additional challenges for correcting distortion and background signal insurmountable by these methods. Imaging live zebrafish relies on visualizing cells throughout the embryo, a system with changing thicknesses and densities throughout the specimen. Due to their

migratory and patrolling role, neutrophils and macrophages are not localized to any particular site in the fish and can be present in any of the tissues at a site of interest such as an injury. Their spread throughout a large cross section of the embryonic tissue leads to a large amount of optical distortion due to the difference in lightpaths through varying thicknesses of tissue resulting in large variations in the signal noise ratio and distortion for cells depending on their location within the fish. However, with Volocity™, it may be possible to generate a background correction to more easily account for the different background rather than relying on background correction built into the FRET applications. Quantitative data was successfully obtained in this study because visualisation was limited to a small area; however, this also greatly limited the number of apoptotic events visualised. To increase the data gathering ability of the acquisition, more image correction is necessary. Foremost, the introduction of deconvolution or image acquisition reducing the unfocused signal, such as confocal microcopy, would be preferential, however corrections for removal of background must also be considered. This could be done in two possible ways; a background correction could be generated from wildtype embryos. Embryos would be mounted in as similar a position as possible and an image would be taken in the relevant fluorescent channels at the same exposure and gain settings as for the transgenic embryos. This background image could then be subtracted from each image acquired in the transgenic fish to create an image with no background signal. The major, and possibly insurmountable problem is the difficulty in finding fish of the same age and mounting them in exactly the same position, though at lower resolutions this would be possible.

An alternative approach would be to use the first image in the sequence as the background correction; this approach has the virtue of being in exactly the same fish embryo and having the same fluorescent background as every other frame in the acquisition, however, with the downside that the initial frame of the video will be lost, and that any cells that remain immotile will also be removed, furthermore, as the health of the embryo changes, or regeneration at the site of injury begins, this correction would lose effectiveness.

It may be possible to remove the requirement for as much background correction by altering the fluorescent properties of the donor. As described, one of

the main issues with the initial pre-correction nF channel, was the relatively low intensity of the CFP fluorophore. If this could be replaced with a more intense fluorophore, such as mTurquoise, then it would be advantageous to imaging FRET (Goedhart et al. 2010).

If the issues surrounding optical distortion and autofluorescence in live samples can be resolved, then FRET could prove a very powerful tool to provide temporal resolution to *in vivo* studies where the advantage of FRET as an almost instantaneous reporter will be most apparent. The sensitivity of FRET to fluorophore separation distance presents rapidly in the intensity of the FRET signal, and at higher resolutions it may be possible for *in vivo* experiments to provide subcellular spatial resolution. However, the imaging demands of FRET can have deleterious consequences on acquired data. The requirement for 3 separate channels for each FRET image exposes specimens to a large amount of energy and results in accelerated bleaching, therefore care must be taken to reduce the effect of overexposure on samples wherever possible.

5.5.3 FRET YVHD as a reporter of inflammasome activation.

A major problem with the FRET approach to measuring inflammasome activation is exposure and intensity of the light used in acquiring the images. Ferrari *et al.* (1997) show that up to 80% of the intracellular IL-1β in macrophages remains uncleaved, with the implication that the scope of action of caspase-1 is therefore limited within the cell. As a cleavage based reporter of caspase-1 activation would compete with native IL-1β for the active site of caspase-1, we would expect an even smaller percentage of the reporter to be cleaved. The loss of FRET signal from such cleavage events may be very low and technically difficult to isolate from the noise of the system. It would be expected that the resulting loss of FRET signal resulting from caspase-1 activation would be smaller than the loss resulting from caspase-3 mediated cleavage of FRET DEVD. Nevertheless, efforts to detect this change were hampered by the difficulty in transfecting cells capable of activating caspase-1 and mediating the processing of IL-1β. If this obstacle were overcome, characterising a FRET YVHD reporter would be possible.

With the publication of recent data supporting a similar role for zebrafish caspase-A to human caspase-1 in the processing of IL-1β (Vojtech et al. 2012), and my generation of Tg(MPEG1:Gal4.VP16) it may be possible to circumvent the requirement for transfectable macrophages by expressing the construct in a zebrafish line. The development of a real time inflammasome reporter remains an important goal for the study of IL-1β processing and release and would be an ideal tool for the study of IL-1β biology.

Regardless of this, I have shown here the characterisation of an *in vivo*, real time caspase-3 reporter in zebrafish, a tool which could be important for the temporal quantification of inflammation resolution in neutrophils and the application of this reporter for anti-inflammatory drug discovery. This also provides an important proof of principle for an *in vivo* caspase-1 reporter as a model of IL-1β processing.

Chapter 6: *in vivo* release of IL-1β

6.1 Introduction

The release mechanism of IL-1β from mammalian cells is a poorly understood and there have been a number of pathways proposed for its secretion. IL-1β is a leaderless protein that does not follow the traditional Golgi-Endoplasmic reticulum release process and so is secreted from cells using other non-conventional pathways. Andrei et al (1999, 2004) have shown that IL-1β is released via endolysosomal related organelles from monocytes, whereas IL-1β release via membrane derived microvesicles has been show by MacKenzie et al., (2001) from THP-1 monocytes, Bianco et al. (2005) in microglia, Pizzirani et al., (2007) in dendritic cells and Qu et al. (2009) in murine macrophages. Qu et al have also shown the release of IL-1β from via smaller exosome derived vesicles in murine macrophages (Qu et al. 2007; Qu et al. 2009).

The proposed release pathways for IL-1β differ according to the cell type used in each study and the stimuli used. However, none of these studies have been performed *in vivo*, and the situation in a living system may be different. An *in vitro* methodology may lead to an incomplete understanding of microvesicle biology due to the innate differences these systems have with *in vivo* models. Monocytes, macrophage and related cells such as microglia exist as a single cell monolayer in *in vitro* studies, whereas *in vivo* macrophages are present within a milieu of living tissue and as such we can expect that the behaviour of *in vivo* microvesicles will more accurately represent the biological situation. The development of an *in vivo* model of IL-1β release will therefore provide a powerful tool for the study of IL-1β biology and provide further insights into its poorly understood release mechanism, as well as allow the investigation of vesicle targeting to IL-1β sensitive cells.

In a number of these studies, mice have been shown to share significant homology in IL-1β release with humans, however visualizing microvesicles in living mouse tissue would be nearly impossible with current techniques due to the lack of contrast and resolution. However, the advantages of the zebrafish as a transgenic model described earlier, especially its optical transparency, make it

ideal for this study. The ease of visualizing specific cell populations *in vivo* using fluorescent markers allows the targeting of specific cells with a reporter of IL-1β release.

In order to visualise the release of IL-1β *in vivo*, a reporter would have to mimic the structure and sequence of IL-1β to interact with the release pathway. As it is unclear which part of IL-1β, a cytokine with no leader sequence, is responsible for its release, and also what mechanism the release pathway takes, it is not possible to generate an artificial version of the sequence or epitope to use as a reporter. Therefore, the remaining option is to fluorescently label a coding sequence for IL-1β itself in order to create a fusion protein. Expression of this reporter on cells capable of releasing IL-1β will allow the visualisation of IL-1β release via tracking the behaviour of the fusion protein. Mammalian IL-1β contains an N-terminal pro-domain; therefore a fluorescent label of bioactive IL-1β is required to be on the N-terminus. There is also a possibility that the size of the fluorophore, which nearly doubles the size of the fusion protein, may interfere with export and the release of the protein, However, IL-1β containing vesicles retain caspase-1 activity and have been shown to contain inflammasome components (MacKenzie et al. 2001), as well as pro-IL-1β implying that the size of these vesicles is already large enough to contain a number of proteins, so the possibility of the fluorophore interacting negatively with the secretion machinery is small.

6.2 Results

6.2.1 IL-1β release from differentiated THP-1 monocytes

To test whether a EGFP tag interfered with the secretion of IL-1β, an IL-1β-EGFP construct a kind gift of David Brough (University of Manchester), was transfected into THP-1 monocytes, which were then differentiated with the addition of phorbol 12-myristate 13-acetate (PMA) (Grahames & Michel 1999). The cells were primed with LPS and stimulated with BzATP. The release of large vesicles was seen following BzATP stimulation (Figure 6.1), however this was only visible on overexposed cells with very strong expression of the plasmid. However, no signal was seen outside cells with a lower level of expression even though

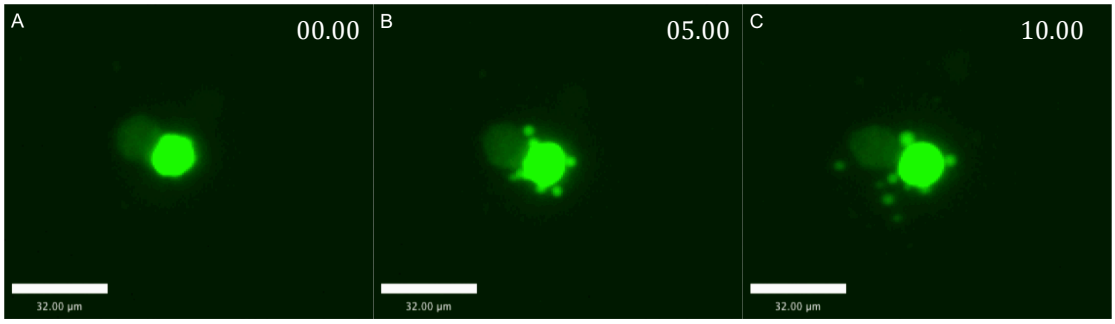

Figure 6.1. IL-1β.EGFP does not appear to interfere with secretion machinery in differentiated THP-1 monocytes. THP-1 monocytes transfected with an IL-1β.EGFP fusion protein encoding plasmid differentiated with PMA and primed for 3 hours with LPS release microvesicles containing the IL-1β fusion protein when stimulated with 500 nM BzATP. Time is mm:ss from start of imaging, scale bar = 32 µm

blebbing was apparent, which was likely due to the low EGFP signal in any vesicles released falling below the detection threshold during imaging.

6.2.2 The Tol2kit and Gateway™ cloning

In this study the primary mode of vector construction was the Tol2Kit (Kwan et al. 2007), itself based on the Gateway™ recombination system (Invitrogen) (Hartley et al. 2000). The Gateway™ process is based on two recombination steps, a BP reaction, recombining AttB and AttP sites; and the LR reaction, recombining AttL and AttR sites using the BP and LR clonase recombinase enzymes respectively. This is a very powerful tool for generating expression plasmids as it allows a single clone to be modularly constructed into vectors with a variety of promoters, tags and reporters. The empty Gateway™ vectors, donor plasmids and destination vectors, code for a *ccdb* suicide gene between the att recombination sites, so are unable to propagate in normal competent cells (Bernard & Couturier 1992)(Figure 6.2 A). Once recombination occurs, the gene is removed allowing for growth of transformed colonies. Furthermore, donor and destination vectors encode different antibiotic

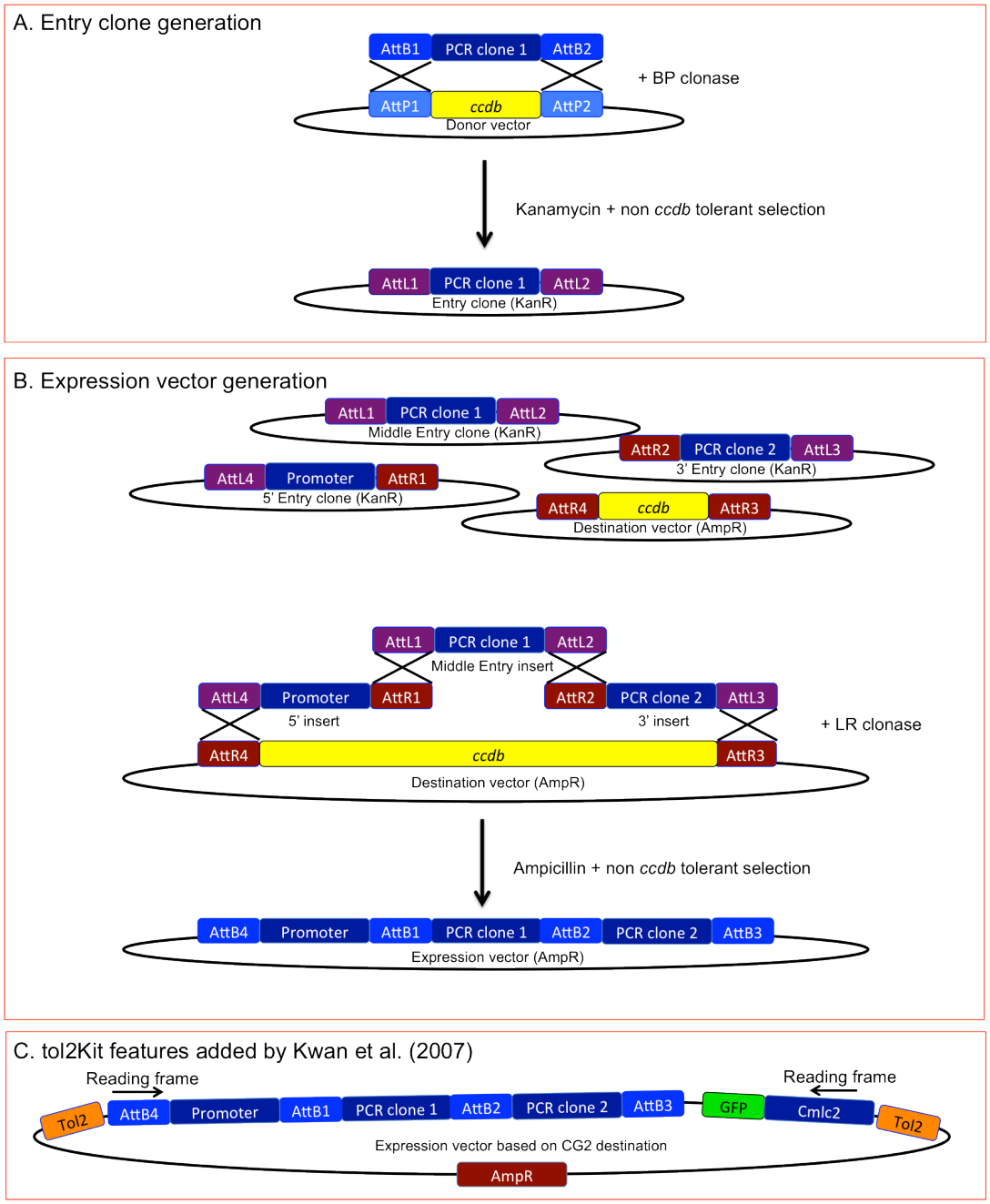

Figure 6.2. Using Invitrogen's Gateway™ recombination system to generate expression constructs. The Gateway™ recombination system allows expression systems to be constructed from two simple recombination reactions. A. A gene of interest is amplified with recombination site containing PCR primers and recombined with a donor vector, generating an entry clone. B. 5', middle and 3' entry clones are combined with a destination vector to generate an expression vector. C. Kwan et al (2007) have generated destination vectors for easy expression in zebrafish by adding Tol2 transposable elements and transgenic markers.

resistances, ensuring that during LR recombination only recombined expression vectors will grow on appropriate selection medium (Figure 6.2 B).

Kwan et al. (2007) used this system to generate a molecular biology toolkit for the easy assembly of zebrafish expression vectors by inserting Tol2 transposable elements on either side of the AttL recombination sites of the attR4-R3 destination vector to enable easy transposition of this vector into the zebrafish genome. Further improvements were made to this vector with the inclusion of a transgenic marker, allowing easy identification of embryos with transgenes by the presence of EGFP expressed under a cmlc2 promoter in the heart, which is clearly visible by 30 hpf. (Figure 6.2 C)

Alongside these destination vectors is the inclusion of a number of modified entry clones to allow fluorescent labelling of proteins of interest and variable strategies for expression, such as tissue specific or whole organism.

6.2.3 IL-1β strain variation.

Using primers complementary to the deposited zebrafish IL-1β sequence (NM_212844.1), the coding sequence for zfIL-1β was amplified from 48 h WIK embryos, then TOPO cloned and sequenced. Two different sequence variants were discovered in the WIK strain, however it was unclear whether these were attributable to PCR error or strain variation. These sequences were translated and aligned (Figure 6.3) to determine where the differences lie. There were five instances there the amino acid sequence was altered between the two sequences, so the structural data described previously in chapter 3 was used to determine where these polymorphisms lay (Figure 6.3). None of the polymorphisms affected residues that were directly conserved between human and zebrafish IL-1β, but some did overlap with regions of secondary structure. To further investigate the source of the polymorphisms, the two alleles were aligned to available database zfIL-1β sequences (Figure 6.4). There was only one instance where the polymorphisms did not align to a deposited sequence, an L/R change on residue 130. These differences were attributed to strain differences between zebrafish in Sheffield and the institutions where these sequences were initially cloned. Further

cloning from AB and Nacre wildtype zebrafish strains only detected allele two. As this variant sequence shared most in common with

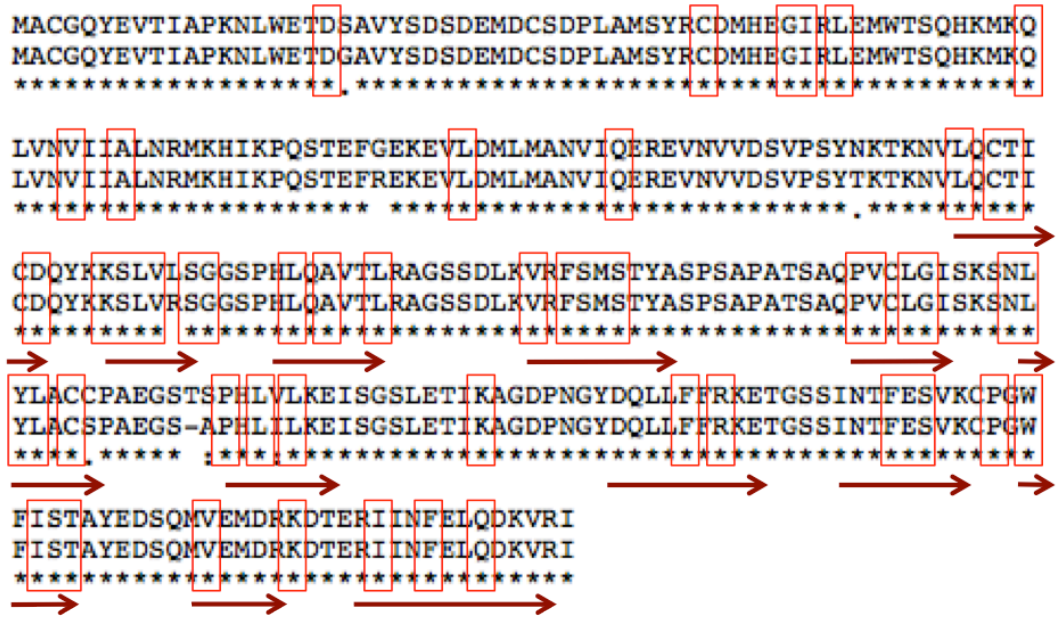

Figure 6.3. IL-1β allele variations in Sheffield WIK wildtype zebrafish are in non conserved residues. Variant alleles aligned and structurally annotated; regions predicted as β-sheets using Phyre (chapter 3) presented as red arrows, with boxes indicating conserved residues between Human and Zebrafish IL-1β sequences show that allele variations are in non conserved residues

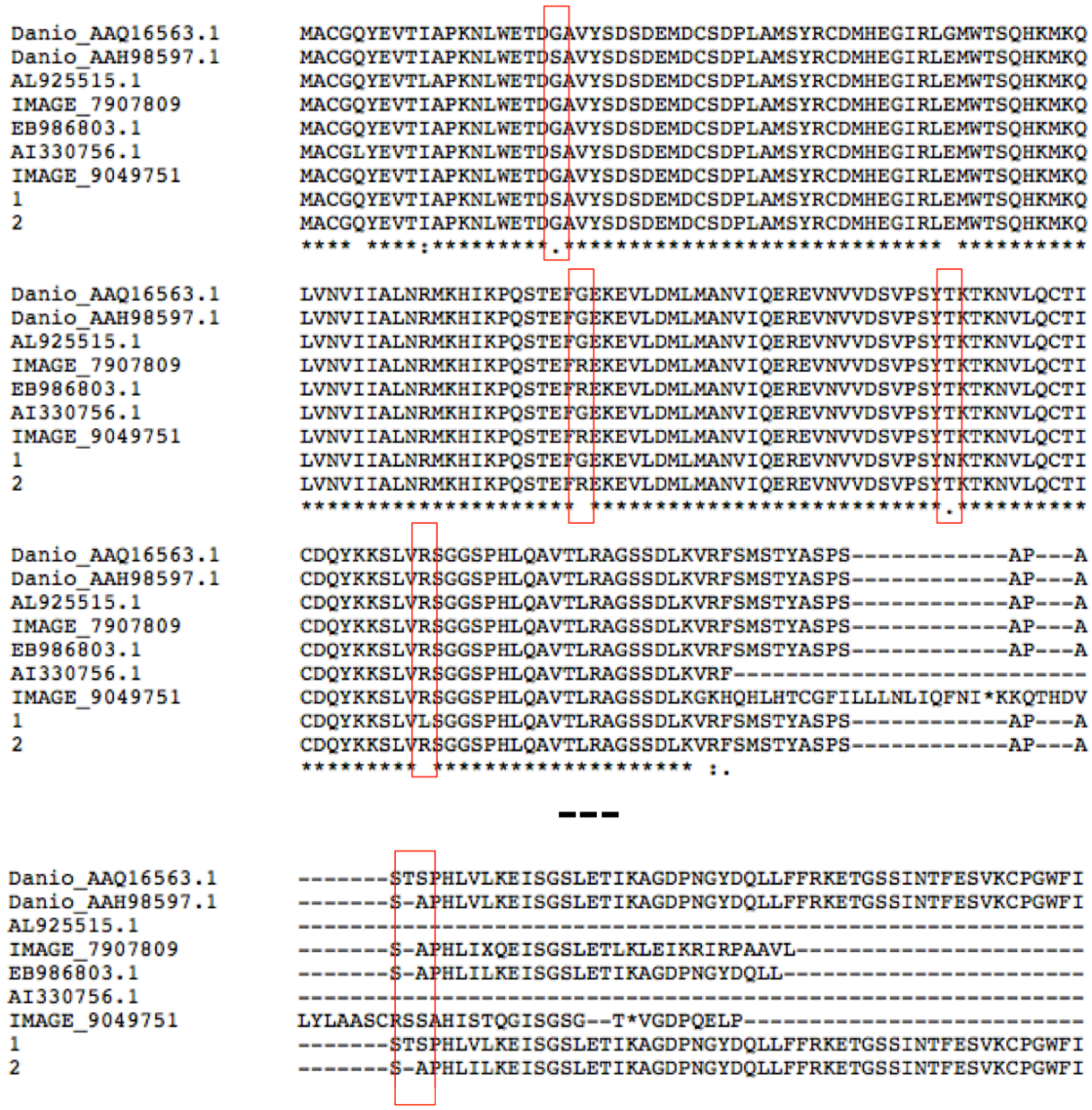

Figure 6.4. Most allele variants in Sheffield WIK IL-1β genotype are conserved between deposited zfIL-1β sequences. Zebrafish WIK allele variants (1, 2) aligned to deposited sequences, ESTs and IMAGE clones for zebrafish IL-1β (accession numbers shown) show most polymorphisms between WIK alleles are shared with at least other deposited IL-1β sequence.

deposited sequences and between strains, alongside retaining the Arg residue as described, it was chosen as the basis for the reporter constructs.

6.2.4 Fluorescently tagged IL-1β EGFP vector construction.

The Variant 2 IL-1β sequence was amplified with restriction site containing primers and ligated into the Gateway™ pME MCS entry clone, which was then combined with the 5' UAS, and either the 3'EGFP or 3' mCherry alongside the pDestTol2CG2 destination vector to generate expression constructs for IL-1β EGFP and IL-1β mCherry respectively using the Gateway™ recombination system (Kwan et al. 2007) (Invitrogen).

The constructs were injected into *Tg(α-Actin:Gal4)* alongside tol2 mRNA to visualise expression. Embryos were selected for EGFP expression in heart muscle from the cmlc2:EGFP transgenesis marker and imaged for expression of EGFP or mCherry in the somite muscle blocks. No fluorescent expression was detected with either pDEST(UAS MCS IL-1β.EGFP) or pDEST(UAS IL-1β.mCherry).

The lack of expression could be due to a number of factors. *Tg(α-Actin:Gal4)* is maintained as an outcross from the original line. With lack of proper maintenance and screening, these fish are a mix of wild type and heterozygous gal4 alleles. Therefore, only 25% of injected embryos from this this line are likely to have actin:Gal4 expression. Furthermore, PME-MCS only has one reading frame not containing a stop codon and is not fully characterised in the original tol2Kit publication (Kwan et al., 2007), so its possible that the cloned IL-1β coding sequence was inserted incorrectly, however, it was later confirmed to be correct by sequencing. A final problem was that using the pME-MCS middle entry clone to build a fusion protein introduces a large linker between the end of the protein coding sequence and the initiation codon of the fluorophore. For MCS IL-1β this encoded an additional 32 amino acids, which increase the size of the IL-1β protein by 12%. This could result in deleterious effects on the translation and expression of the reporter protein and negatively affect its stability.

Instead a new approach to generate the IL-1β middle entry clone was used. The zfIL-1β coding sequence was amplified with primers containing attB recombination sites and recombined with the attB1-2 donor vector (PDONR 221)

to generate pME-zfIL-1β, an IL-1β coding sequence entry clone with no stop codon. This entry clone was used to generate new versions of the EGFP and mCherry tagged IL-1β expression vectors with the same 5' and 3' entry clone and destination vector as described previously. When injected into tg(αActin:Gal4), clear mosaic expression of both EGFP and mCherry can be seen in the muscle tissue at 48 and 72 hpf (Figure 6.5).

I proceeded to test this construct in a macrophage specific gal4 driver line. *pDEST(UAS:IL-1β.EGFP)* was injected into *Tg(fms:Gal4-VP16)i186; Tg(UAS:nfsB.mCherry)i149* (Gray et al., 2011) and the resulting embryos screened for heart marker expression. The resultant *Tg(fms:Gal4-VP16)i186;Tg(UAS:nfsB.mCherry)i149* compound transgenic expresses mCherry tagged nitroreductase in macrophages and a subset of other cells. Macrophages, identified by expression of mCherry, motility and morphology were visualised for EGFP expression, but none was detected. The embryos were subjected to injury by tail transection to recruit macrophages to the site of injury. Very few macrophages were distinguishable by mCherry expression in the transgenic, although a few motile, EGFP positive cells were visible with no mCherry expression at the site of injury (Figure 6.6). Further repeats of this experiment failed to detect anymore EGFP expressing cells and few mCherry labelled macrophages were seen.

The *Tg(fms:Gal4.VP16)i186;Tg(UAS:nfsB.mCherry)i149* has persistent problems with detecting macrophages as discussed in chapter 4 and so poses significant difficulties when using this transgenic as a fluorescent macrophage marker. Furthermore, overexpression of a proinflammatory cytokine in a number of additional tissues such as xanthophores and in the cells of the hindbrain as driven by the *fms* promoter may negatively effect the viability of the embryos, and uncontrolled expression of IL-1β in these tissues could also interfere experimentally with the use of the *pDEST(UAS: IL-1β.EGFP)* line as a reporter by inducing aberrant inflammatory responses.

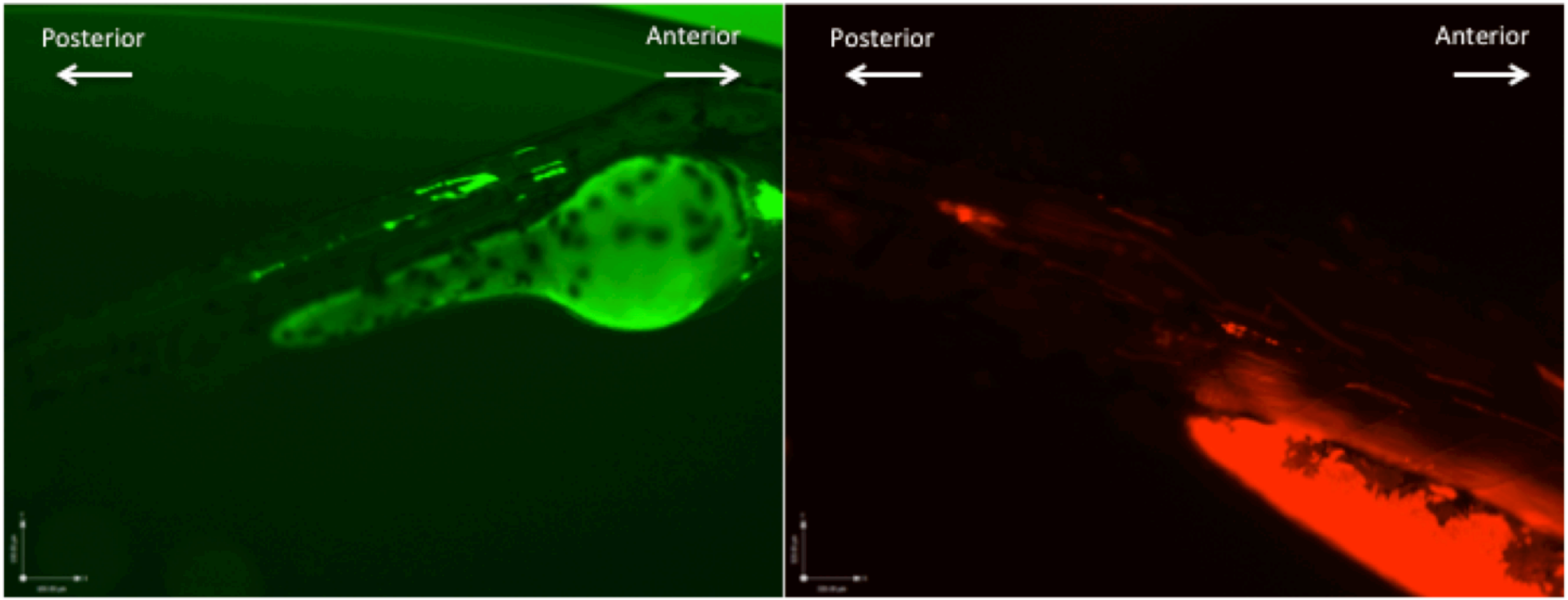

Figure 6.5. zfIL-1β fusion expresses stably in the tg(a-actin:Gal4.VP-16). Microinjection of *pDEST(UAS:zfIL-1β.EGFP)* and *pDEST(UAS:zfIL-1β.mCherry)* into *Tg(a-actin:Gal4.VP-16)* shows mosaic expression in muscle cells when imaged at 72 hpf. Scale=320μm

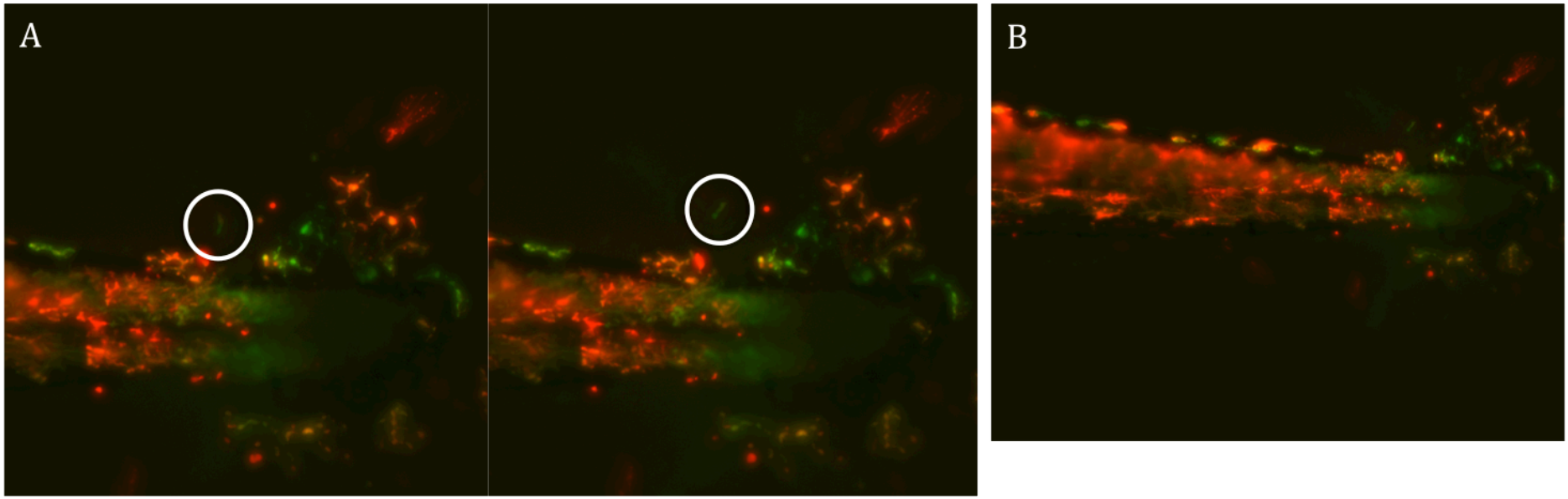

Figure 6.6. The *Tg(fms:Gal4.VP16)i186;Tg(UAS:nfsB.mCherry)i149* compound line has significant silencing and non-macrophage expression. *pDEST(UAS:zfIL-1β.EGFP)* transiently injected into *Tg(fms:Gal4.VP16)i186;Tg(UAS:nfsB.mCherry)i149* embryos shows very little expression of IL-1β.EGFP and no cells labelled with nfsb-mCherry are distinguishable as macrophages. IL-1β.EGFP expressing macrophages are distinguishable by morphology and motility (white circle) A. *Tg(fms:Gal4.VP16)i186; Tg(UAS:nfsB.mCherry)* has significant non macrophage expression, visible in xanthophores, but shows significant silencing of the nfsb-mCherry reporter.

The *Tg(fms:Gal4.VP16)i186;Tg(UAS:nfsB.mCherry)i149* line was therefore found to be unsuitable for the generation of an IL-1β.EGFP reporter. Instead, as described in chapter 4, I was able to generate an *mpeg1*, macrophage specific, gal4 driver, *Tg(mpeg1:Gal4.VP16)sh256*, using the *mpeg1* promoter 5' entry clone generated by Ellett et al. (2010). This approach presents certain advantages over using the *fms* promoter as a driver for an IL-1β.EGFP fusion protein. Access to the *fms* as a macrophage specific driver is limited to the *Tg(fms:Gal4-VP16)i186;Tg(UAS:nfsB.mCherry)i149* compound line, whereas *mpeg1* is a promoter entry clone compatible with the versatile Tol2Kit Gateway™ system. This presented an opportunity for me to address the problem in two different ways. The *mpeg1* entry clone was used to generate a direct driver expression vector, *pDEST(mpeg1:zfIL-1β.EGFP)* for use in transient expression experiments and subsequent stable zebrafish line generation.

A further strategy was also developed, to add increase the likelihood of developing an IL-1β reporter. The UAS silencing issues present in the current version of the Tol2Kit were addressed with the generation of a new UAS 5' entry clone. The phenomenon of UAS silencing has previously been described in detail (Akitake et al. 2011) and is primarily due to the methylation of the CpG rich UAS repeats used in the assembly of these promoters, with the number of concatemers influencing the methylation frequency. However, Akitake et al. (2011) have developed a UAS promoter system based on 4 non-repeating UAS sequences. This new UAS promoter is described as being far less susceptible to promoter methylation and silencing after multiple generations. I used this promoter sequence to generate a new promoter entry clone for a non-repeating UAS using a template clone kindly donated by Mike Parsons (Johns Hopkins) (from hereon this entry clone is referred to as the 4xUAS 5' entry clone). This construct should be less susceptible to methylation, and the appropriate entry clone was used to generate the pDEST(4xUAS:IL-1β.EGFP) expression vector.

The direct driver construct was used in the rest of the study as it gives direct control over the expression of IL-1β.EGFP and provides a transgenic marker for the selection of positive embryos in which IL-1β.EGFP is driven directly by the *mpeg1* promoter. The 4xUAS construct was designed to be used in conjunction with the *Tg(mpeg1:Gal4.VP16)sh256* line as a strategy designed to increase the

likelihood of success, as this has some disadvantages over a direct driver system. Although the original non-repeating UAS sequence has been tested for promoter methylation, the 4xUAS entry clone has not, and therefore may be more susceptible than in the original publication, though this is unlikely. When crossed to *Tg(mpeg1:Gal4.VP16)sh256*, there is only a marker for one transgenic allele as *Tg(mpeg1:Gal4.VP16)sh256* line was not assembled with the cmlc2:EGFP destination vector, therefore it is expected that when crossed to heterozygous Gal4 positive adults, only 50% of the *tg(4xUAS:IL-1β.EGFP)* embryos will be positive for the *Tg(mpeg1:Gal4.VP16)sh256* allele, making selection and experimentation more difficult. However, the major advantages of this construct are that the Gal4:UAS system provides an amplification effect for the promoter driving the Gal4 protein, and that we can use the *pDEST(4xUAS:IL-1β.EGFP)* modularly in any Gal4 driver line to explore IL-1β biology in other cell types.

6.2.5 IL-1β reporter expression.

pDEST(mpeg1:Gal4.VP16) was injected into AB wildtype embryos alongside tol2 transposase mRNA. Embryos were selected by heart marker expression and imaged for green fluorescence in cells with macrophage morphology. There was very little expression of the IL-1β.EGFP transgene. The embryos were injured to recruit macrophages to the tail and imaged using high power confocal microscopy. Macrophages could be clearly distinguished with confocal imaging using a 40x objective at the site of injury. Membrane blebbing could be seen at the leading edges of the macrophages as they moved at the site of injury (Figure 6.7) but very little evidence of microvesicle release was seen.

Contrast enhancement of these macrophage timelapse images at the site of injury revealed that circular vesicles of ≤1 μm could be seen around these cells (Figure 6.8). With no other source of EGFP fluorescence within the embryo, the origin of these vesicles is attributable to the IL-1β.EGFP expressed in macrophages. Furthermore, it is unlikely that this is due to autofluorescence as this is only seen in a subset of the cells visualised. These vesicles have therefore been described

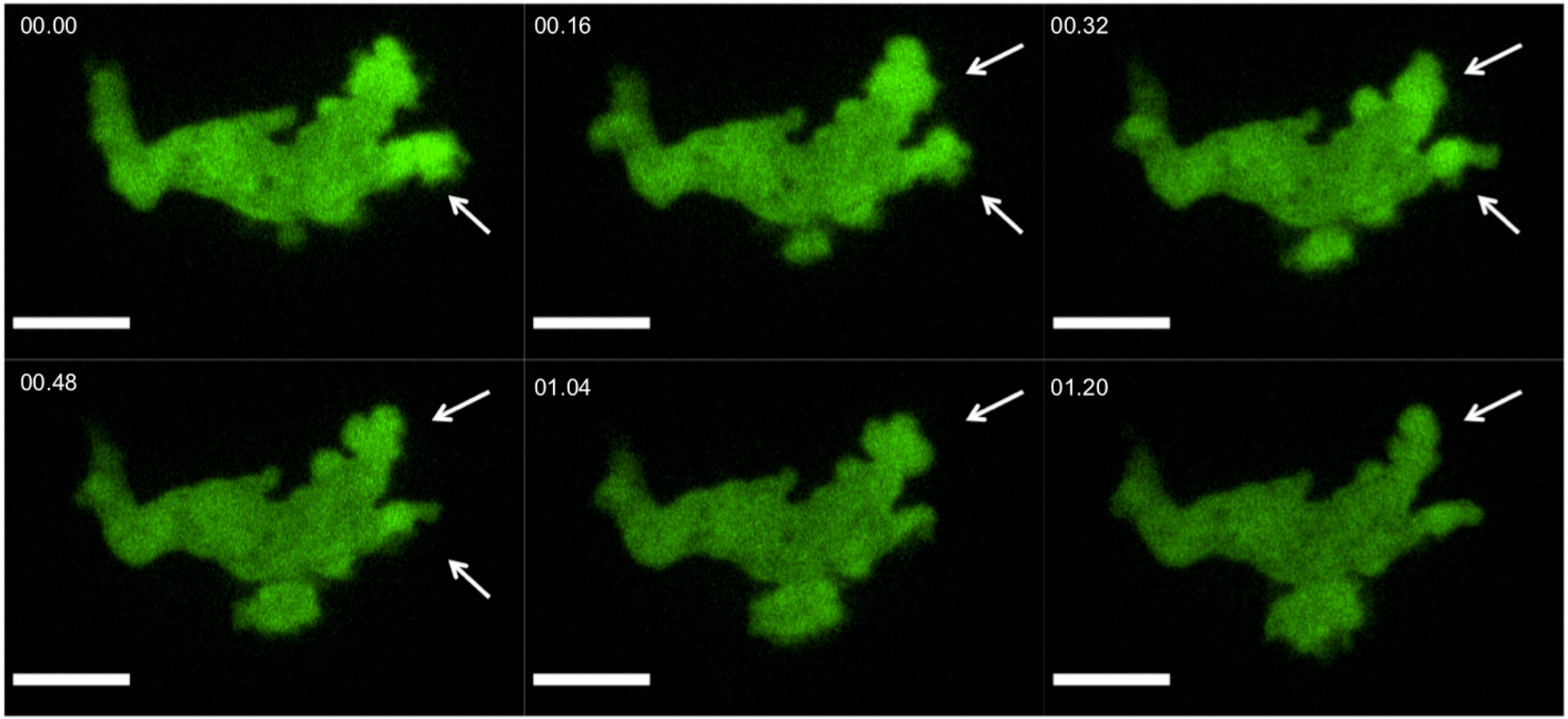

Figure 6.7. *In vivo* IL-1β.EGFP expressing macrophages retain membrane blebbing behaviour *in vivo*.
pDEST(mpeg1:IL-1β.EGFP) injected transiently into AB wildtype zebrafish embryos injured at 72 hpf is expressed in macrophages detected by confocal microscopy at the site of injury. Macrophages exhibit membrane blebbing at the leading edges (white arrows). Scale =7 μm, time os mm:ss from start of imaging.

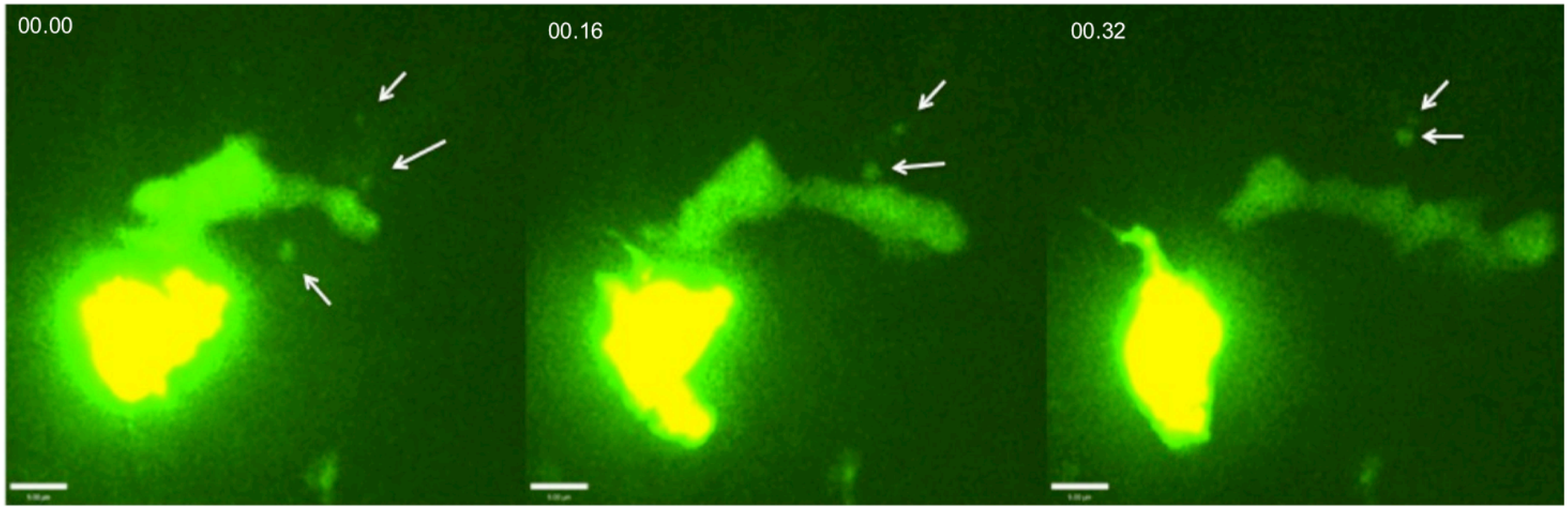

Figure 6.8. Confocal microscopy of transiently expressed *Tg(mpeg1:Gal4.VP16)sh256* in cells at the site of injury reveals the presence of zfIL-1β.EGFP in 0.1-1μm vesicles around these cells. *Tg(mpeg1:Gal4.VP16)sh256* was transiently injected alongside tol2 mRNA into AB wildtype embryos. These embryos were injured 72 hpf and imaged after 1 hour using spinning disc confocal microscopy with a 40x 1.3NA oil immersion objective. Exposure was set on the level of the dimmer cell, therefore cell in the foreground is overexposed. Contrast enhancement was applied using Volocity™. IL-1β.EGFP containing vesicles can be seen putatively released from these cells (arrows). Time is mm:ss from initial frame, scale = 5 μm.

as IL-1β.EGFP containing microvesicles, although further work is required to confirm their origin and biogenesis.

6.3 Discussion

There are many elements of the IL-1β pathway that remain poorly understood. In this chapter I attempted to address the gulf of understanding in the secretion of IL-1β during the inflammatory response by developing an *in vivo* model of IL-1β release, which could be used to visualise this response in a whole intact organism, rather than in the cell culture paradigm to which previous studies have been restricted.

Due to the poorly understood nature of the release pathway of IL-1β, an *in vivo* reporter of release had to be based on the IL-1β sequence itself, the simplest method to design such a reporter being to label IL-1β with a fluorophore. The EGFP label has been shown to not interfere with release of IL-1β so was predicted to serve as an adequate reporter of secretion.

6.3.1 Gateway™ and the Tol2kit for vector construction.

The use of Gateway™ to generate these reporters allowed the construction of a number of vectors from the same basic template. Here, IL-1β.EGFP and mCherry driven by UAS, *mpeg1* and 4xUAS were all generated from a single middle entry clone of zfIL-1β. Throughout this study, the Gateway™ system provided an ideal solution for generating expression vectors and allowed their adaptation to using different promoters, which would have required a substantial change in strategy if using traditional cloning methods. However, the tol2 kit can cause problems if used for generating fusion constructs. In the initial attempt at generating a fusion vector, the linker between the IL-1β coding sequence and the EGFP start site added 41 amino acids in total, which proved to be deleterious for protein expression. By cloning zfIL-1β directly into an entry clone, this linker was reduced to a size of 9 amino acids, the minimum possible due to the inclusion of the Att recombination sites between the two entry clones. This construct was shown to express well *in vivo*, however, with no comparison, it is unclear whether this construct would be more stable or have a stronger signal without this linker.

The tol2 kit based on Invitrogen's Gateway™ system is an incredibly useful tool for the generation of transgenics. There is a sufficient range of available entry clones to generate an array of expression vectors, however over the course of the project I have observed a few problems that I have tried to improve upon. One of the easiest methods for making a middle entry clone from an existing expression construct is to use the middle entry MCS plasmid to generate a clone of your gene of interest in a Gateway™ compatible format. However, a number of problems were encountered in the use of the original PME-MCS. The first was in the cloning error that leads to the addition of a stop site in two out of three reading frames, and the second was the presence of an M13 primer site after the att recombination sites. The presence of an additional primer site disrupts the ease of sequencing a Gateway™ entry clone as all clones have been designed with M13F and M13R sites before the 5' att site and behind the 3' att site both reading into the construct. Gateway™ entry clones are usually easily sequenced, but the presence of an additional M13F site in the Gateway™ insert between the attp1 and attp2 sites interferes with this functionality. The pME-MCS entry clone was itself added to the tol2kit as an afterthought (Chien et al, http://chien.neuro.utah.edu/tol2kitwiki/index.php/Main_Page), as the generation of entry clones from PCR products with ATT site containing primers is much simpler than using a traditional cloning vector such as TOPO to amplify a given sequence, then using restriction site primers to insert it into pME-MCS.

Though an MCS plasmid is not essential, it can be useful to generate constructs from existing plasmids without BP clonase, and in situations where maintaining a reading frame, such as when generating fusion constructs, it is not required. The PCS2 plasmid family is often used to make mRNA for overexpression in fish, and we found that by using AttB primers designed for either side of the PCS2+ multiple cloning site, we could very easily generate entry clones for coding sequences from existing mRNA generation constructs. These clones lack the issues with the pME-MCS constructs described above and allowed the generation of a PCS2+ multiple cloning site entry clone which can be used to generate new entry clones entirely via restriction digest.

As described, a recently discovered problem with Gal4/UAS expression system in zebrafish is the methylation mediated silencing of the UAS promoter sequence (Akitake et al. 2011). The 5' UAS clone provided in the initial release of the tol2 kit is a 10x repeating concatamer construct and remains prone to silencing. I used the 4x non-repeating sequence described to generate a theoretically methylation-resistant entry clone which should prove a useful tool for exploiting the Gal4/UAS system using Gateway™.

6.3.2 Macrophage promoters

A major problem with the generation of the IL-1β-EGFP reporter was the lack of a reliable macrophage specific Gal4 driver line or macrophage promoter with which to express the zfIL-1β EGFP fusion protein. The *fms* promoter (Gray et al. 2011) expressed in too wide a population of cells and caused concerns for the viability and reliability of results recorded in embryos with overexpression of zfIL-1β.EGFP in so many different cell types. Human IL-1β has a very broad range of effects and overexpression in tissues without the internal machinery to process IL-1β could lead to deleterious effects for the health of the zebrafish. These issues were compounded by the availability of this line only as a compound transgenic with *Tg(UAS:nsfB.mCherry)i149*, a line with significant UAS methylation and promoter silencing.

The publication of the much more macrophage specific promoter, *mpeg1* (Ellett et al. 2010), and its available format as an entry clone compatible with the Tol2kit system used to generate the IL-1β expression vectors allowed the expression of zfIL-1β.EGFP in a much more macrophage specific manner, and furthermore allowed a variety of strategies for reporter expression to increase the chances of success.

Though putative macrophage derived microvesicles have been imaged around *mpeg1*:zfIL-1β.EGFP positive cells close to the site of injury, they are not conclusively attributable as the microvesicles described in previous studies of IL-1β release from cells. In order to visualise the release of vesicles from cells, a higher resolution approach is required. These microvesicles, described as between 0.1 and 1 μM, exist at the limit of conventional fluorescence microscopy, and the

images presented here were recorded at an NA of 1.3 in using a Nipkow Spinning disc confocal, close to the state-of-the-art for rapid live imaging. Though higher resolution approaches exist for fluorescence microscopy, they are limited in their application to this study. Super-resolution microscopes could provide the requisite resolution, as could high-end confocal microscopes. However these systems are mostly too slow for imaging of a mechanism described as occurring over such a short timeframe. This limitation must therefore be addressed using a method compatible with the current imaging system.

The tol2kit provides a ready mechanism that could be used to overcome this challenge. If the membrane of the IL-1β.EGFP positive cells could be visualised, separately from the reporter, it may be possible to distinguish the IL-1β release events during a microscopy acquisition. If IL-1β.EGFP cells were also labeled with a membrane mCherry then the simultaneous expression of both transgenes would allow the visualization of events at the cell surface, and would also allow easier tracking of these vesicles following stimulation.

An expression vector for a membrane localized mCherry would not be technically challenging to generate. The tol2kit includes an mCherry vector with an in-frame membrane localization sequence, the latest version of which is available for use. Construction of the vector would simply involve combining this with the correct promoter for the expression system used, either *mpeg1* or 4xUAS. However, the construct may be more reliable if a non Gateway™ system were used for expression. If this membrane fluorophore was combined in a single expression vector with the zfIL-1β.EGFP fusion protein and *mpeg1* as a direct driving promoter then only a single allele would need to be generated to yield a useable transgenic line. This would make animal husbandry and stock maintenance significantly easier and cheaper and would allow the reduction of inbreeding within the fish stock to enhance animal welfare.

Chapter 7: Discussion

In this thesis I aimed to develop a zebrafish model of IL-1β biology. Initially I investigated the function of IL-1β in zebrafish to verify the suitability of the species for this purpose. The predicted structure of zebrafish IL-1β is very similar to the crystal structure of human IL-1β as shown using three different methods for structural prediction, I-TASSER, Phyre and RaptorX. IL-1β mRNA was shown to be induced in response to injury, and treatment of zebrafish larvae with IL-1β pathway inhibitors reduced NF-kB activation and leukocyte recruitment to the site of injury, however one major question was not addressed.

There is considerable disagreement in the literature over the evolutionary conservation of IL-1β. Initial studies of IL-1β outside the mammalian class indicated the lack of a consensus caspase cleavage site on fish, birds and *Xenopus* (Bird, Zou, et al. 2002). However, processing of these IL-1β proteins by non mammalian vertebrates was observed from the earliest experiments of IL-1β biology when Auron et al. (1984) demonstrated that *Xenopus* oocytes produced biologically active IL-1β after injection with the human mRNA sequence. Further evidence for IL-1β processing outside the mammalian lineage has been demonstrated in seabream (Angosto et al. 2012), but was shown to be independent of caspase-1. Conversely a recent study showd that zebrafish IL-1β is cleaved by zebrafish caspase-1 equivalents caspase-A and caspase-B (Vojtech et al. 2012). Zou et al. (1999) investigated trout IL-1β, and showed no evidence of a Caspase-1 cleavage site, but performed no functional tests. From the literature, there are few pieces of evidence describing the cleavage of IL-1β in teleost fish, and the two key studies in the area, Angosto et al. (2012), and Vojtech et al. (Vojtech et al. 2012), disagree on the subject. A key factor in this disagreement is the evolutionary distance between seabream and zebrafish (Sarropoulou et al. 2007), and clear differences in the structure of their domains (López-Castejón et al. 2008). López-Castejón et al (2008) characterise the seabream caspase-1 as more closely related to human caspase-1 based largely on the CARD domain, however, a closer look at these caspase sequences with the CARD domain removed shows a lesser distance between zebrafish and human caspase-1 than seabream caspase-1. This implies closer homology between the active regions of human caspase-1 and

caspase-A, which may explain the difference in IL-1β cleavage potential described (Angosto et al. 2012; Vojtech et al. 2012) (Figure 3.7).

In this study I found that based on structure prediction software, human and zebrafish IL-1β share remarkable structural similarity in the region equivalent to bioactive IL-1β. The structural similarity of the pro domain region is poorer, however, this is expected, as the function of this domain appears to be masking IL-1β bioactivity. Further pathway conservation was found in relation to inflammatory caspase structure, and with regard to IL-1β functional assays. caspase-1 antagonists had a negative effect on inflammatory assays measuring NF-kB activation and leukocyte recruitment, and IL-1β was shown to be highly induced in response to inflammatory insult via injury. P2X7 inhibition had a similar effect on inflammatory function, demonstrating that these results were likely based on response from similar pathways.

The structural similarity and evidence of cleavage (Vojtech et al. 2012), indicate an evolutionary importance placed on IL-1β as a regulator of inflammation, highlighted by increasing complexity during mammalian evolution, which has served to intensify this role. These data support the need for further study and characterisation of IL-1β as a key mediator of inflammation demonstrated by its role in so many inflammatory diseases (Dinarello 2011a) and the effects that anti IL-1β therapies have so far produced (Dinarello 2011b; Dinarello et al. 2012).

Unfortunately, such treatments have thus far taken the form of protein based therapies such as recombinant IL-1RA antagonist Anakinra, Decoy receptor based Rilonocept (Terkeltaub et al. 2009) and monoclonal anti IL-1β antibody Canakinumab (Dhimolea 2010). Protein therapies tend to be more expensive, have a shorter half-life and require intravenous administration; undesirable qualities for the treatment of such a broad range of diseases. And it is our hope that with a better understanding of IL-1β biology, a more effective small molecule inhibitor could be found.

The objectives of the study define the choice of model used for the investigation of IL-1β biology. Our understanding of IL-1β biology has improved significantly from the use of *in vitro* study in cell culture, alongside mouse models and histological studie which have allowed a more systemic approach. However, with these models it would be very difficult to establish the *in vivo* mechanisms of IL-1β secretion, and their downstream function. It was therefore a further aim of this study to develop reporters of these release pathways for use in an *in vivo* investigation of this pathway amenable to chemical and genetic manipulation.

To achieve these aims, the zebrafish presents an ideal model. The transparency of the zebrafish allows the use of fluorescent reporters acting on a temporal and spatial level with minimum of interference in how these pathways function in a living organism, yet its genetic tractability allows these reporters to be readily established.

I have approached the development of an IL-1β model by investigating the use of reporters linked to some of the more confounding questions of IL-1β biology; the development of FRET as a reporter of IL-1β processing is an effort to investigate the activation of caspase-1 on a temporal scale. To date my efforts to develop a caspase-1 reporter have been limited, primarily by the lack of a reliably transfectable human macrophage model has restricted microscopy measurements. Despite this the *in vivo* measurement of FRET was achieved; I have successfully characterised the use of the *Tg(BACmpo:FRET DEVD)i237* as a reporter caspase-3 apoptosis *in vivo*, a tool which should prove more flexible than TUNEL staining only useable on fixed specimens, providing a temporal readout of neutrophil apoptosis. This reporter can easily be incorporated into other tissues under the control of a UAS sequence or other promoters. However, in order to characterise a reporter for caspase-1, I would require a more amenable cell line or a better mode of transfection, such as polymersome based methods. Further improvements to this reporter could be made by using a more effective set of fluorophores; CFP emission is less intense than YFP and allowances have to be made for this in designing experiments. With a brighter blue fluorophore, FRET *in vivo* would be easier to perform, as described by Goedhart et al., (2010) who have developed the more intense and photostable CFP variant mTurquoise, as well as the improved mTurquoise 2 (Goedhart et al. 2012).

A further problem with using CFP/YFP as a reporter of caspase activation (Tyas et al. 2000; Rehm et al. 2002) is the sensitivity of YFP to pH changes (Llopis et al. 1998). A more photostable replacement would be the EYFP derivative Venus, shown to be more effective in the study of apoptosis (K. Takemoto et al. 2003).

One of the most intriguing aspects of IL-1β research is in understanding unconventional release of this cytokine from monocytic cells, and the possible involvement of the same pathway as a more general release mechanism for leaderless proteins. As I have discussed previously, there is much evidence to link IL-1β processing to its secretion; having a live reporter of caspase-1 activation would provide the opportunity to gain new insight to this pathway. Measuring such secretory mechanisms and vesicle biogenesis would require novel specialised reporters.

The molecular machinery of the secretion pathway is currently unknown, and as such we are missing a big part of the larger picture of vesicle biology, a pathway demonstrated to be important in significantly more than IL-1β secretion. As the pathway remains mechanistically opaque, my last aim was to develop a reporter of IL-1β release. It was necessary to base my reporter on a protein known to utilise this leaderless secretory pathway; IL-1β. It is unknown which part of IL-1β structure is necessary for its secretion, and whether any accessory proteins are perhaps responsible This lack of knowledge mandated the use of the entire IL-1β sequence in reporter construction, which was then labelled with a fluorophore for *in vivo* visualisation. Using this reporter, I have recorded the first putative visual evidence *in vivo* of IL-1β containing microvesicles produced in response to injury. At present there are some limitations in the use of this reporter and the interpretations that can be accurately made from the imaging data. It is currently impossible to achieve the resolution necessary to visualise release events themselves due to the lack of visible membrane interaction. In order to use this reporter to successfully investigate mechanisms of release it is therefore necessary to use it alongside a membrane label.

These reporters would be impossible to develop in a mouse or cell line model and here we can clearly see the advantages of zebrafish for this kind of

research. It is important to note that although zebrafish are a useful model, any discoveries made will still need to be validated in a mammalian model if they are to be applied in a therapeutic setting. Therefore zebrafish should be used not as a model in isolation, but alongside mammalian models such as mouse or cell culture techniques.

7.2 Future work

The validation of IL-1beta function in the zebrafish and the generation of reporter lines to measure inflammasome activation, IL-1β secretion and targeting now offer the opportunity to dissect the biological mechanisms underlying these processes, and to screen for small molecular inhibitors of these pathways. However, I feel the limitations of the model should first be addressed.

In order to develop my FRET reporters further it is necessary to use a mammalian tissue culture model more amenable to reporter expression. This study has demonstrated the inefficiency of transfection in THP-1 cells, and with the recently published study demonstrating the ability of caspase-A to process native IL-1β (Vojtech et al. 2012), it may prove more effective to generate this tool *in vivo* than relying on cell culture. Using the data recently published by Vojtech et al. (Vojtech et al. 2012), it will be possible to use site directed mutagenesis to generate a caspase A specific FRET reporter, however, in its initial discovery, Masumoto et al (2003) describe caspase-A to be specific to caspase-1 substrates, so perhaps a strategy incorporating both caspase-A site NVVD and caspase-1 site YVHD would be more prudent. This assay could then be used to investigate caspase-A activation *in vivo* and further characterise its substrate specificity and mechanism of activation via the use of morpholino knockdown and mutant generation strategies, as well as small molecule inhibition. Developing this reporter in human cell lines will, however, prove more technically demanding. It would be necessary to use a macrophage model more amenable to transfection and imaging.

In order, to more robustly observe FRET events related to caspase-1 activation it would also be necessary to modify the FRET reporter with the latest

CFP/YFP fluorophores, mTurquoise 2 and Venus for enhanced photo- and pH stability.

From the *Tg(BACmpo:FRET DEVD)sh237* line, it is possible to see how a FRET based reporter could be used as the foundation of a small molecule inhibitor screen, however, the technique is difficult and both research-time and computing-resource intensive and we found that it is more useful in confirming the mechanism of inflammation resolution enhancing compounds than it could as being the basis of a screen.

This limitation could be reversed *in vitro*, and recently Compan et al., (2012) have described an IL-1β processing reporter based on a very similar principle. Compan et al., (2012) have developed an IL-1β molecule with a BRET reporter (Bioluminescent Resonance Energy Transfer) with both advantages and disadvantages over a FRET based system. BRET uses a luciferase mediated reaction as a fluorescent donor to stimulate an acceptor fluorophore, and therefore does not require fluorescent excitation making it less susceptible to photobleaching and spectral bleedthrough. This is a very viable system for cell based assays, however is less useful *in vivo* because of its dependence on the availability of a luciferase substrate. In essence though, a cell based resonance reporter is more amenable to small molecule screens due to less intense image processing requirements and lower susceptibility to image distortion through living tissue. Although data gathered from these screens should also be validated in a living model for a clearer mechanistic insight.

The improvement of the zebrafish IL-1β fusion protein into a more reliable reporter of release will be simpler. This would require the generation of a macrophage mCherry membrane tag, something achievable with the Tol2Kit (Kwan et al. 2007)and the *mpeg1* promoter entry clone (Ellett et al. 2010) and the subsequent generation of the transgenic zebrafish line. This also provides an exciting opportunity for a more reliable and higher resolution reporter. The literature on IL-1β release tells us that without inflammatory stimuli, IL-1β is subject to constant degradation in lysosomes (Saitoh et al. 2008; Harris et al. 2011), therefore I would predict that IL-1β.EGFP will not provide a constant fluorescent signal. With the use of a Viral 2A sequence (Provost & Rhee 2007) it

would be possible to generate a bicistronic expression construct encoding both the IL-1β fusion protein and the necessary membrane label (Figure 7.1). The virtue of

Figure 7.1. IL-1β reporter Bicistronic cloning strategy. It may be possible to generate a more efficient IL-1β reporter construct using a Bicistronic cloning strategy. A middle entry clone of an IL-1β.EGFP coding sequence would need to be recombined in frame to a 3' entry clone containing a viral 2A autocleaving sequence and a membrane bound mCherry. Such a reporter would allow the translation of both an IL-1β fusion protein and a membrane tag from the same coding sequence allowing improvements to animal husbandry to better comply with Reduction and Refinement objectives in animal welfare by reducing the number of fish necessary and facilitating greater genetic variation as less inbreeding would be required, but importantly, also improving the experimental resolution of the zebrafish line by providing a temporal readout of IL-1β.EGFP protein stability using the mCherry protein as a control.

such a construct is that both proteins will be translated equimolarly, therefore in any macrophage labelled with a red membrane, the IL-1β fusion protein would also be expressed. Under these circumstances, it would be possible to investigate the stability of IL-1β.EGFP in response to inflammatory stimuli, as the presence of a membrane label will indicate expression of the gene; and also to enable the visualisation of membrane-derived microvesicles release events due to the higher contrast provided by the membrane label. The presence of these fluorophores will also enable easier tracking of vesicle trafficking to target cells, and give more insight as to the events responsible for the release of microvesicular contents.

My initial hypotheses were that the ESCRT pathway is responsible for the biogenesis of membrane-derived microvesicles and that this pathway was coupled to caspase-1 via Rab adaptor proteins. We now have the tools to investigate these hypotheses through the use of knockdown technology. The Zebrafish homologue of ESCRT I subunit protein Tsg101 (accession: NP_001002089.1) shares 84% identity with the human protein (accession: Q99816.2) and provides an ideal target for morpholino knockdown in the zebrafish, however, the high conservation implies its evolutionary importance and creates concern that this would have a deleterious effect on a number of other pathways. Perhaps a more appropriate target for knockdown would be adaptor protein Rab39a (accession: NP_059986.1) which shares 59% identity to the zebrafish (accession: NP_998207.1). Rab39a has already been linked to IL-1β release via caspase-1, but its mechanism of action is unclear (C. Becker et al. 2009).

7.3 Thesis summary

In summary, in this thesis I have demonstrated the utility of zebrafish in the study of IL-1β through the validation of zebrafish IL-1 biology justifying the development of fluorescent reporters and transgenic lines investigating IL-1β biology. I undertook a bioinformatics study of IL-1β biology, gaining insight into the structure of IL-1β and possible evolutionary implications in IL-1β. I developed and generated a number of reporter lines from both my own constructs and those of collaborators enabling better characterisation of innate immunity in the zebrafish. This enabled me to undertake a study of the effects of known mammalian IL-1β pathway inhibitors in zebrafish to determine the effects they had on inhibiting inflammation in the zebrafish, alongside characterising zebrafish IL-1β mRNA induction. Some of the reporter lines I have generated have also benefitted our collaborators in the wider community. I have developed a methodology for reporting *in vivo* apoptosis using a FRET based reporter through the adaptation of available software and microscopy equipment allowing better characterisation of a pro-resolution compound, Isopimpinellin, in inflammation. I have also generated a reporter of IL-1β release and observed the first putative microvesicle release events from macrophages in response to inflammatory insult. These tools now provide us with the opportunity to identify the biological mechanism underlying Il-1β secretion *in vivo*, and to screen for small molecule inhibitors of these pathways.

Bibliography

Abbate, A. et al., 2008. Anakinra, a recombinant human interleukin-1 receptor antagonist, inhibits apoptosis in experimental acute myocardial infarction. *Circulation*, 117(20), p.2670.

Ahrens, M. et al., 2013. Whole-brain functional imaging at cellular resolution using light-sheet microscopy. *Nature methods*, p.Epub ahead of print.

Akitake, C. et al., 2011. Transgenerational analysis of transcriptional silencing in zebrafish. *Developmental biology*, 352(2), pp.191–201.

Allan, S., Tyrrell, P. & Rothwell, N., 2005. Interleukin-1 and neuronal injury. *Nature Reviews Immunology*, 5(8), pp.629–640.

Allen, I., Scull, M. & Moore, C., 2009. The NLRP3 Inflammasome Mediates in vivo Innate Immunity to Influenza A Virus through Recognition of Viral RNA. *Immunity*, 30(4), pp.556–565.

Andrei, C. et al., 1999. The secretory route of the leaderless protein interleukin 1β involves exocytosis of endolysosome-related vesicles. *Molecular biology of the cell*, 10(5), pp.1463–1475.

Andrews, D., 1989. A unified theory of radiative and radiationless molecular energy transfer. *Chemical physics*, 135, pp.195–201.

Angosto, D. et al., 2012. Evolution of inflammasome functions in vertebrates: Inflammasome and caspase-1 trigger fish macrophage cell death but are dispensable for the processing of IL-1β. *Innate immunity*.

Aravind, L. & Koonin, E., 1999. Gleaning non-trivial structural, functional and evolutionary information about proteins by iterative database searches. *Journal of molecular biology*, 287(5), pp.1023–1040.

Asakawa, K. & Kawakami, K., 2008. Targeted gene expression by the Gal4-UAS system in zebrafish. *Development, Growth & Differentiation*, 50(6), pp.391–399.

Aupeix, K. et al., 1997. The significance of shed membrane particles during programmed cell death in vitro, and in vivo, in HIV-1 infection. *Journal of clinical investigation*, 99(7), pp.1546–54.

Auron, P. et al., 1987. Studies on the molecular nature of human interleukin 1. *Journal of Immunology*, 138(5), pp.1447–1456.

Auron, P. & Webb, A., 1984. Nucleotide sequence of human monocyte interleukin 1 precursor cDNA. *Proceedings of the …*, 81(December), pp.7907–7911.

Ayala, J. et al., 1994. IL-1 beta-converting enzyme is present in monocytic cells as an inactive 45-kDa precursor. *Journal of immunology*, 153(6), pp.2592–9.

Baeuerle, P., 1988. I kappa B: a specific inhibitor of the NF-kappa B transcription factor. *Science*, 242(4878), pp.540–546.

Baeuerle, P. & Baltimore, D., 1996. NF-κB : Ten Years After Meeting Review. *Cell*, 87, pp.13–20.

Balla, K. et al., 2010. Eosinophils in the zebrafish: prospective isolation, characterization, and eosinophilia induction by helminth determinants. *Blood*, 116(19), pp.3944–54.

Baxendale, S. et al., 2012. Identification of compounds with novel anti-convulsant properties in a zebrafish model of epileptic seizures. *Disease models mechanisms*, (June), pp.1–51.

Beck, G. & Habicht, G., 1996. Immunity and the invertebrates. *Scientific American*, 275(5), pp.60–63, 66.

Beck, G. & Habicht, G., 1991a. primitive cytokines : harbingers of vertebrate defense. *Immunology today*, 12(6), pp.180–183.
Beck, G. & Habicht, G., 1991b. Purification and biochemical characterization of an invertebrate interleukin 1. *Molecular immunology*, 28(6), pp.577–584.
Becker, C., Creagh, E. & O'Neill, L., 2009. Rab39a binds caspase-1 and is required for caspase-1-dependent interleukin-1beta secretion. *Journal of biological chemistry*, 284(50), pp.34531–7.
Bergsbaken, T. & Cookson, B., 2007. Macrophage activation redirects yersinia-infected host cell death from apoptosis to caspase-1-dependent pyroptosis. *PLoS pathogens*, 3(11).
Bergsbaken, T., Fink, S. & Cookson, B., 2010. Pyroptosis: host cell death and inflammation. *Nature Reviews Microbiology*, 7(2), pp.99–109.
Bernard, P. & Couturier, M., 1992. Cell killing by the F plasmid CcdB protein involves poisoning of DNA-topoisomerase II complexes. *Journal of molecular biology*, 226(3), pp.735–45.
Bianco, F. et al., 2009. Acid sphingomyelinase activity triggers microparticle release from glial cells. *EMBO journal*, 28(8), pp.1043–54.
Bianco, F. et al., 2005. Astrocyte-derived ATP induces vesicle shedding and IL-1β release from microglia. *Journal of Immunology*, 174(11), pp.7268–7277.
Bird, S., Zou, J., et al., 2002. Evolution of interleukin-1β. *Cytokine & Growth Factor Reviews*, 13(6), pp.483–502.
Bird, S., Wang, T., et al., 2002. The first cytokine sequence within cartilaginous fish: IL-1 beta in the small spotted catshark (Scyliorhinus canicula). *Journal of immunology*, 168(7), pp.3329–40.
Black, R. et al., 1988. Generation of biologically active interleukin-1 beta by proteolytic cleavage of the inactive precursor. *Journal of biological chemistry*, 263(19), pp.9437–42.
Boutin, H. et al., 2001. Role of IL-1alpha and IL-1beta in ischemic brain damage. *Journal of Neuroscience*, 21(15), pp.5528–5534.
Brennan, M. & Cookson, B., 2000. Salmonella induces macrophage death by caspase-1-dependent necrosis. *Molecular microbiology*, 38(1), pp.31–40.
Bresnihan, B. et al., 1998. Treatment of rheumatoid arthritis with recombinant human interleukin-1 receptor antagonist. *Arthritis and rheumatism*, 41(12), pp.2196–204.
Brocker, C. et al., 2010. Evolutionary divergence and functions of the human interleukin (IL) gene family. *Human Genomics*, 5(1), pp.30–55.
Brough, D. & Rothwell, N., 2007. Caspase-1-dependent processing of pro-interleukin-1beta is cytosolic and precedes cell death. *Journal of Cell Science*, 120(5), pp.772–781.
Bryan, N. & Dorfleutner, A., 2009. Activation of inflammasomes requires intracellular redistribution of the apoptotic speck-like protein containing a caspase recruitment domain. *Journal of Immunology*, 182(5), pp.3173–3182.
Buchan, D. et al., 2010. Protein annotation and modelling servers at University College London. *Nucleic acids research*, 38(Web Server issue), pp.W563–8.
Buck, L. et al., 2012. Ototoxin-induced cellular damage in neuromasts disrupts lateral line function in larval zebrafish. *Hearing research*, 284(1-2), pp.67–81.
Bufler, P., Gamboni-Robertson, F. & Azam, T., 2004. Interleukin-1 homologues IL-1F7b and IL-18 contain functional mRNA instability elements within the

coding region responsive to lipopolysaccharide. *Biochemical Journal*, 381(Pt 2), pp.503–510.
Bujak, M. & Frangogiannis, N., 2009. The role of IL-1 in the pathogenesis of heart disease. *Archivum immunologiae et therapiae experimentalis*, 57(3), pp.165–76.
Bürckstümmer, T. et al., 2009. An orthogonal proteomic-genomic screen identifies AIM2 as a cytoplasmic DNA sensor for the inflammasome. *Nature immunology*, 10(3), pp.266–72.
Carlotti, F., Dower, S. & Qwarnstrom, E., 2000. Dynamic shuttling of nuclear factor kappa B between the nucleus and cytoplasm as a consequence of inhibitor dissociation. *Journal of biological chemistry*, 275(52), pp.41028–34.
Carlton, J. & Martin-Serrano, J., 2007. Parallels between cytokinesis and retroviral budding: a role for the ESCRT machinery. *Science*, 316(5833), pp.1908–12.
Carroll, M., 1998. The role of complement and complement receptors in induction and regulation of immunity. *Annual review of immunology*, 16, pp.545–68.
Casadio, R. et al., 2001. Model of interaction of the IL-1 receptor accessory protein IL-1RAcP with the IL-1beta/IL-1R(I) complex. *FEBS Letters*, 499(1-2), pp.65–68.
Chae, J. et al., 2006. The B30.2 domain of pyrin, the familial Mediterranean fever protein, interacts directly with caspase-1 to modulate IL-1beta production. *Proceedings of the National Academy of Sciences*, 103(26), pp.9982–9987.
Cheng, K. et al., 2011. Whole-animal imaging, gene function, and the Zebrafish Phenome Project. *Current opinion in genetics & development*, 21(5), pp.620–9.
Cohen, S. et al., 2002. Treatment of rheumatoid arthritis with anakinra, a recombinant human interleukin-1 receptor antagonist, in combination with methotrexate: results of a twenty-four-week, multicenter, randomized, double-blind, placebo-controlled trial. *Arthritis and Rheumatism*, 46(3), pp.614–624.
Colotta, F. et al., 1993. Interleukin-1 type II receptor: a decoy target for IL-1 that is regulated by IL-4. *Science*, 261(5120), pp.472–475.
Colucci-Guyon, E. et al., 2011. Strategies of professional phagocytes in vivo: unlike macrophages, neutrophils engulf only surface-associated microbes. *Journal of cell science*, 124(Pt 18), pp.3053–9.
Compan, V. et al., 2012. A Genetically Encoded IL-1β Bioluminescence Resonance Energy Transfer Sensor To Monitor Inflammasome Activity. *Journal of immunology*.
Cooke, E. et al., 2001. Functional analysis of the interleukin-1-receptor-associated kinase (IRAK-1) in interleukin-1 beta-stimulated nuclear factor kappa B (NF-kappa B) pathway activation: *Biochemical Journal*, 359(Pt 2), pp.403–410.
Correa, R. et al., 2004. Characterization of NF-kappa B/I kappa B proteins in zebra fish and their involvement in notochord development. *Molecular and Cellular biology*, 24(12), pp.5257–5268.
Croston, G. et al., 1995. NF-kappa B activation by interleukin-1 (IL-1) requires an IL-1 receptor-associated protein kinase activity. *Journal of Biological Chemistry*, 269(40), pp.24666–24672.
Cruz, C. et al., 2007. ATP activates a reactive oxygen species-dependent oxidative stress response and secretion of proinflammatory cytokines in macrophages. *Journal of biological chemistry*, 282(5), pp.2871–9.

Cui, X. et al., 2003. Shedding of the type II IL-1 decoy receptor requires a multifunctional aminopeptidase, aminopeptidase regulator of TNF receptor type 1 shedding. *Journal of immunology*, 171(12), pp.6814–9.
Cullinan, E., Kwee, L. & Nunes, P., 1998. IL-1 receptor accessory protein is an essential component of the IL-1 receptor. *Journal of Immunology*, 161(10), pp.5614–5620.
Curado, S. et al., 2008. Nitroreductase-mediated cell/tissue ablation in zebrafish: a spatially and temporally controlled ablation method with applications in developmental and regeneration. *Nature protocols*, 3(6), pp.948–954.
Dachary-Prigent, J. et al., 1993. Annexin V as a probe of aminophospholipid exposure and platelet membrane vesiculation: a flow cytometry study showing a role for free sulfhydryl groups. *Blood*, 81(10), pp.2554–65.
Demirov, D. et al., 2002. Overexpression of the N-terminal domain of TSG101 inhibits HIV-1 budding by blocking late domain function. *Proceedings of the National Academy of Sciences*, 99(2), pp.955–60.
Dhimolea, E., 2010. Canakinumab. *Monoclonal Antibodies*, 2(1), pp.3–13.
DiDonato, J. et al., 1997. A cytokine-responsive IkappaB kinase that activates the transcription factor NF-kappaB. *Nature*, 388(6642), pp.548–54.
Dinarello, C., 2011a. A clinical perspective of IL-1β as the gatekeeper of inflammation. *European journal of immunology*, 41(5), pp.1203–17.
Dinarello, C., 1996. Biologic basis for interleukin-1 in disease. *Blood*, 87(6), pp.2095–147.
Dinarello, C., 2011b. Blocking interleukin-1β in acute and chronic autoinflammatory diseases. *Journal of internal medicine*, 269(1), pp.16–28.
Dinarello, C., 2009a. Immunological and inflammatory functions of the interleukin-1 family. *Annual review of immunology*, 27, pp.519–50.
Dinarello, C., 2009b. Interleukin-1beta and the autoinflammatory diseases. *New England Journal of Medicine*, 360(23), pp.2467–2470.
Dinarello, C., Ikejima, T. & Warner, S., 1987. Interleukin 1 induces interleukin 1. I. Induction of circulating interleukin 1 in rabbits in vivo and in human mononuclear cells in vitro. *Journal of Immunology*, 139(6), pp.1902–1910.
Dinarello, C., Simon, A. & Van der Meer, J., 2012. Treating inflammation by blocking interleukin-1 in a broad spectrum of diseases. *Nature Reviews Drug Discovery*, 11(8), pp.633–652.
Dostert, C. et al., 2008. Innate immune activation through Nalp3 inflammasome sensing of asbestos and silica. *Science*, 320(5876), pp.674–7.
Draper, B., Morcos, P. & Kimmel, C., 2001. Inhibition of zebrafish fgf8 preâ€↓mRNA splicing with morpholino oligos: A quantifiable method for gene knockdown. *genesis*, 156, pp.154–156.
Dukes, J. et al., 2008. A dominant-negative ESCRT-III protein perturbs cytokinesis and trafficking to lysosomes. *Biochemical journal*, 411(2), pp.233–9.
Dunn, E. et al., 2001. Annotating genes with potential roles in the immune system: six new members of the IL-1 family. *Trends in immunology*, 22(10), pp.533–6.
Eimon, P. et al., 2006. Delineation of the cell-extrinsic apoptosis pathway in the zebrafish. *Cell death and differentiation*, 13(10), pp.1619–30.
Eisenberg, S. et al., 1990. Primary structure and functional expression from complementary DNA of a human interleukin-1 receptor antagonist. *Nature*, 343(6256), pp.341–6.

Ekker, S., 2000. Morphants: a new systematic vertebrate functional genomics approach. *Yeast*, 17(4), pp.302–306.
Elhage, R. et al., 1998. Differential effects of interleukin-1 receptor antagonist and tumor necrosis factor binding protein on fatty-streak formation in apolipoprotein E-deficient mice. *Circulation*, 97(3), pp.242–244.
Elks, P. et al., 2011. Activation of hypoxia-inducible factor-1α (Hif-1α) delays inflammation resolution by reducing neutrophil apoptosis and reverse migration in a zebrafish inflammation model. *Blood*, 118(3), pp.712–22.
Ellett, F. et al., 2010. Mpeg1 Promoter Transgenes Direct Macrophage-Lineage Expression in Zebrafish. *Blood*, 117(4), pp.49–56.
Fadok, V. et al., 1993. The Ability to Recognize Phosphatidylserine on Apoptotic Cells Is an Inducible Function in Murine Phosphatidylserine Following the Passage of Bone marrow-derived macrophages. *Chest*, 103(2 Suppl), p.102S.
Fadok, V., Voelker, D. & Campbell, P., 1992. Exposure of phosphatidylserine on the surface of apoptotic lymphocytes triggers specific recognition and removal by macrophages. *Journal of Immunology*, 148(7), pp.2207–2216.
Fantuzzi, G. et al., 1997. Response to local inflammation of IL-1 beta-converting enzyme- deficient mice. *Journal of immunology*, 158(4), pp.1818–24.
Feige, J. et al., 2005. PixFRET, an ImageJ plug-in for FRET calculation that can accommodate variations in spectral bleed-throughs. *Microscopy research and technique*, 68(1), pp.51–8.
Feng, Y. et al., 2010. Live imaging of innate immune cell sensing of transformed cells in zebrafish larvae: parallels between tumor initiation and wound inflammation. *PLoS biology*, 8(12), p.e1000562.
Feng, Y., Renshaw, S. & Martin, P., 2012. Live Imaging of Tumor Initiation in Zebrafish Larvae Reveals a Trophic Role for Leukocyte-Derived PGE(2). *Current biology : CB*, 22(13), pp.1253–9.
Fenton, M. et al., 1988. Human pro-IL-1 beta gene expression in monocytic cells is regulated by two distinct pathways. *Journal of Immunology*, 140(7), pp.2267–2273.
Fenton, M. et al., 1987. Transcriptional regulation of the human prointerleukin 1 beta gene. *Journal of immunology*, 138(11), pp.3972–9.
Ferrari, D. et al., 1997. Extracellular ATP triggers IL-1 beta release by activating the purinergic P2Z receptor of human macrophages. *Journal of Immunology*, 159(3), pp.1451–1458.
Ferrari, D. et al., 2006. The P2X7 receptor: a key player in IL-1 processing and release. *Journal of immunology*, 176(7), pp.3877–83.
Le Feuvre, R. et al., 2002. Priming of macrophages with lipopolysaccharide potentiates P2X7-mediated cell death via a caspase-1-dependent mechanism, independently of cytokine production. *Journal of biological chemistry*, 277(5), pp.3210–8.
Fink, S., Bergsbaken, T. & Cookson, B., 2008. Anthrax lethal toxin and Salmonella elicit the common cell death pathway of caspase-1-dependent pyroptosis via distinct mechanisms. *Proceedings of the National Academy of Sciences*, 105(11), pp.4312–7.
Fink, S. & Cookson, B., 2006. Caspase-1-dependent pore formation during pyroptosis leads to osmotic lysis of infected host macrophages. *Cellular microbiology*, 8(11), pp.1812–25.

Flajnik, M. & Du Pasquier, L., 2004. Evolution of innate and adaptive immunity: can we draw a line? *Trends in immunology*, 25(12), pp.640–4.
Fleischmann, R. et al., 2006. Safety of extended treatment with anakinra in patients with rheumatoid arthritis. *Annals of the rheumatic diseases*, 65(8), pp.1006–12.
Franchi, L. et al., 2006. Cytosolic flagellin requires Ipaf for activation of caspase-1 and interleukin 1beta in salmonella-infected macrophages. *Nature immunology*, 7(6), pp.576–82.
Fujii, T., Nakagawa, H. & Murakawa, S., 1979. Immunity in lamprey I. Production of haemolytic and haemagglutinating antibody to sheep red blood cells in Japanese lampreys. *Developmental & Comparative …*, 3(c), pp.441–451.
Gan, X. & Gould, S., 2011. Identification of an inhibitory budding signal that blocks the release of HIV particles and exosome/microvesicle proteins. *Molecular biology of the cell*, 22(6), pp.817–30.
Gao, L.Y. & Abu Kwaik, Y., 1999. Activation of caspase 3 during Legionella pneumophila-induced apoptosis. *Infection and immunity*, 67(9), pp.4886–94.
Garrus, J. et al., 2001. Tsg101 and the vacuolar protein sorting pathway are essential for HIV-1 budding. *Cell*, 107(1), pp.55–65.
Gasse, P. et al., 2009. Uric acid is a danger signal activating NALP3 inflammasome in lung injury inflammation and fibrosis. *American journal of respiratory and critical care medicine*, 179(10), pp.903–13.
Goedhart, J. et al., 2010. Bright cyan fluorescent protein variants identified by fluorescence lifetime screening. *Nature methods*, 7(2), pp.137–9.
Goedhart, J. et al., 2012. Structure-guided evolution of cyan fluorescent proteins towards a quantum yield of 93%. *Nature communications*, 3, p.751.
Gordon, G. et al., 1998. Quantitative Fluorescence Resonance Energy transfer Measurements Using Fluorescence Microscopy. *Biophysical journal*, 74(May), pp.2702–2713.
Grahames, C. & Michel, A., 1999. Pharmacological characterization of ATP- and LPS-induced IL-1beta release in human monocytes. *British journal of pharmacology*, 127, pp.1915–1921.
Gray, C. et al., 2011. Simultaneous intravital imaging of macrophage and neutrophil behaviour during inflammation using a novel transgenic zebrafish. *Thrombosis and haemostasis*, 105(5), pp.811–9.
Greenfeder, S. et al., 1995. Molecular cloning and characterization of a second subunit of the interleukin 1 receptor complex. *Journal of Biological Chemistry*, 270(23), pp.13757–13765.
Guma, M. et al., 2009. Caspase 1-independent activation of interleukin-1beta in neutrophil-predominant inflammation. *Arthritis and rheumatism*, 60(12), pp.3642–50.
Hall, CJ et al., 2007. The zebrafish lysozyme C promoter drives myeloid-specific expression in transgenic fish. *BMC developmental biology*, 7, p.42.
Hall, CJ et al., 2009. Transgenic zebrafish reporter lines reveal conserved Toll-like receptor signaling potential in embryonic myeloid leukocytes and adult immune cell lineages. *Journal of leukocyte biology*, 85(5), pp.751–65.
Van Ham, T. et al., 2010. Live imaging of apoptotic cells in zebrafish. *Faseb Journal*, 24(11), pp.4336–42.
Harris, J. et al., 2011. Autophagy controls IL-1beta secretion by targeting pro-IL-1beta for degradation. *Journal of biological chemistry*, 286(11), pp.9587–97.

Hartley, J., Temple, G. & Brasch, M., 2000. DNA cloning using in vitro site-specific recombination. *Genome Research*, 10(11), pp.1788–1795.
Heijnen, H. et al., 1999. Activated platelets release two types of membrane vesicles: microvesicles by surface shedding and exosomes derived from exocytosis of multivesicular bodies and alpha-granules. *Blood*, 94(11), pp.3791–9.
Hemmrich, G., Miller, DJ & Bosch, T., 2007. The evolution of immunity: a low-life perspective. *Trends in immunology*, 28(10), pp.449–54.
Henne, W., Buchkovich, N. & Emr, S., 2011. The ESCRT pathway. *Developmental cell*, 21(1), pp.77–91.
Henry, K. et al., 2013. Zebrafish as a model for the study of neutrophil biology. *Journal of leukocyte biology*, 94(October), pp.1–10.
Herbomel, P., Thisse, B. & Thisse, C., 1999. Ontogeny and behaviour of early macrophages in the zebrafish embryo. *Development*, 126(17), pp.3735–3745.
Herbomel, P., Thisse, B. & Thisse, C., 2001. Zebrafish early macrophages colonize cephalic mesenchyme and developing brain, retina, and epidermis through a M-CSF receptor-dependent invasive process. *Developmental biology*, 238(2), pp.274–288.
Hersh, D. et al., 1999. The Salmonella invasin SipB induces macrophage apoptosis by binding to caspase-1. *Proceedings of the National Academy of Sciences*, 96(5), pp.2396–401.
Hong, S. et al., 2004. Analysis and characterisation of IL-1beta processing in rainbow trout, Oncorhynchus mykiss. *Fish & shellfish immunology*, 16(3), pp.453–9.
Hornung, V. et al., 2009. AIM2 recognizes cytosolic dsDNA and forms a caspase-1-activating inflammasome with ASC. *Nature*, 458(7237), pp.514–8.
Hornung, V. et al., 2008. Silica crystals and aluminum salts activate the NALP3 inflammasome through phagosomal destabilization. *Nature immunology*, 9(8), pp.847–56.
Huber, J. et al., 2002. Oxidized Membrane Vesicles and Blebs From Apoptotic Cells Contain Biologically Active Oxidized Phospholipids That Induce Monocyte-Endothelial Interactions. *Arteriosclerosis, Thrombosis, and Vascular Biology*, 22(1), pp.101–107.
Hugel, B. & Martínez, M., 2005. Membrane microparticles: two sides of the coin. *Physiology*, 20, pp.22–27.
Hughes, A., 1997. Rapid Evolution of Immunoglobulin Immune System Cells Superfamily C2 Domains Expressed in. *Molecular Biology and Evolution*, 14(1), pp.1–5.
Huising, M. et al., 2004. The molecular evolution of the interleukin-1 family of cytokines; IL-18 in teleost fish. *Developmental and comparative immunology*, 28(5), pp.395–413.
Ingham, P., 2009. The power of the zebrafish for disease analysis. *Human molecular genetics*, 18(R1), pp.R107–12.
Irmler, M. et al., 1995. Granzyme A Is an Interleukin 1 beta converting Ensyme. *Journal of experimental medicine*, 181(May), pp.1917–22.
Isoda, K. et al., 2005. Deficiency of interleukin-1 receptor antagonist deteriorates fatty liver and cholesterol metabolism in hypercholesterolemic mice. *Journal of Biological Chemistry*, 280(8), pp.7002–7009.

Isoda, K. et al., 2004. Lack of interleukin-1 receptor antagonist modulates plaque composition in apolipoprotein E-deficient mice. *Arteriosclerosis, thrombosis, and vascular biology*, 24(6), pp.1068–73.
Jacobs, M. & Harrison, S., 1998. Structure of an IκBα/NF-κB Complex. *Cell*, 95(6), pp.749–758.
Jault, C., Pichon, L. & Chluba, J., 2004. Toll-like receptor gene family and TIR-domain adapters in Danio rerio. *Molecular Immunology*, 40(11), pp.759–771.
Jiang, Y. et al., 2000. A multicenter, double-blind, dose-ranging, randomized, placebo-controlled study of recombinant human interleukin-1 receptor antagonist in patients with rheumatoid arthritis: radiologic progression and correlation of Genant and Larsen scores. *Arthritis and rheumatism*, 43(5), pp.1001–9.
Jin, C. & Flavell, R., 2010. Molecular mechanism of NLRP3 inflammasome activation. *Journal of clinical immunology*, 30(5), pp.628–31.
Jones, DA & Takemoto, D., 2004. Plant innate immunity – direct and indirect recognition of general and specific pathogen-associated molecules. *Current Opinion in Immunology*, 16(1), pp.48–62.
Joosten, L. & Netea, M., 2009. inflammatory arthritis in caspase-1 gene deficient mice: Contribution of proteinase 3 for caspase-1-independent production of bioactive IL-1β. *Arthritis and rheumatism*, 60(12), pp.3651–3662.
Källberg, M. et al., 2012. Template-based protein structure modeling using the RaptorX web server. *Nature Protocols*, 7, pp.1511–1522.
Kanneganti, T. et al., 2007. Pannexin-1-mediated recognition of bacterial molecules activates the cryopyrin inflammasome independent of Toll-like receptor signaling. *Immunity*, 26(4), pp.433–443.
Kanther, M. et al., 2011. Microbial colonization induces dynamic temporal and spatial patterns of NF-kappaB activation in the zebrafish digestive tract. *Gastroenterology*, 141(1), pp.197–207.
Kasahara, S. & Bosch, T., 2003. Enhanced antibacterial activity in Hydra polyps lacking nerve cells. *Developmental and comparative immunology*, 27(2), pp.79–85.
Kaspar, R. & Gehrke, L., 1994. Peripheral blood mononuclear cells stimulated with C5a or lipopolysaccharide to synthesize equivalent levels of IL-1 beta mRNA show unequal IL-1 beta protein accumulation but similar polyribosome profiles. *Journal of Immunology*, 129(1), p.2865.
Kasza, A., Wyrzykowska, P. & Horwacik, I., 2010. Transcription factors Elk-1 and SRF are engaged in IL1-dependent regulation of ZC3H12A expression. *BMC molecular Biology*, 11, p.14.
Kaufman, J., 2002. The origins of the adaptive immune system : whatever next ? *Nature immunology*, 3(12), pp.1124–25.
Kawakami, K. et al., 2004. A transposon-mediated gene trap approach identifies developmentally regulated genes in zebrafish. *Developmental cell*, 7(1), pp.133–44.
Keller, H., Lorizate, M. & Schwille, P., 2009. PI(4,5)P2 degradation promotes the formation of cytoskeleton-free model membrane systems. *Chemphyschem*, 10(16), pp.2805–12.
Keller, M. et al., 2008. Active caspase-1 is a regulator of unconventional protein secretion. *Cell*, 132(5), pp.818–31.

Kelley, L. & Sternberg, M., 2009. Protein structure prediction on the Web: a case study using the Phyre server. *Nature protocols*, 4(3), pp.363–71.
Kim, S. & Bauernfeind, F., 2010. Listeria monocytogenes is sensed by the NLRP3 and AIM2 Inflammasome. *European journal of immunology*, 40(6), pp.1545–1551.
Kimmel, C., 1989. Genetics and early development of zebrafish. *Trends in Genetics*, 5(8), pp.283–288.
Kleiner, H. et al., 2001. Oral administration of naturally occurring coumarins leads to altered phase I and II enzyme activities and reduced DNA adduct formation by polycyclic aromatic hydrocarbons in various tissues of SENCAR mice. *Carcinogenesis*, 22(1), pp.73–82.
Kofoed, E. & Vance, R., 2011. Innate immune recognition of bacterial ligands by NAIPs determines inflammasome specificity. *Nature*, 477(7366), pp.592–5.
Kollewe, C., Neumann, D. & Martin, M., 2000. The first two N-terminal immunoglobulin-like domains of soluble human IL-1 receptor type II are sufficient to bind and neutralize IL-1beta. *FEBS letters*, 487(2), pp.189–93.
Kominato, Y. et al., 1995. Monocyte expression of the human prointerleukin 1 beta gene (IL1B) is dependent on promoter sequences which bind the hematopoietic transcription factor Spi-1/PU.1. *Molecular and Cellular biology*, 15(1), pp.58–68.
Kono, T., Watanuki, H. & Sakai, M., 2002. The activation of interleukin-1[beta] in serum of carp, Cyprinus carpio, injected with peptidoglycan. *Aquaculture*, 212(1-4), pp.1–10.
Koopmans, W. et al., 2007. Single-pair FRET microscopy reveals mononucleosome dynamics. *Journal of fluorescence*, 17(6), pp.785–95.
Korherr, C. et al., 1997. A critical role for interleukin-1 receptor accessory protein in interleukin-1 signaling. *European Journal of Immunology*, 27(1), pp.262–267.
Kudo, S. et al., 1990. Clearance and Tissue Distribution of Recombinant Human Interleukin 1 β in Rats Clearance and Tissue Distribution of Recombinant Human Interleukin IÃŸ in Rats. *Cancer research*, pp.5751–5755.
Kwan, K. et al., 2007. The Tol2kit: a multisite gateway-based construction kit for Tol2 transposon transgenesis constructs. *Developmental dynamics*, 236(11), pp.3088–99.
Laing, K. et al., 2008. A genomic view of the NOD-like receptor family in teleost fish: identification of a novel NLR subfamily in zebrafish. *BMC evolutionary Biology*, 8, p.42.
Lang, D., Knop, J. & Wesche, H., 1998. The type II IL-1 receptor interacts with the IL-1 receptor accessory protein: a novel mechanism of regulation of IL-1 responsiveness. *Journal of Immunology*, 161(12), pp.6871–6877.
Langenau, D. et al., 2004. In vivo tracking of T cell development, ablation, and engraftment in transgenic zebrafish. *Proceedings of the National Academy of Sciences of the United States of America*, 101(19), pp.7369–74.
Lanot, R. et al., 2001. Postembryonic hematopoiesis in Drosophila. *Developmental biology*, 230(2), pp.243–57.
Lata, S. et al., 2008. Helical structures of ESCRT-III are disassembled by VPS4. *Science*, 321(5894), pp.1354–1357.

Lee, E. et al., 2001. A highly efficient Escherichia coli-based chromosome engineering system adapted for recombinogenic targeting and subcloning of BAC DNA. *Genomics*, 73(1), pp.56–65.
Lenz, M., Crow, D. & Joanny, J., 2009. Membrane buckling induced by curved filaments. *Physical review letters*, (c), pp.1–4.
Lépine, S. et al., 2006. ATP-induced apoptosis of thymocytes is mediated by activation of P2 X 7 receptor and involves de novo ceramide synthesis and mitochondria. *Biochimica et biophysica acta*, 1761(1), pp.73–82.
Li, L. et al., 2012. Live Imaging Reveals Differing Roles of Macrophages and Neutrophils during Zebrafish Tail Fin Regeneration. *Journal of biological chemistry*, 287(30), pp.25353–60.
Li, P. et al., 1995. Mice deficient in IL-1 beta-converting enzyme are defective in production of mature IL-1 beta and resistant to endotoxic shock. *Cell*, 80(3), pp.401–11.
Liang, M. et al., 2006. The interleukin-1beta gene is transcribed from a poised promoter architecture in monocytes. *Journal of Biological Chemistry*, 281(14), pp.9227–9237.
Lieschke, G. et al., 2001. Morphologic and functional characterization of granulocytes and macrophages in embryonic and adult zebrafish. *Blood*, 98(10), pp.3087–3096.
Lieschke, G. & Currie, P., 2007. Animal models of human disease: zebrafish swim into view. *Nature reviews. Genetics*, 8(5), pp.353–67.
Llopis, J. et al., 1998. Measurement of cytosolic, mitochondrial, and Golgi pH in single living cells with green fluorescent proteins. *Proceedings of the National Academy of Sciences*, 95(12), pp.6803–8.
Locovei, S. et al., 2007. Pannexin1 is part of the pore forming unit of the P2X(7) receptor death complex. *FEBS Letters*, 581(3), pp.483–488.
López-Castejón, G., Young, M., et al., 2007. Characterization of ATP-gated P2X7 receptors in fish provides new insights into the mechanism of release of the leaderless cytokine interleukin-1 beta. *Molecular immunology*, 44(6), pp.1286–99.
López-Castejón, G. et al., 2008. Molecular and functional characterization of gilthead seabream Sparus aurata caspase-1: the first identification of an inflammatory caspase in fish. *Molecular immunology*, 45(1), pp.49–57.
López-Castejón, G., Sepulcre, M, et al., 2007. The type II interleukin-1 receptor (IL-1RII) of the bony fish gilthead seabream Sparus aurata is strongly induced after infection and tightly regulated at transcriptional and post-transcriptional levels. *Molecular immunology*, 44(10), pp.2772–80.
López-Castejón, G. & Brough, D., 2011. Understanding the mechanism of IL-1β secretion. *Cytokine & growth factor reviews*, 22(4), pp.189–95.
Loynes, C. et al., 2010. Pharmacological manipulation of inflammation resolution during spontaneously resolving tissue neutrophilia in the zebrafish. *Journal of leukocyte biology*, 87(2), pp.203–12.
Lugo-Villarino, G. et al., 2010. Identification of dendritic antigen-presenting cells in the zebrafish. *Proceedings of the National Academy of Sciences of the United States of America*, 107(36), pp.15850–5.
MacKenzie, A. et al., 2001. Rapid secretion of interleukin-1beta by microvesicle shedding. *Immunity*, 15(5), pp.825–835.

Maelfait, J. et al., 2008. Stimulation of Toll-like receptor 3 and 4 induces interleukin-1beta maturation by caspase-8. *The Journal of experimental medicine*, 205(9), pp.1967–73.
Malinowsky, D. & Lundkvist, J., 1998. Interleukin-1 receptor accessory protein interacts with the type II interleukin-1 receptor. *FEBS letters*, 429(3), pp.299–302.
Marguet, D. et al., 1999. Engulfment of apoptotic cells involves the redistribution of membrane phosphatidylserine on phagocyte and prey. *Nature cell biology*, 1(7), pp.454–6.
Mariathasan, S. et al., 2004. Differential activation of the inflammasome by caspase-1 adaptors ASC and Ipaf. *Nature*, 430(6996), pp.213–8.
Martin, S. et al., 1995. Early redistribution of plasma membrane phosphatidylserine is a general feature of apoptosis regardless of the initiating stimulus: inhibition by overexpression of Bcl-2 and Abl. *The Journal of experimental medicine*, 182(5), pp.1545–56.
Martinet, W., Schrijvers, D. & Kockx, M., 2003. Nucleofection as an efficient nonviral transfection method for human monocytic cells. *Biotechnology Letters*, 25(13), pp.1025–1029.
Martinez, F., Gordon, S. & Locati, M., 2006. Transcriptional profiling of the human monocyte-to-macrophage differentiation and polarization: new molecules and patterns of gene expression. *Journal of Immunology*, 177(10), pp.7303–7311.
Martinon, F., Burns, K. & Tschopp, J., 2002. The inflammasome: a molecular platform triggering activation of inflammatory caspases and processing of proIL-beta. *Molecular cell*, 10(2), pp.417–26.
Martinon, F., Hofmann, K. & Tschopp, J., 2001. The pyrin domain: a possible member of the death domain-fold family implicated in apoptosis and inflammation. *Current biology*, 11(4), pp.R118–20.
Masumoto, J. et al., 2003. Caspy, a zebrafish caspase, activated by ASC oligomerization is required for pharyngeal arch development. *Journal of biological chemistry*, 278(6), pp.4268–76.
Mcmahan, C. et al., 1991. A novel IL-1 receptor, cloned from B cells by mammalian expression, is expressed in many cell types. *EMBO Journal*, 10(10), pp.2821–2832.
Medzhitov, R., Preston-hurlburt, P. & Janeway, C., 1997. A human homologue of the Drosophila Toll protein signals activation of adaptive immunity. *Nature*, 388(July), pp.6–9.
Meeker, N. & Trede, N., 2008. Immunology and zebrafish: spawning new models of human disease. *Developmental and comparative immunology*, 32(7), pp.745–57.
Meijer, A. et al., 2004. Expression analysis of the Toll-like receptor and TIR domain adaptor families of zebrafish. *Molecular Immunology*, 40(11), pp.773–783.
Meijer, A. & Spaink, H., 2011. Host-pathogen interactions made transparent with the zebrafish model. *Current drug targets*, 12(7), pp.1000–17.
Meixenberger, K. et al., 2010. Listeria monocytogenes-infected human peripheral blood mononuclear cells produce IL-1beta, depending on listeriolysin O and NLRP3. *Journal of immunology*, 184(2), pp.922–30.
Mercurio, F. et al., 1997. IKK-1 and IKK-2: cytokine-activated IkappaB kinases essential for NF-kappaB activation. *Science*, 278(5339), pp.860–866.

Mertens, M. & Singh, J., 2009. Anakinra for rheumatoid arthritis. *Cochrane database of systematic reviews (Online)*, 36(1), p.CD005121.
Miao, A. et al., 2006. Cytoplasmic flagellin activates caspase-1 and secretion of interleukin 1beta via Ipaf. *Nature immunology*, 7(6), pp.569–75.
Miller, B. et al., 1995. Inhibition of mature IL-1 beta production in murine macrophages and a murine model of inflammation by WIN 67694, an inhibitor of IL-1 beta converting enzyme. *Journal of Immunology*, 154(3), pp.1331–1338.
Miller, DJ et al., 2007. The innate immune repertoire in cnidaria--ancestral complexity and stochastic gene loss. *Genome biology*, 8(4), p.R59.
Miller, DK et al., 1993. Purification and Characterisation of Active human Interleukin-1β-converting enzyme from THP.1 Monocytic cells. *Journal of Biological Chemistry*, 268(24), pp.18062–18069.
Mitcham, J., Parnet, P. & Bonnert, T., 1996. T1/ST2 signaling establishes it as a member of an expanding interleukin-1 receptor family. *Journal of Biological Chemistry*, 271(10), pp.5777–5783.
Mizgalska, D. et al., 2009. Interleukin-1-inducible MCPIP protein has structural and functional properties of RNase and participates in degradation of IL-1beta mRNA. *FEBS Journal*, 276(24), pp.7386–7399.
Morgan, M. et al., 2001. An apoptosis signaling pathway induced by the death domain of FADD selectively kills normal but not cancerous prostate epithelial cells. *Cell death and differentiation*, 8(7), pp.696–705.
Morita, E. et al., 2011. ESCRT-III protein requirements for HIV-1 budding. *Cell host & microbe*, 9(3), pp.235–42.
Morita, E. et al., 2007. Human ESCRT and ALIX proteins interact with proteins of the midbody and function in cytokinesis. *EMBO journal*, 26(19), pp.4215–27.
Muto, A. et al., 2013. Real-Time Visualization of Neuronal Activity during Perception. *Current biology*, 23(4), pp.307–11.
Nasevicius, A. & Ekker, S., 2000. Effective targeted gene "knockdown" in zebrafish. *Nature genetics*, 26(2), pp.216–20.
Neumann, D., Kollewe, C. & Martin, M., 2000. The membrane form of the type II IL-1 receptor accounts for inhibitory function. *Journal of Immunology*, 165(6), pp.3350–3357.
Nicklin, M. & Weith, A., 1994. A Physical map of the region encompassing the Human Interleukin-1α, Interleukin-1β and interleukin-1 Receptor Antagonist Genes. *Genomics*, 19(2), pp.382–384.
Niethammer, P. et al., 2009. A tissue-scale gradient of hydrogen peroxide mediates rapid wound detection in zebrafish. *Nature*, 459(7249), pp.996–9.
Nomura, S. et al., 1995. Platelet-derived microparticles may influence the development of atherosclerosis in diabetes mellitus. *Atherosclerosis*, 116(2), pp.235–40.
Nuki, G. et al., 2002. Long-term safety and maintenance of clinical improvement following treatment with anakinra (recombinant human interleukin-1 receptor antagonist) in patients with rheumatoid arthritis: extension phase of a randomized, double-blind, placebo-controlled trial. *Arthritis and rheumatism*, 46(11), pp.2838–46.
Nurminen, T. et al., 2002. Observation of topical catalysis by sphingomyelinase coupled to microspheres. *Journal of the American Chemical Society*, 124(41), pp.12129–34.

Nürnberger, T. et al., 2004. Innate immunity in plants and animals: striking similarities and obvious differences. *Immunological reviews*, 198, pp.249–66.
Oehlers, S. et al., 2010. Expression of zebrafish cxcl8 (interleukin-8) and its receptors during development and in response to immune stimulation. *Developmental and comparative immunology*, 34(3), pp.352–9.
Pancer, Z. et al., 2004. Somatic diversification of variable lymphocyte receptors in the agnathan sea lamprey. *Nature*, 430(6996), pp.174–80.
Pancer, Z. & Cooper, M., 2006. The evolution of adaptive immunity. *Annual review of immunology*, 24, pp.497–518.
Pawley, J., 2006. *Handbook of Biological confocal microscopy 3rd edition*,
Pelegrín, P., Barroso-Gutierrez, C. & Surprenant, A., 2008. P2X7 receptor differentially couples to distinct release pathways for IL-1beta in mouse macrophage. *Journal of Immunology*, 180(11), pp.7147–7157.
Pelegrín, P. & Surprenant, A., 2009a. Dynamics of macrophage polarization reveal new mechanism to inhibit IL-1beta release through pyrophosphates. *EMBO journal*, 28(14), pp.2114–27.
Pelegrín, P. & Surprenant, A., 2006. Pannexin-1 mediates large pore formation and interleukin-1beta release by the ATP-gated P2X7 receptor. *EMBO journal*, 25(21), pp.5071–82.
Pelegrín, P. & Surprenant, A., 2009b. The P2X(7) receptor-pannexin connection to dye uptake and IL-1beta release. *Purinergic signalling*, 5(2), pp.129–37.
Peng, J. & Xu, J., 2011. RaptorX: exploiting structure information for protein alignment by statistical inference. *PROTEINS: Structure, Function, and Genetics Structure Function And Bioinformatics*, 79 Suppl 1(S10), pp.161–71.
Peri, F. & Nüsslein-Volhard, C., 2008. Live imaging of neuronal degradation by microglia reveals a role for v0-ATPase a1 in phagosomal fusion in vivo. *Cell*, 133(5), pp.916–27.
Perregaux, D. & Gabels, A., 1994. Interleukin-1 beta maturation and release in response to ATP and nigericin. Evidence that potassium depletion mediated by these agents is a necessary and common. *Journal of Biological Chemistry*, 269(21), pp.15195–15203.
Pétrilli, V. et al., 2007. Activation of the NALP3 inflammasome is triggered by low intracellular potassium concentration. *Cell Death and Differentiation*, 14(9), pp.1583–1589.
Pizzirani, C. et al., 2007. Stimulation of P2 receptors causes release of IL-1beta-loaded microvesicles from human dendritic cells. *Blood*, 109(9), pp.3856–3864.
Prajsnar, T. et al., 2008. A novel vertebrate model of Staphylococcus aureus infection reveals phagocyte-dependent resistance of zebrafish to non-host specialized pathogens. *Cellular microbiology*, 10(11), pp.2312–25.
Prajsnar, T. et al., 2012. A privileged intraphagocyte niche is responsible for disseminated infection of Staphylococcus aureus in a zebrafish model. *Cellular microbiology*, 14(10), pp.1600–19.
Priestle, J., Schär, H. & Grütter, M., 1988. Crystal structure of the cytokine interleukin-1 beta. *EMBO journal*, 7(2), pp.339–43.
Prince, M. et al., 2006. Naturally occurring coumarins inhibit 7,12-dimethylbenz[a]anthracene DNA adduct formation in mouse mammary gland. *Carcinogenesis*, 27(6), pp.1204–13.

Prochnow, N. et al., 2009. Pannexin1 in the outer retina of the zebrafish, Danio rerio. *Neuroscience*, 162(4), pp.1039–1054.
Provost, E. & Rhee, J., 2007. Viral 2A peptides allow expression of multiple proteins from a single ORF in transgenic zebrafish embryos. *Genesis*, 629(October), pp.625–629.
Qu, Y. et al., 2007. Nonclassical IL-1 beta secretion stimulated by P2X7 receptors is dependent on inflammasome activation and correlated with exosome release in murine macrophages. *Journal of Immunology*, 179(3), pp.1913–1925.
Qu, Y. et al., 2009. P2X7 receptor-stimulated secretion of MHC class II-containing exosomes requires the ASC/NLRP3 inflammasome but is independent of caspase-1. *Journal of immunology*, 182(8), pp.5052–62.
Qwarnstrom, E. et al., 1988. Binding, internalization, and intracellular localization of interleukin-1 beta in human diploid fibroblasts. *Journal of Biological Chemistry*, 263(17), pp.8261–8269.
Rano, T. et al., 1997. A combinatorial approach for determining protease specificities: application to interleukin-1β converting enzyme (ICE). *Chemistry & Biology*, 4(2), pp.149–155.
Rassendren, F. et al., 1997. The permeabilizing ATP receptor, P2X7. Cloning and expression of a human cDNA. *Journal of Biological Chemistry*, 272(9), pp.5482–5486.
Rathinam, V., Vanaja, S. & Fitzgerald, K., 2012. Regulation of inflammasome signaling. *Nature immunology*, 13(4), pp.333–2.
Regnier, C. et al., 1997. Identification and characterization of an IkappaB kinase. *Cell*, 90(2), pp.373–383.
Rehm, M. et al., 2002. Single-cell fluorescence resonance energy transfer analysis demonstrates that caspase activation during apoptosis is a rapid process. Role of caspase-3. *Journal of Biological Chemistry*, 277(27), pp.24506–24514.
Relton, J. & Rothwell, N., 1992. Interleukin-1 receptor antagonist inhibits ischaemic and excitotoxic neuronal damage in the rat. *Brain Research Bulletin*, 29(2), pp.243–246.
Renshaw, S. et al., 2006. A transgenic zebrafish model of neutrophilic inflammation. *Blood*, 108(13), pp.3976–8.
Renshaw, S. et al., 2004. Three novel Bid proteins generated by alternative splicing of the human Bid gene. *Journal of biological chemistry*, 279(4), pp.2846–55.
Renshaw, S. & Trede, N., 2012. A model 450 million years in the making: zebrafish and vertebrate immunity. *Disease models & mechanisms*, 5(1), pp.38–47.
Rothwarf, D. et al., 1998. IKK-gamma is an essential regulatory subunit of the IkappaB kinase complex. *Nature*, 395(6699), pp.297–300.
Roy, A., Kucukural, A. & Zhang, Y., 2010. I-TASSER: a unified platform for automated protein structure and function prediction. *Nature protocols*, 5(4), pp.725–38.
Rubartelli, A. et al., 1990. A novel secretory pathway for interleukin-lbeta, a protein lacking a signal sequence. *EMBO Journal*, 9(5), pp.1503–1510.
Sabroe, I. et al., 2008. The role of TLR activation in inflammation. *Journal of pathology*, 214(2), pp.126–35.
Saitoh, T. et al., 2008. Loss of the autophagy protein Atg16L1 enhances endotoxin-induced IL-1beta production. *Nature*, 456(7219), pp.264–8.

Salloum, F. et al., 2009. Anakinra in experimental acute myocardial infarction--does dosage or duration of treatment matter? *Cardiovascular drugs and therapy*, 23(2), pp.129–35.
Sanz, J.M. & Di Virgilio, F., 2000. Kinetics and mechanism of ATP-dependent IL-1 beta release from microglial cells. *Journal of immunology*, 164(9), pp.4893–8.
Van der Sar, A. et al., 2006. MyD88 Innate Immune Function in a Zebrafish Embryo Infection Model. *Infection and Immunity*, 74(4), pp.2436–2441.
Sarropoulou, E. et al., 2007. A gene-based radiation hybrid map of the gilthead sea bream Sparus aurata refines and exploits conserved synteny with Tetraodon nigroviridis. *BMC genomics*, 8, p.44.
Satta, N., Toti, F. & Feugeas, O., 1994. Monocyte vesiculation is a possible mechanism for dissemination of membrane-associated procoagulant activities and adhesion molecules after stimulation by. *The Journal of …*, 153(7), pp.3245–3255.
Scheer, N., 1999. Use of the Gal4-UAS technique for targeted gene expression in the zebrafish. *Mechanisms of development*, 80(2), pp.153–158.
Schindler, R., Clark, B. & Dinarello, C., 1990. Dissociation between interleukin-1 beta mRNA and protein synthesis in human peripheral blood mononuclear cells. *Journal of biological chemistry*, 265(18), pp.10232–7.
Schönbeck, U., Mach, F. & Libby, P., 1998. Generation of biologically active IL-1 beta by matrix metalloproteinases: a novel caspase-1-independent pathway of IL-1 beta processing. *Journal of immunology*, 161(7), pp.3340–6.
Schreuder, H. et al., 1997. A new cytokine-receptor binding mode revealed by the crystal structure of the IL-1 receptor with an antagonist. *Nature*, 386(6621), pp.194–200.
Von Schwedler, U. et al., 2003. The protein network of HIV budding. *Cell*, 114(6), pp.701–13.
Scott, E. et al., 2007. Targeting neural circuitry in zebrafish using GAL4 enhancer trapping. *Nature Methods*, 4(4), pp.323–326.
Scotton, C. et al., 2005. Transcriptional profiling reveals complex regulation of the monocyte IL-1 beta system by IL-13. *Journal of immunology*, 174(2), pp.834–45.
Seigneuret, M., 1984. ATP-dependent asymmetric distribution of spin-labeled phospholipids in the erythrocyte membrane: relation to shape changes. *Proceedings of the National Academy of Sciences*, 81(12), pp.3751–3755.
Sepulcre, MP et al., 2009. Evolution of lipopolysaccharide (LPS) recognition and signaling: fish TLR4 does not recognize LPS and negatively regulates NF-kappaB activation. *Journal of immunology*, 182(4), pp.1836–45.
Shintani, S. & Terzic, J., 2000. Do lampreys have lymphocytes? The Spi evidence. *Proceedings of the …*, 97(13), pp.7417–22.
Shumway, S., Maki, M. & Miyamoto, S., 1999. The PEST domain of IkappaBalpha is necessary and sufficient for in vitro degradation by mu-calpain. *Journal of Biological Chemistry*, 274(43), pp.30874–30881.
Sieger, D. et al., 2012. Long-range Ca2+ waves transmit brain-damage signals to microglia. *Developmental cell*, 22(6), pp.1138–48.
Silverman, W. & Vaccari, J. de R., 2009. The pannexin 1 channel activates the inflammasome in neurons and astrocytes. *Journal of Biological …*, 284(27), pp.18143–18151.

Sims, J. et al., 1988. cDNA expression cloning of the IL-1 receptor, a member of the immunoglobulin superfamily. *Science*, 241(4865), pp.585–589.
Smith, D. et al., 2003. The soluble form of IL-1 receptor accessory protein enhances the ability of soluble type II IL-1 receptor to inhibit IL-1 action. *Immunity*, 18(1), pp.87–96.
So, A. & De Smedt, T., 2007. A pilot study of IL-1 inhibition by anakinra in acute gout. *Arthritis Research and …*, 9(2), p.R28.
Stein, C. et al., 2007. Conservation and divergence of gene families encoding components of innate immune response systems in zebrafish. *Genome Biology*, 8(11), p.R251.
Stenmark, H., Olkkonen, V. & M, 2001. The Rab GTPase family. *Genome Biology*, 2(5), pp.1–7.
Stoletov, K. et al., 2009. Vascular lipid accumulation, lipoprotein oxidation, and macrophage lipid uptake in hypercholesterolemic zebrafish. *Circ Res*, 104(8), pp.952–960.
Stout, J., Sims, P. & Wiedmer, T., 1996. Isolation of an erythrocyte membrane protein that mediates Ca2+-dependent transbilayer movement of phospholipid. *Journal of Biological Chemistry*, 271(29), pp.17205–17210.
Sullivan, C. & Kim, C., 2008. Zebrafish as a model for infectious disease and immune function. *Fish & shellfish immunology*, 25(4), pp.341–50.
Sullivan, J. et al., 2007. Rel homology domain-containing transcription factors in the cnidarian Nematostella vectensis. *Development genes and evolution*, 217(1), pp.63–72.
Sun, Y. et al., 2008. Molecular cloning and expression analysis of the ASC gene from mandarin fish and its regulation of NF-kappaB activation. *Developmental and Comparative Immunology*, 32(4), pp.391–399.
Surprenant, A. et al., 1996. The cytolytic P2Z receptor for extracellular ATP identified as a P2X receptor (P2X7). *Science*, 272(5262), pp.735–738.
Sutterwala, F., Ogura, Y., Szczepanik, M., et al., 2006. Critical role for NALP3/CIAS1/Cryopyrin in innate and adaptive immunity through its regulation of caspase-1. *Immunity*, 24(3), pp.317–27.
Sutterwala, F., Ogura, Y., Zamboni, D., et al., 2006. NALP3: a key player in caspase-1 activation. *Journal of endotoxin research*, 12(4), pp.251–6.
Takemoto, K. et al., 2003. Spatio-temporal activation of caspase revealed by indicator that is insensitive to environmental effects. *Journal of cell biology*, 160(2), pp.235–43.
Tepper, A. et al., 2000. Sphingomyelin hydrolysis to ceramide during the execution phase of apoptosis results from phospholipid scrambling and alters cell-surface morphology. *Journal of cell biology*, 150(1), pp.155–64.
Terkeltaub, R. et al., 2009. The IL-1 Inhibitor Rilonacept in Treatment of Chronic Gouty Arthritis: Results of a Placebo-Controlled, Monosequence Crossover, Nonrandomized, Single-Blind Pilot Study. *Annals of the Rheumatic Diseases*, 68(10), pp.1613–7.
Thornberry, N. et al., 1997. A combinatorial approach defines specificities of members of the caspase family and granzyme B. Functional relationships established for key mediators of apoptosis. *Journal of biological chemistry*, 272(29), pp.17907–11.

Tian, H. et al., 2007. A high throughput drug screen based on fluorescence resonance energy transfer (FRET) for anticancer activity of compounds from herbal medicine. *British journal of pharmacology*, 150(3), pp.321–34.
Tierney, M. & Medcalf, R., 2001. Plasminogen activator inhibitor type 2 contains mRNA instability elements within exon 4 of the coding region. Sequence homology to coding region instability determinants in other mRNAs. *Journal of Biological Chemistry*, 276(17), pp.13675–13684.
Tobin, D. et al., 2010. The lta4h locus modulates susceptibility to mycobacterial infection in zebrafish and humans. *Cell*, 140(5), pp.717–30.
Tyas, L. et al., 2000. Rapid caspase-3 activation during apoptosis revealed using fluorescence-resonance energy transfer. *EMBO reports*, 1(3), pp.266–70.
Unlu, S. et al., 2007. Phosphorylation of IRF8 in a pre-associated complex with Spi-1/PU. 1 and non-phosphorylated Stat1 is critical for LPS induction of the IL1B gene. *Molecular Immunology*, 44(13), pp.3364–3379.
Urasaki, A. & Asakawa, K., 2008. Efficient transposition of the Tol2 transposable element from a single-copy donor in zebrafish. *Proceedings of the National Academy of Sciences*, 105(50), pp.19827–19832.
Verhoef, P. & Estacion, M., 2003. P2X7 receptor-dependent blebbing and the activation of Rho-effector kinases, caspases, and IL-1beta release. *Journal of Immunology*, 170(11), pp.5728–5738.
Verhoef, P., Kertesy, S. & Estacion, M., 2004. Maitotoxin induces biphasic interleukin-1β secretion and membrane blebbing in murine macrophages. *Molecular Pharmacology*, 66(4), pp.909–920.
Vigers, G. et al., 1997. Crystal structure of the type-I interleukin-1 receptor complexed with interleukin-1beta. *Nature*, 386(6621), pp.190–4.
Vojtech, L. et al., 2009. Host immune response and acute disease in a zebrafish model of Francisella pathogenesis. *Infection and immunity*, 77(2), pp.914–25.
Vojtech, L. et al., 2012. Roles of inflammatory caspases during processing of zebrafish interleukin-1β in Francisella noatunensis infection. *Infection and immunity*, 80(8), pp.2878–85.
Wilson, K. et al., 1994. Structure and mechanism of interleukin-1 beta converting enzyme. *Nature*, 370(6487), pp.270–5.
Wollert, T. et al., 2009. Membrane scission by the ESCRT-III complex. *Nature*, 458(7235), pp.172–177.
Xia, Z. & Liu, Y., 2001. Reliable and global measurement of fluorescence resonance energy transfer using fluorescence microscopes. *Biophysical journal*, 81(4), pp.2395–402.
Xu, X. et al., 1998. Detection of programmed cell death using fluorescence energy transfer. *Nucleic acids research*, 26(8), pp.2034–5.
Xu, Y. et al., 2000. Structural basis for signal transduction by the Toll/interleukin-1 receptor domains. *Nature*, 408(6808), pp.111–115.
Xu, Z. et al., 2011. Mutation of a novel virulence-related gene mltD in Vibrio anguillarum enhances lethality in zebra fish. *Research in microbiology*, 162(2), pp.144–50.
Yang, C. et al., 2012. Neutrophils Exert Protection in the Early Tuberculous Granuloma by Oxidative Killing of Mycobacteria Phagocytosed from Infected Macrophages supplemental data. *Cell host & microbe*, 12, pp.301–312.

Youvan, D. et al., 1997. Calibration of Fluorescence Resonance Energy Transfer in Microscopy Using Genetically Engineered GFP Derivatives on Nickel Chelating Beads. *Biotechnology*, 3, pp.1–18.
Zerial, M. & McBride, H., 2001. Rab proteins as membrane organizers. *Nature reviews Molecular cell biology*, 2(2), pp.107–17.
Zhang, Y., 2008. I-TASSER server for protein 3D structure prediction. *BMC bioinformatics*, 9, p.40.
Zhao, X., Ellingsen, S. & Fjose, A., 2009. Labelling and targeted ablation of specific bipolar cell types in the zebrafish retina. *BMC neuroscience*, 10, p.107.
Zhao, Y. et al., 2011. The NLRC4 inflammasome receptors for bacterial flagellin and type III secretion apparatus. *Nature*, 477(7366), pp.596–600.
Zhou, Q. et al., 1997. Molecular cloning of human plasma membrane phospholipid scramblase. A protein mediating transbilayer movement of plasma membrane phospholipids. *Journal of Biological Chemistry*, 272(29), pp.18240–18244.
Zhu, Y. et al., 2005. The ancient origin of the complement system. *EMBO journal*, 24(2), pp.382–94.
Zou, J., Grabowski, P. & Cunningham, C., 1999. Molecular cloning of interleukin 1 from rainbow trout Oncorhynchus mykiss reveals no evidence of an ICE cut site. *Cytokine*, 11(8), pp.552–560.
Zwaal, R. & Schroit, A., 1997. Pathophysiologic implications of membrane phospholipid asymmetry in blood cells. *Blood*, 89(4), pp.1121–1132.